Huan Pang *Editor*

Nano/Micro Metal-Organic Frameworks

A Platform for Electrochemical Energy Applications

Springer

Nano/Micro Metal-Organic Frameworks

Huan Pang
Editor

Nano/Micro Metal-Organic Frameworks

A Platform for Electrochemical Energy Applications

Springer

Editor
Huan Pang
School of Chemistry and Chemical Engineering
Yangzhou University
Yangzhou, Jiangsu, China

ISBN 978-981-16-4070-4 ISBN 978-981-16-4071-1 (eBook)
https://doi.org/10.1007/978-981-16-4071-1

This Springer imprint is published by the registered company Springer Nature Singapore Pte Ltd.
The registered company address is: 152 Beach Road, #21-01/04 Gateway East, Singapore 189721, Singapore

Contents

1 Nano/Micro MOF-Based Materials 1
Huan Pang and Yijian Tang

2 MOF Derivatives 41
Bingjun Zhu

3 Batteries 79
Lin-Hai Pan, Hai-Yan He, Jian-Hua Wang, Xin Liu, Jia-Wei Qian, Jingwei Chen, and Li-Feng Chen

4 Supercapacitors 143
Jianan Zhang, Xiaoyu Zhang, Dongping Xue, Huicong Xia, and Su Jiang

5 MOF-Derived Materials for Energy Conversion 165
Jianan Zhang, Su Jiang, Dongping Xue, and Xiaoyu Zhang

6 Summary and Perspectives 211
Huan Pang

Chapter 1
Nano/Micro MOF-Based Materials

Huan Pang and Yijian Tang

1.1 Introduction

Metal–organic frameworks (MOFs) are the structures of highly ordered polymer connected by coordination bonds. Due to the diversity of organic ligands and metal ions, as well as the principles of some successful crystal engineering, MOFs are famous for their modular design capabilities to construct framework topology, the size/shape of pore and the characteristics of pore surface as needed. In addition to their structures and applications, MOFs are also known for the response of their flexible structures to external stimuli (object changes, light irradiation, temperature change and mechanical forces) [1–4]. For most MOFs, the host framework of different parts can rotate around a single bond in an organic ligand or can rotate between an organic ligand and a metal ion. The reversible nature of coordination bonds and weaker supramolecular interactions also enables the internal connections within the MOF crystals to reversibly break and reform. These structural features give rise to multiple, easily accessible thermodynamic metastable states. Consequently, flexible MOFs can show diverse types and magnitudes of structural dynamism. Importantly, many of the structure changes occur with the retention of the periodicity and even the single-crystallinity, which enable the transformed structures and host–guest interactions to be visualized at the atomic level by crystallography techniques including the convenient inhouse single-crystal X-ray diffraction [5].

MOFs are a novel type of crystalline porous material with a periodic network structure, which consists of inorganic vertices and organic linkers that are coupled to each other through coordination bonds [6]. There are now more than 20,000

H. Pang (✉) · Y. Tang
School of Chemistry and Chemical Engineering, Institute for Innovative Materials and Energy, Yangzhou University, Yangzhou 225009, Jiangsu, PR China
e-mail: huanpangchem@hotmail.com; panghuan@yzu.edu.cn

Y. Tang
e-mail: yijiantangchem@126.com

H. Pang (ed.), *Nano/Micro Metal-Organic Frameworks*,
https://doi.org/10.1007/978-981-16-4071-1_1

MOFs with various compositions, morphologies and crystal structures. Owing to the unique advantages such as porous crystal structure, highly dispersed metal components, adjustable pore size, MOFs have excellent application performance in energy storage, drug delivery, catalysis. As a new electrode material, MOFs have unique advantages such as high specific surface area, low density, controllable pore size and great thermal stability, which can be used as the electrodes of batteries and supercapacitors. MOFs materials introduce design concepts and concepts in crystal engineering into supramolecular disciplines, which is an emerging cross-field that spans inorganic chemistry, organic chemistry, crystal engineering, and materials science. Through nearly two decades of research and development, MOFs materials have made a series of progress in synthesis and preparation, design, performance, and theoretical research. Compared with traditional materials, MOF materials have obvious advantages. Firstly, the structure of the MOFs material has certain adjustability. The size and shape of the crystal pores can be adjusted by selecting the size of the organic ligand. At the same time, the surface of the pores of the MOFs material can be modified to achieve the target performance. Secondly, the composition of MOFs materials is highly diverse. By choosing different organic ligands and metals, MOF materials with different structures can be constructed to achieve different target properties. Thirdly, the method for synthesizing MOFs is simple. Fourthly, MOF materials have porous characteristics, and a high specific surface area can be obtained through reasonable design. Fifthly, as a kind of organic–inorganic hybrid materials linked by coordination bonds, MOFs materials have high thermal and chemical stability [7–10].

In 1995, Yaghi and coworkers [11] reported a two-dimensional (2D) structure material, which is connected by rigid organic ligand trimesic acid (BTC) and transition metal Co. In 1999, Yaghi'team [12] reported that a three-dimensional (3D) metal organic framework material with a simple cubic structure-MOF-5, constructed with rigid organic ligand terephthalic acid (BDC) and transition metal Zn, is composed of benzene-containing metal nodes at the eight vertices of the cube. The unique merits of crystalline porous structure, highly dispersed metal components and adjustable pore size of MOFs grant them outstanding performances in a variety of applications,16 for example, energy storage. In 2004 and 2005, Gérard Férey of the University of Versailles in France successively reported two molecular sieve-like MOFs with the characteristics of super-large pores-MIL-100 and MIL-101 [13, 14]. It combines target chemistry and computer simulation methods, and uses conventional organic ligands BTC and BDC and trivalent metal Cr to construct a MOF with a super-large cage MTN-type molecular sieve topology. They both have two mesoporous cages with sizes of 25 Å, 29 Å and 29 Å, 34 Å. The specific surface area is as high as 3100 $m^2\ g^{-1}$ and 5900 $m^2\ g^{-1}$. This contribution of Férey's research not only solves the problem that single-crystal X-ray diffraction methods are unable to solve the huge unit cell volume when analyzing the crystal structure, but also proposes a new strategy for designing and synthesizing the target structure with the aid of computer simulation, which can be said to be MOF materials. The development has revealed a new page. In 2006, Yaghi's research team [5] turned their attention to traditional molecular sieve materials with superior stability and reported that they had

synthesized 12 molecular sieve-like imidazole framework materials with 7 typical silica-alumina molecular sieve topologies-ZIF-1 to ZIF-12, these materials exhibit superior thermal and chemical stability, among which ZIF-8 and ZIF-11 can not only be stable to 550 °C, but also remain stable in boiling alkaline aqueous solutions and organic solvents. Later, it was favored by many scientific researchers and developed many applications. Subsequently, from 2007 to 2008, the Yaghi research team successively reported on ZIF-20 to ZIF-23, ZIF-68, ZIF-69, ZIF-70, ZIF-95 and ZIF-100 structures have greatly expanded the ZIF family [5, 15].

In addition, the materials with hybrid micro/nanostructure play an important role in energy storage and conversion applications (rechargeable batteries, supercapacitors and fuel cells) with high performance. Although they are complex, these multicomponent structures have the potential to overcome the weaknesses of a single counterpart. The unique characteristics of this hybrid structural material, as well as the unlimited selection of components having various properties, provides methods to optimize application performance. To date, various kinds of micro/nano hybrid structures have been obtained through a variety of synthesis methods, which usually require precursors and sacrificial templates to construct complex hybrid structures. This is because the thermodynamic and kinetic processes of various reactions occurring at the interface of micro/nanocrystals are affected by the surface energy, so the design and control of various morphologies of MOF nanocrystals has become a hot topic in recent years [16, 17].

MOFs can be designed into specific geometrical micro/nano structures (one dimension, two dimensions and three dimensions) to be partially eliminated. These morphological strategies give new functions and properties to traditional MOF materials. For example, compared with bulk MOF counterparts, ultrathin size MOF nanosheets have great conductivity and stability in electrocatalysis. Mass transfer limitations are weakened by increasing the texture porosity and exposed specific surface area.

The economic development and increasing prosperity of the last few decades have been supported by increasingly large energy consumption that has led to the sacrifice of natural environment because of the blind exploitation and abuse of fossil energy. It will be difficult for mankind to deal with the consequence of the further deterioration of the environment in the future, and hence, the exploration and development of renewable energy sources are especially important. Progress has also been made in the past few decades by exploiting renewable energy sources such as solar, tide and wind. However, in most cases, due to their intermittent characteristics, it is difficult for these energy source to consistently provide sufficient power as needed. As a result, it is necessary to either develop some more controllable and flexible energy forms or more efficient energy storage technology [18].

MOFs as a well-established class of crystalline porous materials, constructed from metal ions or clusters, which are interconnected by organic ligand molecules based on a modular principle and form 3D frameworks with various topologies. This results in the formation of the precisely defined pore system, which differentiate MOFs from less ordered activated carbons, porous metal oxides and silica's. Well-defined crystal structure of MOFs opens unique functionalization possibilities, which in turns further

expand their application potential ranging from catalysis, capture of the greenhouse gases and even fabrication of electronic devices etc. Among the broad application field for MOFs, energy-related applications are connected with energy storage and transformation. The use of redox-active metals provides improved charge transfer between the ligand and metal nodes and therefore makes them prospective as active materials for electrochemical energy applications.

Recently, due to the high specific surface area, controllable morphology, abundant pores and versatility, MOFs have become a research hotspot in the field of electrochemistry. The growing number of publications on energy-related applications of MOFs in the recent 2 years indicates a great progress in this field. For example, through a review of previous studies, some researchers have outlined various synthesis methods for MOFs and synthesized various morphologies of nanomaterials with MOFs as precursors, such as nanosheets, nanoparticles, nanospheres, nanorods, and so on.

Among the various applications of MOFs, the electrochemical sensor based on MOF is a potential application. In recent years, several researchers have outlined MOFs and their derivatives applications in the field of sensors. In recent years, with the development of nanotechnology and nanoscience, important progress has been made in the application of nanostructured MOFs in electrochemical sensors. MOFs are endowed with electrochemical sensing capabilities through the introduction of redox and catalytic active sites using active metal ions and/or ligands Therefore, MOFs have made outstanding achievements in the latest progress of electrochemical sensing detection of H_2O_2, glucose, heavy metal ions, etc. ZIF-67 crystallites with porous {1 10} plane were synthesized through a simple and rapid method by Zhao and co-workers, and weres used for the determination of glutathione (GSH) [19]. The prepared ZIF-67-modified electrode can significantly increase the GSH signal during testing. Additionally, Co-MOFs can also be used for the high efficiency H_2O_2 sensors as the active substance. The modified electrode has the advantages of low detection limit, wide linear range and high sensitivity for the detection of H_2O_2 [20].

At present, the study of pure MOFs in electrochemical sensors has not made historical progress, so people try to study some MOF composites to improve the performance of H_2O_2 and glucose sensitivity. A non-enzyme sensor used a unique flower-like solvothermal reduction graphene oxide (SGO)@HKUST-1 as a substrate for the detection of H_2O_2 was designed by Wang and co-workers. As an effective structural guiding agent, all the octahedral HKUST-1 particles changed into layered flowers SGO@HKUST-1 when the addition amount of GO reached 0.13 mg mL^{-1}. The synergistic effect between SGO and HKUST-1 improves the electrochemical properties of the composites [21].

In addition to decarbonizing our energy, the world energy needs can be met sustainably through energy efficiency and conservation [22]. By introducing abundant renewable energy sources, such as solar, wind and hydropower, these needs can be met without damaging the environment, diversifying the global energy mix. By converting and storing renewable energy sources in chemical bonds, the intermittent nature of renewable energy sources can be reduced and dependence on traditional fossil fuels in the transport and industrial sectors reduced. The stored energy can

be converted into electricity, used as feedstock for the production of high-value industrial-related chemicals, or used directly for the transportation sector as liquid fuel. The splitting of water into O_2 and H_2 is an attractive strategy for the sustainable production of H_2, which has received significant attention as an energy carrier that can be utilized in fuel cell technology to convert chemical energy into electrical energy [23]. The design and implementation of catalysts to facilitate these transformations is necessary for reducing the activation barrier for the energy conversions of interest.

In recent years, MOF-based materials (original MOFs, MOF composite materials and MOF-derived materials) have attracted extensive attention in the terms of energy storage and conversion [24, 25].

Compared with conventional rechargeable batteries, supercapacitors have attracted more and more attention because of their higher power density, faster charge and discharge rates and longer cycling life. Compared with the porosity of conventional MOFs, which is often associated with poor electrical conductivity and structural stability, the high porosity of MOFs and MOF composites makes the composites have great potential in the field of supercapacitors, especially in the field of electrochemical double layer capacitors (EDLCs) [26]. Since the activated carbon widely used at present can only provide limited theoretical capacitance for EDLCs, it is of great significance to overcome these inherent shortcomings and make full use of the high specific surface area of the original MOFs in the electrochemical process. A composite composed of 10% reduced graphene oxide (rGO) and HKUST-1 was synthesized by Sawangphruk and co-workers to enhance the electrical conductivity of pure HKUST-1. In addition, the introduction of rGO contributes to the distribution of micropores and mesopores with an average pore size of 8.2 nm, which is conducive to the absorption and release of ions from the electrolyte. When tested in three-electrode confguration with 0.5 M Na_2SO_4 as electrolyte, the resulting composite exhibited a desirable specifc capacitance of 385 F g^{-1}, whereas the pure HKUST-1 without rGO stored very limited charges. CNT is another carbon material used to improve the conductivity of the MOF composites [27]. Lin and co-workers synthesized a composite material of CNTs and Mn-MOF ($Mn(C_2H_4O_2)_2(H_2O)_4$). The addition of CNTs increased the capacitance of Mn-MOF/CNT composites from 43.2 F g^{-1} of pure Mn-MOF to 203.1 F g^{-1} of Mn-MOF/CNT composites in 1 M Na_2SO_4 [28].

MOFs can also be used as an effective active material and substrate for supercapacitor composites. For example, Chen et al. have successfully prepared a double-layer composite material (NiHCF@MnO_2) composed of a MOF structure (NiHCF) and MnO_2 as the electrode material for supercapacitors [29]. The CV and galvanostatic charging-discharge curves of the composite show that the specific capacitance of NiHCF@MnO_2 composite is larger than that of NiHCF and MnO_2 alone due to the synergistic effect of NiHCF and MnO_2. The capacitance of this composite from three-electrode test can reach 224 F g^{-1} at 50 mV s^{-1} in 0.5 M Na_2SO_4, much higher than those of individual NiHCF (177.5 F g^{-1}) and MnO_2 (172 F g^{-1}).

Because of the limited resources of fossil fuels on one hand, and constantly increasing energy demand on another hand, fuel cells could be a reasonable alternative for environmentally unfriendly internal combustion engines. Additionally,

many researchers have summarized the latest research on the applications of nanostructured MOFs and MOF-derived materials in batteries. Recently, new types of rechargeable batteries have been introduced, such as lithiumsulfur (Li–S) batteries, lithium-ion batteries (LIBs), sodium-ion batteries (SIBs) and metal–air batteries, which are emerging as promising candidates for post-lithium-ion batteries [7, 30–33]. LIBs have become popular power supplies, not only for various portable electronic devices, but also for EVs, due to their unique advantages, such as high energy and high power density, environmental benignity, long lifetime, and no memory effects. Apart from the direct use of pristine MOFs as electrode materials for LIBs, a large number of MOF-derived nanostructures with desirable electrochemical properties have been designed and synthesized by using various MOFs as sacrificial templates. Xu et al. first encapsulated sulfur in the porous carbon nanoplates obtained by one-step pyrolysis of MOF-5. The obtained C–S composite cathode displayed good cycling performance and a high specific capacity of 730 mAh g^{-1} after 50 cycles charge/discharge at a current density of 837.5 mA g^{-1} [34]. Later on, Wu et al. reported ZIF-8 derived microporous carbon polyhedrons as carbon host to form C–S composites. Well-prepared carbonic polyhedrons that have sufficient and unvarying micropores were later on used as carbon host for preparation of carbon/sulfur mixtures [35]. Their research showed that the temperature for sulfur loading, sulfur content and the electrolyte affected the performance of Li–S batteries.

Recently, SIBs have gained great attention as a promising alternative to LIBs due to the abundance of sodium, low cost, and appropriate redox potential. Nevertheless, as compared to lithium, insertion/extraction of sodium ions lead to much larger volume change in the electrode due to its larger ionic radius. Therefore, exploring high-performance electrode materials is of great importance for the advancement of SIBs [36, 37].

MOFs as versatile precursors to produce various porous nanomaterials, including porous carbons, metal oxides, metal sulfides, metal phosphides, and metal carbides, as well as new multifunctional hybrid materials. Fang et al. reported 2D bimetallic oxide (Co_3O_4/ZnO) nanosheets using bimetallic MOF as the precursor. The Co_3O_4/ZnO hybrid nanosheets with rich oxygen vacancies have abundant porosity and high surface areas. When used as anode of SIBs, the Co_3O_4/ZnO hybrid nanosheets exhibited high rate capability with a specific capacity of 242 mAh g^{-1} at a current density as high as 2000 mA g^{-1}. In addition, it delivered a capacity retention of 91% after 1000 cycles charge/discharge [38]. The enhanced performance is believed to be due to its 2D structure and synergistic effect of the hybrid materials.

Developing advanced electrode materials is of great importance for next-generation rechargeable batteries. Recently, MOFs have been utilized as precursors or sacrificial templates to prepare various nanostructured materials, such as porous carbon, metal oxides, other metal compounds and their composites. MOF-derived materials have large surface area, narrow distributed pore size, abundant porosity and designable structures, which made them potential candidates as the electrode of high-performance post-lithium-ion batteries.

1.2 1D MOFs

In consideration of the unique anisotropic characteristics of 1D nanostructures, the fabrication of 1D MOF nanomaterials for specific applications has greatly increased. By selecting organic ligands and inorganic metal ions, 1D nanoscaled MOF materials with attractive properties and customizable configurations can be realized, such as nanowires [39], nanorods [40, 41] and nanofibers [42, 43]. So far, the most common method to fabricate these structures is the self-assembly of organic ligands and inorganic metal ions through a one-pot approach. However, it is more challenging to produce micro/nanoscaled 1D MOFs with controllable morphology and structure compared with 0D nanoparticles.

1.2.1 Template Strategy

Among all nanostructured materials, nanotubes are particularly attractive because these fascinating tubular nanostructures offer access to three different contact regions, namely inner, outer surfaces and both ends [44, 45]. Therefore, unique properties for applications in adsorption, catalysis, sensing, and nanodevices are presented. Although various technologies have been used to make a variety of nanotubes from different kinds of materials, the strategies for designing MOF nanotubes (MOFNTs) remain largely unexplored. In 2012, Qiu and co-workers reported a rational self-sacrificing template strategy to obtain tubular nanostructures by combining the advantages of ultrasonic synthesis and vapor diffusion technique [46]. The cadmium ion and benzene-1,3,5-tricarboxylate (btc^{3-}) were chosen as the metal connector and the bridging ligand to illustrate such a self-sacrificing template strategy. Ultrasound irradiation was employed as an energy source, because it not only facilitates the structural transformation of MOFs and shortens the reaction time, but also accelerates dissolution of the initially formed thermodynamically unstable nanorod template. Using triethylamine (TEA) as a deprotonation agent, MOF nanorod templates for forming MOF nanotubes (MOFNTs) were firstly synthetized by ultrasonic and vapor-phase diffusion technique, as shown in Fig. 1.1a. After removing the excess TEA, continuous ultrasonic irradiation caused the dissolution of the initial MOF nanorods and the formation of a new MOF phase, thus resulting in the formation of MOFNTs. The scanning electron microscopy (SEM) images showed that an initial rodlike product was formed at 5 min under ultrasonic conditions in the presence of TEA vapor. A large number of MOFNTs with inner diameters of 50–150 nm and outer diameters of 100–300 nm were obtained at 20 min after removing the small vial containing TEA. The ultrasonic irradiation effect and removal of TEA are the reasons that cause the initial nanorods to grow into the final nanotubes. The removal of TEA prevented continued growth of the kinetic phase. The ultrasonic treatment caused an equilibration to generate the more thermodynamically stable phase as a tubular coating, as well as simultaneous dissolving of unstable nanorod templates. Figure 1.1b showed the

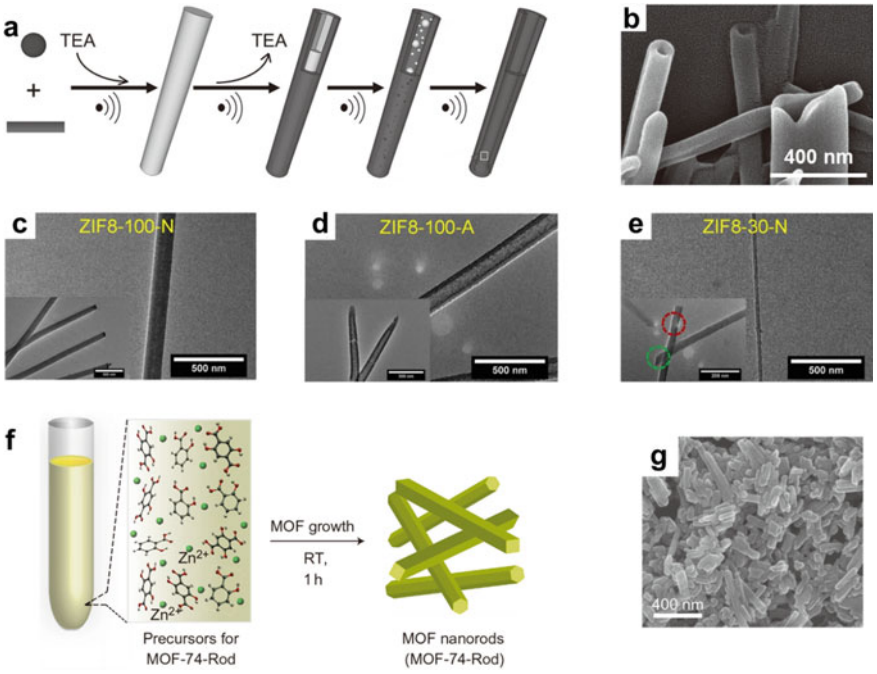

Fig. 1.1 **a** Illustration of the fabrication process of MOFNTs by the self-sacrificing template strategy. **b** Close-up SEM image of open-ended MOFNTs. Transmission electron microscopy (TEM) images of ZIF8-100-N (**c**), ZIF8-100-A (**d**), and ZIF8-30-N (**e**). **f** Scheme of synthesis of MOF-74-Rod. **g** SEM images of MOF-74-Rod showing the formation of uniform rod-shaped MOFs. **a** and **b** Adapted with permission [46]. Copyright 2012, WILEY–VCH. **c–e** Adapted with permission [47]. Copyright 2018, WILEY–VCH. **f** and **g** Adapted with permission [48]. Copyright 2016, Nature Publishing Group

unprecedented success of this synthesis. The growth mechanism of MOFNTs helps us understand the crystal growth and self-assembly process of nanostructured MOF materials. By selecting suitable metal ions, organic ligands and deprotonation agents, this simple strategy can also be extended to the synthesis of other novel MOF-based nanostructures, such as hollow MOF spheres and MOF core–shell structures.

In subsequent research, Qin et al. discovered controlled growth mechanisms of 1D MOF nanotubes (Fig. 1.1c), nanorods (Fig. 1.1d), and nanowires (Fig. 1.1e) under size-confinement and surface directing effects [47]. Through employing interfacial synthesis templated by tracketched polycarbonate (PCTE) membranes, zeolitic imidazolate framework-8 (ZIF-8) 1D nano- and super-structures can be tailored by changing the size of template pores and type/concentration of reactants, resulting in different morphologies. In order to impart hydrophilicity, the pore walls of PCTE membranes are coated with a thin layer of poly(N-vinylpyrrolidinone) (PVP). During the initially interfacial synthesis, PVP acted as anchors for the initially formed ZIF-8 seed crystals that induce further growth from the pore wall inward, gradually forming

hollow tubes and solid rods. It was found that polycrystalline ZIF-8 solid nanorods and hollow nanotubes were formed within 100 nm membrane pores, while single crystalline ZIF-8 nanowires grew inside 30 nm pores. The Brunauer – Emmett–Teller (BET) surface area existed discrepancies, which may be caused by the difference in ZIF-8 crystal quality. ZIF8-100-A possesses the worst crystal quality since the growth of nanotubes is stopped at early stage. ZIF8-30-N was displayed to be single crystalline and thus showed the highest porosity, while the polycrystalline ZIF8-100-N sample fall somewhere in between. Result demonstrated the MOF nanostructure can be controllably incorporated into the porous polymer templates, so that the composite membranes possessed assessible nanopore surfaces, thereby rendering them potentially useful in gas/liquid separation applications. Although the template strategy is prone to control the morphology of the MOFs, the length and diameter of the products are restrained by the pore shape and template thickness, so it is not suitable for manufacturing large-length MOFs. This discovery provides a general method for controlling size, morphology, and lattice orientation of MOF nanomaterials.

1.2.2 Modulation Method

Modulation method can effectively control the morphologies/sizes and functionalities of MOFs by using modulators. The modulators can not only control the kinetics of various processes such as nucleation, but also induce the growth process of MOF crystals along a specific direction, thereby forming MOFs with distinct morphologies and sizes. Kitagawa et al. developed a strategy to modulate the coordination equilibria simply by adding capping reagents with the same chemical functionality as the linkers [41]. The rate of framework extension and crystal growth is regulated by impeding the coordination interaction between the metal ions and the organic linkers. The $[\{Cu_2(ndc)_2(dabco)\}_n]$ (ndc = 1,4-naphthalene dicarboxylate; dabco = 1,4-diazabicyclo[2.2.2]octane) with tetragonal crystal system was selected to investigate the crystal growth mechanisms of porous coordination polymers (PCPs). Its anisotropic framework characteristics were dominated by two coordination modes (ndc-copper and dabco-copper). By adding monocarboxylic acid as a modulator, one coordination mode (ndc-copper) can be selectively adjusted. The modulator can also physically prevent crystal aggregation, thereby leading to anisotropic growth. In this research, acetic acid was used to directly influence the coordination equilibria. The increase in the concentration of acetic acid significantly reduced the growth rate of crystals, and promoted the formation of high aspect ratio nanorods by inhibiting the growth in the [99] direction. The presence of acetic acid as a modulator hindered the ndc-copper interaction that forms the two-dimensional layer because both ndc and acetate had the same carboxylate functionality. The selective coordination modulation method enhanced the relative crystal growth in the [001] direction. In addition, the correlation between the adsorption properties and crystallinity of the nanorods suggested that the coordination modulation method can produce nanorods with high porosity and high crystallinity, which was equivalent

to bulk crystals synthesized by conventional solvothermal methods. As a result, it is proved that coordination modulation method can control the crystal growth of nanosized PCP crystals [$\{Cu_2(ndc)_2(dabco)\}_n$]. In another report, a self-templated and catalyst-free strategy for the fabrication of 1D carbon nanorods by morphology-maintained thermal transformation of rod-shaped MOFs was presented [48]. By selecting salicylic acid as a modulator, the room-temperature reaction of zinc acetate and 2,5-dihydroxyterephthalic acid formed rod-shaped MOF-74 with a width of 30–60 nm and a length of 200–500 nm, as shown in Fig. 1.1 g. The corresponding synthesis process of MOF-74-Rod is shown in Fig. 1.1f. The addition of the salicylic acid modulator stabilizes the active metal sites on the surface of the MOF crystal, resulting in MOF growth in a rod-shaped morphology. In addition, non-hollow 1D carbon nanorods with moderate aspect ratio was achieved by thermal transformation of MOF-74. This approach is readily scalable and can be employed to generate carbon nanorods and graphene nanoribbons on industrial levels.

1.2.3 Recrystallization Process

The kinetic control of crystallization has a significant impact on the crystal morphology and crystallinity, and the low reaction rate is conducive to the formation of anisotropic nanostructures and single crystals. The kinetics of crystallization can be controlled by using different precursors with different solubility in specific solvents. Xu and co-workers reported the fabrication of the first single-crystal MOF nanotubes [49]. They successfully synthesized superlong single-crystal Co-MOF nanotubes with a diameter of $\sim$70 nm and length of $20 - 35$ μm via an amorphous MOF-mediated recrystallization approach. The reaction of cobalt acetate tetrahydrate and 2,5-dihydroxyterephthalic acid at room temperature first given amorphous MOF-74 nanoparticles, which then recrystallized into superlong single-crystal Co-MOF nanotubes in water at 175 °C. The growth process of these nanotubes was analyzed by changing the solvent, acidity/basicity, reaction time, and temperature. Results indicated the water solvent was beneficial to the formation of the 1D anisotropic nanostructure of Co-MOF-74. Moreover, both the length and the crystallinity of Co-MOF-74 nanotubes increased with the concentration of water in the reaction solvent. By studying the pH values of the original mixture solution, the superlong Co-MOF-74 nanotubes were obtained at a pH value ranging from 6 to 10. MOF rods were achieved at pH $\leq$ 5 and pH = 11. At the reaction time of 12 h, uniform MOF nanotubes can be synthesized above 150 °C, whereas only gel-like products were obtained at 100 °C. The synthesized uniform and monodisperse morphology of MOF nanotubes can be employed as a nanocolumn for separating large molecules. In addition, the MOF nanotubes were excellent precursors for synthesizing 1D carbon nano-fibers. In an argon atmosphere, carbonization of the Co-MOF nanotubes maintained the 1D morphology, providing long carbon nano-fibers. Using dicyandiamide as a nitrogen and a secondary carbon source, a hierarchical architecture composed of carbon nanofibers wrapped by carbon nanotubes with cobalt nano-particles on the

top was formed. The resulting hierarchical dendrites with carbon nanofiber trunks and carbon nanotube branches not only have excellent electrocatalytic activity for oxygen reduction reaction, but also have special applications in rechargeable Zn-air batteries. In general, this work demonstrates a new strategy to fabricate MOF nanotubes and related 1D nanostructures.

1.2.4 Microemulsion Strategy

The microemulsion strategy is also an effective way to regulate the growth of MOF in a specific direction. Lin et al. developed a general reverse microemulsion-based methodology for the fabrication of uniform MOF nanorods ($Gd(BDC)_{1.5}(H_2O)_2$, BDC = 1,4-benzenedicarboxylate) with a length of 100–125 nm and diameter of 40 nm in a water-in-oil microemulsion system [40]. In addition, the morphologies and sizes of the nanorods were influenced by the water/surfactant molar ratio of the microemulsion systems. In order to explore the generality of nanoscale MOF synthesis in reverse microemulsions, they also carried out the reactions of $GdCl_3$ and 1,2,4-BTC (tri-(methylammonium)benzene-1,2,4-tricarboxylate). As a result, irregularly shaped and crystalline nanoplates of $[Gd(1,2,4\text{-BTC})(H_2O)_3]\cdot H_2O$ with a diameter of ~100 nm and an average thickness of 35 nm were successfully synthesized in a water/surfactant molar ratio of 15. Luminescent nanorods were successfully synthesized by using Eu^{3+} or Tb^{3+} dopants. The ethanol dispersions of these doped nanorods were highly luminescent under ultraviolet excitation with characteristic red and green luminescence from Eu^{3+} and Tb^{3+}, respectively. These results suggest that nanoscale MOFs can be used as potential contrast agents for multimodal imaging.

1.2.5 Lab-On-A-Chip Approach

Microfluidic synthesis is another charming method to synthesize nanomaterials with controllable morphology and size. Compared with traditional methods, excellent and unique properties appear when shrinking dimensions inside a microreactor. The presence of laminar flow makes microfluidic technologies ideal synthetic and assembly tools. Under laminar flow conditions, a stable interface can be established between two reactive streams, while mixing happens only by diffusion. The reaction time can be adjusted by changing the flow rate. Maspoch and co-workers reported the first case of coordination polymer nanofibers assembled using microfluidic technologies [42]. Unlike common synthetic procedures, this approach enabled parallel synthesis and facilitated the formation of 1D coordination polymer assemblies at the nanometer length scale. They demonstrated that microfluidic synthesis can control the assembly of metal ions and organic building blocks, thus resulting in the formation of 1D coordination polymer nanostructures. Two aqueous solutions were first added in the

microfluidic platform that has four input channels through a syringe pump system to synthesize Cu(II)-Asp (amino acid aspartate) nanofibers. As a result, the formation of bundles of well-aligned nanofibers with diameters ranging from 50 to 200 nm can be found. Furthermore, this synthesis strategy can be extended to design other 1D nanostructures, such as Ag(I)-Cys (cysteine) nanofibers and Zn(II)-4,4'-bipyridine nanofibers with rather a uniform diameter below 100 nm.

1.2.6 Hydrothermal/Solvothermal Method

In addition to the above mentioned, hydrothermal/solvothermal synthesis are also widely used to synthesize 1D MOFs. The synthesis of 1D MOFs (HKUST-1 nanobelts) from Cu nanowires (ligand-free) was achieved by a traditional hydrothermal method [50]. During the transformation process of HKUST-1 nanobelts, the Cu nanowires act as a copper source and template. The molar ratio of Cu nanowires/H_3BTC (H_3BTC = 1,3,5-Benzenetricarboxylic acid) and the reaction time play important roles in the morphology of the final products. When the molar ratio of Cu/H_3BTC reached 1:40, only nanobelts can be found in the final products. When the reaction time was 2 h, the thin layer of HKUST-1 appeared on the copper nanowire. With the prolonging of hydrothermal reaction, the HKUST-1 layer on the surface of copper nanowires became thicker and the crystallinity got better. Finally, the Cu nanowires were completely transformed into nanobelts at 20 h. This work provides a strategy for the future design and synthesis 1D MOF.

1.2.7 Ultrasonic-Assisted Synthesis

A sonochemical method was used to synthesize nano-rods of a novel cadmium(II) metal–organic coordination polymer, $[Cd(p\text{-}2yeinh)(NO_2)]_n$ (1) (p-2yeinh = pyridin-2-yl ethylidene-isonicotinohydrazide) [51]. The thickness of sheets metal–organic coordination polymer has changed 27–45 nm upon increasing the sonication time. Thinner rods with the thickness ranging from 25 to 50 nm were achieved at lower concentrations. At the ultrasonic power of 36 W, rods of uniform morphology with thickness of 53–55 nm were obtained. The results of sonochemical methods indicated that lower concentrations of reagents caused particle size reduction. In addition, increasing the power of ultrasound irradiation resulted in a uniform rod-like morphology.

1.3 2D MOFs

Since the discovery of graphene stripping from graphite in 2004, two-dimensional (2D) nanomaterials have attracted extensive attention [52]. 2D nanomaterials are characterized by 2D planar structures with atomic or molecular thickness, especially ultra-thin 2D nanomaterials whose carriers can move freely on two dimensions of non-nanoscale (2D plane). This endows them high carrier mobility, gives them excellent electrical conductivity, and makes them favorable materials for electrodes and semiconductor devices [53]. The synthesis of 2D MOF nanosheets still remains a great challenge, because the growth of MOF crystals should be suppressed to the nanometer scale only along the vertical direction without affecting the other two lateral directions. Preparation of ultrathin 2D MOFs with desired features, such as composition, size, thickness, crystal phase, defect, and surface property are of particular importance, which enables further investigation of their physical, chemical, electronic, and optical properties, as well as exploration of various potential applications [54]. Many approach have been developed for the synthesis of 2D MOF nanosheets, such as sonication exfoliation, mechanical exfoliation, Li-intercalation exfoliation, chemical exfoliation, interfacial synthesis, three-layer synthesis, surfactant-assisted synthesis, modulated synthesis, and sonication synthesis. These methods can be classified into two crucial strategies, bottom-up and top-down approaches. The top-down approach is achieved by the exfoliation of bulk MOFs, which includes mechanical or chemical exfoliation and so on [55]. The bottom-up method generally focuses on interfacial synthesis and modulated synthesis. A significant merit of the bottom-up synthesis is that the structures can be customized via the selection of components (metal ions and/or organic ligand molecules). Therefore, the bottom-up method may broaden the diversity and utility of 2D nanosheets. Figure 1.2 shows typical methods to develop the preparation of 2D MOFs in the past decade. Generally, these methods

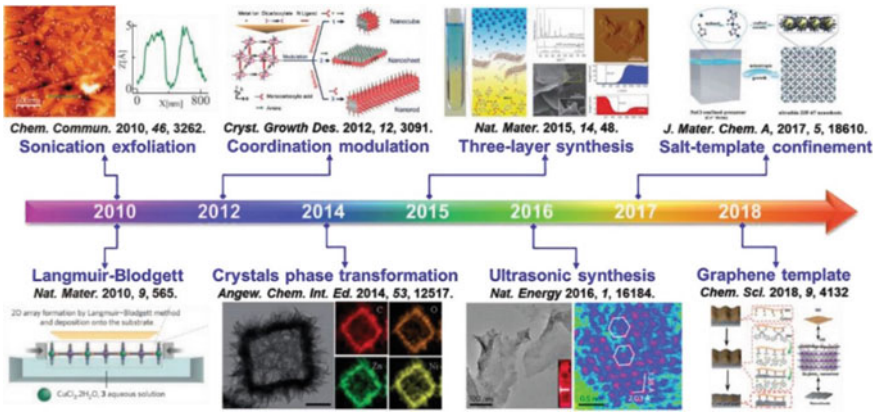

Fig. 1.2 Timeline of important breakthroughs in the synthesis of 2D MOF nanosheets [56]

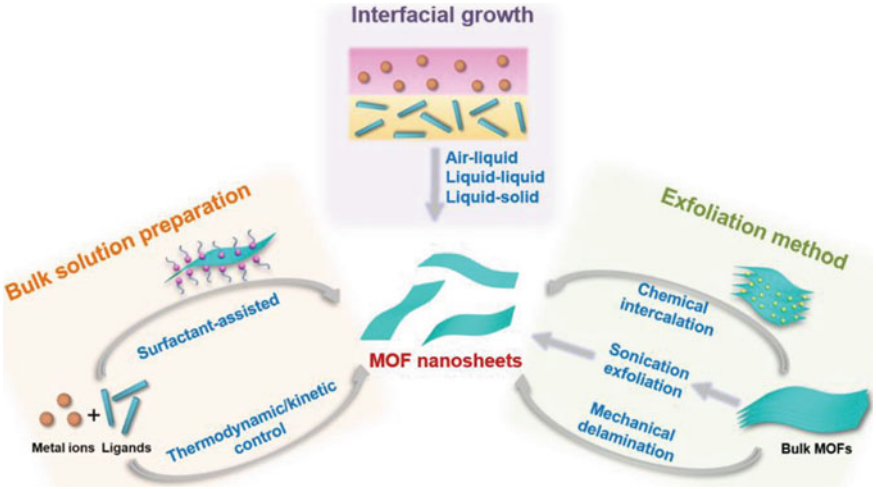

Fig. 1.3 Schematic illustration of the three typical preparation strategies for 2D MOFs [56]

can be classified into exfoliation, bulk solution preparation, and interfacial grow approach. The synthetic procedures for these methods are schematically illustrated in Fig. 1.3.

1.3.1 Exfoliation Process

Layered bulk 2D MOF crystals are constructed by stacking each layer along the vertical direction via weak interactions, such as van der Waals forces and/or hydrogen bonding. Layered bulk MOF crystals is able to be exfoliated into ultrathin 2D MOF nanosheets when proper mechanical forces are applied. The exfoliation strategy, such as solvent-induced delamination synthesis and ultrasonic exfoliation, is another approach for fabricating 2D MOF nanostructures, and is considered as a top-down synthesis strategy [57]. In this method, layered bulk MOFs are first synthesized by a general method, and are then transformed into single-layered or few-layered MOF nanosheets by a physical or chemical exfoliation process.

As ultrasonic exfoliation is a common method to obtain micro/nanosized materials, it is a favorable choice to exfoliate bulk MOFs by the ultrasound-assisted strategy. In 2008, Nielsen et al. [58] first reported the delamination of $Zn(C_{12}H_{14}O_4)$ MOF in acetone and ethanol. The compound is a metal organic layered structure where each of the layers is constructed on a basis of infinite chains of tetrahedrally coordinated Zn atoms. The Zn chain atoms are solely bound together by carboxylate groups. The crystallographic analysis proved the weak van der Waals bonding between the layers of this metal–organic compound. After ultrasonication of $Zn(C_{12}H_{14}O_4)$ MOF for 3 h at room temperature along with evaporation

of acetone, delaminated single layers were observed. The thickness of particles is 2 nm, corresponding to two layers. This subsequently provide interesting opportunities to restack ordered layered hybrid composites. Later on, Amo-Ochoa et al. [59] reported weakening of the interlayer interactions within $[Cu_2Br(IN)_2]_n$ (IN = isonicotinato) to produce 2D nanosheets by a similar sonication process. To prepare 2D $[Cu_2Br(IN)_2]_n$ nanosheets, sonication was applied to overcome the interlayer π–π interaction. The bulk $[Cu_2Br(IN)_2]_n$ MOF was successfully exfoliated and dispersed by probe sonication for 30 min. Atomic Force Microscopy (AFM) topography image showed a homogenous distribution of nanosheets with thickness of 5 ± 0.5 Å, which is in agreement with the thickness of single-layer $[Cu_2Br(IN)_2]_n$. Foster et al. [59] designed a layered MOF with bulky 3-methoxypropoxy groups to make it easy to exfoliate and disperse in divers solvents. As expected, the 3-methoxypropoxy group-functionalized MOF could be easily exfoliated in many solvents, including water, N,N-dimethylformamide (DMF), acetonitrile, ethanol and acetone. In Gallego's work, layered MOF material have been fully exfoliated just by solvent-assisted interaction [59]. Since the solvent-assisted procedure is very soft in terms of energy, this method avoids the potential complications of exfoliation of sheets from laminar crystals or isolation of sheets from solid substrates.

In general, it is an easy and feasible way to obtain 2D MOF nanosheets via exfoliation of layered bulk MOFs with assistance of external force. Morphological distortion and structural destruction occur in this process, which hinder the preparation of high quality MOF nanosheets. In addition, the thickness of the MOF nanosheets is difficult to control due to the lack of precise adjustment of the applied force intensity and the restacking of the obtained MOF nanosheets. In addition, the exfoliation method is merely applicable to layered MOFs with weak interaction between layers, and its scalability is limited. In order to satisfy the application of exfoliation method in actual industrial production, it is necessary to consider the above problems and formulate feasible solutions.

1.3.2 Bulk Solution Preparation

Compared to exfoliation methods which generally have low yield and may cause morphological/structural destruction. Direct synthesis of 2D MOFs in bulk solution is relatively effective in regulating the size and thickness of 2D nanosheets. The key issue for this method is to selectively control the growth direction of the MOF crystals, i.e., to restrict the growth in the vertical direction. To realize this, diverse techniques are utilized to control the growth of MOF crystals.

Surfactant molecules, which are important in controlling the nucleation and growth process of MOF crystals, are widely utilize in material synthesis. During the growth process, the surfactant selectively attaches to the MOF surface, resulting in the formation of ultrathin MOF nano-sheets and anisotropic growth of the MOF. This strategy has been also used for the preparation of MOF nanosheets. Zhao et al.

[60] synthesized a series of tetrakis(4-carboxyphenyl)porphyrin (TCPP) based ultrathin 2D MOFs through a surfactant-assisted method, such as Zn-TCPP, Cu-TCPP and Cd-TCPP nanosheets. In each layer of bulk Zn-TCPP, one $Zn_2(COO)_4$ paddlewheel metal node is coordinated with four TCPP ligands. The introduced surfactant of polyvinyl pyrrolidone (PVP) restricted the growth of Zn-TCPP along the specific direction, leading to the formation of ultrathin Zn-TCPP nanosheets with thickness of sub-10 nm. Other surfactants, such as sodium lauryl sulfate and cetyltrimethyl ammonium bromide (CTAB) have also been demonstrated effective to the synthesis of MOF nanosheets [61]. In Zhao's work, ultra-thin Zn(bim)(OAc) nanosheets with a thickness of 1.0–6.5 nm were synthesized by using gluconate salts as modulators with a high yields of 65% [62]. In addition to surfactants, small capping molecules (e.g., acetic acid, pyridine) have also been used for the preparation of MOF nanosheets. Lin et al. used the functional group of formate as modulators to reduce the surface energy of the crystal without blocking the active site and generate 2D MOF nanosheets [56].

Using surfactants or small molecule modulators for the synthesis of 2D MOFs may block part of the active sites. So, the synthetic methods without adding other molecules to obtain anisotropic growth of MOF nanosheets have received widely attentions, such as the means of kinetic and/or thermodynamic control of the growth process, or by the utilize of properly designed ligands and secondary building units, it tends to preferentially grow to a 2D structure. The direct synthesis of 2D MOF nanosheets in bulk solution is capable of overcoming the insufficient of the exfoliation method mentioned in Sect. 2.2.1, which produces high-quality MOF nanosheets with tunable thickness. Nevertheless, the synthesis of 2D MOF nanosheets in bulk solution usually utilizes surfactants or modulators to confine the growth of MOF crystals in a certain direction. This inevitably blocks part of active sites of MOFs. Therefore, it is desirable to develop a suitable synthetic method which effectively controls the growth direction of crystal without using surfactant/modulator.

1.3.3 Interfacial Growth Approach

Interfacial synthesis is one of the most widely used bottom-up methods for the synthesis of 2D MOF nanosheets. In this method, the reaction takes place at the solvent interface, ensuring favorable control of the MOF nucleation and growth. Depending on the diffusion-mediated process, the MOFs only grow in the confined 2D interface region, leading to the formation of 2D nanosheets. Especially, the liquid/air interfacial synthesis utilizes the well-dispersed monolayer of organic ligands on the liquid surface to control the thickness of the MOF nanosheets [63]. This method has been widely used in the preparation of MOF nanomaterials [64, 65]. The synthesis of single-layer and few-layer nickel bis(dithiolene) nanosheets through the coordination reaction between nickel(II) acetate and benzenehexathiol (BHT) at the liquid air interface was reported [64]. Nishihara et al. reported the fabrication of multilayer bis(dipyrrinato)zinc complex nanosheets [66]. The present work describes a bis(dipyrrinato)zinc complex nanosheet synthesized from a three-way

dipyrrin ligand and zinc(II) acetate. The spontaneous and reversible coordination of dipyrrin ligands with metal ions makes them suitable as building blocks for bottom-up nanosheets. A liquid/liquid interfacial synthesis between a three-way dipyrrin ligand and zinc(II) ions results in a multi-layer nanosheet, while an air/liquid interfacial reaction produces a single-layer or few-layer nanosheet with domain sizes of >10 μm on one side.

For interfacial synthesis, the yield of the resulting 2D MOF nanosheets is highly dependent on the area of the interface, limiting its utilization for the large-scale synthesis of 2D MOF nanosheets. Gascon et al. [67] obtained a three-layer synthesis strategy to prepare CuBDC (BDC = terephthalate) MOF nanosheets with a high yield. The synthesis medium consists of three liquid layers prepared by vertically aligning a mixture of acetonitrile and DMF in diverse ratios. The top layer contains more acetonitrile, while the bottom layer contains more DMF. The $Cu(NO_3)_2$ is dissolved into the top layer, and the BDC ligand is dissolved in the bottom layer. These two layers are separated by a middle layer containing an equal amount of DMF and acetonitrile. When Cu^{2+} and the BDC ligands slowly diffuse into the middle layer, the growth of the MOF nanosheets occurs. The nascent MOF nanosheets are naturally separated from the middle layer by sedimentation, which avoids over-growth, while new CuBDC 2D nanosheets are produced when fresh Cu^{2+} cations and BDC ligands continue to diffuse into the middle layer, resulting in a much higher yield production of MOF nanosheets.

1.3.4 Summary

The preparation strategies of 2D MOF nanosheets have been highlighted, such as sonication exfoliation, surfactant-assisted synthesis, interfacial synthesis and three-layer synthesis. The interfacial synthesis method is very promising in the preparation of single-and few-layer MOF nanosheets with large size, but the crystallinity of these MOF nanosheets is not high enough, as evidenced by the weak diffraction spots and XRD patterns. Despite all the recent achievements in this exciting research area, many challenges still remain in the high-yield synthesis of well-dispersed 2D MOF nanosheets. It is urgent to find other methods to develop for the synthesis of 2D MOF nanosheets based the aforementioned methods and the future directions lies in the synthesis of high-quality 2D MOF nanosheets with large size. Particularly, finding surfactants or other compounds with weak binding on the MOF nanosheets surface, which can be easily removed after the formation of MOF nanosheets, is very crucial in the synthesis of 2D MOF nanosheets.

1.4 Hierarchical MOFs

Metal–organic frameworks (MOFs) were originally known as a kind of simple extended coordination compound "Prussian Blue". Subsequently, Yaghi and colleagues reported a MOF-5 constructed from Zn_4O clusters and linear dicarboxylic acid linkers, which has permanent porosity [12, 68]. In addition, further exploration of MOF includes the construction of flexible MOFs (MIL-88), ultrastable MOFs (UiO-66), and ultraporous MOFs (MIL-101) [69–71]. Nowadays, more and more attention has been paid to the evolution of hierarchical MOFs with controllable structure and internal sequence and the heterarchical MOFs with enhanced diversity, because these MOF structures may simulate the sequence behavior and perform complex functions of organisms [72–74]. As shown in Fig. 1.4, building units are randomly distributed in the frame lattice in many heterarchical MOFs. However, in order controlled hierarchical MOF, these units are arranged in a specific order in the lattice, which has a great influence on the molecular and macroscopic properties of the framework materials [75–77].

The superstructure of MOF can establish a hierarchical system. For example, Kitagawa and coworkers have reported the mesoscopic architectures [79]. The primary structure of MOF (unit cell) is composed of organic linkers and inorganic clusters. MOF crystallites (secondary architectures), self-assembly of MOF crystallites (tertiary architectures), and quaternary architectures should be further explored [80]. However, the evolution of MOF materials is mainly concentrated in molecular

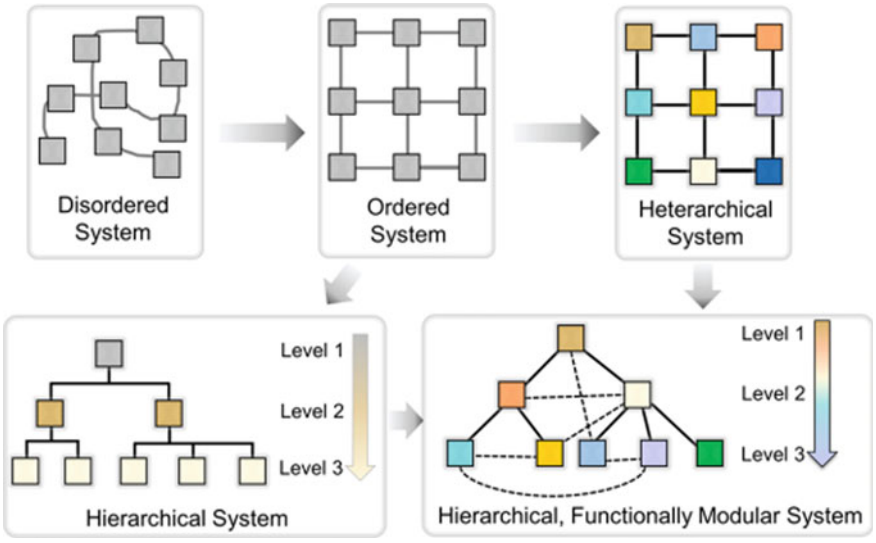

Fig. 1.4 The concepts of hierarchy and heterarchy are used in the design of materials. Reproduced with permission [79]. Copyright 2020, American Chemical Society

assembly. For instance, in order to construct a primary structure of MOF, the principles of coordination chemistry are used to guide the controllable synthesis. Moreover, the geometric structure and connectivity adjustability of organic binders and inorganic clusters have also been widely studied, which enhances the basic diversity and function of framework materials. The latest development of MOF focuses on the introduction of hierarchy into the synthesis tools of higher level MOF architecture (secondary MOF), such as controlled assembly, epitaxial growth, and labilization methods, resulting in MOF three-level architecture with exceptional characteristics and complexity. Unfortunately, in coordination chemistry, there are few discovers about artificial framework superstructures with four-level structure or more complex structure, and there are few synthetic guidelines to guide the study of these structures.

It is difficult to synchronize MOF molecular assembly with functional mesoscopic architectures construction. Therefore, it is very important to study the multi-scale control of MOF structure formation and propose a reasonable synthesis route of hierarchical MOFs or MOF composites. It is necessary to adjust these hierarchical structures on multiple scales to promote cooperative catalysis in MOFs, because it needs to optimize the selectivity of porous frameworks and the activity of catalytic centers [81–83]. The geometric and electronic properties of the active metal centers are the main factors affecting the catalytic activity, and the design principles are based on active effects in homogeneous systems [84–86]. At the same time, larger scale effect (pore window, crystal size and pore environment etc.) is beneficial to the selectivity of porous framework, all of which make the selected substrates can effectively diffuse to or from the active centers. Substrate partitioning and high activity centers are the breakthrough points for the development of the cooperative catalyst. As shown in Fig. 1.5, Porous hierarchy, architecture hierarchy and composition hierarchy are the three main hierarchies of MOFs.

The multi-scale pores (macroporosity, mesoporosity, and microporosity) in a framework are the performance of hierarchical pores in MOF [87–89]. These hierarchical pores can be assembled by components or synthesized by template etching. The hierarchical porous (HP) MOF structure has the advantages of changing the reaction pathway, easily adjusting the pore size, accessibility of active sites and enhancing the diffusion kinetics in the reaction process, which promotes the progress of the synthesis method of HP-MOFs. Modulated synthesis has been widely used in the crystallization of HP MOFs, where the modulators play a larger role. HP-MOF-5 was reported by Yaghi and co-workers in the early stage. They found sponge shaped MOF-5 crystals, which have macropores and mesopores throughout the crystal. Sponge MOF-5 and pomegranate MOF-5 can be prepared by adding 4-(dodecyloxy)benzoic acid (DBA) as a modulator while maintaining the microporosity of MOF-5. Here, the alkyl chain of DBA is used as template, while the carboxylic group can be combined with Zn clusters [90]. The precise control of MOF size and crystal morphology has been achieved well, but creating more complex structures in MOF crystal has become a research point. Complete crystals with specific morphology are the characteristics of most MOFs. Although their specific morphology can give aesthetic feeling intuitively, mass transfer and diffusion will be affected, which limits their application in gas separation, catalysis and so on. The HP structure with enhanced diffusion rate can

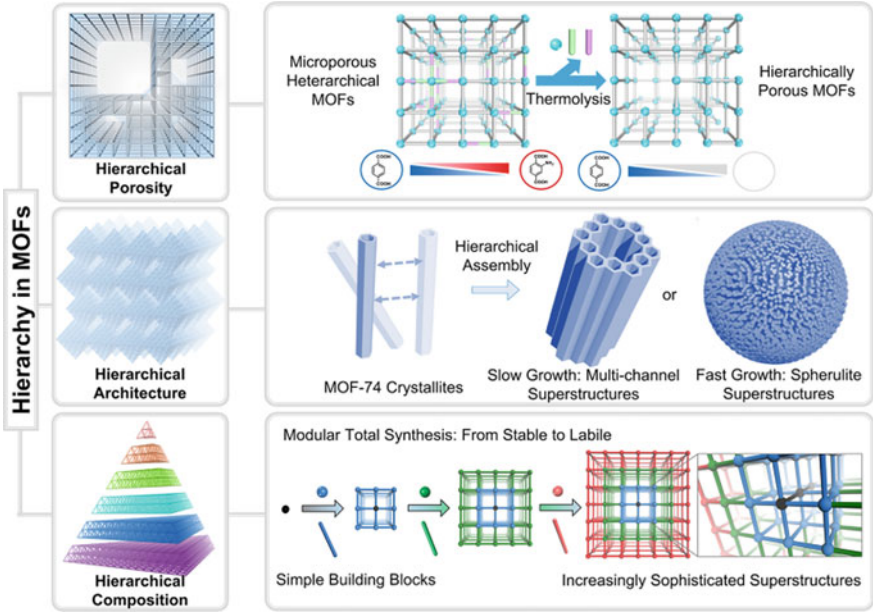

Fig. 1.5 Hierarchical MOFs from three different perspectives. Reproduced with permission [78]. Copyright 2020, American Chemical Society

be constructed by adding macropores or mesoporous into MOF crystals, which can be realized by template-free or template method. For example, Shen and coworkers achieved ZIF-8 with oriented and highly ordered macropores (Fig. 1.6). In this case, polystyrene (PS) nanospheres were mixed with ZIF-8 precursor and then crystallized in ammonia and methanol. The template PS nanospheres can then be removed and the ordered hierarchical structure of single-crystalline ZIF-8 is formed [89]. Moreover, HP-MOFs can be synthesized without templates. The assembly of MOF nanoparticles was controlled by adjusting the synthesis conditions. For example, Lyu et al. designed a 3D printing method to fabricate related MOF structures, in which Co-MOF crystals were mixed with Pluronic F127 and eventually printed into specific structures [91]. It is also a method to produce mesopores or macropores by post synthesis, which usually requires an etchant. Kim et al. found that mesoporous pores could be formed in a microporous MOF called post-66 (y) by using an etchant (water) [92].

It is an important method to assemble MOF crystal into layered superstructure to increase framework packing density and prepare multi-component structure. By adjusting the kinetics of nucleation and growth, MOF superstructures with different morphologies should be prepared, and then assemble superior layered structures as blocks [93–95]. Unique crystal structures can be produced by adjusting the crystallization conditions. These structures usually present adjustable pore sizes and chemical environments. The process of hierarchical assembly needs precise control of

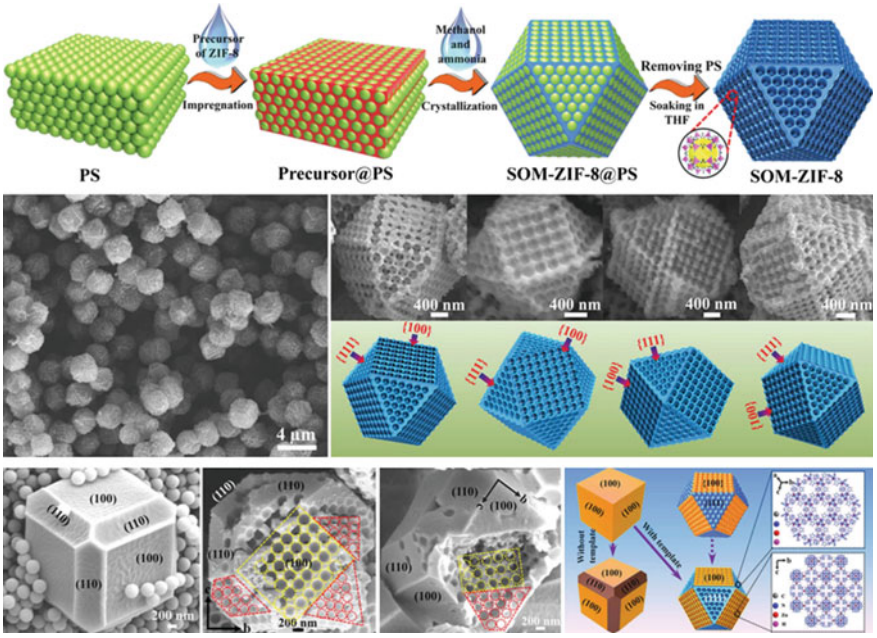

Fig. 1.6 PS templated approachs to prepare ordered macro-microporous single-crystalline ZIF-8. Reproduced with permission [89]. Copyright 2018, American Association for the Advancement of Science

MOF nucleation, directional growth and stability. Zhou's team found that in a simple one-pot synthesis process, as long as a suitable evolution temperature was found, a series of hollow tube crystals could be used to assemble the hierarchically porous tube structure with multiple channel sizes [96]. The directional assembly of a well-defined MOF-74 tube at 85 °C ensured an orderly arrangement of the MOF inherent micropores and macropores formed by the template. Through a correction and self-healing method, the interface between the adjacent tubes is melted to integrate a single MOF crystal into a unified superstructure [97]. The evolution from secondary structure to tertiary structure of MOF indicates the importance of coordination bond in the evolution of superstructure. To create more complicated architectures, a three-level seed architecture can be used in the assembly process (Fig. 1.7) [98]. For instance, Zhou's team observed that when MOF-74-III spherulite superstructures mixed with solutions containing organic linkers of different lengths, MOF-74-II plumose superstructures showed secondary growth. Two kinds of tertiary superstructures (MOF-74-III spherulites and MOF-74-II dendrites) exist in the resulting quaternary superstructure. This seed-mediated approach reveals a synthetic route to produce complex hetero-structures. The hierarchical MOF structures include atoms, building blocks, crystallites, and superstructures. These superstructures contain accurately defined

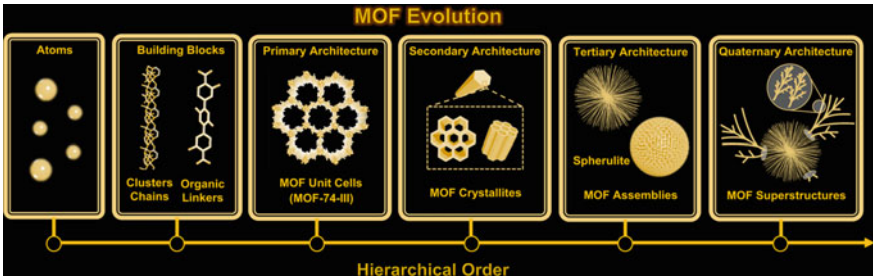

Fig. 1.7 Schematic diagram of hierarchical MOF evolution. Reproduced with permission [78]. Copyright 2020, American Chemical Society

modules designed to perform specific tasks in order. Due to its controllable morphologies, porous framework material is an ideal prototype for the development of hierarchical architectures (hollow structure, core–shell structure and multi-functional hybrid composites, etc.). It is of great significance to study the mechanism of these suprastructural assemblies. This can not only deepen our understanding of the nucleation and growth of MOF structure, but also guide us to prepare more intricate crystal framework structure.

This research area will continue to expand, focusing on improving the ability to control MOF structures with unprecedented temporal and spatial accuracy at the molecular, supramolecular and mesoscopic levels. Advanced technologies, such as lithography, may be introduced into engineering models and layered MOFs in porous environments. It is expected to develop a new assembly mode between components to connect various functional framework materials, so as to form a collaborative system with enhanced performance. In addition, another direction is to study the formation mechanism of hierarchical structure of the system, which will provide guidance for the design of functional buildings based on porous crystal materials. Multi scale control over the formation of MOF architecture is expected to bring new opportunities for layered framework materials with integrated functions.

1.5 Hybrid MOFs

In order to overcome the weak point of MOFs (e.g., chemical instability and poor electrical conductivity) and introduce new functionalities, combining MOFs with a variety of functional materials is of great interest. In hybrid MOFs, the advantages of both MOFs (topologies, porosities, structural adaptivity) and various kinds of functional materials (unique optical, electrical, magnetic and catalytic properties) can be combined effectively [99, 100]. To date, there are many active materials selected to construct hybrid MOFs, such as carbon materials, metals, polyoxometalates (POMs), polymers, framework materials, etc.

1.5.1 MOF-Metal Nanoparticles Composites

Metal nanoparticles (MNPs) usually have high surface energies and tend to aggregate. The porous properties and large specific surface area of MOFs are beneficial to immobilize MNPs, meanwhile prevent the aggregation of MNPs. In general, there are two main synthetic approaches for the immobilization of MNPs in MOFs. One is to immerse the metal precursor in the MOFs, followed by reduction of the precursor to metal atoms. In this synthetic route, various techniques can be applied such as chemical vapor deposition, solid grinding, and solution infiltration. For example, the Pt@UiO-66-NH_2 composites was synthesized by impregnating UiO-66-NH_2 with different contents of structural defects into the Pt precursor solution, followed by reduction at 200 ºC in an H_2/Ar atmosphere. As the result, Pt NPs with an average size of 1.2–1.4 nm can be dispersed in UiO-66-NH_2 particles [101]. The Ru NPs with a size range of 1.5–1.7 nm embedded into the otherwise unchanged MOF-5 were successfully obtained via a gas-phase loading of MOF-5 with the volatile compound [Ru(cod)(cot)] (cod = 1,5-cyclooctadiene, cot = 1,3,5-cyclooctatriene) followed by the hydrogenolysis of the adsorbed complex inside the porous structure of MOF-5 [102]. Xiao et al. dispersed the re-synthesized Pt NPs (~3 nm) into the synthetic system of UiO-66-NH_2, and obtained the Pt@UiO-66-NH_2 composites with 2.87 wt % Pt loading [103]. Another approach involves the synthesis of MNPs initially, and then the MOFs are allowed to grow around the MNPs by adding suitable chemicals, which still remains to be explored. Lu et al. reported an effective strategy to encapsulate various nanoparticles within ZIF-8 in a controllable way. Polyvinylpyrrolidone (PVP) was introduced into the synthesis system to modified Au NPs, which result in the successive adsorption of nanoparticles onto the continuously forming surfaces of the growing MOF crystals. After mixing PVP-capped Au NPs with methanolic solutions of zinc nitrate and 2-methylimidazole at room temperature, Au@ZIF can be achieved [104].

1.5.2 MOF-Metal Oxide Composites

Metal oxide nanomaterials have attracted many attentions due to the advantages of controllable shape and size, nontoxicity, thermal and chemical stability [105, 106]. Typically, the preparation method of MOF-metal oxide composites is similar to that of MOF-Metal nanoparticles composites. They are considered to be ideal pseudocapacitance electrode materials due to the high theoretical specific capacitance and high reversibility. However, they have high surface energies and are easy to accumulate, which lead to the loss of pseudocapacitance performance [107]. In this vein, construct MOF-metal oxide composites can not only reduce the aggregation of metal oxide nanomaterials, but also integrate the advantages of both metal oxides and MOFs. Zheng et al. synthesized Co-MOF sheet (Co-MOF, Co_2(ptcda)·$2H_2O$, ptcda = perylene-3,4,9,10-tetracarboxylic dianhydride) via a simple one-pot hydrothermal

method. Specifically, Co_3O_4 nanocubes grew on the surface of Co-MOF sheet at pH = 11–13 and formed the Co_3O_4@Co-MOF composite.[108] In order to enhance the photocatalytic efficiency, Zhang et al. designed a double-shell TiO_2@ZIF-8 hollow nanospheres through sonocrystallization [109]. Sonocrystallization can inhibit the self-nucleus growth of ZIF-8 to some degree, and ZIF-8 tended to grow along with the surface of TiO_2 hollow nanospheres carboxylation.

Dekrafft et al. applied the MOF-template strategy by coating MIL-101 particles with an amorphous shell of TiO_2 based on the acid-catalyzed hydrolysis and condensation of titanium(IV) bis(ammonium lactato)dihydroxide (TALH) in water. Besides, the thickness of the TiO_2 coating could be controlled by changing the ratios of acid or the reaction time [110].

1.5.3 MOF-POM Composites

POMs, defined as $[XM_{12}O_{40}]^{n-}$ (i.e., X = Co^{2+}, P^{5+}, Si^{4+} etc.; M = W^{6+}, Mo^{6+} etc.), belongs to transition metal-oxo clusters. Owing to its nanosize, complete inorganic skeleton and multi-electron redox properties, POMs have great potential in many research fields (e.g., catalysis, energy storage, etc.) [111–113]. Particularly, the combination of POMs with organic ligands attracts much attention due to their intrinsic differences in properties and corresponding synergistic effects. Simultaneously, ZIFs as a kind of unique MOF, have large chambers limited by narrow windows filled with imidazolate rings, which can capture molecules of the right size, even store. In this regard, ZIFs provide a suitable storage facilities for POMs [114]. In view of that POMs belong to highly polar molecules, they can't adhere to the surface of particles or get stuck between particles, they can only be encapsulated inside the ZIFs cages [115]. Traditionally, POMs are confined into MOFs though a one-pot method for the preparation of MOF@POM, i.e., "POMOF"-based route, besides the size of POMs clusters should match that of MOFs is more importantly. For example, as shown in Fig. 1.8a, first put metal ions (Zinc oxide), ligands (2-MIM) and heteropolyacid (e.g., phosphotungstic acid, silicotungstic acid and phosphomolybdic acid) into the stainless steel, after a series of ball-mill, washing and drying, ZIF@POM composites were obtained (ZIF-8@$H_3PW_{12}O_{40}$, ZIF-8@$H_4SiW_{12}O_{40}$ and ZIF-8@$H_3PMo_{12}O_{40}$) respectively, which were shown in Fig. 1.8b. Also, Mukhopadhyay et al. [113] mixed Zn^{2+}, POM ($K_6[CoW_{12}O_{40}]\cdot 6H_2O$), and 2-MIM in a methanolic solution with stirring to synthesize POM@ZIF-8, and the composites was highly efficient, stable and is able to perform water oxidation reaction in neutral pH. Zhang et al. encapsulated a $H_3PMo_{12}O_{40}$ in the customized cavities of ZIF-67, and constructed a kind of hollow structure, which resulted from the coordination modulator role of POMs and the anisotropic etch action of POMs in the self-assembly process [116]. However, such a simple and direct route is difficult to control the rate of reaction at various stages to some extent, resulting in the uncontrolled assembly. Therefore, Chen et al. proposed a new non-POMOF-based route to combine POMs and ZIFs, which can controls the amount of encapsulated POMs and maintain the uniformity of morphology [117].

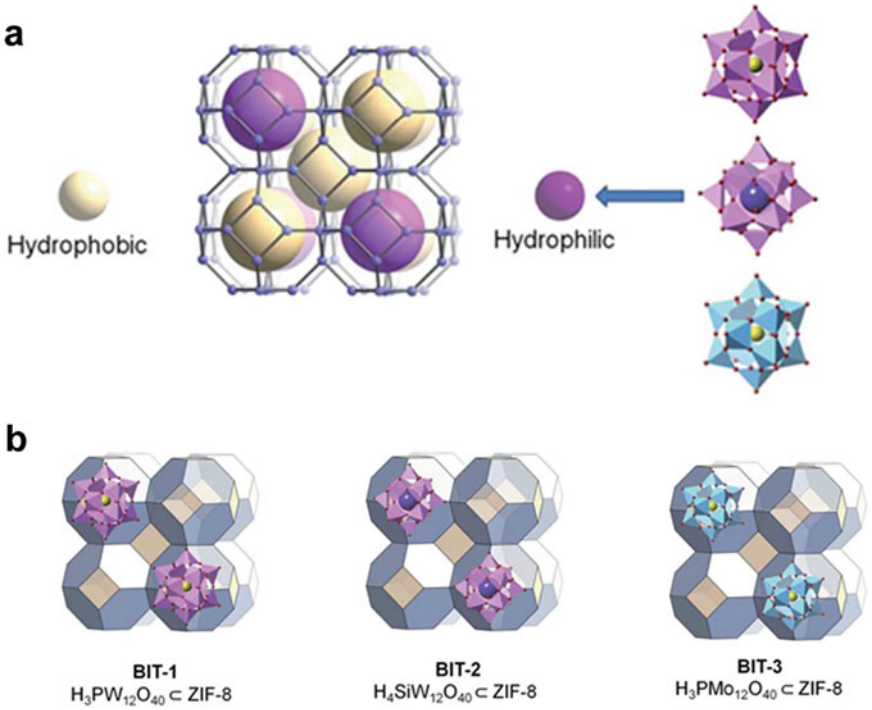

Fig. 1.8 **a** Representation of POM ⊂ ZIF composites affording inherent interconnected compartments with distinct functionalities. Yellow and purple spheres represent hydrophobic and hydrophilic interiors of the cages, respectively. **b** Structural representations of ZIF-8@$H_3PW_{12}O_{40}$, ZIF-8@$H_4SiW_{12}O_{40}$ and ZIF-8@$H_3PMo_{12}O_{40}$ [115]. Copyright 2014, The Royal Society of Chemistry

Specifically, the imidazolate rings of ZIF-67 were opened by heating to provide a channel for the entry of PMo_{12}, and the 2-MIM also can react with PMo_{12} to stabilize the whole structure. After that, the free Co^{2+} and 2-MIM were reassembled so that PMo_{12} was completely encapsulated in ZIF-67. Except encapsulating POMs in MOFs, simple coating is also common. Wang et al. coated the POM on the outer surface of ZIF-67@ZIF-8 hybrids by using a facile coprecipitation method [118].

1.5.4 MOF-Carbon Composites

Carbon materials, such as graphene, graphene oxide (GO), carbon nanotubes (CNTs) and carbon black, are of particular interest due to the excellent electrical conductivity, remarkable mechanical strength, high specific surface area, and low density. They improve MOF formation by increasing the dispersive forces within the MOFs, meanwhile suppress their aggregation. Among them, GO and CNTs are appropriate

materials for the synthesis of MOF composites. CNTs are well-ordered, high aspect ratio allotropes of carbon. According to the structure and diameter of CNTs, they also have significant adsorption and metal and semiconductor electronic properties. There are two main variants of carbon nanotubes, i.e., single-walled carbon nanotubes (SWCNTs) and multi-walled carbon nanotubes (MWCNTs) [119]. A commonly used method for preparing CNT-MOF composites involves dispersing CNTs into the MOF precursor solutions to support the in-situ growth of MOF crystals. Yang et al. combined an acid-treated MWCNTs and MOF-5 by introducing CNTs into the preparation system of MOF-5 [120]. Graphite oxide (GO), also called graphene oxide or graphitic, which is derived from the oxidative exfoliation of graphite [121]. The coexistence of ionic groups and aromatic SP^2 domains enables GO to become a structural node and participate in the bonding interactions in MOFs [122]. Owing to the facile delamination and functional nature of the GO surface, MOF-GO composites can be easily obtained by simply dispersing GO into the MOF synthesis systems [123–125]. Since epoxy and carboxylic groups on GO, they may fix zinc oxide clusters. Petit et al. dispersed GO powder ino the well-dissolved zinc nitrate/BDC mixture [126]. Then, the mixture were subsequently subjected to the same synthesis procedure as for MOF-5. Owing to the strong chemical bonds between MOF-5 and GO, i.e., the coordination between the GO oxygen groups and the metallic centers of MOF-5, GO/MOF-5 composites were obtained. Similarly, Abdi et al. first dispersed GO into methanol, after that introduced H-methylimidazole and zinc solution respectively for the in-suit growth of ZIF-8, and formed ZIF-8@GO hybrid [127]. Further, Travlou et al. incorporate aminated GO to MOF for the improvement of adsorption selectivity. During the initial exposure, ammonia was able to connect with the copper sites of HKUST-1 and formed complexes, subsequently the released BTC ligands reacted with ammonia [128].

1.5.5 MOF-MOM Composites

To date, the design of MOF-based hybrid frameworks is attached much attention. MOF-on-MOF strategy is fundamental for the conjugation of MOFs and form layered or core–shell MOFs. The growth process of MOF-MOF composites is initiated by the coordination interaction from the addition of metal ions with the ligands exposed on the surface of MOF template [129]. In most cases, the growth of the daughter MOF onto the preformed MOF based on their well-matched cell lattices. Choi et al. demonstrated the different type growth of two MOFs on the same template. The secondary MIL-68-Br have virtually identical structures with the initial MIL-68 template, which resulted the isotropic growth and the formation of core–shell-type MIL-68@MIL-68-Br, while the anisotropic growth of MOF-NDC on MIL-68 lead to a semi–tubular-type hybrid [130]. Hereafter, Wang et al. verified the heteroepitaxy growth can be carried out smoothly by increasing the lattice constant with the obvious lattice mismatch up to 20% [131]. Ikigaki et al. employed an layer-by-layer approach to fabricate the MOF-on-MOF structure [132]. Firstly, they chose the $Cu(OH)_2$

substrate which is consisted of oriented copper hydroxides nanobelts, and the grew 2D MOF $Cu_2(BPDC)_2$ (BPDC = biphenyl-4,4'-dicarboxylate) onto it with the assistance of BPDC, and then deposited $Cu_2(BDC)_2$ layer onto the $Cu_2(BPDC)_2$. Additionally, many other strategies have been explored to treat with the mismatched cell lattices between two MOFs, e.g., Van der Waals (vdW) integration [133], internal extended growth method [134]. etc. Take the vdW integration as the example, as shown in Fig. 1.9, Yao et al. assembled Cu-TCPP Cu-HHTP (TCPP = 5,10,15,20-tetrakis (4-carboxyphenyl), HHTP = 2,3,6,7,10,11-hexahydrotriphenylene) nanosheets based on the "modular assembly" stamping method because of the different sql topology. They first dispersed the Cu-TCPP nanosheets in ethanol to form a translucent suspension, then dripped onto the surface of water in the beaker to promote the integration of the continuous layer [133]. Gu et al. [134] exploited a new strategy called internal extended growth method, i.e., from the outside and inside, to overcome the limitation of mismatched crystallographic parameters. Although NH_2-UiO-66(Zr) and NH_2-MIL-125(Ti) have distinct morphologies and crystal structures, they can be hybridized easily through microwave heating, and NH_2-UiO-66(Zr) is exposed to NH_2-MIL-125(Ti) precursors under the effect of the extra structure-director agent (polyvinylpyrrolidone). The pyrrolidone ring from PVP tend to interact with metallic ions [135, 136], after stirring for a long time, PVP layers were coated on the surface of NH_2-UiO-66(Zr) nanoparticles, which was conducive to the adsorption of Ti^{4+}, and promote the aggregation of the NH_2-MIL-125(Ti) nuclei. Subsequently, NH_2-MIL-125(Ti) grew into a three-dimensional nanotablet via the self-assembly.

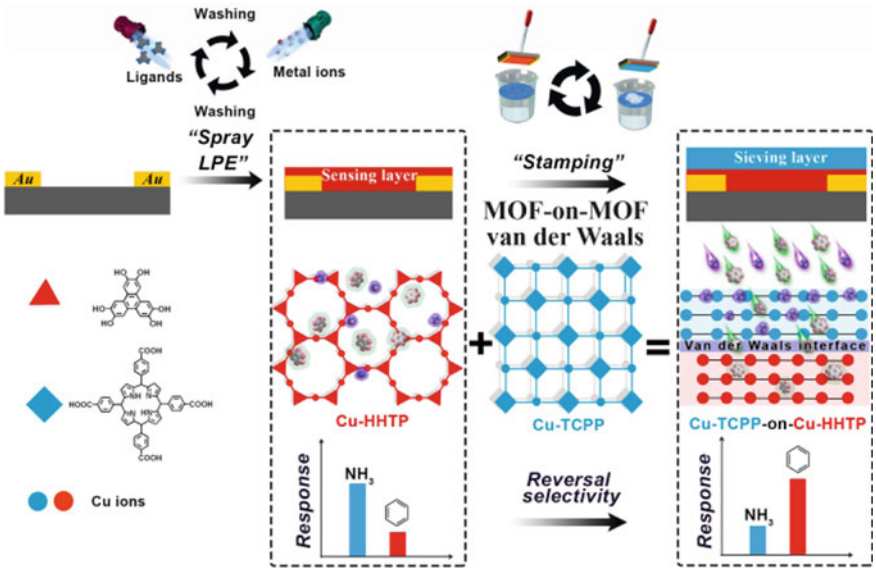

Fig. 1.9 Illustration of the preparation of MOF-on-MOF thin films by vdW integration and their application as highly selective benzene sensing materials [133]. Copyright 2019, Wiley–VCH

1.6 Conclusion

In summary, the synthesis strategy for morphology control of micro/nano MOF materials with one-dimensional, two-dimensional and three-dimensional structures is summarized. It is well known that the high specific surface area and porosity of micro-nano MOFs can alleviate volume changes during chemical processes and promote electrolyte penetration. However, further applications in practice still need more in-depth exploration to overcome its own shortcomings.

Firstly, 1D structure has unique anisotropy, which attracts a large number of researchers to prepare micro-nanomaterials with specific structure and components. Solvothermal method is the most common synthesis method. Solvothermal method can adjust the particle size, morphology and crystal surface exposure of MOF by controlling the reaction temperature, solvent concentration and reaction time, so as to obtain the ideal MOF material. The template strategy enables MOF nanostructures to be incorporated into porous polymer templates to achieve gas–liquid separation effect. However, the size of the product is affected by the template, and this method provides an idea for the synthesis of small-size MOF materials. In order to effectively control the size and morphology of MOFs, the nucleation kinetics can be controlled by adding modulators and the MOFs crystal can be grown in a specific direction. Since the modifier is a unit-point linker, it generally regulates the framework expansion and growth rate by hindering the coordination interaction between the metal ion and the organic ligand, and can prevent the agglomeration of the crystal structure. The widely used modulators are acetic acid and salicylic acid. This method is easy to extend and can be used to synthesize 1D MOF materials at an industrial level. In addition, the crystallization kinetics process can also be controlled by adding precursors with different solubility to the solvent, so as to achieve control of the crystal morphology and size. This method is mainly suitable for the synthesis of single crystal MOF. Similarly, the 1D micro/nano structure is affected by the molar ratio of water/surfactant in the microemulsion system, and the microemulsion strategy can also adjust the MOF to grow in a specific direction. In addition, the crystallization kinetics process can also be controlled by adding precursors with different solubility to the solvent, so as to achieve control of the crystal morphology and size. This method is mainly suitable for the synthesis of single crystal MOF. The microfluidic synthesis method is to form a stable interface between two reaction streams under laminar flow conditions, and the reaction time can be controlled by adjusting the flow rate, which helps to form 1D complexes on the micro-nano scale. In addition, the sonochemical method can also change the thickness and particle size of the MOF by using a lower concentration of reagents to obtain a uniform micro-nano size morphology.

Secondly, nanomaterials with 2D planar structures with atomic or molecular thickness have become ideal semiconductor and electrode materials due to their excellent conductivity. However, without affecting the growth of MOF in other directions, it is still a challenge to only inhibit the growth in the vertical direction to the micro-nano level. The more mature methods for preparing 2D MOF can be roughly divided into bottom-up and top-down. From top to bottom, the bulk MOF is usually peeled

off, such as mechanical peeling or chemical peeling. Since the layered bulk MOF is stacked in a vertical direction by weak interaction, it can be converted into a thin layer of micro-nano structure by applying appropriate mechanical peeling. However, the precision of the applied mechanical force is difficult to adjust, and the structure may be deformed or damaged during the peeling process, and the application range of this peeling method is very limited. Bottom-up usually select components to control the structure, and the more commonly used methods are solution preparation or interface growth method. The solution preparation method can selectively attach to the surface of MOF crystals to induce anisotropic growth of MOF. However, the use of surfactants or small molecule modulators may block some of the active sites of MOF. Therefore, dynamics or thermodynamics, which do not use any modifiers, are highly anticipated. The most widely used bottom-up method is the interface growth method. Liquid/gas interface synthesis uses a well-dispersed monolayer of organic ligands on the liquid surface to control the growth of MOF.

Third, because the MOF architecture has the potential to perform complex functions, hierarchical MOFs with diversity and internal controllable sequences have received widespread attention. The hierarchical structure of MOF mainly includes porous layer, system structure layer and composition hierarchy. Hierarchical systems can be established in the MOF structure, such as level 1, level 2, level 3, and level 4. Multi-scale control of MOF is formed by adjusting the layered structure ability of MOF on multiple scales to improve the activity of catalytic center and the selectivity of porous framework. The construction of primary structure is mainly influenced by coordination chemistry theory and acid–base theory, through controlled synthesis of the connectivity of inorganic clusters and organic linkers. The construction of the secondary system requires the formation of a complex MOF system structure through epitaxial growth, controlled assembly or laboratory methods. Artificial skeleton structures with higher-level structures are still relatively rare. Synthesis strategies are mainly divided into top-down and bottom-up. From top to bottom, the mesoporous or macroporous structure is usually obtained by etching the synthesized material. Bottom-up, but by adjusting the synthesis conditions to control the assembly of MOF particles into high-level structures. By adjusting the nucleation and growth kinetics of the MOF, the packing density of the frame can be increased and a multi-component architecture can be fabricated to assemble the advanced layered MOF. The use of a three-level seed structure to mediate the growth of MOF during the assembly process can form a complex superstructure. The study of layered MOF can improve the understanding of the nucleation and growth of MOF structure and guide the synthesis of more complex structures. Surface modification and reverse synthesis stability are the main considerations of MOF layering principle. Surface modification can more effectively use the secondary MOF phase on the seed MOF, and ensure the structural integrity of the MOF during the secondary growth process by combining synthetic stability. Through controllable synthesis, the layered MOF is used as a template, and the MOF is further modified and transformed into different phases, including polymer phase, original MOF phase and void phase. Fourth, combining MOF with other functional materials can also overcome some of the defects of MOF and add new functions to MOF. Currently, carbon materials,

polymers, polyoxometalates and other materials are widely used to construct MOF composite materials. Since metal nanoparticles generally have higher surface energy and are easy to aggregate, the porous structure of MOF can prevent the aggregation of MNPs and the larger specific surface area can fix MNPs. In addition, metal oxide materials have a higher theoretical specific capacitance, and the size and morphology are easy to control. Therefore, constructing MOF-metal oxide composite materials can not only have the advantages of MOF and metal oxide, but also overcome their respective shortcomings. Because POMs have a complete inorganic framework and multi-electron redox characteristics, they have great potential in the field of energy storage and conversion. In particular, the combination of POMs and organic ligands makes them have inherent characteristic differences and corresponding synergistic effects, which has attracted the attention of a large number of researchers. In addition, carbon materials have excellent electrical conductivity, strong mechanical strength and high specific surface area, which can increase the dispersion force inside the MOF to improve the structural properties of the MOF. Among them, the structure of CNT makes it have significant adsorption capacity and semiconductor electronic properties, and it is usually dispersed in the MOF precursor solution to support the in-situ growth of MOF. The coexistence of ionic groups and aromatic sp2 domains in GO can make GO participate in the bonding of MOF as a structural node. Since GO is easy to disperse, the composite material can be obtained by dispersing GO into the MOF synthesis system. The conjugation of MOF and the hybrid frame design forming layered or core–shell MOF have attracted much attention. In most cases, the sub-MOF will grow on the pre-formed MOF according to its well-matched cell lattice, which is caused by the coordination of metal ions with ligands exposed on the surface of the MOF template.

The rapid development of MOFs in recent years, on the one hand, the wide application prospect of MOFs is prompting the majority of scholars and researchers to carry out experimental research, on the other hand, the progress of science and technology promotes us to quickly develop new material products to replace the old ones. The variable one-dimensional, two-dimensional and three-dimensional structure of MOFs makes it have a variety of properties and applications, and the synthesis of MOFs is also diverse. Different ligands or different synthesis conditions will get different dimensions of crystal materials.

MOFs materials have been developed for more than 20 years, and have come to prominence in the fields of separation, purification, capture, storage, selective catalysis, drug delivery, photoelectromagnetic materials and host–guest chemistry of energy gases.This material is easy to prepare and can be obtained directly from the mixture of metal ions and organic ligands, and the coordination ability of ligands can be changed. The synthesized MOFs has acid–base amphoteric properties. In addition to the Lewis base site, the metal–organic framework also provides Lewis acid site. At the same time, metal ions play two roles in the skeleton: one is to provide the skeleton center as nodes, and the other is to form branches in the center, thus enhancing the physical properties of MOFs (such as porosity and chirality). It shows attractive application prospects in the development of new functional materials, such as selective catalysis, molecular recognition, reversible host–guest molecular (ion)

exchange, ultra-high purity separation, bioconductive materials, optoelectronic materials, magnetic materials and chips. Because metal–organic framework materials have many advantages and a wide range of applications, more and more attention has been paid to the synthesis of metal–organic framework materials.

But after all, the time of development is too short, compared with the industrial application of traditional porous materials, many problems need to be solved urgently. The research of industrial synthesis methods of metal–organic framework porous materials and their development in industrial applications will be a challenge for scientists. Such as: how to design and synthesize functional MOFs materials according to the needs, how to synthesize stable metal–organic skeleton materials, how to produce more functional materials with practical application value, and so far there is no MOF material that can fully meet the requirements of industrial production applications, either because of the lack of hydrothermal stability, chemical stability, or because the performance in the practical application environment is not perfect. This is due to: first, the output of MOFs is small, and the yield of some materials with excellent properties is low, so they can not be used on a large scale; second, some materials are still in the conceptual and laboratory stage, and can not adapt to the complex situation of reality; third, because the synthesis cost is high, its precious metals and expensive ligands are used more, so the economic benefit is low. Therefore, at present, according to the actual situation, MOFs synthesizes commercial products that can be produced and applied on a large scale, which will be the focus of future research. In other words, the study of performance in industrial applications and the development of industrial synthesis methods will be another challenge for scientists.

As the study of metal–organic framework has not yet entered a mature stage of development, there is still a lot of room for development. In view of the unique pores of the metal–organic framework system and its interaction with guest molecules, the assembly, structural and functional recombination of metal oxides / oxalates, molecular sieves and other highly chemically stable systems is still an important direction in the ascendant. Any emerging material will encounter resistance in the process of development, and breaking through one difficulty after another and solving one problem after another is the inexhaustible driving force for its development. With more and more MOFs materials with superior properties being designed and developed, we have every reason to look forward to the good prospect of industrial application of MOFs materials. From the perspective of application prospect, the application of metal–organic framework materials in new energy sources based on small molecules such as hydrogen and methane has an inestimable prospect in the research and application of major environmental science problems, such as C–C, C–H, C–N, C–O, and N–N bonds activation and conversion of related substances, as well as CO_2 storage, transformation and nuclide storage and separation.

There are many methods for the synthesis of metal–organic MOFs. The conventional synthesis methods include diffusion method (including gas phase diffusion, liquid phase diffusion and gel diffusion), volatilization method and hydrothermal/solvothermal method. With the development of coordination chemistry and material chemistry, new methods such as ultrasonic synthesis, ionic liquid

method, solid state reaction, sublimation, microwave synthesis and biphasic synthesis have been applied to the synthesis of MOFs materials. A variety of different synthesis methods have their own advantages and disadvantages, such as: microwave synthesis method uses microwave as a means of synthesis, metal complexes can be obtained in more than 10 min or dozens of minutes, saving time and high efficiency. However, due to the short reaction time, the obtained crystal is often poor, and its structure can not be determined by X-ray single crystal diffraction. Complexes with different structures may be formed by different synthesis methods. Therefore, the choice of synthesis method is very important to the synthesis of MOFs, and even affect its structure and properties. At present, synthetic MOFs tends to develop in the direction of green environmental protection, and it will be more diversified in the future research and development. Finding more synthesis methods and how to apply MOFs more widely to practical applications instead of continuing to imagine is a very important topic, which is worthy of our consideration and active response.

References

1. Serre C, Millange F, Thouvenot C, Nogue M, Loue D (2002) Very large breathing effect in the first nanoporous chromium(III)-based solids: MIL-53 or Cr(III)(OH) x [O(2)C-C(6)H(4)-CO(2)] x [HO(2)C-C(6)H(4)-CO(2)H](x) x H(2)O(y). J Am Chem Soc 124(45):13519–13526. https://doi.org/10.1021/ja0276974
2. Kitagawa S, Kitaura R, Noro S (2004) Functional porous coordination polymers. Angew Chem Int Ed 43(18):2334–2375. https://doi.org/10.1002/anie.200300610
3. Furukawa H, Cordova KE, Keeffe MO, Yaghi OM (2013) The chemistry and applications of metal-organic frameworks. Science 341(6149):1230444. https://doi.org/10.1126/science.1230444
4. Islamoglu T, Goswami S, Li Z, Howarth AJ, Farha OK, Hupp JT (2017) Postsynthetic tuning of metal–organic frameworks for targeted applications. Acc Chem Res 50(4):805–813. https://doi.org/10.1021/acs.accounts.6b00577
5. Eustis SN, Radisic D, Bowen KH, Bachorz RA, Haranczyk M, Schenter GK, Gutowski M (2008) Electron-driven acid-base chemistry: proton transfer from hydrogen chloride to ammonia. Science 319(5865):936–939. https://doi.org/10.1126/science.1151614
6. Li Y, Xu Y, Yang W, Shen W, Xue H, Pang H (2018) MOF-derived metal oxide composites for advanced electrochemical energy storage. Small 14:1704435. https://doi.org/10.1002/smll.201704435
7. Li W, Hu S, Luo X, Li Z, Sun X, Li M, Liu F, Yu Y (2017) Confined amorphous red phosphorus in MOF-derived n-doped microporous carbon as a superior anode for sodium-ion battery. Adv Mater 29:1605820. https://doi.org/10.1002/adma.201605820
8. Liu B, Shioyama H, Jiang H, Zhang X, Xu Q (2010) Metal–organic framework (MOF) as a template for syntheses of nanoporous carbons as electrode materials for supercapacitor. Carbon N Y 48:456–463. https://doi.org/10.1016/j.carbon.2009.09.061
9. Han Y, Qi P, Zhou J, Feng X, Li S, Fu X, Zhao J, Yu D, Wang B (2015) Metal-organic frameworks (MOFs) as sandwich coating cushion for silicon anode in lithium ion batteries. ACS Appl Mater Interfaces 7:26608–26613. https://doi.org/10.1021/acsami.5b08109
10. Wang S, McGuirk CM, d'Aquino A, Mason JA, Mirkin CA (2018) Metal-organic framework nanoparticles. Adv Mater 30:1–14. https://doi.org/10.1002/adma.201800202

11. Yaghi OM, Li G, Li H (1995) Selective binding and removal of guests in a microporous metal–organic framework. Nature 378:703–706. https://doi.org/10.1038/378703a0
12. Li H, Eddaoudi M, O'Keeffe M, Yaghi OM (1999) Design and synthesis of an exceptionally stable and highly porous metal-organic framework. Nature 402:276–279. https://doi.org/10.1038/46248
13. Férey G, Serre C, Mellot-Draznieks C, Millange F, Surblé S, Dutour J, Margiolaki I (2004) A hybrid solid with giant pores prepared by a combination of targeted chemistry, simulation, and powder diffraction. Angew Chem 116:6456–6461. https://doi.org/10.1002/ange.200460592
14. Rosi NL, Kim J, Eddaoudi M, Chen B, O'Keeffe M, Yaghi OM (2005) Rod packings and metal-organic frameworks constructed from rod-shaped secondary building units. J Am Chem Soc 127:1504–1518. https://doi.org/10.1021/ja045123o
15. Furukawa H, Keeffe MO, Hayashi H, Ot APC, Yaghi OM (2007) Zeolite A imidazolate frameworks. Nat Mater 6(7):501–506. https://doi.org/10.1038/nmat1927
16. Huang X, Tan C, Yin Z, Zhang H (2014) 25th anniversary article: hybrid nanostructures based on two-dimensional nanomaterials. Adv Mater 26(14):2185–2204. https://doi.org/10.1002/adma.201304964
17. Leela A, Reddy M, Gowda SR, Shaijumon MM, Ajayan PM (2012) Hybrid nanostructures for energy storage applications. Adv Mater 24(37):5045–5064. https://doi.org/10.1002/adma.201104502
18. Jingling M, Fengzhang R, Guangxin W, Yi X, Yaqiong L, Jiuba W (2017) Electrochemical performance of melt-spinning Al–Mg–Sn based anode alloys. Int J Hydrogen Energy 42:11654–11661. https://doi.org/10.1016/j.ijhydene.2017.02.185
19. Zhao J, Wei C, Pang H (2015) Zeolitic imidazolate framework-67 rhombic dodecahedral microcrystals with porous 110 facets as a new electrocatalyst for sensing glutathione. Part Part Syst Charact 32:429–433. https://doi.org/10.1002/ppsc.201400177
20. Yang L, Xu C, Ye W, Liu W (2015) An electrochemical sensor for H_2O_2 based on a new Co-metal-organic framework modified electrode. Sens Actuators, B 215:489–496. https://doi.org/10.1016/j.snb.2015.03.104
21. Wang Q, Yang Y, Gao F, Ni J, Zhang Y, Lin Z (2016) Graphene oxide directed one-step synthesis of flowerlike graphene@HKUST-1 for enzyme-free detection of hydrogen peroxide in biological samples. ACS Appl Mater Interfaces 8:32477–32487. https://doi.org/10.1021/acsami.6b11965
22. El-Dairi M, House RJ (2019) Optic nerve hypoplasia. In: Handbook of pediatric retinal OCT and the eye-brain connection. Elsevier, Amsterdam, pp 285–287
23. Seh ZW, Kibsgaard J, Dickens CF, Chorkendorff I, Nørskov JK, Jaramillo TF (2017) Combining theory and experiment in electrocatalysis: Insights into materials design. Science 355:eaad4998. https://doi.org/10.1126/science.aad4998
24. Li SL, Xu Q (2013) Metal-organic frameworks as platforms for clean energy. Energy Environ Sci 6:1656–1683. https://doi.org/10.1039/c3ee40507a
25. Schoedel A, Ji Z, Yaghi OM (2016) The role of metal–organic frameworks in a carbon-neutral energy cycle. Nat Energy 1:1–13. https://doi.org/10.1038/nenergy.2016.34
26. Xie Z, Xu W, Cui X, Wang Y (2017) Recent progress in metal-organic frameworks and their derived nanostructures for energy and environmental applications. Chemsuschem 10:1645–1663. https://doi.org/10.1002/cssc.201601855
27. Srimuk P, Luanwuthi S, Krittayavathananon A, Sawangphruk M (2015) Solid-type supercapacitor of reduced graphene oxide-metal organic framework composite coated on carbon fiber paper. Electrochim Acta 157:69–77. https://doi.org/10.1016/j.electacta.2015.01.082
28. Zhang Y, Lin B, Sun Y, Zhang X, Yang H, Wang J (2015) Carbon nanotubes@metal–organic frameworks as Mn-based symmetrical supercapacitor electrodes for enhanced charge storage. RSC Adv 5:58100–58106. https://doi.org/10.1039/c5ra11597c
29. Wang Y, Chen Q (2014) Dual-layer-structured nickel hexacyanoferrate/MnO_2 composite as a high-energy supercapacitive material based on the complementarity and interlayer concentration enhancement effect. ACS Appl Mater Interfaces 6:6196–6201. https://doi.org/10.1021/am5011173

30. Cao X, Tan C, Zhang X, Zhao W, Zhang H (2016) Solution-processed two-dimensional metal dichalcogenide-based nanomaterials for energy storage and conversion. Adv Mater 28:6167–6196. https://doi.org/10.1002/adma.201504833
31. Zhang M, Dai Q, Zheng H, Chen M, Dai L (2018) Novel MOF-derived Co@N-C bifunctional catalysts for highly efficient Zn–air batteries and water splitting. Adv Mater 30:1–10. https://doi.org/10.1002/adma.201705431
32. Ni J, Wang W, Wu C, Liang H, Maier J, Yu Y, Li L (2017) Highly reversible and durable na storage in niobium pentoxide through optimizing structure, composition, and nanoarchitecture. Adv Mater 29:1–6. https://doi.org/10.1002/adma.201605607
33. Jiang H, Liu X-C, Wu Y, Shu Y, Gong X, Ke F-S, Deng H (2018) Innentitelbild: metal-organic frameworks for high charge-discharge rates in lithium-sulfur batteries. Angew Chemie 130:3900–3900. https://doi.org/10.1002/ange.201802341
34. Xu G, Ding B, Shen L, Nie P, Han J, Zhang X (2013) Sulfur embedded in metal organic framework-derived hierarchically porous carbon nanoplates for high performance lithium-sulfur battery. J Mater Chem A 1:4490–4496. https://doi.org/10.1039/c3ta00004d
35. Bin WuH, Wei S, Zhang L, Xu R, Hng HH, Lou XW (2013) Embedding sulfur in MOF-derived microporous carbon polyhedrons for lithium-sulfur batteries. Chem A Eur J 19:10804–10808. https://doi.org/10.1002/chem.201301689
36. Li C, Hu Q, Li Y, Zhou H, Lv Z, Yang X, Liu L, Guo H (2016) Hierarchical hollow Fe_2O_3 @MIL-101(Fe)/C derived from metal-organic frameworks for superior sodium storage. Sci Rep 6:1–8. https://doi.org/10.1038/srep25556
37. Guo Y, Zhu Y, Yuan C, Wang C (2017) $MgFe_2O_4$ hollow microboxes derived from metal-organic-frameworks as anode material for sodium-ion batteries. Mater Lett 199:101–104. https://doi.org/10.1016/j.matlet.2017.04.069
38. Fang G, Zhou J, Cai Y, Liu S, Tan X, Pan A, Liang S (2017) Metal-organic framework-templated two-dimensional hybrid bimetallic metal oxides with enhanced lithium/sodium storage capability. J Mater Chem A 5:13983–13993. https://doi.org/10.1039/c7ta01961k
39. Song H, Shen L, Wang J, Wang C (2016) Reversible lithiation–delithiation chemistry in cobalt based metal organic framework nanowire electrode engineering for advanced lithium-ion batteries. J Mater Chem A 4:15411–15419. https://doi.org/10.1039/C6TA05925B
40. Rieter WJ, Taylor KML, An H, Lin W, Lin W (2006) Nanoscale metal−organic frameworks as potential multimodal contrast enhancing agents. J Am Chem Soc 128:9024–9025. https://doi.org/10.1021/ja0627444
41. Tsuruoka T, Furukawa S, Takashima Y, Yoshida K, Isoda S, Kitagawa S (2009) Nanoporous nanorods fabricated by coordination modulation and oriented attachment growth. Angew Chemie Int Ed 48:4739–4743. https://doi.org/10.1002/anie.200901177
42. Puigmartí-Luis J, Rubio-Martínez M, Hartfelder U, Imaz I, Maspoch D, Dittrich PS (2011) Coordination polymer nanofibers generated by microfluidic synthesis. J Am Chem Soc 133:4216–4219. https://doi.org/10.1021/ja110834j
43. Shi J, Zhang J, Tan D, Cheng X, Tan X, Zhang B, Han B, Liu L, Zhang F, Liu M, Xiang J (2019) Rapid, room-temperature and template-free synthesis of metal-organic framework nanowires in alcohol. ChemCatChem 11:2058–2062. https://doi.org/10.1002/cctc.201900124
44. Aijaz A, Masa J, Rösler C, Xia W, Weide P, Botz AJR, Fischer RA, Schuhmann W, Muhler M (2016) $Co@Co_3O_4$ encapsulated in carbon nanotube-grafted nitrogen-doped carbon polyhedra as an advanced bifunctional oxygen electrode. Angew Chemie Int Ed 55:4087–4091. https://doi.org/10.1002/anie.201509382
45. Zhang Z, Kong L-L, Liu S, Li G-R, Gao X-P (2017) A high-efficiency sulfur/carbon composite based on 3D graphene nanosheet@carbon nanotube matrix as cathode for lithium-sulfur battery. Adv Energy Mater 7:1602543. https://doi.org/10.1002/aenm.201602543
46. Li R, Yuan Y-P, Qiu L-G, Zhang W, Zhu J-F (2012) A rational self-sacrificing template route to metal-organic framework nanotubes and reversible vapor-phase detection of nitroaromatic explosives. Small 8:225–230. https://doi.org/10.1002/smll.201101699
47. Arbulu RC, Jiang Y-B, Peterson EJ, Qin Y (2018) Metal-organic framework (MOF) nanorods, nanotubes, and nanowires. Angew Chemie Int Ed 57:5813–5817. https://doi.org/10.1002/anie.201802694

48. Pachfule P, Shinde D, Majumder M, Xu Q (2016) Fabrication of carbon nanorods and graphene nanoribbons from a metal–organic framework. Nat Chem 8:718–724. https://doi.org/10.1038/nchem.2515
49. Zou L, Hou C-C, Liu Z, Pang H, Xu Q (2018) Superlong single-crystal metal-organic framework nanotubes. J Am Chem Soc 140:15393–15401. https://doi.org/10.1021/jacs.8b09092
50. Li Q, Zhu W, Lian Y, Peng Y, Deng Z (2020) One-dimensional HKUST-1 nanobelts from Cu nanowires. Chin Chem Lett 31:517–520. https://doi.org/10.1016/j.cclet.2019.05.005
51. Mojtabazade F, Mirtamizdoust B, Morsali A, Talemi P (2018) Ultrasonic-assisted synthesis and the structural characterization of novel the zig-zag Cd(II) metal-organic polymer and their nanostructures. Ultrason Sonochem 42:134–140. https://doi.org/10.1016/j.ultsonch.2017.11.018
52. Novoselov KS (2004) Electric field effect in atomically thin carbon films. Science 306:666–669. https://doi.org/10.1126/science.1102896
53. Liu C, Bai Y, Zhao Y, Yao H, Pang H (2020) MoS2/graphene composites: fabrication and electrochemical energy storage. Energy Storage Mater 33:470–502. https://doi.org/10.1016/j.ensm.2020.06.020
54. Liu J, Yu H, Wang L, Deng Z, Naveed K-R, Nazir A, Haq F (2018) Two-dimensional metal-organic frameworks nanosheets: synthesis strategies and applications. Inorg Chim Acta 483:550–564. https://doi.org/10.1016/j.ica.2018.09.011
55. Huang J, Li Y, Huang R-K, He C-T, Gong L, Hu Q, Wang L, Xu Y-T, Tian X-Y, Liu S-Y, Ye Z-M, Wang F, Zhou D-D, Zhang W-X, Zhang J-P (2018) Electrochemical exfoliation of pillared-layer metal-organic framework to boost the oxygen evolution reaction. Angew Chemie 130:4722–4726. https://doi.org/10.1002/ange.201801029
56. Liu W, Yin R, Xu X, Zhang L, Shi W, Cao X (2019) Structural engineering of low-dimensional metal-organic frameworks: synthesis, properties, and applications. Adv Sci 6:1802373. https://doi.org/10.1002/advs.201802373
57. Xiao X, Zou L, Pang H, Xu Q (2020) Synthesis of micro/nanoscaled metal-organic frameworks and their direct electrochemical applications. Chem Soc Rev 49:301–331. https://doi.org/10.1039/c7cs00614d
58. Nielsen RB, Kongshaug KO, Fjellvåg H (2008) Delamination, synthesis, crystal structure and thermal properties of the layered metal-organic compound $Zn(C_{12}H_{14}O_4)$. J Mater Chem 18:1002. https://doi.org/10.1039/b712479a
59. Amo-Ochoa P, Welte L, González-Prieto R, Sanz Miguel PJ, Gómez-García CJ, Mateo-Martí E, Delgado S, Gómez-Herrero J, Zamora F (2010) Single layers of a multifunctional laminar Cu(i, ii) coordination polymer. Chem Commun 46:3262. https://doi.org/10.1039/b919647a
60. Zhao M, Wang Y, Ma Q, Huang Y, Zhang X, Ping J, Zhang Z, Lu Q, Yu Y, Xu H, Zhao Y, Zhang H (2015) Ultrathin 2D metal-organic framework nanosheets. Adv Mater 27:7372–7378. https://doi.org/10.1002/adma.201503648
61. Junggeburth SC, Diehl L, Werner S, Duppel V, Sigle W, Lotsch BV (2013) Ultrathin 2D coordination polymer nanosheets by surfactant-mediated synthesis. J Am Chem Soc 135:6157–6164. https://doi.org/10.1021/ja312567v
62. Zhao K, Liu S, Ye G, Gan Q, Zhou Z, He Z (2018) High-yield bottom-up synthesis of 2D metal–organic frameworks and their derived ultrathin carbon nanosheets for energy storage. J Mater Chem A 6:2166–2175. https://doi.org/10.1039/C7TA06916B
63. Zhao M, Lu Q, Ma Q, Zhang H (2017) Two-dimensional metal-organic framework nanosheets. Small Methods 1:1600030. https://doi.org/10.1002/smtd.201600030
64. Kambe T, Sakamoto R, Hoshiko K, Takada K, Miyachi M, Ryu J-H, Sasaki S, Kim J, Nakazato K, Takata M, Nishihara H (2013) π-conjugated nickel bis(dithiolene) complex nanosheet. J Am Chem Soc 135:2462–2465. https://doi.org/10.1021/ja312380b
65. Clough AJ, Yoo JW, Mecklenburg MH, Marinescu SC (2015) Two-dimensional metal-organic surfaces for efficient hydrogen evolution from water. J Am Chem Soc 137:118–121. https://doi.org/10.1021/ja5116937

66. Sakamoto R, Hoshiko K, Liu Q, Yagi T, Nagayama T, Kusaka S, Tsuchiya M, Kitagawa Y, Wong W-Y, Nishihara H (2015) A photofunctional bottom-up bis(dipyrrinato)zinc(II) complex nanosheet. Nat Commun 6:6713. https://doi.org/10.1038/ncomms7713
67. Rodenas T, Luz I, Prieto G, Seoane B, Miro H, Kapteijn F, LlabrésiXamena FX, Gascon J (2015) Metal–organic framework nanosheets in polymer composite materials for gas separation. Nat Mater 14(48):55. https://doi.org/10.1038/nmat4113
68. Diercks CS, Kalmutzki MJ, Diercks NJ, Yaghi OM (2018) Conceptual advances from werner complexes to metal-organic frameworks. ACS Cent Sci 4:1457–1464. https://doi.org/10.1021/acscentsci.8b00677
69. Ferey G (2005) A chromium terephthalate-based solid with unusually large pore volumes and surface area. Science 309:2040–2042. https://doi.org/10.1126/science.1116275
70. Cavka JH, Jakobsen S, Olsbye U, Guillou N, Lamberti C, Bordiga S, Lillerud KP (2008) A new zirconium inorganic building brick forming metal organic frameworks with exceptional stability. J Am Chem Soc 130:13850–13851. https://doi.org/10.1021/ja8057953
71. Serre C, Mellot-Draznieks C, Surble S, Audebrand N, Filinchuk Y, Ferey G (2007) Role of solvent-host interactions that lead to very large swelling of hybrid frameworks. Science 315:1828–1831. https://doi.org/10.1126/science.1137975
72. Luo Y, Ahmad M, Schug A, Tsotsalas M (2019) Rising up: hierarchical metal-organic frameworks in experiments and simulations. Adv Mater 31:1901744. https://doi.org/10.1002/adma.201901744
73. Feng L, Wang K-Y, Lv X-L, Powell JA, Yan T-H, Willman J, Zhou H-C (2019) Imprinted apportionment of functional groups in multivariate metal-organic frameworks. J Am Chem Soc 141:14524–14529. https://doi.org/10.1021/jacs.9b06917
74. Xiao X, Zou L, Pang H, Xu Q (2020) Synthesis of micro/nanoscaled metal–organic frameworks and their direct electrochemical applications. Chem Soc Rev 49:301–331. https://doi.org/10.1039/C7CS00614D
75. Feng L, Yuan S, Li J-L, Wang K-Y, Day GS, Zhang P, Wang Y, Zhou H-C (2018) Uncovering two principles of multivariate hierarchical metal-organic framework synthesis via retrosynthetic design. ACS Cent Sci 4:1719–1726. https://doi.org/10.1021/acscentsci.8b00722
76. Feng L, Wang K-Y, Day GS, Zhou H-C (2019) The chemistry of multi-component and hierarchical framework compounds. Chem Soc Rev 48:4823–4853. https://doi.org/10.1039/C9CS00250B
77. Liang Z, Zhao R, Qiu T, Zou R, Xu Q (2019) Metal-organic framework-derived materials for electrochemical energy applications. EnergyChem 1:100001. https://doi.org/10.1016/j.enchem.2019.100001
78. Feng L, Wang K-Y, Willman J, Zhou H-C (2020) Hierarchy in metal-organic frameworks. ACS Cent Sci 6:359–367. https://doi.org/10.1021/acscentsci.0c00158
79. Reboul J, Furukawa S, Horike N, Tsotsalas M, Hirai K, Uehara H, Kondo M, Louvain N, Sakata O, Kitagawa S (2012) Mesoscopic architectures of porous coordination polymers fabricated by pseudomorphic replication. Nat Mater 11:717–723. https://doi.org/10.1038/nmat3359
80. Cölfen H, Antonietti M (2005) Mesocrystals: inorganic superstructures made by highly parallel crystallization and controlled alignment. Angew Chemie Int Ed 44:5576–5591. https://doi.org/10.1002/anie.200500496
81. Peng Y, Zhao M, Chen B, Zhang Z, Huang Y, Dai F, Lai Z, Cui X, Tan C, Zhang H (2018) Hybridization of MOFs and COFs: a new strategy for construction of MOF@COF core-shell hybrid materials. Adv Mater 30:1705454. https://doi.org/10.1002/adma.201705454
82. Zhu R, Ding J, Jin L, Pang H (2019) Interpenetrated structures appeared in supramolecular cages, MOFs, COFs. Coord Chem Rev 389:119–140. https://doi.org/10.1016/j.ccr.2019.03.002
83. Luo L, Lo W-S, Si X, Li H, Wu Y, An Y, Zhu Q, Chou L-Y, Li T, Tsung C-K (2019) Directional engraving within single crystalline metal-organic framework particles via oxidative linker cleaving. J Am Chem Soc 141:20365–20370. https://doi.org/10.1021/jacs.9b10499

84. Pérez-Ramírez J, Christensen CH, Egeblad K, Christensen CH, Groen JC (2008) Hierarchical zeolites: enhanced utilisation of microporous crystals in catalysis by advances in materials design. Chem Soc Rev 37:2530. https://doi.org/10.1039/b809030k
85. Schwieger W, Machoke AG, Weissenberger T, Inayat A, Selvam T, Klumpp M, Inayat A (2016) Hierarchy concepts: classification and preparation strategies for zeolite containing materials with hierarchical porosity. Chem Soc Rev 45:3353–3376. https://doi.org/10.1039/C5CS00599J
86. Xu Y, Li Q, Xue H, Pang H (2018) Metal-organic frameworks for direct electrochemical applications. Coord Chem Rev 376:292–318. https://doi.org/10.1016/j.ccr.2018.08.010
87. Feng L, Wang K-Y, Lv X-L, Yan T-H, Zhou H-C (2019) Hierarchically porous metal–organic frameworks: synthetic strategies and applications. Natl Sci Rev. https://doi.org/10.1093/nsr/nwz170
88. Feng L, Yuan S, Zhang L-L, Tan K, Li J-L, Kirchon A, Liu L-M, Zhang P, Han Y, Chabal YJ, Zhou H-C (2018) Creating hierarchical pores by controlled linker thermolysis in multivariate metal-organic frameworks. J Am Chem Soc 140:2363–2372. https://doi.org/10.1021/jacs.7b12916
89. Shen K, Zhang L, Chen X, Liu L, Zhang D, Han Y, Chen J, Long J, Luque R, Li Y, Chen B (2018) Ordered macro-microporous metal-organic framework single crystals. Science 359:206–210. https://doi.org/10.1126/science.aao3403
90. Eddaoudi M, Li H, Yaghi OM (2000) Highly porous and stable metal−organic frameworks: structure design and sorption properties. J Am Chem Soc 122:1391–1397. https://doi.org/10.1021/ja9933386
91. Lyu Z, Lim GJH, Guo R, Kou Z, Wang T, Guan C, Ding J, Chen W, Wang J (2019) 3D-printed MOF-derived hierarchically porous frameworks for practical high-energy density Li-O_2 batteries. Adv Funct Mater 29:1806658. https://doi.org/10.1002/adfm.201806658
92. Kim Y, Yang T, Yun G, Ghasemian MB, Koo J, Lee E, Cho SJ, Kim K (2015) Hydrolytic transformation of microporous metal-organic frameworks to hierarchical micro- and mesoporous MOFs. Angew Chemie Int Ed 54:13273–13278. https://doi.org/10.1002/anie.201506391
93. Carné-Sánchez A, Imaz I, Cano-Sarabia M, Maspoch D (2013) A spray-drying strategy for synthesis of nanoscale metal–organic frameworks and their assembly into hollow superstructures. Nat Chem 5:203–211. https://doi.org/10.1038/nchem.1569
94. Lee J, Kwak JH, Choe W (2017) Evolution of form in metal–organic frameworks. Nat Commun 8:14070. https://doi.org/10.1038/ncomms14070
95. Yanai N, Granick S (2012) Directional self-assembly of a colloidal metal-organic framework. Angew Chemie 124:5736–5739. https://doi.org/10.1002/ange.201109132
96. Feng L, Li J-L, Day GS, Lv X-L, Zhou H-C (2019) Temperature-controlled evolution of nanoporous MOF crystallites into hierarchically porous superstructures. Chem 5:1265–1274. https://doi.org/10.1016/j.chempr.2019.03.003
97. Deng H, Grunder S, Cordova KE, Valente C, Furukawa H, Hmadeh M, Gandara F, Whalley AC, Liu Z, Asahina S, Kazumori H, O'Keeffe M, Terasaki O, Stoddart JF, Yaghi OM (2012) Large-pore apertures in a series of metal-organic frameworks. Science 336:1018–1023. https://doi.org/10.1126/science.1220131
98. Feng L, Wang K-Y, Yan T-H, Zhou H-C (2020) Seed-mediated evolution of hierarchical metal–organic framework quaternary superstructures. Chem Sci 11:1643–1648. https://doi.org/10.1039/C9SC06064B
99. Li X, Yang X, Xue H, Pang H, Xu Q (2020) Metal–organic frameworks as a platform for clean energy applications. EnergyChem 2:100027. https://doi.org/10.1016/j.enchem.2020.100027
100. Wang K-B, Xun Q, Zhang Q (2019) Recent progress in metal-organic frameworks as active materials for supercapacitors. EnergyChem 2:100025. https://doi.org/10.1016/j.enchem.2019.100025
101. Ma X, Wang L, Zhang Q, Jiang HL (2019) Switching on the photocatalysis of metal-organic frameworks by engineering structural defects. Angew Chemie - Int Ed 58:12175–12179. https://doi.org/10.1002/anie.201907074

102. Schröder F, Esken D, Cokoja M, van den Berg M (2008) Ruthenium Nanoparticles inside Porous [Zn4O(bdc)3] by hydrogenolysis of adsorbed [Ru(cod)(cot)]: a solid-state reference system for surfactant-stabilized ruthenium colloids. J Am Chem Soc 130:6119–6130
103. Xiao J, Shang Q, Xiong Y, Zhang Q, Luo Y, Yu S, Jiang H (2016) Boosting photocatalytic hydrogen production of a metal-organic framework decorated with platinum nanoparticles: the platinum location matters. Angew Chemie 128:9535–9539. https://doi.org/10.1002/ange.201603990
104. Lu G, Li S, Guo Z, Farha OK, Hauser BG, Qi X, Wang Y, Wang X, Han S, Liu X, Duchene JS, Zhang H, Zhang Q, Chen X, Ma J, Loo SCJ, Wei WD, Yang Y, Hupp JT, Huo F (2012) Imparting functionality to a metal-organic framework material by controlled nanoparticle encapsulation. Nat Chem 4:310–316. https://doi.org/10.1038/nchem.1272
105. Jiang J, Li Y, Liu J, Huang X, Yuan C, Lou XWD (2012) Recent advances in metal oxide-based electrode architecture design for electrochemical energy storage. Adv Mater 24:5166–5180. https://doi.org/10.1002/adma.201202146
106. Chen L-F, Yu Z-Y, Wang J-J, Li Q-X, Tan Z-Q, Zhu Y-W, Yu S-H (2015) Metal-like fluorine-doped β-FeOOH nanorods grown on carbon cloth for scalable high-performance supercapacitors. Nano Energy 11:119–128. https://doi.org/10.1016/j.nanoen.2014.10.005
107. Zhai T, Wan L, Sun S, Chen Q, Sun J, Xia Q, Xia H (2017) Phosphate ion functionalized Co_3O_4 ultrathin nanosheets with greatly improved surface reactivity for high performance pseudocapacitors. Adv Mater 29:1604167. https://doi.org/10.1002/adma.201604167
108. Zheng S, Li Q, Xue H, Pang H, Xu Q (2020) A highly alkaline-stable metal oxide@metal–organic framework composite for high-performance electrochemical energy storage. Natl Sci Rev 7:305–314. https://doi.org/10.1093/nsr/nwz137
109. Zhang M, Shang Q, Wan Y, Cheng Q, Liao G, Pan Z (2019) Self-template synthesis of double-shell TiO_2@ZIF-8 hollow nanospheres via sonocrystallization with enhanced photocatalytic activities in hydrogen generation. Appl Catal B Environ 241:149–158. https://doi.org/10.1016/j.apcatb.2018.09.036
110. Dekrafft KE, Wang C, Lin W (2012) Metal-organic framework templated synthesis of Fe_2O_3/TiO_2 nanocomposite for hydrogen production. Adv Mater 24:2014–2018. https://doi.org/10.1002/adma.201200330
111. Fukuzumi S (2014) Hong D (2013) Homogeneous versus heterogeneous catalysts in water oxidation. Eur J Inorg Chem 4:645–659. https://doi.org/10.1002/ejic.201300684
112. Wei T, Zhang M, Wu P, Tang YJ, Li SL, Shen FC, Wang XL, Zhou XP, Lan YQ (2017) POM-based metal-organic framework/reduced graphene oxide nanocomposites with hybrid behavior of battery-supercapacitor for superior lithium storage. Nano Energy 34:205–214. https://doi.org/10.1016/j.nanoen.2017.02.028
113. Mukhopadhyay S, Debgupta J, Singh C, Kar A, Das SK (2018) A Keggin polyoxometalate shows water oxidation activity at neutral pH: POM@ZIF-8, an efficient and robust electrocatalyst. Angew Chemie Int Ed 57:1918–1923. https://doi.org/10.1002/anie.201711920
114. Park KS, Ni Z, Cote AP, Choi JY, Huang R, Uribe-Romo FJ, Chae HK, O'Keeffe M, Yaghi OM (2006) ZIFs—first synthesis. Proc Natl Acad Sci 103:10186–10191. https://doi.org/10.1073/pnas.0602439103
115. Li R, Ren X, Zhao J, Feng X, Jiang X, Fan X, Lin Z, Li X, Hu C, Wang B (2014) Polyoxometallates trapped in a zeolitic imidazolate framework leading to high uptake and selectivity of bioactive molecules. J Mater Chem A 2:2168–2173. https://doi.org/10.1039/c3ta14267a
116. Zhang L, Mi T, Ziaee MA, Liang L, Wang R (2018) Hollow POM@MOF hybrid-derived porous Co_3O_4/$CoMoO_4$ nanocages for enhanced electrocatalytic water oxidation. J Mater Chem A 6:1639–1647. https://doi.org/10.1039/c7ta08683k
117. Chen C, Wu A, Yan H, Xiao Y, Tian C, Fu H (2018) Trapping $[PMo_{12}O_40]^{3-}$ clusters into pre-synthesized ZIF-67 toward Mo_XCo_XC particles confined in uniform carbon polyhedrons for efficient overall water splitting. Chem Sci 9:4746–4755. https://doi.org/10.1039/c8sc01454j

118. Wang Y, Wang Y, Zhang L, Sen LC, Pang H (2019) Core-shell-type ZIF-8@ZIF-67@POM hybrids as efficient electrocatalysts for the oxygen evolution reaction. Inorg Chem Front 6:2514–2520. https://doi.org/10.1039/c9qi00798a
119. Smart SK, Cassady AI, Lu GQ, Martin DJ (2006) The biocompatibility of carbon nanotubes. Carbon N Y 44:1034–1047. https://doi.org/10.1016/j.carbon.2005.10.011
120. Yang SJ, Choi JY, Chae HK, Cho JH, Nahm KS, Park CR (2009) Preparation and enhanced hydrostability and hydrogen storage capacity of CNT©MOF-5 hybrid composite. Chem Mater 21:1893–1897. https://doi.org/10.1021/cm803502y
121. Stankovich S, Dikin DA, Dommett GHB, Kohlhaas KM, Zimney EJ, Stach EA, Piner RD, Nguyen ST, Ruoff RS (2006) Graphene-based composite materials. Nature 442:282–286. https://doi.org/10.1038/nature04969
122. Zhu QL, Xu Q (2014) Metal-organic framework composites. Chem Soc Rev 43:5468–5512. https://doi.org/10.1039/c3cs60472a
123. Jabbari V, Veleta JM, Zarei-Chaleshtori M, Gardea-Torresdey J, Villagrán D (2016) Green synthesis of magnetic MOF@GO and MOF@CNT hybrid nanocomposites with high adsorption capacity towards organic pollutants. Chem Eng J 304:774–783. https://doi.org/10.1016/j.cej.2016.06.034
124. Castarlenas S, Téllez C, Coronas J (2017) Gas separation with mixed matrix membranes obtained from MOF UiO-66-graphite oxide hybrids. J Memb Sci 526:205–211. https://doi.org/10.1016/j.memsci.2016.12.041
125. Jayaramulu K, Masa J, Tomanec O, Peeters D, Ranc V, Schneemann A, Zboril R, Schuhmann W, Fischer RA (2017) Nanoporous nitrogen-doped graphene oxide/nickel sulfide composite sheets derived from a metal-organic framework as an efficient electrocatalyst for hydrogen and oxygen evolution. Adv Funct Mater 27:1–10. https://doi.org/10.1002/adfm.201700451
126. Petit C, Bandosz TJ (2009) MOF-graphite oxide composites: Combining the uniqueness of graphene layers and metal-organic frameworks. Adv Mater 21:4753–4757. https://doi.org/10.1002/adma.200901581
127. Abdi J, Vossoughi M, Mahmoodi NM, Alemzadeh I (2017) Synthesis of metal-organic framework hybrid nanocomposites based on GO and CNT with high adsorption capacity for dye removal. Chem Eng J 326:1145–1158. https://doi.org/10.1016/j.cej.2017.06.054
128. Travlou NA, Singh K, Rodríguez-Castellón E, Bandosz TJ (2015) Cu-BTC MOF-graphene-based hybrid materials as low concentration ammonia sensors. J Mater Chem A 3:11417–11429. https://doi.org/10.1039/c5ta01738f
129. Lee S, Oh S, Oh M (2020) Atypical hybrid metal-organic frameworks (MOFs): a combinative process for MOF-on-MOF growth, etching, and structure transformation. Angew Chem Int Ed 59:1327–1333. https://doi.org/10.1002/anie.201912986
130. Choi S, Kim T, Ji H, Lee HJ, Oh M (2016) Isotropic and anisotropic growth of metal-organic framework (MOF) on MOF: logical inference on MOF structure based on growth behavior and morphological feature. J Am Chem Soc 138:14434–14440. https://doi.org/10.1021/jacs.6b08821
131. Wang Z, Liu J, Lukose B, Gu Z, Weidler PG, Gliemann H, Heine T, Wöll C (2014) Nanoporous designer solids with huge lattice constant gradients: Multiheteroepitaxy of metal-organic frameworks. Nano Lett 14:1526–1529. https://doi.org/10.1021/nl404767k
132. Ikigaki K, Okada K, Tokudome Y, Toyao T, Falcaro P, Doonan CJ, Takahashi M (2019) MOF-on-MOF: oriented growth of multiple layered thin films of metal-organic frameworks. Angew Chem Int Ed 58:6886–6890. https://doi.org/10.1002/anie.201901707
133. Yao MS, Xiu JW, Huang QQ, Li WH, Wu WW, Wu AQ, Cao LA, Deng WH, Wang GE, Xu G (2019) Van der Waals heterostructured MOF-on-MOF thin films: cascading functionality to realize advanced chemiresistive sensing. Angew Chem Int Ed 58:14915–14919. https://doi.org/10.1002/anie.201907772
134. Gu Y, Wu YN, Li L, Chen W, Li F, Kitagawa S (2017) Controllable modular growth of hierarchical MOF-on-MOF architectures. Angew Chem Int Ed 56:15658–15662. https://doi.org/10.1002/anie.201709738

135. He J, Yap RCC, Yee Wong S, Zhang Y, Hu Y, Chen C, Zhang X, Wang J, Li X (2016) Controlled growth of a metal-organic framework on gold nanoparticles. CrystEngComm 18:5262–5266. https://doi.org/10.1039/c6ce00733c
136. Sindoro M, Granick S (2014) Voids and yolk-shells from crystals that coat particles. J Am Chem Soc 136:13471–13473. https://doi.org/10.1021/ja507274n

Chapter 2
MOF Derivatives

Bingjun Zhu

2.1 Introduction

Metal–organic frameworks (MOFs) are a family of crystalline porous materials, where their framework structures are constructed by the coordination interactions between metal ion/cluster nodes and organic linkers. Thanks to their unique structural and chemical properties, MOFs have been under intensive studies for their applications in modern energy and environmental technologies, such as fuel cells [1], metal-air batteries [2], water electrolysis [3], supercapacitors [4], hydrogen storage [5]. However, the utilisation of MOFs in the above-mentioned energy and environmental technologies is not limited to their pristine forms. After thermal or chemical treatments in either inert or reactive environments, pristine MOFs can be converted into many different derivative materials, including MOF-derived porous carbon (such as metal-doped or metal-free carbon) and MOF-derived metal compounds (such as metal oxides, sulphides and phosphides). These MOF derivatives do not just partially inherit the structural and chemical characteristics of their MOF precursors, but also exhibit some more interesting porous networks and chemical components, leading to even improved performance of the materials.

In order to describe the characteristic advantages of MOF-derived materials, it is inevitable to recapture the unique structural and chemical characteristics of their MOF precursors. The distinct merits of pristine MOFs are mainly reflected in the following aspects: (1) Crystalline porous structure with variable structures from two-dimensional (2D) to three-dimensional (3D) constructions. (2) Diverse combinations of metal cations with organic ligands, leading to the formation of a variety of porous framework structures and the possession of different metallic and non-metallic active elements (such as N, P and S). (3) Metal cation/cluster nodes are separated by the surrounding organic ligands, forming atomically dispersed metallic sites. Thanks to

B. Zhu (✉)
School of Aeronautic Science and Engineering, Beihang University, Beijing, China
e-mail: zhubingjun@buaa.edu.cn

H. Pang (ed.), *Nano/Micro Metal-Organic Frameworks*,
https://doi.org/10.1007/978-981-16-4071-1_2

the above-mentioned merits of pristine MOFs, those advantageous characteristics may be not just partially inherited by MOF derivatives but can also evolve into some more interesting structural and chemical features, which may be beneficial in terms of their utilisation in energy and environmental applications [6]. The key attractions of MOF derivatives are summarised as follows:

(1) Hierarchically porous structures

Due to the removal of carbon or non-carbon elements, thermal treatments of pristine MOFs usually result in the collapse of their crystalline porous structures. This process can change the arrangement of the remaining atoms (such as carbon, metal or metal compounds) and thus the original pore sizes, leading to the formation of pores of different sizes, covering the pore size range of macropores, mesopores and micropores. According to the classification by International Union of Pure and Applied Chemistry (IUPAC), the sizes of macropores are above 50 nm, those of mesopores are between 50 and 2 nm, while those of micropores are below 2 nm [7]. These pores of different sizes are usually interconnected with each other, leading to the formation of hierarchically porous networks. When compared with many MOFs, which mainly compose of micropores, MOF derivatives with hierarchically porous structures may be more favourable in the circumstance when mass transfer within the pore network is an important consideration for material design. For example, in the case of MOF-derived porous carbon for gas adsorption, macropores more likely play the role of "lobby", which provide a spacious entrance for adsorbent molecules, while mesopores offer smooth "passageways" for the diffusion of adsorbent molecules within the pore networks. The adsorption of those molecules usually take place in the connected micropores due to their comparatively large adsorption potentials [8]. The significance of hierarchically porous structure is also widely recognised in many electrochemical studies in terms of mass transport of reactants and reaction products within pore networks (such as the design of electrocatalysts and electrode materials) [9].

In addition, the variable porous framework structures of pristine MOFs also lead to the formation of variable porous structures of their derivatives. For example, 2D MOFs are usually used for the manufacture of 2D porous membranes, while 3D MOFs are sometimes used for the construction of porous carbon materials with 3D porous networks as well. Furthermore, it is important to note that well-developed porous structure is not a unique merit for pristine MOFs or their derivatives, since it can be found in many other porous functional materials, such as activated carbon produced by activation methods. However, in the latter case, it is difficult to keep the resulting porous structures the same in different batches of products, because it is hard to control the distribution and dispersion of activating agents within carbon precursor materials. In the case of MOFs, the formation of their crystalline porous structures is a direct consequence of metal–organic coordination. This makes the ordered structures of MOFs designable and predictable prior to synthesis. In this case, the porous structure of MOF derivatives can also be designed and predicted prior

to thermal treatments, which is an important factor be considered for the future stable mass production.

(2) Nanoscale metallic active sites

The diversity of MOFs is attributed to the diverse combinations of metal modes and organic linkers. This also makes it possible to synthesise a wide range of MOF derivatives with different metallic active sites to fulfil various functions of the materials. More importantly, it is previously mentioned that metal cation/cluster nodes are separated by the surrounding organic ligands, forming atomically dispersed metal sites. After thermal treatments, metallic elements are usually still preserved in the resulting MOF derivatives. In this case, the orderly arranged and isolated metallic sites in pristine MOFs can promote the formation of highly dispersed and uniformly distributed metal nanoparticles in their corresponding MOF derivatives. This is particularly true in terms of MOF-derived carbon materials. The carbonisation of organic ligands lead to the formation of carbon frameworks, where metal nanoparticles are embedded, which prevents them from agglomerating into larger particles. The formation of large agglomerates of metal particles results in the reduced number of exposed active sites because only those on the surface of metal particles can take the effects of enhanced interactions between active sites and reactants/adsorbents. In contrast, the formation of highly dispersed and uniformly distributed metal nanoparticles as active sites is beneficial in terms of enlarged active interface for adsorption and reaction to take place. Particularly in the case of transition metal-based MOFs and their derived materials, transition metal nanoparticles can catalyse the formation of graphitic carbon shells around them, which does not just prevent them from agglomeration but also protect them from external corrosion and poisoning. In recent years, there is a fast-growing interest in the design and synthesis of advanced materials with atomically dispersed metallic active sites. In this case, metallic active sites are dispersed and distributed in the porous substrates in the form of single atom sites, which maximises their exposure to the surrounding interaction environment. These atomically dispersed metallic sites can also interact with neighbouring atoms or functional groups, such as carbon and nitrogen. This can cause the redistribution of electrons at the metallic sites and thus tailors their reactivity [10]. It is aforementioned that orderly arranged and isolated metal nodes are a unique characteristic of MOFs. Therefore, it offers the possibility to utilise this characteristic to produce atomically dispersed metal sites in the resulting MOF derivatives [11].

Furthermore, it is also possible to design and synthesise MOFs with orderly arranged bimetallic sites, which provides an opportunity to produce MOF-derived carbon with highly dispersed and uniformly distributed bimetallic active sites. The possession of bimetallic active sites in MOF derivatives are favourable in terms of achieving the following two functions:

On the one hand, the two metallic elements may exhibit different affinities/activities towards different adsorbents/reactants, which grants MOF derivatives bifunctionalities in some specific applications, for instance, oxygen

reduction reaction (ORR) and oxygen evolution reaction (OER) for metal-air batteries, hydrogen evolution reaction (HER) and OER for water electrolysis. On the other hand, synergistic effects may occur between the two metallic elements, which can improve the performance of MOF derivatives through facilitating their spatial distribution, electron distribution and electron transfer pathway.

(3) Diverse choices of organic ligands

Sometimes, organic ligands are also called organic linkers because they play the role of "bridges" to link metal nodes and form the "skeletons" to build framework structures of MOFs and separate metal nodes from each other. In addition, organic ligands are the source of carbon to produce MOF-derived carbonaceous materials by means of high temperature thermal treatments in inert gas atmospheres. These processes are usually referred to as the carbonisation of MOFs, which leads to the formation of carbon frameworks with embedded metal nanoparticles. Apart from the role of carbon source, organic ligands can also possess other non-metallic elements, such as oxygen, nitrogen, sulphur and phosphorus, which may incorporate into the structures of the resulting MOF derivatives as active sites in the following two forms:

On the one hand, non-metallic elements can incorporate into the resulting carbon structures of MOF derivatives as defect dopants. A frequently applied non-metallic dopant is nitrogen element. It can incorporate into the carbon structure in the form of pyridinic, pyrrolic, pyridonic and graphitic nitrogen. The activities of the above-mentioned nitrogen functional groups are different from each other due to varied electron distributions at these active sites. For example, pyridinic nitrogen possess lone pair electrons, which offers this type of nitrogen comparatively higher affinity and activity [12].

On the other hand, non-metallic elements can also react with the metallic elements during the thermal treatments of MOFs, converting or partially converting metal nanoparticles into metallic compounds, such as metal phosphides and metal sulphides. These chemical transformations can help to enhance the activities of metallic sites through the modification of electron distribution and the facilitation of electron transfer at active sites. Moreover, the association with non-metallic elements may tailor the affinities of active sites towards specific adsorbents or reactants, which is also an effective way to introduce bifunctionalities to MOF derivatives [13]. In the past, conventional modification methods usually involve multi-step thermal treatments in inert and reactive gas environments. This is a common approach for many studies on the modification of metallic active sites in MOF derivatives. However, with the purpose choice among diverse organic ligands, the modification of metallic active sites can be carried out in a single step-thermal treatment, which is favoured in terms of reduced material and energy consumptions.

In summary, the attractions of MOF derivatives originate from the unique structural and chemical characteristics of their pristine MOF precursors. These advantageous characteristics of pristine MOFs can evolve into more favourable porous structures and chemical constituents, including hierarchically porous

structures, nanoscale metallic active sites and non-metallic functional groups. In this chapter, selected examples from earlier published research works are used to demonstrate the advance of design and synthesis strategies for a variety of MOF derivatives, most of which can be classified into MOF-derived carbon materials (metal-doped carbon, metal-free carbon and MOF-derived carbon with atomically dispersed metallic active sites) and MOF-derived metal compounds (metal oxides, hydroxides, phosphides, sulphides, selenides and nitrides). Particular attentions are paid to the design of metal–organic coordination structures and chemical components of MOFs and its influence on the resulting porous structures and chemical compositions of MOF derivatives, in order to demonstrate the "uniqueness" of using MOFs as precursor materials.

2.2 MOF-Derived Porous Carbon

Thanks to the crystalline porous structures and carbon-rich organic ligands of MOFs, porous carbon is a major form of MOF derivatives, which can be produced by means of thermal treatments at high temperatures and in inert gas atmospheres (such as Ar and N_2). This process is well-known as the carbonisation of MOFs. On the one hand, metal and most of carbon elements can be preserved in the resulting MOF derivatives after carbonisation, leading to the formation of porous carbon frameworks with embedded metal nanoparticles, that is, metal-doped carbon. In the meantime, the other non-carbon elements, such as O, N and P, are removed or partially removed from the resulting carbon structures during the carbonisation process. The remaining non-metallic elements either incorporate into carbon structures as active sites or react with metal nanoparticles to modify metallic active sites. The doping of both metallic and non-metallic elements in MOF-derived porous carbon contributes to the formation of heteroatom-doped carbon. On the other hand, metallic elements can be removed by either acid washing after thermal treatments or vaporisation at high temperatures during thermal treatments, leading to the formation metal-free carbon with non-metallic dopants or missing carbon vacancies as active sites. Herein, this section focuses on the summary of recent advance in the design and synthesis of MOF-derived heteroatom-doped carbon and metal-free defective carbon.

2.2.1 MOF-Derived Heteroatom-Doped Carbon

The diverse combinations of metals and organic linkers make it possible to produce MOF-derived porous carbon with different combinations of heteroatom dopants. Zeolitic imidazolate frameworks (ZIFs) are a distinctive group of MOFs, which are constructed by the coordination between metal cations and imidazolate ligands [14]. As the term suggests, ZIFs possess structures similar to those of aluminosilicate zeolites, where imidazolate ligands play the role of "bridges" to connect two metal

cations (M-IM-M, IM = imidazolate), similar to the Si–O–Si bonds in zeolites [15]. Apart from the common characteristic of crystalline porous structure, the attractions of ZIFs are also reflected in their isolated metallic cation sites and nitrogen-containing imidazolate ligands. Because of the above-mentioned two characteristic features, it is possible to make use of ZIFs as precursor materials to produce ZIF-derived, metal- and nitrogen-doped porous carbon derivatives.

ZIF-67 is one of the most intensively studied ZIFs, which composes of cobalt cation as the metallic node and 2-methylimidazole as the organic ligands [16]. It usually possesses purple colour and polyhedral shape. Thanks to the isolated metallic sites and N-containing ligands, ZIF-67 is also widely used as the precursor materials to produce Co- and N-doped porous carbon materials for a wide range of energy and environmental applications, including gas adsorption and separation, electrochemical energy conversion and storage [16]. ZIF-67 can be synthesised by means of either solvothermal methods [17] or simple mix and stir methods [18]. Different synthetic methods and conditions can influence the sizes and morphologies of ZIF precursors and their carbon derivatives. Xia et al. synthesised a series of ZIF-67 crystals by means of both the solvothermal method at 120 °C and the mix and stir method at different temperatures (60 and 25 °C, respectively) and in different solvents (water and methanol, respectively). Figure 2.1a shows that ZIF-67 prepared with the mix & stir method at room temperature in methanol exhibits the smallest particle size of 300 nm, which can be attributed to the comparatively slower crystal growth at a lower temperature and a less polar solvent. This ZIF-67 nanocrystal sample is chosen to be further carbonised in the argon flow in the temperatures ranging from 600 to 900 °C. Figure 2.1c–e show the scanning electron microscope (SEM) and transmission electron microscope (TEM) images of the 750 °C carbonised ZIF-67, which suggests that the polyhedral shape of pristine ZIF-67 is relatively well-preserved even after carbonisation. Figure 2.1d also reveals a relatively uniformly dispersed black dots, that is, Co nanoparticles, embedded in the carbon polyhedron. A higher magnification TEM image (as shown in Fig. 2.1e) further shows that the size of Co nanoparticles is about 10 nm. In addition, due to the catalytic effect of Co, a few layers of carbon shells are also formed around these nanoparticles, which helps to improve the stability of Co nanoparticles. The X-ray photoelectron spectroscopy (XPS) surface chemistry analysis shows that nitrogen from the ligands incorporates into the resulting carbon structure mainly in its pyridinic forms, while Co tends to form Co–N active sites due to the abundant Co-N_4 moieties in the ZIF-67 precursors (as shown Fig. 2.1b). The specific surface area of both pristine ZIF-67 and their carbon derivatives are investigated by the nitrogen sorption methods. The characterisation results show that the specific surface area of pristine ZIF-67 decreases with the increasing crystal size. The 300 nm ZIF-67 shows a high Brunauer–Emmett–Teller (BET) surface area of 1512 $m^2\ g^{-1}$. This value drops to 386 $m^2\ g^{-1}$ after thermal treatments, however, the original crystalline porous framework evolves into a hierarchical structure as well, which is beneficial in terms of mass transfer within the pore network.

With the advance in the design and synthesis of innovative MOFs, more Co-based MOFs can become the candidate precursor materials for the production of MOF-derived Co- and N-doped porous carbon. Jagadeesh et al. reported a cobalt

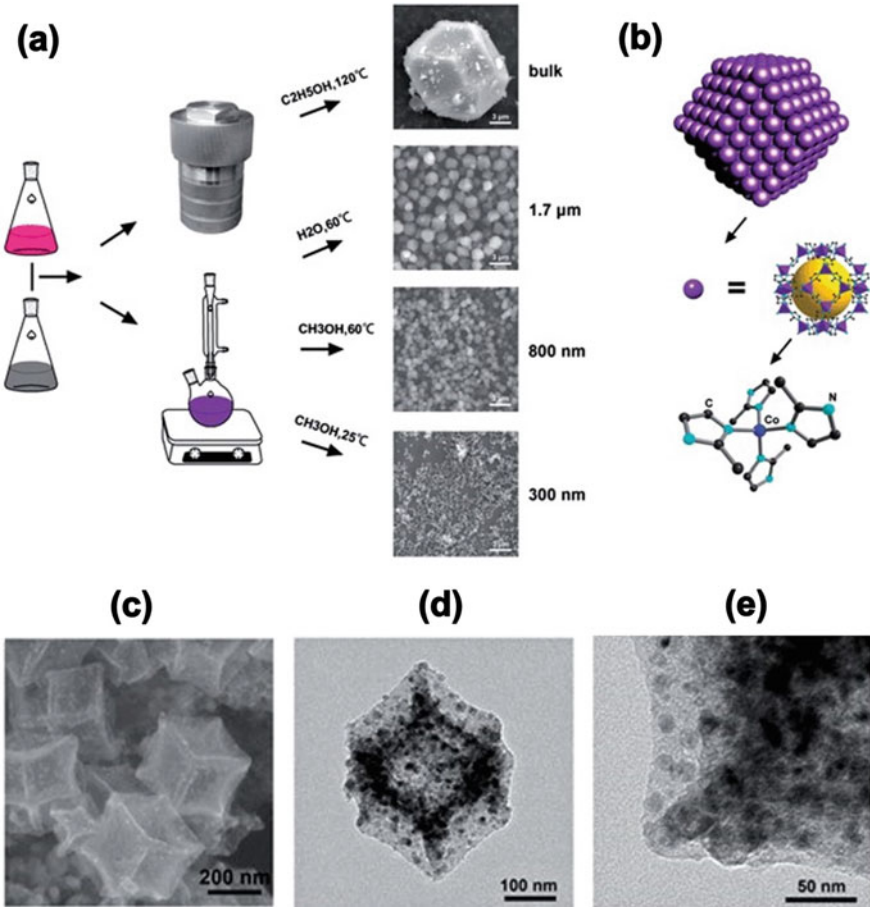

Fig. 2.1 **a** Synthesis of ZIF-67 with different methods and conditions. **b** Schematic illustration of ZIF-67 polyhedron, its microscopic porous framework structure and the coordination structure with Co cation and 2-methylimidazolate ligands. **c** SEM image of ZIF-67-derived carbon polyhedrons after thermal treatments at 750 °C. **d** and **e** TEM images of ZIF-67-derived polyhedron with Co nanoparticles (black dots). Reproduced with permission [18]. © 2014 Royal Society of Chemistry

nanoparticle-based porous carbon material, which is derived from a cobalt-diamine-dicarboxylic acid MOF precursor [19]. Figure 2.2a illustrates the synthetic procedure of this Co-MOF-derived porous carbon. In this case, cobalt nitrate is used as the source of metal cation and,4-diazabicyclo[2.2.2]octane (DABCO) and terephthalic acid (TPA) are applied as the organic ligands. The Co-MOF precursor is synthesised by the simple mix & stir method in dimethylformamide (DMF) and immobilized on Vulcan XC 72R carbon substrate. The corresponding Co-doped carbon is then produced by the carbonisation at 800 °C in Ar. The aberration-corrected scanning transmission electron microscope (STEM) image (as shown in Fig. 2.2b) does not just reveal Co nanoparticles with sizes from 5 to 30 nm, but also shows that graphitic

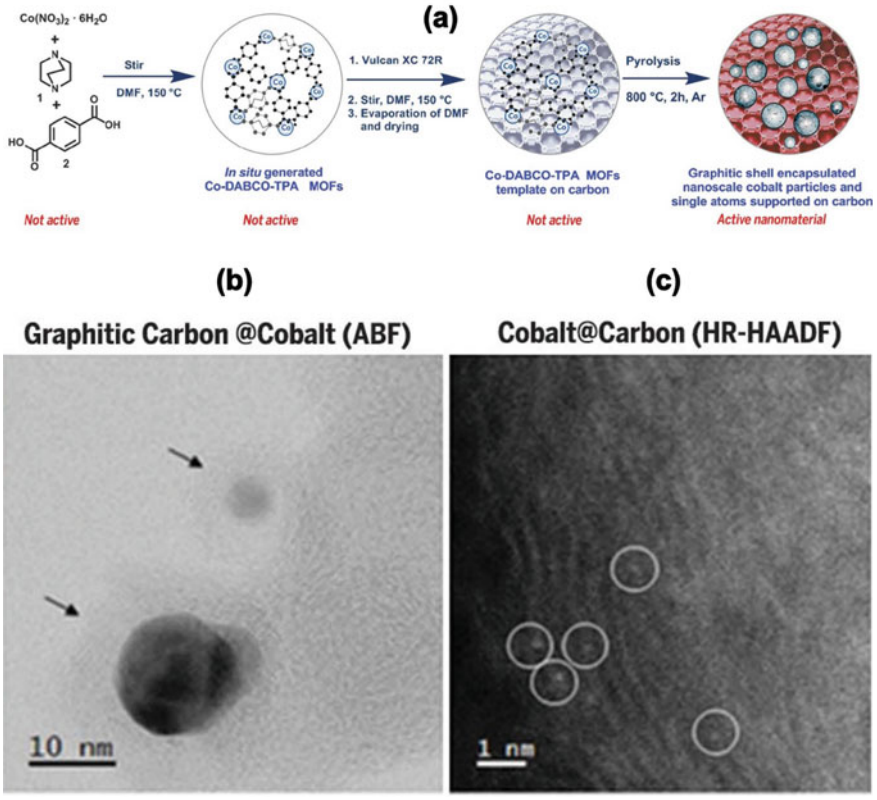

Fig. 2.2 **a** An illustration of the synthesis of Co nanoparticle-encapsulated Co-DABCO-TPA-derived porous carbon. **b** Aberration-corrected STEM image of Co nanoparticles encapsulated in the graphitic carbon shells. **c** HAADF image of single Co atom sites (white dots) in MOF-derived carbon. Reproduced with permission [19]. © 2017 Science

layers and short-range ordered graphitic shells are formed around the nanoparticles due to the catalytic effect of Co. More interestingly, the high-angle annular dark field (HAADF) image demonstrates the existence of single Co atom sites in short-range ordered carbon regions. By combining TEM imaging and XPS analysis, it is discovered that some Co nanoparticles exhibit a Co–Co_3O_4 core–shell nanostructure and nitrogen from DABCO ligands incorporates into the resulting Co-doped carbon in the form of pyridinic nitrogen and bonding with Co cation (CoN_x).

Apart from heteroatom-doped carbon derived from Co-based MOFs, there are numerous published research works on MOF-derived porous carbons embedded with many other metallic nanoparticles. Zou et al. reported a hierarchical hollow Ni/NiO nanoparticle-graphene composite derived by means of carbonisation and oxidation of a Ni-based MOF (ligand: trimesic acid) [20]. Yun et al. introduced a Fe/Fe_2O_3-doped porous carbon, which is derived from another famous group of MOFs, that is, MIL-101 (Fe) (MIL = Materials Institute Lavoisier) [21]. Many other metal-doped

carbon derivatives can also be produced from MILs, such as MIL-101(Cr) [22], MIL-125(Ti) [23] and MIL-53(Al) [24]. Cai et al. synthesised Cu/Cu_2O-supported graphitic carbon composite from the widely studied MOF-74 (Cu) [25]. Thanks to the large number of possible combinations between metal and organic ligands, a wide range of heteroatom-doped porous carbons can be produced from MOF precursors. Moreover, the existence of bimetallic MOFs makes it possible to synthesise bimetal-doped porous carbon materials. By controlling the molar ratio of the bimetallic elements in MOF precursors, it is possible to control the molar ratio of the bimetallic elements in the resulting carbon derivatives.

An interesting example was a ZnCo co-doped carbon nanotube networks derived from a ZnCo bimetallic MOF, which was published by Li et al. [26]. It is previously mentioned that ZIF-67 is an intensively studied Co-based MOF, which is widely used as the precursor to produce Co- and N-doped porous carbon. ZIF-8 is another well-known ZIF-type MOF, which possesses the isostructure of ZIF-67 but substitutes Co with Zn as the metallic cation centre. Therefore, it brings the opportunity to use both Co and Zn salts ($Co(NO_3)_2$ and $Zn(NO_3)_2$) to react 2-methylimidazole ligands, leading to the formation of ZnCo bimetallic MOFs (as shown in Fig. 2.3a). In this work, ZnCo bimetallic MOF is synthesised with the 1:1 molar ratio of $Co(NO_3)_2$/$Zn(NO_3)_2$. The as-prepared bimetallic MOF is then pyrolysed at 700 °C in Ar flow. Since the boiling point of Zn is 908 °C [27], Zn is preserved in the resulting porous carbon with Co as the co-dopant, leading to the formation of ZnCo bimetallic nanoparticles, which catalyses the graphitization of carbon and the growth of carbon nanotubes on the surface of carbonised bimetallic MOF (as shown in Fig. 2.3b). Figure 2.3c and d show the ZnCo nanoparticle at the tip of the carbon nanotube. It is worth mentioning that ZnCo bimetallic MOFs based on ZIF-8 and ZIF-67 frequently appear in many other studies on MOF-derived heteroatom-doped carbon as well. However, in many cases, Zn plays the role of "structure modifier", where the corresponding carbonisation temperature is set to be above its boiling point, resulting in the evaporation of Zn and the formation monometal-doped carbon. On the one hand, the volatilisation of Zn can may induce the formation of pores and thus improve the porous structure of MOF-derived carbon [28–30]. On the other hand, the evaporation of Zn can also help facilitate the distribution and dispersion of the other metal nanoparticles, preventing the formation of large agglomerates [31, 32].

In summary, thanks to the unique structural and chemical characteristics of MOFs, they can be utilised as precursors to produce a wide range of MOF-derived porous carbon materials, which are doped with a variety of metallic and non-metallic heteroatoms in the form of nanoparticles, functional groups and moieties. These highly dispersed and uniformly distributed active sites can help to improve the performance of MOF-derived carbon in energy and environmental applications. With the further pursuit of optimised performance, MOF-derived porous carbon materials with atomically dispersed metal sites have attracted great attention from chemists and materials scientists.

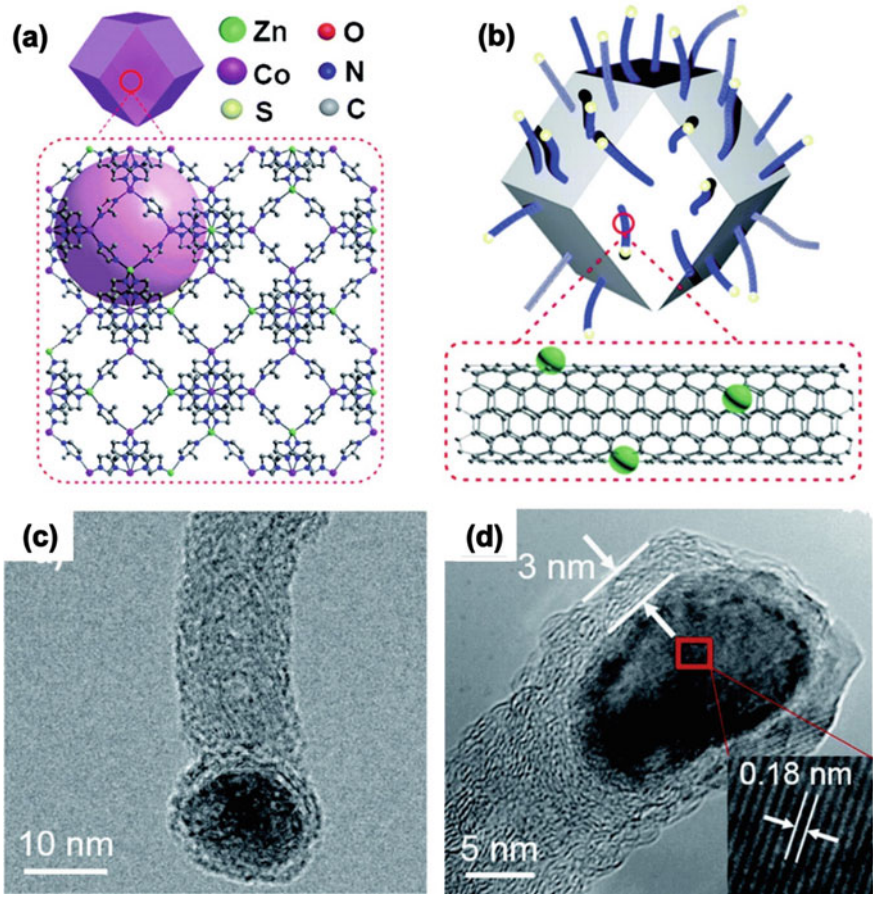

Fig. 2.3 **a** The framework structure of ZnCo bimetallic MOF. **b** The growth of carbon nanotubes on the surface of the carbonized bimetallic MOF. **c** and **d** ZnCo bimetallic nanoparticle at the tip of the carbon nanotube. Reproduced with permission [26]. © 2018 Royal Society of Chemistry

2.2.2 MOF-Derived Carbon with Atomically Dispersed Metal Sites

The significance of metal nanoparticles in porous carbon is to promote the exposure of highly dispersed and uniformly distributed active sites for optimised material performance. In this case, the formation of atomically dispersed metal sites (ADMSs) can maximise the exposure and interfacial contact of active sites with adsorbents/reactants, and thus release the "full potential" of an active site. In addition, the single-atom metallic site may interact with the neighbouring atoms (such as N, S and P), which can modify the electron distribution and transfer at the active site and thus tailor the material performance as well. However, the production of porous

carbon with ADMSs usually involves the careful control over the concentration of metal source and the complicated synthetic method to induce the formation of M–N–C coordination structure. Owing to isolated metal sites and active non-metallic elements (particularly nitrogen) in organic ligands, the carbonisation of MOFs becomes a more convenient and controllable route to produce porous carbon with ADMSs. It is previously mentioned that, besides Co nanoparticles, Jagadeesh and co-workers also found atomically dispersed Co sites in a cobalt-diamine-dicarboxylic acid MOF-derived porous carbon [19].

Yang et al. reported the synthesis of a carbon framework with atomically dispersed Mn sites by means of the carbonisation of a Mn-BTC MOF (BTC = 1,3,5-benzenetricarboxylic acid), followed by the HCl etching treatment and NH_3 annealing (as shown in Fig. 2.4a) [33]. Aberration corrected high-angle annular dark-field scanning transmission electron microscope imaging (HAADF-STEM, Fig. 2.4b) and Extended X-ray absorption fine structure spectra (EXAFS, Fig. 2.4c) demonstrate the existence of single Mn atom sites and the formation of Mn–O and Mn-N coordination in the MOF-derived carbon framework. In Fig. 2.4c, Mn foil is used as the reference material to show the peak for Mn–Mn bond (black curve), which is absent in the sample with ADMSs (orange curve). This apparent difference further proves that Mn metallic sites exist in the form of single atoms.

Similar to the case of bimetallic MOF-derived bimetal nanoparticle-doped carbon, it is possible to produce porous carbon atomically dispersed bimetallic sites with bimetallic MOFs as well. Han et al. presented a hollow carbon nanocubes with atomically dispersed CoNi bimetallic sites derived from a CoNi bimetallic MOF (as shown in Fig. 2.5a) [34]. This bimetallic MOF is fabricated by the chemical precipitation of Ni^{2+} cations and $Co(CN)_6^{3-}$ and coated with polydopamine for the formation of the core–shell hollow carbon nanotube after 500 °C annealing in NH_3 flow. The last step of acid etching is to remove the excessive Co and Ni nanoparticles, leaving only the diatomic Co–Ni sites, which form coordination structures with the neighbouring N atoms. In this way, the Co–Ni diatomic site still fulfil the purpose of atomic dispersion, which acts like a "single-atom" site. These atomically dispersed bimetal sites are imaged by the aberration-corrected HAADF-STEM in Fig. 2.5b. Figure 2.5c shows the Fourier transformed EXAFS spectra of MOF-derived porous carbon nanocubes with bimetallic ADMSs (red curve) and nanoparticles (black curve). It evidences the existence of only Co–N and Co–Ni interactions in the sample with ADMSs, while the sample with bimetallic nanoparticles shows a clear peak for Co–Co bonds.

Apart from intrinsic isolated metal cation centres, ADMSs can be produced by the introduction of external metal sources in accompany with the carbonisation of MOFs. For example, Zhu et al. demonstrated a hierarchical carbon architecture with atomically dispersed Fe sites derived from $FeCl_3$- and DCD-encapsulated MIL-101-NH_2 (DCD = dicyandiamide) [35]. In this case, DCD does not just play the role of additional source of carbon and nitrogen, but also prevent the collapse of porous structure and the agglomeration of metallic components. This is further in favour of the formation of ADMSs in addition to the merits of the MOF precursor. Again, the HAADF-STEM imaging and EXAFS analysis demonstrate the existence of single Fe atom sites with the formation of FeN_x coordination structure.

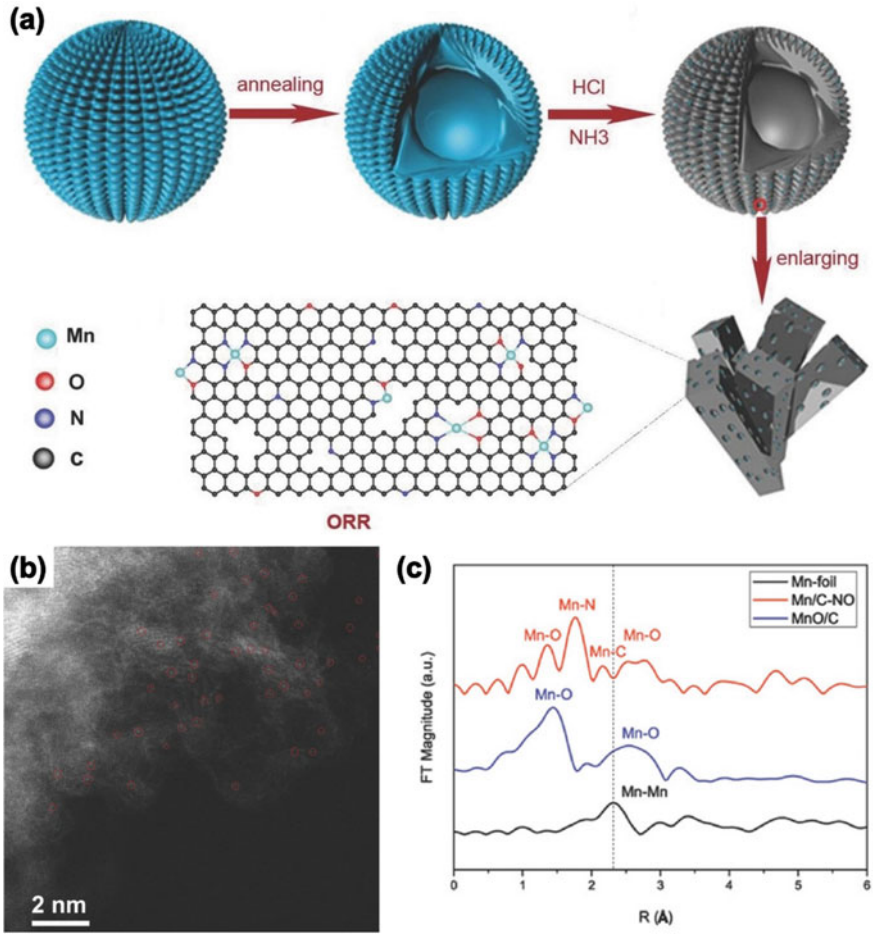

Fig. 2.4 **a** A flow chart of the synthesis procedure for the carbon framework with atomically dispersed Mn sites from Mn-BTC, which are coordinated with O and N atoms at the edges of pores and frameworks. **b** Aberration-corrected HAADF-STEM shows single Mn atom sites (red circles). **c** Fourier transform of Mn K-edge x-ray EXAFS spectra indicate the existence of Mn-N and Mn–O coordination and the absence of Mn–Mn bond in Mn-BTC-derived carbon (Mn/C-NO, orange curve). Reproduced with permission [33]. © 2018 WILEY–VCH Verlag GmbH & Co. KGaA

Besides the above-discussed examples, there are a large number of reported works on MOF-derived porous carbon with either mono- or bimetallic ADMSs [11, 36]. In most cases, ADMSs in MOF-derived carbon can be achieved by either the one-step carbonisation of MOF precursors with intrinsic metal cations or the encapsulation and dispersion of external metal sources in crystalline porous frameworks of MOF precursors before carbonisation. The formation of ADMSs can be attributed to isolated metal sites, well-developed porous structures and coordination interactions with neighbouring non-metallic sites from organic ligands. Since ADMSs represent

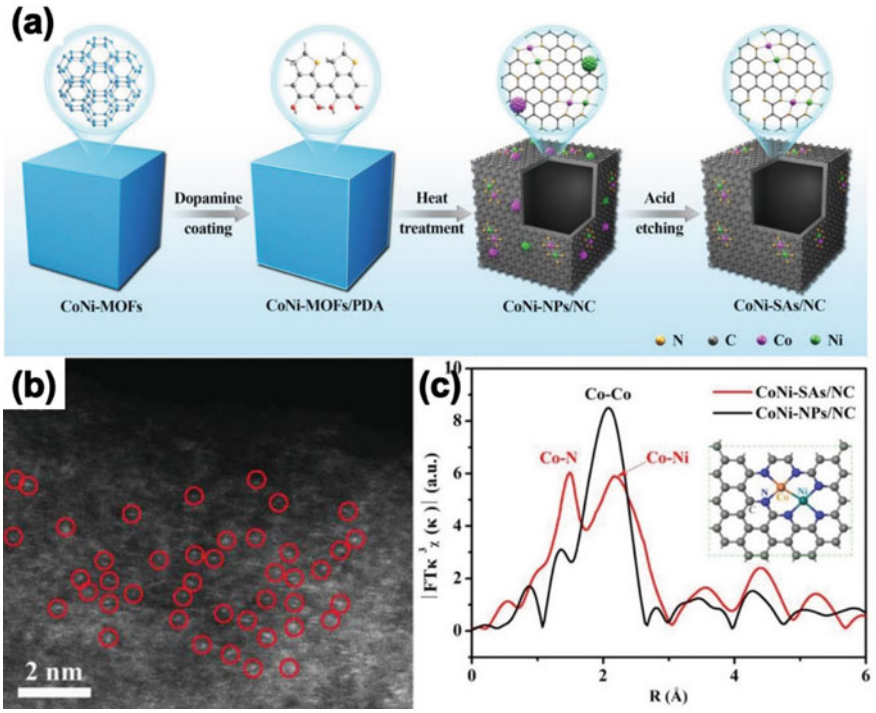

Fig. 2.5 **a** An illustration of the synthesis of CoNi bimetallic MOF-derived carbon nanotube with atomically dispersed bimetallic Co–Ni sites. **b** HAADF-STEM image of atomically dispersed Co–Ni sites (red circles). **c** Fourier transformed Co K-edge EXAFS spectra of the sample with atomic Co–Ni sites (red curve), indicating Co–Ni and Co–N bonds. The sample with CoNi nanoparticles (black curve) is used as the reference material for Co–Co bond. Reproduced with permission [34]. © 2019 WILEY–VCH Verlag GmbH & Co. KGaA

the non-stopping pursue of higher performance of functional materials, it can be expected the on-going research on ADMSs will continue to bring excitement and pleasant surprise with the exploitation of MOF-derived porous carbon.

2.3 MOF-Derived Metal-Free Defective Carbon

Apart from the rich progress of MOF-derived metal-doped carbon, there is also a growing interest in the development of MOF-derived metal-free carbon. The functional performance of metal-doped carbon heavily relies their metallic active sites. However, this also makes them susceptible to acidic and alkaline environments due to metal leaching and etching [37]. In the absence of metallic elements, the activity of metal-free carbon depends on the defective sites in the carbon structures, which frequently exist in the form of chemical defects (non-metallic dopants, such as N,

P and S) and structural defects (vacancies, edges and holes) [38]. The formation of these defective sites can modify the local charge distribution and thus play the role of active sites in metal-free carbon. Furthermore, these active sites may possess higher stabilities when compared with those of metallic sites in acidic and alkaline environments. When MOFs are applied to produce metal-free carbon, the diverse choices of organic ligands make it possible to introduce multiple non-metallic dopants as chemical defects, while the rearrangement of carbon atoms during thermal treatments may create all kinds of structural defective sites in the resulting carbon structures. Metallic elements from the MOF precursors are removed either by means of acid washing or volatilisation at high temperatures.

In the case of the acid washing method, Wang et al. produced a nanoporous carbon from ZIF-67 [39]. It is previously introduced that ZIF-67 is a Co-based MOF with 2-methylimidazolate linkers. Therefore, the pyrolysis of ZIF-67 in the inert gas atmosphere (Ar in this work) leads to the formation of MOF-derived carbon with embedded Co nanoparticles. As illustrated in Fig. 2.6a, in order to produce metal-free carbon, this ZIF-67-derived carbon is further washed with aqua regia. This acid washing process does not just remove Co nanoparticles but also promotes the formation of new nanopores. Figure 2.6b and c are the high resolution TEM images of ZIF-67-derived porous carbon before and after acid washing, respectively. It clearly shows the formation of new nanopores due to the removal of Co nanoparticles by acid washing. Porosity analysis results show that both specific surface areas and pore volumes of ZIF-67-derived carbon increase after acid treatments.

It is mentioned in the previous example that Zn can be used as a "structural modifier" in bimetallic MOF-derived heteroatom-doped carbon due to its volatilisation at high temperatures above its boiling temperature (908 °C). Based on the same consideration, Zn-based MOFs are widely used as precursor materials to produce metal-free porous carbon [40–42]. In contrast, if the temperatures of thermal treatments are below the boiling point of Zn, Zn element is still preserved in MOF-derived carbon in the form of metallic nanoparticles. In this case, acid washing is required to produce metal-free carbon [43]. When compared with the acid washing process, the volatilisation of Zn may be recognised as a more convenient one-step method and a more environmentally friendly way to produce MOF-derived metal-free carbon. As early as 2014, Zhang and co-workers reported the synthesis of metal-free and N-doped porous carbon from ZIF-7, which is a Zn-based ZIF-type MOF with the benzimidazole ligands [44]. In the authors' work, the ZIF-7 precursor is mixed with glucose and then carbonised at 950 °C, where glucose is used as an additional source of carbon. The analytical results of XPS, X-ray diffraction (XRD) and Energy Dispersive X-ray (EDX) confirm the removal of Zn after the carbonisation of ZIF-7 due to the evaporation of Zn. In this case, nitrogen becomes the only dopant and the main active sties in the resulting carbon structure to fulfil its functional performance (i.e. electrocatalysis in this work).

Apart from ZIF-7 from the above-discussed case, ZIF-8 is another Zn-based MOF, which is widely studied for the production of MOF-derived metal-free carbon due to its merit of easy synthesis at ambient conditions and the volatilisation of Zn as well [45]. It is previously mentioned that ZIF-8 possesses the same framework

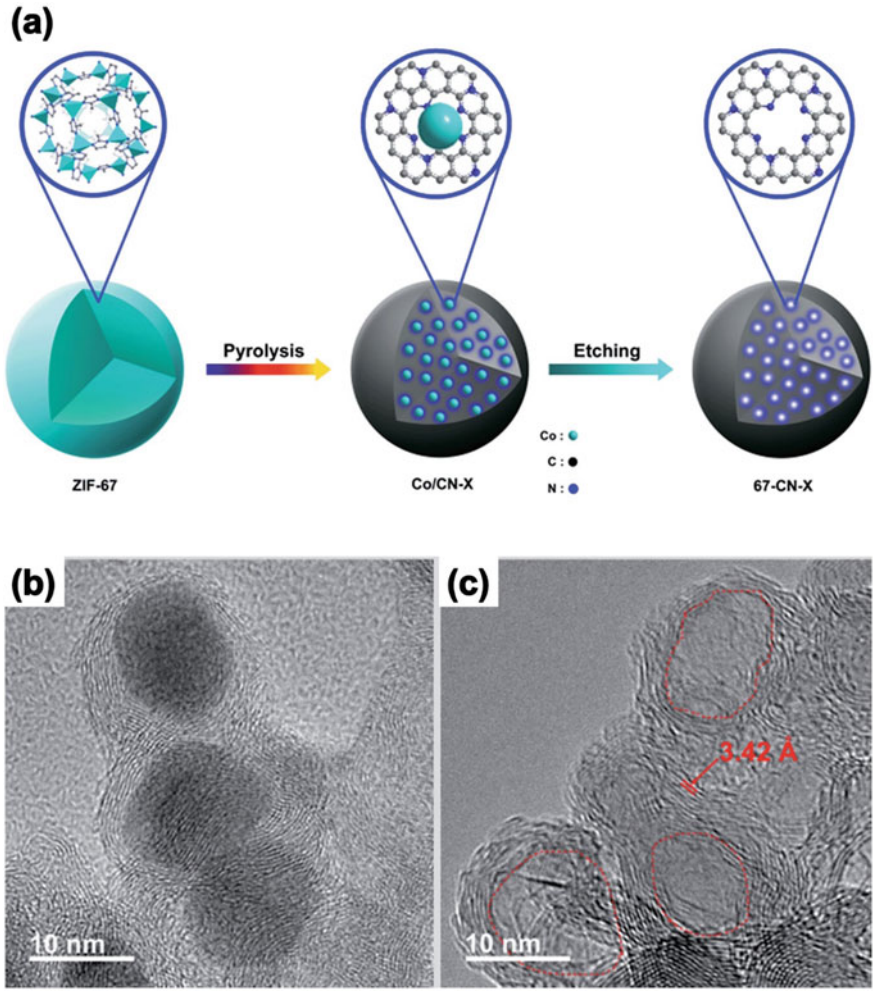

Fig. 2.6 **a** An illustration of Co-doped nanoporous carbon derived from ZIF-67, followed by the acid treatment to produce metal-free carbon. TEM images of ZIF-67-derived carbon (**b**) before and (**c**) after the acid treatment by aqua regia, showing the removal of Co nanoparticles and the formation of nanopores. Reproduced with permission [39]. © 2016 Royal Society of Chemistry

structure of ZIF-67 and use the same ligands of 2-methylimidazole. Recently, Pan et al. reported such a metal-free and heteroatom-doped carbon derived from phytic-acid-functionalized ZIF-8 by means of 1050 °C annealing in NH_3 (as shown in Fig. 2.7a) [46]. Again, Zn is removed from ZIF-8-derived carbon due to its evaporation, where no apparent Zn nanoparticle is shown in the high magnification TEM image in Fig. 2.7b. N and P elements are introduced into the resulting carbon structure as dopant defects from the 2-methylimidazolate ligands and phytic acid functional

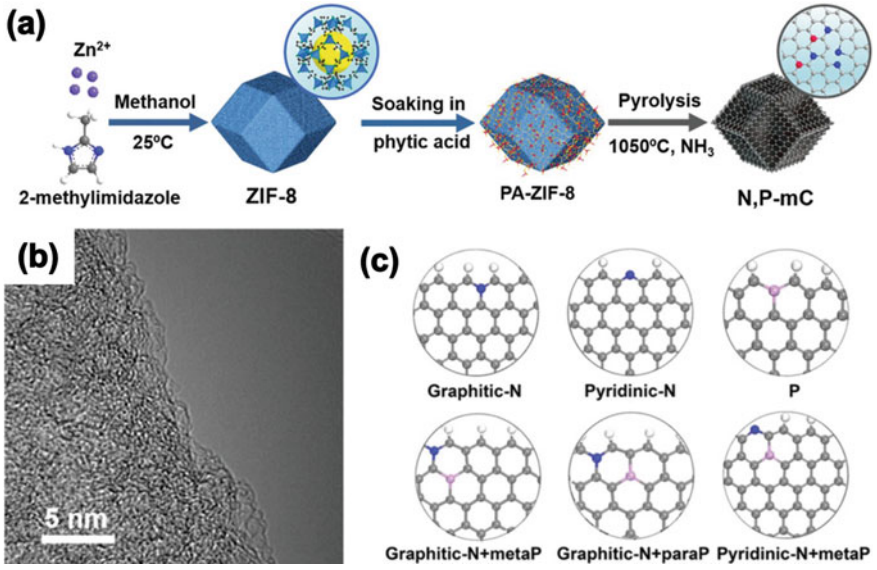

Fig. 2.7 **a** A schematic flow chart of metal-free and N, P-co-doped carbon derived from phytic-acid-functionalized ZIF-8. **b** A high magnification TEM of ZIF-8-derived carbon shows no apparent Zn nanoparticles. **c** Simulated N and P doping in carbon structures. Reproduced with permission [46]. © 2020 WILEY–VCH Verlag GmbH & Co. KGaA

groups, respectively (as shown in Fig. 2.7c). In another work by Zhao et al., a metal-free N-doped graphitic carbon photocatalyst is produced from ZIF-8 as well [47]. In this case, besides the role of N as dopant defect active site, N dopants also promote the formation of vacancy-type defects in this MOF-derived carbon (as shown in Fig. 2.8).

It is also worth mentioning that, although the volatilisation of Zn is a more effective and environmentally friendly way to produce MOF-derived metal-free carbon. Many laboratory works still carry out acid washing after thermal treatments, in order to to remove any possible residual Zn in MOF-derived carbon for the purpose of research preciseness [48, 49]. Furthermore, Zn-based MOFs can also be used as hosts and

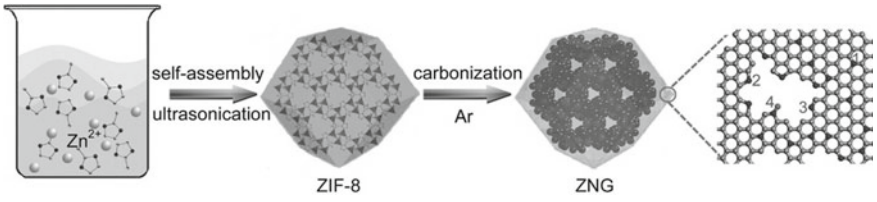

Fig. 2.8 An illustration of the synthesis of ZIF-8-derived carbon with vacancy-type defects. Reproduced with permission [47]. © 2016 WILEY–VCH Verlag GmbH & Co. KGaA

templates to load external metal elements as active dopants, where Zn is vaporised during carbonisation and only monometal-doped carbon is formed [50].

In summary, thanks to the porosity and diversity of MOFs, they can be utilised to produce a variety of porous carbon materials with or without metallic dopants. On the one hand, in the case of MOF-derived metal-free carbon, metallic elements can be removed by means of either acid washing or high temperature volatilisation. In this case, the performance of MOF-derived carbon heavily relies on its porous structure, non-metallic dopant and structural defect sites in the resulting carbon structure. On the other hand, in the case of MOF-derived metal-doped carbon, metallic elements can exist in the form of nanoparticles or ADMSs, which become the major active sites to fulfil the functions of the materials. Non-metallic elements from organic linkers can co-dope with metallic elements in MOF-derived carbon as active sites. They can either modify the electron distribution and transfer at metallic active sites or form coordination interactions with metal cations to promote the formation of ADMSs. Furthermore, it is also possible for non-metallic elements to react with metallic elements during thermal treatments, which can lead to the formation of metal compound active sites and thus tailor the activities of metallic sites.

2.4 MOF-Derived Metal Compounds

In the case of MOF-derived metal-doped carbon, the majority of metal dopants frequently exist in their elemental forms due to their reduction reactions with carbon. These elemental metals can further react with non-metallic elements, such as O, N, P, S and Se, forming metal compounds, which can improve or tailor the activities of metallic sites. These non-metallic elements can come from external chemical sources (such as NH_3, CS_2, S powder and NaH_2PO_4) or organic linkers of MOF precursors. In the former case, MOF precursors are subject to thermal treatments in either inert or oxidative gas atmospheres to produce MOF-derived metal-doped carbon or metal oxides. Then, metallic elements in MOF derivatives can further react with the above-mentioned chemical sources of non-metallic elements in the form of either continuous gas flows, decomposed products in inert carrier gas flows or solid mixtures. In the latter case, non-metallic elements are released upon thermal decompositions of organic linkers. Some of them may be lost in the form of decomposed gas molecules, while the other may dope into the resulting carbon structures or react with metallic elements to form metal compounds. Apart from the methods of thermal treatments, MOF-derived metal compounds can also be produced by means of chemical etching methods at ambient conditions. To date, there are reports of metal oxides [51], hydroxides [52], phosphides [53], sulphides [54], selenides [55] and nitrides [56] derived from MOF precursors, which are discussed in the following subsections, respectively.

2.4.1 MOF-Derived Metal Oxides

Metal oxide is a common form of active metal compounds. Thanks to their porous frameworks and isolated metal nodes, MOFs can be used as precursor materials to produce both metal oxides and metal oxide-doped carbon with inherited porosities and metallic active sites. In the case of MOF-derived metal oxides, they can be produced by means of high temperature calcination in air, which completely removes the carbon content from the original MOFs. In the case of MOF-derived metal oxide-doped carbon, they can be produced by either post-oxidation treatments in air at comparatively lower temperatures after carbonisation or reactions with intrinsic oxygen elements from decomposed organic linkers during carbonisation.

A typical example for MOF-derived metal oxides was presented by Yu and coworkers. In their work, a bimetallic oxide hollow nanowire ($NiO/NiCo_2O_4$) is synthesised from MOF-74 with Ni/Co bimetallic nodes and 2,5-dihydroxyterephthalic acid (DHTA) linkers [57]. Similar to ZIF-67, MOF-74 is another group of frequently studied and utilised MOF due to its high specific surface area and a variety of tailorable metal cation nodes, including the possibility of bimetallic cation nodes. In this case, Ni and Co acetates are simultaneously added to the reaction solution for the synthesis bimetallic MOF-74. The MOF precursor is then subject to oxidation in air at 350 °C in air. The mechanism for the formation of hollow nanowires is proposed to the result of Kirkendall effect [58], which can be explained by the different diffusivities of inner and outer components during the high temperature oxidation treatment [59]. In the case of MOF-derived metal oxide-doped carbon, Zhou et al. synthesised a range of transition metal oxide-doped carbon materials from a variety of transition metal-based MOFs, including Co-BTC, Co-BDC (BDC = 1,4-dicarboxybenzene acid), Co-DHTP (DHTP = 2,5-dihydroxyterephthalic acid) and the same MOFs but with Ni nodes [60]. Since all the MOF precursors are carbonised in high-purity N_2 gas flow, organic linkers become the only source of oxygen for the formation of metal oxides. In addition, as shown in Fig. 2.9, the use of different organic ligands can also lead to the formation of 1D, 2D and 3D MOFs and corresponding MOF derivatives as well.

Zhang et al. reported the synthesis of Fe_2O_3 with microboxes and hierarchical shell structures from a Prussian blue (PB)-type MOF, which is an iron(III) hexacyanoferrate(II) compound ($Fe_4[Fe(CN)_6]_3$) that possesses a cubic shape [61]. Prussian blue is an accidently synthesized and discovered cubic crystal materials, where substitutional and interstitial modifications lead to the formation of a variety of structures analogous to that of PB [62–64]. Therefore, this group of MOFs are well-known as Prussian blue analogues (PBAs). In this work, Fe_2O_3 microboxes are produced by the calcination of $Fe_4[Fe(CN)_6]_3$ in air. The authors conclude the 3-stage formation of hierarchical Fe_2O_3 microboxes, which is illustrated in Fig. 2.10a. Figure 2.10b–j show the SEM and TEM images of PB-derived Fe_2O_3 microboxes, which are calcined at 350, 550 and 650 °C, demonstrating different structures of PB-derived Fe_2O_3 at different stages illustrated in Fig. 2.10a.

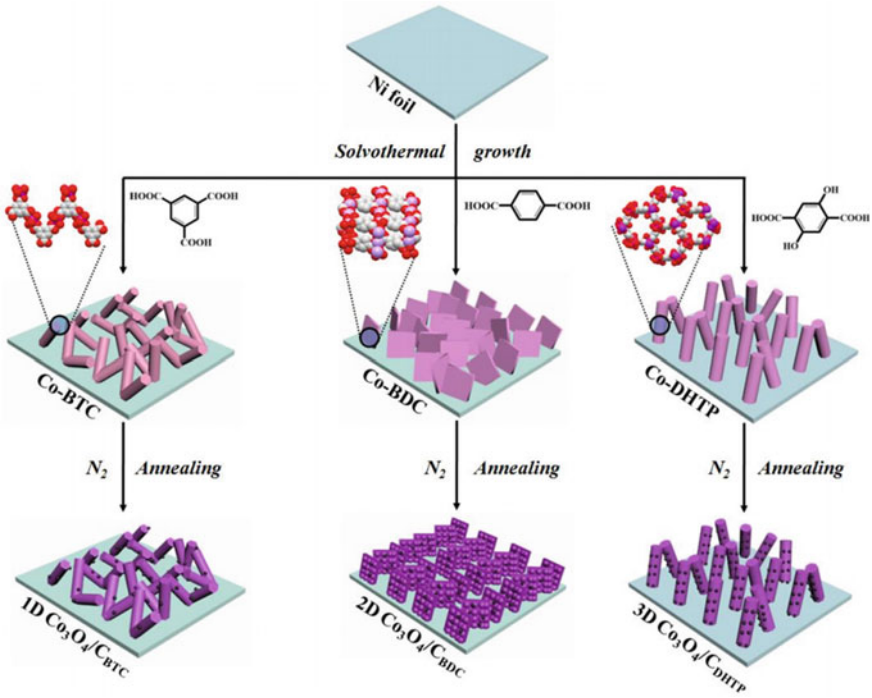

Fig. 2.9 The direct production of various Co_3O_4-doped carbon materials from MOFs with different O-containing organic ligands, leading to the formation of 1D–3D structures. Reproduced with permission [60]. © 2018 American Chemical Society

2.4.2 MOF-Derived Metal Hydroxides

Metal hydroxide is another common form of active metal compound, which is frequently synthesised and utilised in the form of layered double hydroxides (LDHs). LDHs is a large group of layered compound materials, which consist of positively charged layers (e.g., metal cations) and interlayer regions filled with charge balancing anions and water molecules [65]. Similar to both structural and chemical diversities of MOFs, LDHs also possess the merit of flexible combinations of metal cations and charge compensating anions. This common advantage interlinks these two large families of functional materials, and make it possible to use MOFs as precursors to produce LDHs with a variety of nanostructures and chemical properties [66, 67], and vice versa [68]. Differing from the high temperature oxidative treatments for MOF-derived metal oxides, MOF-derived metal hydroxides can be produced through alkaline hydrolysis reactions between MOFs and hydroxide ions in the alkaline solutions at ambient conditions. The framework structures of MOFs collapse as a result of chemical etching. Organic linkers are removed during the etching process, while metal cations react with hydroxide ions or water molecules to form metal hydroxides.

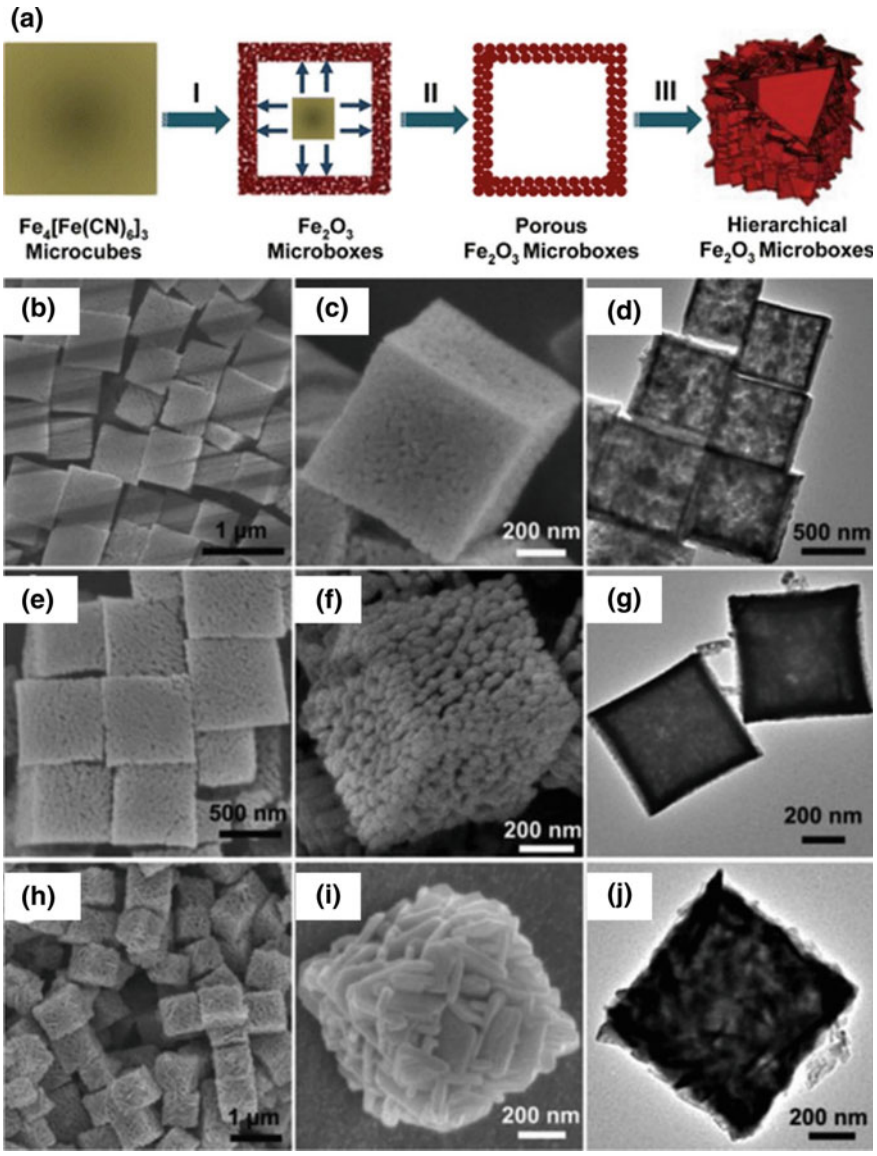

Fig. 2.10 **a** An illustration of hierarchical Fe_2O_3 microboxes from $Fe_4[Fe(CN)_6]_3$ PBA precursors. SEM and TEM images of PB-derived Fe_2O_3 microboxes after calcination in air at (**b**–**d**) 350 °C, (**e**–**g**)550 °C and (**h**–**j**) 650 °C. Reproduced with permission [61]. © 2012 American Chemical Society

Zhang et al. reported an ultrathin $Co(OH)_2$ nanoarray derived from a Co-based MOF with 2-methylimidazolate linkers, which is grown on a piece of Ni foam [69]. The growth of MOFs is carried out by simply immersing the Ni foam in the mixture aqueous solution of cobalt chloride and 2-methylimidazole. Then, the synthesis of $Co(OH)_2$ nanoarrays is carried out by the further immersion of Co-MOF/Ni foam in the cobalt chloride ethanol solution with a pH value between 5 and 6, allowing the alkaline hydrolysis reaction to take place. The porous nature of MOF precursors ensures the easy access of cobalt chloride solution, leading to the formation of ultrathin layers of $Co(OH)_2$ sheets. Figure 2.11 also indicates that $Co(OH)_2$ nanosheets also inherit the nanoarray structure of MOFs, leading to the formation of $Co(OH)_2$ nanonetworks on Ni foam. Furthermore, as emphasised in Fig. 2.11, all the above-mentioned reactions are carried out at room temperature, which is beneficial in terms of easy synthesis and energy saving.

It is demonstrated in the above section of "MOF-derived metal oxides" that PB-type MOF $Fe_4[Fe(CN)_6]_3$ is used for the production of Fe_2O_3 microboxes. Later on, the same research group reported their continued work on the synthesis of $Fe(OH)_3$ from the same MOF precursor [70]. In this case, other than calcination in air, $Fe(OH)_3$ with different structures are produced by either simple "mix & shake" reactions at ambient conditions or hydrothermal reactions at 80 °C, both with NaOH. The former method leads to the yolk-shelled $Fe(OH)_3$ microboxes, while the latter induces the formation of multishelled $Fe(OH)_3$ microboxes. The different architectures of $Fe(OH)_3$ microboxes can be attributed to varied diffusion of OH^- and precipitation of $Fe(OH)_3$ at different temperatures and concentrations of NaOH solutions.

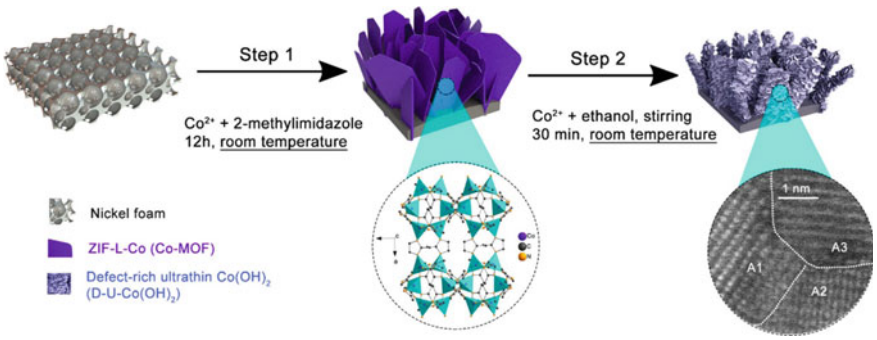

Fig. 2.11 An schematic synthesis procedure of $Co(OH)_2$ nanonetworks from the growth of a Co-based MOF nanoarrays on Ni foam. Reproduced with permission [69]. © 2018 American Chemical Society

2.4.3 MOF-Derived Metal Phosphides

Owing to the diverse bonding types in metal phosphides (M_xP_y), the combination of metal and phosphorus can bring about many interesting physical and chemical properties [71]. Thanks to the high electronegativity of phosphorus, they can draw electrons from metallic elements, which may tune M_xP_y into "electron sinks", making them more attractive to positively charged protons [58, 72]. This characteristic is particularly useful in catalysing proton-involved reactions, such as HER for water electrolysis. This arouses interests from researchers to develop and study a wide range of M_xP_y either in the form of pure compounds or active dopants in carbon materials. Similar to the case of metal oxides and hydroxides, MOFs have been studied as precursor materials because of the unique advantages of their structural and chemical characteristics. Both M_xP_y compounds and M_xP_y-doped carbon can be produced by the two-step thermal treatment processes, which involve high temperature calcination in air or carbonisation in inert gas atmospheres as the first step, followed by the additional step of phosphorisation at elevated temperatures as well. The phosphorisation reaction is usually carried out by the decomposition of phosphorous compounds (sodium hypophosphite in most cases) and subsequent reactions between metallic elements and P-containing decomposed gaseous products in carrier gases (e.g., N_2 or Ar). Phosphorous compounds are placed at the upstream of the carrier gas, while MOF derivatives are placed at the downstream. Therefore, decomposed products follow the carrier gas flow and reach MOF derivatives, where phosphorisation reactions take place. In some other cases, metal phosphides are produced just in a single-step phosphorisation of MOFs with phosphorous compounds.

In the case of MOF-derived M_xP_y compounds, Chu et al. reported the synthesis of Zn-Co phosphide porous nanosheets ($Zn_{0.33}Co_{0.67}P$), which was derived from a ZnCo bimetallic MOF with the 2-methylimidazolate linkers [73]. In this work, the authors calcine this bimetallic MOF in air at 400 °C to produce $ZnCo_2O_4$, and thus proceed with the phosphorisation treatment at 300 °C. Sodium hypophosphite (NaH_2PO_2) is used as the source of phosphorus, which decomposes and releases phosphine (PH_3) upon heating. N_2 is used as the carrier gas for PH_3 to reach the calcined MOF and convert Zn-Co oxides into Zn-Co phosphides. In some other cases, for example, in Xiao et al.'s work [74], they adopted a one-step phosphorisation process to convert a wide range of CoM bimetallic ZIFs (M = Ni^{2+}, Mn^{2+}, Cu^{2+} and Zn^{2+}) into a variety of CoM bimetallic phosphide nanosheets. In the case of MOF-derived M_xP_y-doped carbon, Liu et al. reported a Ni_2P-doped porous carbon derived from a Ni-MOF with the BTC linkers [75]. This Ni-MOF is firstly carbonised in Ar at 600 °C. Again, sodium hypophosphite (NaH_2PO_2) is used as the source of phosphine for the phosphorisation of carbonised Ni-MOF at 350 °C. Chemical analysis on the carbonised and phosphorised Ni-MOF indicates that Ni_2P and Ni co-exist in the resulting carbon framework and form hybrid nanoparticles. Synergistic effects can occur between Ni_2P and Ni, which can help to optimise the electronic structure and charge transfer within this MOF-derived Ni_2P/Ni-doped carbon.

The above-mentioned research works adopt the straightforward carbonisation and phosphorisation method to produce M_xP_y and M_xP_y-doped carbon. With some clever material design strategies, it is possible to introduce both interesting structural and compositional features to M_xP_y with the utilisation of MOFs. He and co-workers demonstrate their effort to design and synthesise such a carbon-incorporated Ni–Co mixed metal phosphide nanoboxes through a two-step modification of ZIF-67 [76]. In their work, ZIF-67 is not subject to direct carbonisation and phosphorisation treatments to produce Ni_xP_y-doped carbon. Instead, ZIF-67 nanocubes are firstly immersed in a $Ni(NO_3)_2$ ethanol solution, which is a previously mentioned method to produce MOF-derived metal hydroxides. As suggested by Fig. 2.12a, the reaction between ZIF-67 and $Ni(NO_3)_2$ takes place at the surface of the nanocubes in the first place, forming Ni-Co bimetallic LDH on the surface. In the meantime, the diffusion of ZIF-67 from inside out leads to the formation of ZIF-67@LDH nanoboxes. Then, ZIF-67@LDH nanoboxes are phosphorised with NaH_2PO_2 in N_2 flow at 350 °C and organic linkers of ZIF-67 are also carbonised at the same time, leading to the formation of carbon-incorporated Ni-Co mixed metal phosphide nanoboxes. Again, the existence of bimetallic elements in the phosphide compound brings the potential of bimetallic synergy in terms of improved performance (enhanced electrocatalytic activity in this work), while the incorporation of carbon enhances the structural stability, electron transfer efficiency and electrical conductivity of this MOF-derived bimetallic phosphide material. Apart from He et al.'s work, a similar approach was adopted by Guan and co-workers to produce hollow Mo-doped CoP nanoarrays from a 2D Co-based MOF [77]. In this case, the 2D Co-based MOF firstly reacts Na_2MoO_4

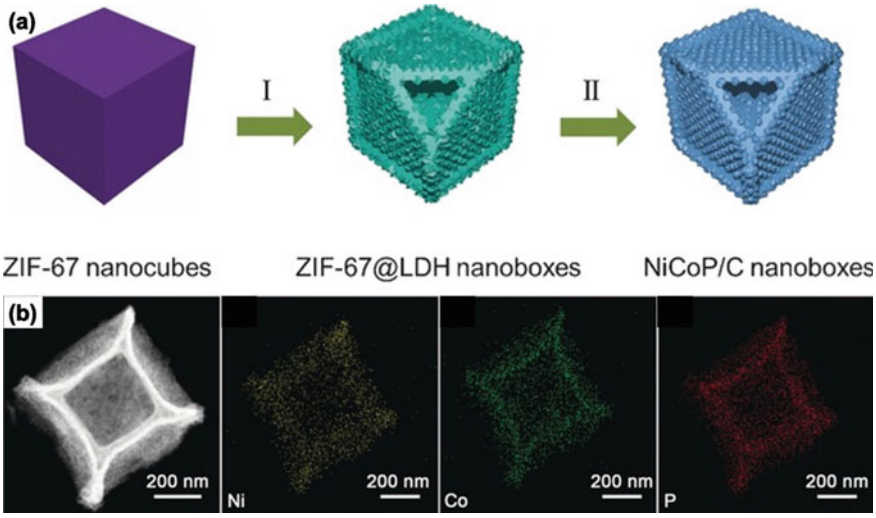

Fig. 2.12 **a** An illustration of the two-step formation process from ZIF-67 nanocubes to carbon-incorporated NiCoP nanoboxes: I. LDH formation; II phosphorisation. **b** HAADF-STEM image of a carbon-incorporated NiCoP nanoboxe and its corresponding elemental mapping images of Ni, Co and P. Reproduced with permission [76]. © 2017 WILEY–VCH Verlag GmbH & Co. KGaA

to produce Mo-Co LDH arrays, and is then phosphorised with NaH_2PO_2 to generate hollow CoP nanoarrays.

It is previously mentioned that non-metallic elements can be released from the organic linkers during the thermal treatments of MOFs and take part in the reaction with metallic elements to form metal compound active sites. This is a more favourable route based on the consideration of material and energy saving. In the case of MOF-derived metal phosphides, P-containing organic ligands can be applied as an intrinsic source of phosphorus. In addition to the merits of material and energy saving, considering the toxicity of PH_3, the use of P-containing ligands also become a less toxic and more environmentally friendly way to produce MOF-derived metal phosphides. A representative example was demonstrated by Wang and co-workers to produce FeNi bimetallic phosphide (FeNiP) nanoparticles anchored on hollow carbon structures, which are derived from a Ni-based MOF with H_3TPO (H_3TPO = tris-(4-carboxylphenyl)phosphine oxide)) and DABCO (DABCO = 1,4-diazabicyclo[2.2.2]-octane) as the linkers, denoted as BMM-10 [78]. As illustrated in Fig. 2.13a, after the synthesis of this Ni-based MOF BMM-10, it is acid-etched by the hydrolysis of $Fe(NO_3)_3$ in ethanol solution to form Fe–Ni hollow nanoparticles (Fe–Ni-HNP), where the crystalline structure of BMM-10 is destroyed. As depicted in Fig. 2.13b, chemical analysis suggests that the uncoordinated P = O bonds in TPO-2 linkers tend to be transformed into P-O during the $Fe(NO_3)_3$ etching process, while the coordinated P = O bonds in TPO-1 linkers tend to decompose during carbonisation at low temperatures. Then, the decomposition of a large amount of P-O and C-P bonds promotes the conversion from FeNi to FeNiP. It is worth mentioning that the direct carbonisation of MOFs with P-containing organic linkers is not always applicable for the formation of functional MOF-derived metal phosphides. In one of the authors' earlier work [79], they developed a cage-like Zn-based MOF with

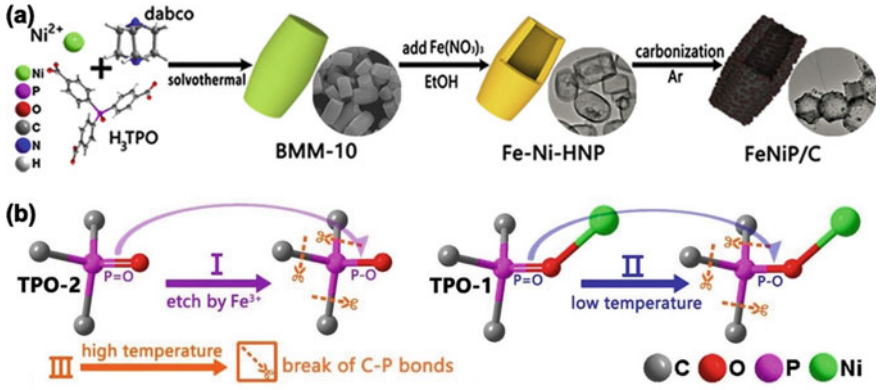

Fig. 2.13 **a** An illustration of the synthesis of a FeNi bimetallic phosphide hollow carbon composite from a Ni-based MOF with P-containing organic linker H3TPO as the intrinsic source of phosphorus. **b** A schematic of structural change from P = O to P–O bonds during $Fe(NO_3)_3$ etching and low temperature treatments, and the breaking of C–P bonds at high temperature carbonisation. Reproduced with permission [78]. © 2017 Elsevier

the same H_3TPO and DABCO as organic linkers. However, its direct carbonisation results in the formation of corrosive phosphates, which causes the collapse of the cage-like structure and the formation of large agglomerates of metallic phosphide particles.

2.4.4 MOF-Derived Metal Sulphides

Metal sulphides (M_xS_y) are another group of frequently encountered in MOF derivative-related studies. S atom in M_xS_y plays a similar active role in comparison with that of P atom in M_xP_y due to its high electronegativity as well. However, S is even more electronegative than that of P, which is not necessarily an advantage for S as an active site [58]. The stronger interaction can enhance the adsorption of reactants (e.g. protons in HER) on S active sites. However, it can also make it more difficult for the reaction products being desorbed from S active sites (e.g., H_2 in HER) [80]. The overall activity of M_xS_y can be tailored by the choice of different metals, metal/sulphur ratios and material structures. In this case, thanks to the diversity of MOFs, they can be used to produce MOF-derived M_xS_y with varied structural and compositional characteristics. The synthesis methods for MOF-derived M_xS_y are very similar to those for MOF-derived M_xP_y. They can exist in the form of either M_xS_y or M_xS_y-doped carbon, which can be obtained by means of either thermal treatments with external sources of S (such as CS_2 and S powders) or direct calcination/carbonisation of MOFs with S-containing organic linkers. There are also reports of converting MOFs to M_xS_y through chemical reaction routes at ambient conditions without the need for thermal treatments.

In the case of MOF-derived M_xS_y, Zhou and colleagues adopted the two-step LDH formation and sulfuration method to produce MOF-derived NiCo bimetallic sulphides [81]. In their work, ZIF-67 is firstly grown on $Ti_3C_2T_x$ nanosheets (T_x stands for surface terminal groups such as -F_x and -OH_x), followed by the immersion of ZIF-67@ $Ti_3C_2T_x$ nanosheets into a $Ni(NO_3)_2$ ethanol solution, where ZIF-67 is etched and converted into NiCo bimetallic LDH. Then, this bimetallic LDH is sulfurised by means of thermal treatments at 400 °C in the CS_2 gas flow. In the case of MOF-derived M_xS_y-doped carbon, Shao et al. synthesised FeS2-doped porous carbon by means of the two-step carbonisation and sulfuration of MIL-88 (Fe), which is a Fe-based MOF with the 2-aminoterephthalic acid linkers. The authors firstly carbonised MIL-88 (Fe) at 600 °C in the N_2 gas flow to produce MOF-derived porous carbon with Fe nanoparticles [82]. Then, this Fe-doped porous carbon is further mixed with sulphur powder, which are placed at the downstream and upstream of the carrier gas (N_2 in this work), respectively. The sulfuration reaction is carried out at 500 °C.

Apart from the use of external sources of S, M_xS_y can also be produced by the direct carbonisation/calcination of MOF precursors with S-containing linkers. A representative work was published by Zhao et al., where they designed and synthesised a 2D Co-based MOF with two organic ligands H_2BDC and SPDP (SPDP =

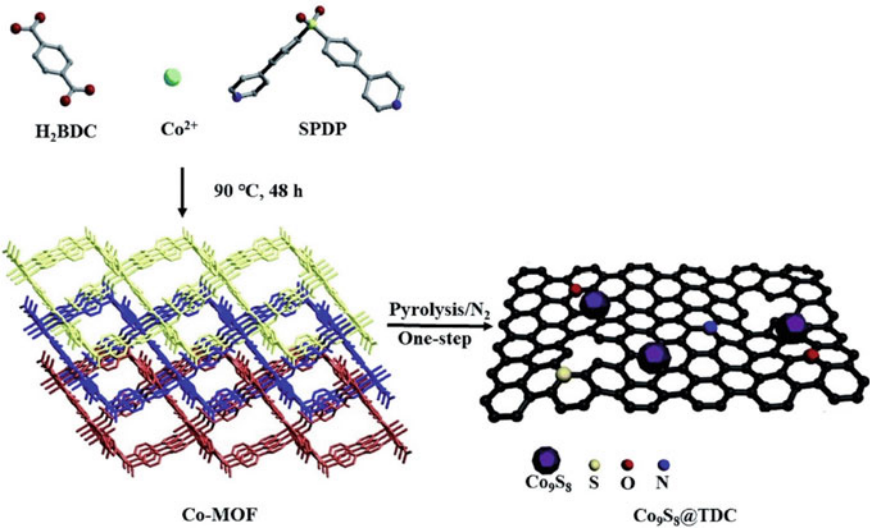

Fig. 2.14 An illustration of the synthesis of a Co-based MOF with both H_2BDC and S-containing SPDP as the bridging ligands, making it possible to produce Co_9S_8 in the resulting porous carbon in a single-step carbonisation. Reproduced with permission [83]. © 2019 Royal Society of Chemistry

4,4′-(sulfonylbis(4,1-phenylene))dipyridine) [83]. As illustrated in Fig. 2.14, since SPDP is a S-containing ligand, a simple one-step carbonisation is able to promote the formation of Co_9S_8 nanoparticles encapsulated in MOF-derived carbon matrix.

In addition to the thermal treatment methods, the synthesis of metal sulphides can be carried out by means of chemical reactions as well. Similar to the cases of MOF-derived metal oxides and hydroxides, PBA-type MOFs can be utilised to produce metal sulphides with interesting structures and morphologies. Again, the same research group, which presented their works on PB-derived Fe_2O_3 and $Fe(OH)_3$, reported another continued research on the synthesis of NiS nanoframes from Ni-Co PBA nanocube templates ($Ni_3[Co(CN)_6]_2$) [84]. In this work, NiS is synthesised by the direct reaction between the Ni-Co PBA and the Na_2S solution, which is carried out by means of the solvothermal method in autoclaves at 100 °C. As illustrated in Fig. 2.15a, an anisotropic chemical etching and anion exchange mechanism is proposed, where the reaction tends to start at the edge of the PBA cube due to higher curvature and roughness with more defects. SEM images in Fig. 2.15b–e demonstrate gradual structural change from the PBA cubic form to NiS nanoframes at different passing hours. Dong et al. employed a similar approach with ZIF-8 but using a different chemical source of S, that is, thioacetamide (TAA). In this work, the as-prepared ZIF-8 is mixed with TAA in the ethanol solution and sealed in an autoclave for the solvothermal reaction at 85 °C, which converts ZIF-8 into ZnS [85]. This solvothermal sulfuration method was also adopted by Yilmaz et al. to produce Co_9S_8 by the sealed reaction between ZIF-67 and TAA at 100 °C [66].

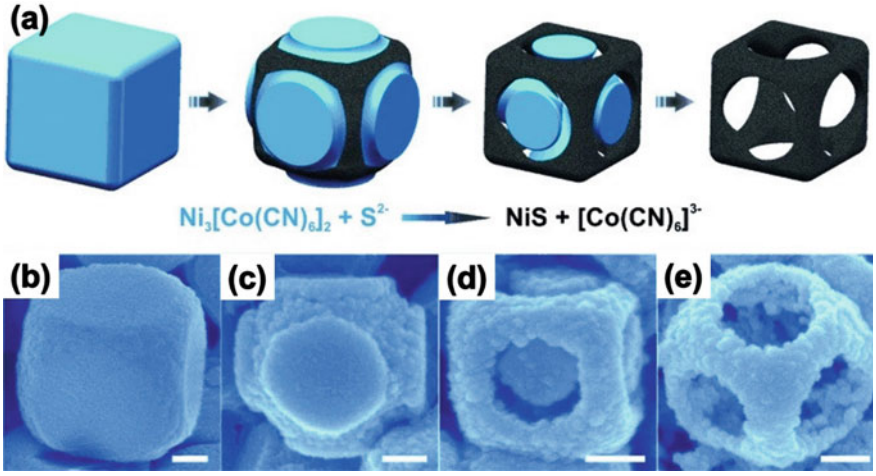

Fig. 2.15 **a** An illustration of the synthetic procedure of NiS nanoframes by means of the reaction between $Ni_3[Co(CN)_6]_2$ and Na_2S. SEM images show the gradual structural change from $Ni_3[Co(CN)_6]_2$ nanocubes to NiS nanoframes in (**b**) 0 h. **c** 0.5 h. **d** 2 h. **e** 6 h (scale bar: 100 nm). Reproduced with permission [84]. © 2015 WILEY–VCH Verlag GmbH & Co. KGaA

2.4.5 MOF-Derived Metal Selenides

Owing to their unique electronic structure and electrical properties, in recent years, metal selenides (M_xSe_y) arise like a "rising star" in the field of transition metal chalcogenides for energy conversion and storage applications, once which mainly focused on M_xS_y- and M_xP_y-based materials. When compared with many other transition metal chalcogenides, M_xSe_y demonstrates more appealing performance on the aspects of charge transfer and electronic conductivity [86, 87]. In addition, while M_xSe_y can also attract protons, Se sites in M_xSe_y exhibit weaker bonding strengths with reactants, which is favourable for the desorption of reaction products in some catalytic reactions. For example, Se–H show a lower bonding strength (276 kJ mol^{-1}) than those of P–H (322 kJ mol^{-1}) and S–H (363 kJ mol^{-1}), which is in favour of hydrogen desorption from the active sites [80]. The excellence of M_xSe_y motivates the enthusiasm of researchers to look into the design and synthesis of M_xSe_y with different structural and compositional features, in order to the tailor the functionality of M_xSe_y for a wide range of applications. The above-mentioned merits of M_xSe_y encourages material researchers to take the advantages of MOFs as effective precursors to fabricate M_xSe_y-based materials, in order to fully explore their potentials.

The synthesis methods of MOF-derived M_xSe_y almost resemble those for MOF-derived M_xS_y and M_xP_y, which mainly involve single- or multi-step carbonisation/calcination and selenisation processes. For example, in the case of MOF-derived M_xSe_y compounds, the two-step calcination and selenisation process was utilised by

Zhao et al. to produce $CoSe_2$ with a hierarchical nanosheet structure from a Co-based MOF with methylamine and formic acid as organic linkers. At first, this Co-based MOF is calcined at 400 °C in air to produce Co_3O_4 microcubes. Then, $CoSe_2$ microcubes are produced through another two-step hydrothermal reaction, where Se reacts with NaOH to generate Se^{2-} ions at 200 °C, followed by the subsequent anion exchange reaction between Se^{2-} and Co_3O_4 to generate $CoSe_2$ at different temperatures from 140 to 200 °C. 160 °C is found to be the optimised hydrothermal temperature because of the formation of the hierarchical nanosheet structure, which maximises the surface to volume ratio of the material and increase the interfacial contact area. A lower hydrothermal temperature can result in an incomplete selenisation process, while a higher hydrothermal temperature promotes the formation of nanorods rather than nanosheets. Besides hydrothermal reactions, selenisation reactions can also be carried out by means of carbonising the mixture of MOFs and Se powders. For example, in Yuan et al.'s work [88], the mixture of Fe-Zn bimetallic MOF-5 (ligands: H_2BDC) and Se powder is carbonised at 350 °C in Ar atmosphere to fabricate ZnSe-FSe_2.

Despite the wide adoption of the above-mentioned thermal selenisation treatment, it faces a major issue with the loss of Se due to its evaporation if the heating temperature is above its boiling point (~685 °C) [89]. A large amount of vaporised Se is carried away by the carrier gas before they can react with MOFs or MOF derivatives. This issue is not just applicable to the synthesis of metal selenides but also in the case of phosphorisation and sulphurisation. In this case, as illustrated in Fig. 2.16, Yang and colleagues proposed a confined thermal treatment method to fabricate $Se/CoSe_2/C$ composite from ZIF-67 [90]. In their work, the single-step carbonisation and selenisation process is carried out in a vacuum-sealed glass vessel. This confined reaction space helps to preserve vaporised Se, which can maximise the Se loading in the MOF-derived carbon composite. This does not just mean a thorough

Fig. 2.16 An illustration of the single-step carbonisation and selenisation treatment of ZIF-67 with the Se powder in a vacuum-sealed glass vessel, leading to the formation of MOF-derived $Se/CoSe_2/C$ composite. Reproduced with permission [90]. © 2019 Elsevier

selenisation reaction between Co and Se to generate $CoSe_2$ but also facilitates the vapor deposition of elemental Se, leading to the formation of $Se/CoSe_2/C$ composite.

2.4.6 MOF-Derived Metal Nitrides

Metal nitrides (M_xN_y) are a group of interstitial compounds, which means nitrogen atoms in M_xN_y usually occupy the interstitial sites of the parent metals. Thanks to their characteristic chemical structures, metal nitrides demonstrate promising electrical conductivity, chemical stability and electrocatalytic activity, particularly in terms of their application in electrochemical energy conversion and storage [91]. Therefore, it is inevitable for material researchers to take the structural and compositional advantages of MOFs to engineer the nanostructures and chemical compositions of M_xN_y.

NH_3 was the most frequently used the source of nitrogen to react with metals and form MOF-derived M_xN_y [92, 93]. For example, in Liu et al.'s work [94], The authors firstly convert a Co-MOF (ligands: 2-methylimidazole) into $NiCo_2O_4$ in two steps: the hydrolysis of Co-MOF by $Ni(NO_3)_2$ ethanol solution to generate Ni-Co LDH and the oxidation of Ni-Co LDH in air at 350 °C to generate $NiCo_2O_4$. Then, $NiCo_2O_4$ is nitridised by means of thermal treatments with NH_3 to form a heterostructure of Ni-doped Co–Co_2N at 350 °C. Lower NH_3 treatment temperatures of 250 and 300 °C lead to the formation of Ni-doped CoN and Co_2N, respectively. This is due to the simultaneous reduction and nitridisation of $NiCo_2O_4$ by NH_3 at these comparatively lower temperatures. However, when the treatment temperature increases to 350 °C, NH_3 decomposes into N_2 and H_2, leading to an enhanced reduction effect and thus elemental Co appears to form a heterostructure with Co_2N. When the temperature is further elevated to 400 °C, the nitridisation effect is superior than that of reduction, and all Co components are nitridised into the Co_3N phase. Lai et al. synthesised a Ni–Co nitrides/carbon hybrid nanocages from ZIF-67 by using NH_3 as the source of nitrogen and following the same two-step of LDH formation and nitridisation process [95]. Instead of multiple stages of transformation, there are also reports of fabricating MOF-derived M_xN_y through just a in situ single carbonisation and nitridisation step in NH_3. For example, a porous carbon doped with $Co_{5.47}$ N nanoparticles was directly formed by the in situ carbonisation and nitridisation of ZIF-67 at 700 °C in Chen et al.'s work [96]. Another example was demonstrated by Kang et al. for the in situ formation of Co_3N-doped carbon nanocubes derived from a PBA-type MOF $Co_3[Co(CN)_6]_2$ in a single-step carbonisation and nitridisation in NH_3 at 450 °C [97] (Fig. 2.17).

In terms of the formation of metal nitrides with intrinsic nitrogen from organic linkers, there is a report of the derivation of $Co/CoN/Co_2P$ ternary carbon composite from a Co-based MOF ($[Co_3(pimda)_2(H_2O)_5]$) with H_3pimda (H_3pimda = 2-propyl-1H-imidazole-4,5-dicarboxylic acid) as the bridging ligands [98, 99]. Although the formation of Co_2P is carried out by the frequently applied thermal treatment method with NaH_2PO_2, since H_3pimda is a N-containing ligand, the formation of CoN purely

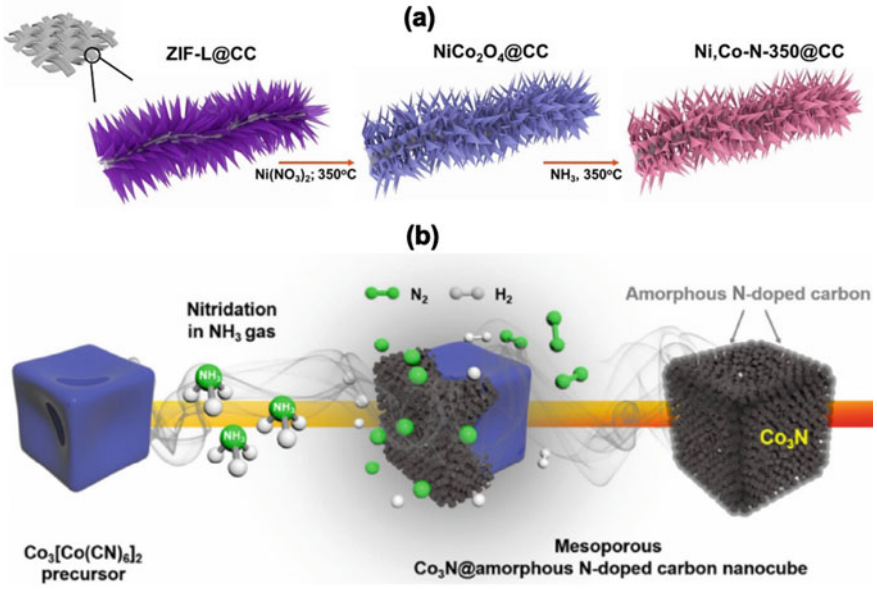

Fig. 2.17 **a** The two-step oxide formation and nitridisation process in Liu et al.'s work [94]. Reproduced with permission. © 2018 American Chemical Society. **b** The single-step carbonisation and nitridisation process in Kang et al. work. Reproduced with permission [97]. © 2019 Springer

relies on this intrinsic source of nitrogen from the H_3pimda ligand rather than any external chemical source. Apart from the above-discussed example, there is another report of the synthesis of CoN_3-doped carbon derived from Zn-ZIF-67, that is, CoZn bimetallic MOFs with a range of Co/Zn ratios [100]. The authors propose that the formation of CoN_3 species is attributed to the release of NH_3 from decomposed 2-mehylimidazole ligands. The formation of the microporous channels by Zn evaporation is also important for the diffusion of NH_3 to the Co sites, where nitridisation reactions can take place. In order to demonstrate the determining role of ZIF-67 in the formation of CoN_3, the authors pyrolysed a mixture of Co and Zn salts with the 2-methylimidazole ligands, where no CoN_3 is found in the pyrolysis products.

In summary, the structural and chemical diversities of MOFs make them ideal precursor materials to fabricate a variety of MOF-derived metal compounds with designed nanostructures and chemical compositions, in order to fulfil their functions in a wide range of applications. Metal compounds can be derived MOF precursors by means of either high temperature thermal treatments or chemical reactions at comparatively lower temperatures (such as room temperature). In the case of high temperature thermal treatments, on the one hand, non-metallic elements in MOF-derived metal compounds can come from extrinsic chemical sources in the form of reactive gas atmospheres, decomposed products from reactive solid chemicals and elementary substances in powdery form. On the other hand, they can come from

decomposed organic linkers during thermal treatments. In the case of chemical reactions at comparatively lower temperatures, non-metallic elements can convert MOF precursors into metal compounds by means of either hydrothermal or solvothermal reactions based on the hydrolysis and anion exchange mechanisms. In comparison, the latter material synthesis route is more favourable due to the consideration of material and energy savings.

References

1. Furukawa H, Cordova KE, O'Keeffe M, Yaghi OM (2013) The chemistry and applications of metal-organic frameworks. Science 341(6149):1230444. https://doi.org/10.1126/science.1230444
2. Zhu B, Liang Z, Xia D, Zou R (2019) Metal-organic frameworks and their derivatives for metal-air batteries. Energy Storage Mater 23:757–771. https://doi.org/10.1016/j.ensm.2019.05.022
3. Zhu B, Zou R, Xu Q (2018) Metal-organic framework based catalysts for hydrogen evolution. Adv Energy Mater 8(24):1801193. https://doi.org/10.1002/aenm.201801193
4. Xu G, Nie P, Dou H, Ding B, Li L, Zhang X (2017) Exploring metal organic frameworks for energy storage in batteries and supercapacitors. Mater Today 20(4):191–209. https://doi.org/10.1016/j.mattod.2016.10.003
5. Langmi HW, Ren J, North B, Mathe M, Bessarabov D (2014) Hydrogen storage in metal-organic frameworks: a review. Electrochim Acta 128:368–392. https://doi.org/10.1016/j.electacta.2013.10.190
6. Yang W, Li X, Li Y, Zhu R, Pang H (2019) Applications of metal–organic-framework-derived carbon materials. Adv Energy Mater 31(6):1804740. https://doi.org/10.1002/adma.201804740
7. Qi L, Tang X, Wang Z, Peng X (2017) Pore characterization of different types of coal from coal and gas outburst disaster sites using low temperature nitrogen adsorption approach. Int J Min Sci Technol 27(2):371–377. https://doi.org/10.1016/j.ijmst.2017.01.005
8. Rodríguez-Reinoso F, Sepúlveda-Escribano A (2001) Chapter 9: porous carbons in adsorption and catalysis. In: Nalwa HS (ed) Handbook of surfaces and interfaces of materials. Academic Press, Burlington, pp 309–355
9. Yang X-Y, Chen L-H, Li Y, Rooke JC, Sanchez C, Su B-L (2017) Hierarchically porous materials: synthesis strategies and structure design. Chem Soc Rev 46(2):481–558. https://doi.org/10.1039/C6CS00829A
10. Yilmaz G, Peh SB, Zhao D, Ho GW (2019) Atomic- and molecular-level design of functional metal–organic frameworks (MOFs) and derivatives for energy and environmental applications. Adv Sci 6(21):1901129. https://doi.org/10.1002/advs.201901129
11. Liang Z, Qu C, Xia D, Zou R, Xu Q (2018) Atomically dispersed metal sites in MOF-based materials for electrocatalytic and photocatalytic energy conversion. Angew Chem Int Ed 57(31):9604–9633. https://doi.org/10.1002/anie.201800269
12. Ejaz A, Jeon S (2018) The individual role of pyrrolic, pyridinic and graphitic nitrogen in the growth kinetics of Pd NPs on N-rGO followed by a comprehensive study on ORR. Int J Hydrogen Energy 43(11):5690–5702. https://doi.org/10.1016/j.ijhydene.2017.12.184
13. Zhu B, Xia D, Zou R (2018) Metal-organic frameworks and their derivatives as bifunctional electrocatalysts. Coord Chem Rev 376:430–448. https://doi.org/10.1016/j.ccr.2018.07.020
14. Chen B, Yang Z, Zhu Y, Xia Y (2014) Zeolitic imidazolate framework materials: recent progress in synthesis and applications. J Mater Chem A 2(40):16811–16831. https://doi.org/10.1039/C4TA02984D

15. Park KS, Ni Z, Côté AP, Choi JY, Huang R, Uribe-Romo FJ, Chae HK, O'Keeffe M, Yaghi OM (2006) Exceptional chemical and thermal stability of zeolitic imidazolate frameworks. Proc Nat Acad Sci USA 103(27):10186–10191. https://doi.org/10.1073/pnas.0602439103%JProceedingsoftheNationalAcademyofSciences
16. Zhong G, Liu D, Zhang J (2018) The application of ZIF-67 and its derivatives: adsorption, separation, electrochemistry and catalysts. J Mater Chem A 6(5):1887–1899. https://doi.org/10.1039/C7TA08268A
17. Qian J, Sun F, Qin L (2012) Hydrothermal synthesis of zeolitic imidazolate framework-67 (ZIF-67) nanocrystals. Mater Lett 82:220–223. https://doi.org/10.1016/j.matlet.2012.05.077
18. Xia W, Zhu J, Guo W, An L, Xia D, Zou R (2014) Well-defined carbon polyhedrons prepared from nano metal–organic frameworks for oxygen reduction. J Mater Chem A 2(30):11606–11613. https://doi.org/10.1039/C4TA01656D
19. Jagadeesh RV, Murugesan K, Alshammari AS, Neumann H, Pohl M-M, Radnik J, Beller M (2017) MOF-derived cobalt nanoparticles catalyze a general synthesis of amines. Science 358(6361):326–332. https://doi.org/10.1126/science.aan6245%JScience
20. Zou F, Chen Y-M, Liu K, Yu Z, Liang W, Bhaway SM, Gao M, Zhu Y (2016) Metal organic frameworks derived hierarchical hollow NiO/Ni/graphene composites for lithium and sodium storage. ACS Nano 10(1):377–386. https://doi.org/10.1021/acsnano.5b05041
21. Yun R, Hong L, Ma W, Jia W, Liu S, Zheng B (2019) Fe/Fe_2O_3@N-dopped porous carbon: a high-performance catalyst for selective hydrogenation of nitro compounds. ChemCatChem 11(2):724–728. https://doi.org/10.1002/cctc.201801626
22. Farisabadi A, Moradi M, Hajati S, Kiani MA, Espinos JP (2019) Controlled thermolysis of MIL-101(Fe, Cr) for synthesis of FexOy/porous carbon as negative electrode and Cr_2O_3/porous carbon as positive electrode of supercapacitor. Appl Surf Sci 469:192–203. https://doi.org/10.1016/j.apsusc.2018.11.053
23. McNamara ND, Kim J, Hicks JC (2016) Controlling the pyrolysis conditions of microporous/mesoporous MIL-125 to synthesize porous, carbon-supported Ti catalysts with targeted Ti phases for the oxidation of dibenzothiophene. Energy Fuels 30(1):594–602. https://doi.org/10.1021/acs.energyfuels.5b01946
24. Zong M, Huo S, Liu Y, Zhang X, Li K (2021) Hydrangea-like nitrogen-doped porous carbons derived from NH2-MIL-53(Al) for high-performance capacitive deionization. Sep Purif Technol 256:117818. https://doi.org/10.1016/j.seppur.2020.117818
25. Cai J, Li Y, Zhang M, Li Z (2019) Cooperation in Cu-MOF-74-Derived Cu–Cu_2O–C nanocomposites to enable efficient visible-light-initiated phenylacetylene coupling. Inorg Chem 58(12):7997–8002. https://doi.org/10.1021/acs.inorgchem.9b00733
26. Li Q, Wu J, Huang L, Gao J, Zhou H, Shi Y, Pan Q, Zhang G, Du Y, Liang W (2018) Sulfur dioxide gas-sensitive materials based on zeolitic imidazolate framework-derived carbon nanotubes. J Mater Chem A 6(25):12115–12124. https://doi.org/10.1039/C8TA02036A
27. Liu B, Shioyama H, Akita T, Xu Q (2008) Metal-organic framework as a template for porous carbon synthesis. J Am Chem Soc 130(16):5390–5391. https://doi.org/10.1021/ja7106146
28. Tan J, He X, Yin F, Chen B, Liang X, Li G, Yin H (2020) Bimetallic ZnCo zeolitic imidazolate framework/polypyrrole-polyaniline derived Co/N-doped carbon for oxygen reduction reaction. Int J Hydrogen Energy 45(31):15453–15464. https://doi.org/10.1016/j.ijhydene.2020.04.018
29. Meng Z, Cai S, Wang R, Tang H, Song S, Tsiakaras P (2019) Bimetallic−organic framework-derived hierarchically porous Co-Zn-N-C as efficient catalyst for acidic oxygen reduction reaction. Appl Catal B 244:120–127. https://doi.org/10.1016/j.apcatb.2018.11.037
30. Ding M, Shi W, Guo L, Leong ZY, Baji A, Yang HY (2017) Bimetallic metal–organic framework derived porous carbon nanostructures for high performance membrane capacitive desalination. J Mater Chem A 5(13):6113–6121. https://doi.org/10.1039/C7TA00339K
31. Gao Y, Zhu Y, Chen Z, Hu C (2020) Nitrogen-coordinated cobalt embedded in a hollow carbon polyhedron for superior catalytic oxidation of organic contaminants with peroxymonosulfate. ACS ES&T Eng 1:76–85. https://doi.org/10.1021/acsestengg.0c00039

32. Huo Q, Li J, Qi X, Liu G, Zhang X, Zhang B, Ning Y, Fu Y, Liu J, Liu S (2019) Cu, Zn-embedded MOF-derived bimetallic porous carbon for adsorption desulfurization. Chem Eng J 378:122106. https://doi.org/10.1016/j.cej.2019.122106
33. Yang Y, Mao K, Gao S, Huang H, Xia G, Lin Z, Jiang P, Wang C, Wang H, Chen Q (2018) O-, N-atoms-coordinated mn cofactors within a graphene framework as bioinspired oxygen reduction reaction electrocatalysts. Adv Mater 30(28):1801732. https://doi.org/10.1002/adma.201801732
34. Han X, Ling X, Yu D, Xie D, Li L, Peng S, Zhong C, Zhao N, Deng Y, Hu W (2019) Atomically dispersed binary Co-Ni sites in nitrogen-doped hollow carbon nanocubes for reversible oxygen reduction and evolution. Adv Mater 31(49):1905622. https://doi.org/10.1002/adma.201905622
35. Zhu Q-L, Xia W, Zheng L-R, Zou R, Liu Z, Xu Q (2017) Atomically dispersed Fe/N-doped hierarchical carbon architectures derived from a metal-organic framework composite for extremely efficient electrocatalysis. ACS Energy Lett 2(2):504–511. https://doi.org/10.1021/acsenergylett.6b00686
36. Huang H, Shen K, Chen F, Li Y (2020) Metal-organic frameworks as a good platform for the fabrication of single-atom catalysts. ACS Catal 10(12):6579–6586. https://doi.org/10.1021/acscatal.0c01459
37. Ren Q, Wang H, Lu X-F, Tong Y-X, Li G-R (2018) Recent progress on MOF-derived heteroatom-doped carbon-based electrocatalysts for oxygen reduction reaction. Adv Sci 5(3):1700515. https://doi.org/10.1002/advs.201700515
38. Tang C, Zhang Q (2017) Nanocarbon for oxygen reduction electrocatalysis: dopants. Edges and Defects. 29(13):1604103. https://doi.org/10.1002/adma.201604103
39. Wang X, Li Y (2016) Nanoporous carbons derived from MOFs as metal-free catalysts for selective aerobic oxidations. J Mater Chem A 4(14):5247–5257. https://doi.org/10.1039/C6TA00324A
40. Yang L, Xu G, Ban J, Zhang L, Xu G, Lv Y, Jia D (2019) Metal-organic framework-derived metal-free highly graphitized nitrogen-doped porous carbon with a hierarchical porous structure as an efficient and stable electrocatalyst for oxygen reduction reaction. J Colloid Interface Sci 535:415–424. https://doi.org/10.1016/j.jcis.2018.10.007
41. Qian Y, Hu Z, Ge X, Yang S, Peng Y, Kang Z, Liu Z, Lee JY, Zhao D (2017) A metal-free ORR/OER bifunctional electrocatalyst derived from metal-organic frameworks for rechargeable Zn-air batteries. Carbon 111:641–650. https://doi.org/10.1016/j.carbon.2016.10.046
42. Wang X, Li X, Ouyang C, Li Z, Dou S, Ma Z, Tao L, Huo J, Wang S (2016) Nonporous MOF-derived dopant-free mesoporous carbon as an efficient metal-free electrocatalyst for the oxygen reduction reaction. J Mater Chem A 4(24):9370–9374. https://doi.org/10.1039/C6TA03015G
43. He F, Chen G, Zhou Y, Yu Y, Li L, Hao S, Liu B (2016) ZIF-8 derived carbon (C-ZIF) as a bifunctional electron acceptor and HER cocatalyst for g-C3N4: construction of a metal-free, all carbon-based photocatalytic system for efficient hydrogen evolution. J Mater Chem A 4(10):3822–3827. https://doi.org/10.1039/C6TA00497K
44. Zhang P, Sun F, Xiang Z, Shen Z, Yun J, Cao D (2014) ZIF-derived in situ nitrogen-doped porous carbons as efficient metal-free electrocatalysts for oxygen reduction reaction. Energy Environ Sci 7(1):442–450. https://doi.org/10.1039/C3EE42799D
45. Wu M, Wang K, Yi M, Tong Y, Wang Y, Song S (2017) A facile activation strategy for an MOF-derived metal-free oxygen reduction reaction catalyst: direct access to optimized pore structure and nitrogen species. ACS Catal 7(9):6082–6088. https://doi.org/10.1021/acscatal.7b01649
46. Pan B, Zhu X, Wu Y, Liu T, Bi X, Feng K, Han N, Zhong J, Lu J, Li Y, Li Y (2020) Toward highly selective electrochemical CO_2 reduction using metal-free heteroatom-doped carbon. Adv Sci 7(16):2001002. https://doi.org/10.1002/advs.202001002
47. Zhao X, Yang H, Jing P, Shi W, Yang G, Cheng P (2017) A metal-organic framework approach toward highly nitrogen-doped graphitic carbon as a metal-free photocatalyst for hydrogen evolution. Small 13(9):1603279. https://doi.org/10.1002/smll.201603279

48. Liu Y, Miao W, Fang X, Tang Y, Wu D, Mao S (2020) MOF-derived metal-free N-doped porous carbon mediated peroxydisulfate activation via radical and non-radical pathways: Role of graphitic N and CO. Chem Eng J 380:122584. https://doi.org/10.1016/j.cej.2019.122584
49. Yang M, Zhang Y, Jian J, Fang L, Li J, Fang Z, Yuan Z, Dai L, Chen X, Yu D (2019) Donor-acceptor nanocarbon ensembles to boost metal-free All-pH hydrogen evolution catalysis by combined surface and dual electronic modulation. Angew Chem Int Ed 58(45):16217–16222. https://doi.org/10.1002/anie.201907826
50. Gadipelli S, Li Z, Zhao T, Yang Y, Yildirim T, Guo Z (2017) Graphitic nanostructures in a porous carbon framework significantly enhance electrocatalytic oxygen evolution. J Mater Chem A 5(47):24686–24694. https://doi.org/10.1039/C7TA03027D
51. Li Y, Xu Y, Yang W, Shen W, Xue H, Pang H (2018) MOF-derived metal oxide composites for advanced electrochemical energy storage. Small 14(25):1704435. https://doi.org/10.1002/smll.201704435
52. Liang Q, Chen J, Wang F, Li Y (2020) Transition metal-based metal-organic frameworks for oxygen evolution reaction. Coord Chem Rev 424:213488. https://doi.org/10.1016/j.ccr.2020.213488
53. Li Z, Zheng Y, Liu Q, Wang Y, Wang D, Li Z, Zheng P, Liu Z (2020) Recent advances in nanostructured metal phosphides as promising anode materials for rechargeable batteries. J Mater Chem A 8(37):19113–19132. https://doi.org/10.1039/D0TA06533A
54. Li T, Bai Y, Wang Y, Xu H, Jin H (2020) Advances in transition-metal (Zn, Mn, Cu)-based MOFs and their derivatives for anode of lithium-ion batteries. Coord Chem Rev 410:213221. https://doi.org/10.1016/j.ccr.2020.213221
55. Xu X, Liu J, Liu J, Ouyang L, Hu R, Wang H, Yang L, Zhu M (2018) Na-ion batteries: a general metal-organic framework (MOF)-derived selenidation strategy for in situ carbon-encapsulated metal selenides as high-rate anodes for Na-ion batteries (Adv. Funct. Mater. 16/2018). Adv Funct Mater 28(16):1870108. https://doi.org/10.1002/adfm.201870108
56. Li X, Ao Z, Liu J, Sun H, Rykov AI, Wang J (2016) Topotactic transformation of metal-organic frameworks to graphene-encapsulated transition-metal nitrides as efficient fenton-like catalysts. ACS Nano 10(12):11532–11540. https://doi.org/10.1021/acsnano.6b07522
57. Yu C, Wang Y, Cui J, Yu D, Zhang X, Shu X, Zhang J, Zhang Y, Vajtai R, Ajayan Pulickel M, Wu Y (2018) MOF-74 derived porous hybrid metal oxide hollow nanowires for high-performance electrochemical energy storage. J Mater Chem A 6(18):8396–8404. https://doi.org/10.1039/C8TA01426D
58. Joo J, Kim T, Lee J, Choi S-I, Lee K (2019) Morphology-controlled metal sulfides and phosphides for electrochemical water splitting. Adv Mater 31(14):1806682. https://doi.org/10.1002/adma.201806682
59. Pieraggi B (2008) Diffusion and solid state reactions. In: Gao W, Li Z (eds) Developments in high temperature corrosion and protection of materials. Woodhead Publishing, Cambridge, UK, pp 9–35
60. Zhou J, Dou Y, Zhou A, Shu L, Chen Y, Li J-R (2018) Layered metal-organic framework-derived metal oxide/carbon nanosheet arrays for catalyzing the oxygen evolution reaction. ACS Energy Lett 3(7):1655–1661. https://doi.org/10.1021/acsenergylett.8b00809
61. Zhang L, Wu HB, Madhavi S, Hng HH, Lou XW (2012) Formation of Fe_2O_3 microboxes with hierarchical shell structures from metal-organic frameworks and their lithium storage properties. J Am Chem Soc 134(42):17388–17391. https://doi.org/10.1021/ja307475c
62. Wang B, Han Y, Wang X, Bahlawane N, Pan H, Yan M, Jiang Y (2018) Prussian blue analogs for rechargeable batteries. iScience 3:110–133. https://doi.org/10.1016/j.isci.2018.04.008
63. Xu Y, Zheng S, Tang H, Guo X, Xue H, Pang H (2017) Prussian blue and its derivatives as electrode materials for electrochemical energy storage. Energy Storage Mater 9:11–30. https://doi.org/10.1016/j.ensm.2017.06.002
64. Hurlbutt K, Wheeler S, Capone I, Pasta M (2018) Prussian blue analogs as battery materials. Joule 2(10):1950–1960. https://doi.org/10.1016/j.joule.2018.07.017
65. Fan G, Li F, Evans DG, Duan X (2014) Catalytic applications of layered double hydroxides: recent advances and perspectives. Chem Soc Rev 43(20):7040–7066. https://doi.org/10.1039/C4CS00160E

66. Yilmaz G, Yam KM, Zhang C, Fan HJ, Ho GW (2017) Situ transformation of MOFs into layered double hydroxide embedded metal sulfides for improved electrocatalytic and supercapacitive performance. Adv Master 29(26):1606814. https://doi.org/10.1002/adma.201606814
67. Zhao M, Zhao Q, Li B, Xue H, Pang H, Chen C (2017) Recent progress in layered double hydroxide based materials for electrochemical capacitors: design, synthesis and performance. Nanoscale 9(40):15206–15225. https://doi.org/10.1039/C7NR04752E
68. Cai M, Liu Q, Xue Z, Li Y, Fan Y, Huang A, Li M-R, Croft M, Tyson TA, Ke Z, Li G (2020) Constructing 2D MOFs from 2D LDHs: a highly efficient and durable electrocatalyst for water oxidation. J Mater Chem A 8(1):190–195. https://doi.org/10.1039/C9TA09397D
69. Zhang B, Qi Z, Wu Z, Lui YH, Kim T-H, Tang X, Zhou L, Huang W, Hu S (2019) Defect-rich 2D material networks for advanced oxygen evolution catalysts. ACS Energy Lett 4(1):328–336. https://doi.org/10.1021/acsenergylett.8b02343
70. Zhang L, Wu HB, Lou XW (2013) Metal–Organic-frameworks-derived general formation of hollow structures with high complexity. J Am Chem Soc 135(29):10664–10672. https://doi.org/10.1021/ja401727n
71. Callejas JF, Read CG, Roske CW, Lewis NS, Schaak RE (2016) Synthesis, characterization, and properties of metal phosphide catalysts for the hydrogen-evolution reaction. Chem Mater 28(17):6017–6044. https://doi.org/10.1021/acs.chemmater.6b02148
72. Yang Y, Zhou C, Wang W, Xiong W, Zeng G, Huang D, Zhang C, Song B, Xue W, Li X, Wang Z, He D, Luo H, Ouyang Z (2021) Recent advances in application of transition metal phosphides for photocatalytic hydrogen production. Chem Eng J 405:126547. https://doi.org/10.1016/j.cej.2020.126547
73. Chu W, Hou Y, Liu J, Bai X, Yf G, Cao Z (2020) Zn-Co phosphide porous nanosheets derived from metal-organic-frameworks as battery-type positive electrodes for high-performance alkaline supercapacitors. Electrochim Acta 364:137063. https://doi.org/10.1016/j.electacta.2020.137063
74. Xiao X, He C-T, Zhao S, Li J, Lin W, Yuan Z, Zhang Q, Wang S, Dai L, Yu D (2017) A general approach to cobalt-based homobimetallic phosphide ultrathin nanosheets for highly efficient oxygen evolution in alkaline media. Energy Environ Sci 10(4):893–899. https://doi.org/10.1039/C6EE03145E
75. Liu X, Li W, Zhao X, Liu Y, Nan C-W, Fan L-Z (2019) two birds with one stone: metal-organic framework derived micro-/nanostructured Ni_2P/Ni hybrids embedded in porous carbon for electrocatalysis and energy storage. Adv Funct Mater 29(35):1901510. https://doi.org/10.1002/adfm.201901510
76. He P, Yu X-Y, Lou XW (2017) Carbon-incorporated nickel-cobalt mixed metal phosphide nanoboxes with enhanced electrocatalytic activity for oxygen evolution. Angew Chem Int Ed 56(14):3897–3900. https://doi.org/10.1002/anie.201612635
77. Guan C, Xiao W, Wu H, Liu X, Zang W, Zhang H, Ding J, Feng YP, Pennycook SJ, Wang J (2018) Hollow Mo-doped CoP nanoarrays for efficient overall water splitting. Nano Energy 48:73–80. https://doi.org/10.1016/j.nanoen.2018.03.034
78. Wang X, Chai L, Ding J, Zhong L, Du Y, Li T-T, Hu Y, Qian J, Huang S (2019) Chemical and morphological transformation of MOF-derived bimetallic phosphide for efficient oxygen evolution. Nano Energy 62:745–753. https://doi.org/10.1016/j.nanoen.2019.06.002
79. Qian J, Wang X, Chai L, Liang L-F, Li T-T, Hu Y, Huang S (2018) Robust cage-based zinc-organic frameworks derived dual-doped carbon materials for supercapacitor. Cryst Growth Des 18(4):2358–2364. https://doi.org/10.1021/acs.cgd.7b01765
80. Anantharaj S, Ede SR, Sakthikumar K, Karthick K, Mishra S, Kundu S (2016) Recent trends and perspectives in electrochemical water splitting with an emphasis on sulfide, selenide, and phosphide catalysts of Fe Co, and Ni: a review. ACS Catal 6(12):8069–8097. https://doi.org/10.1021/acscatal.6b02479
81. Zou H, He B, Kuang P, Yu J, Fan K (2018) Metal-organic framework-derived nickel-cobalt sulfide on ultrathin mxene nanosheets for electrocatalytic oxygen evolution. ACS Appl Mater Interfaces 10(26):22311–22319. https://doi.org/10.1021/acsami.8b06272

82. Shao M, Cheng Y, Zhang T, Li S, Zhang W, Zheng B, Wu J, Xiong W-W, Huo F, Lu J (2018) Designing MOFs-derived FeS_2@carbon composites for high-rate sodium ion storage with capacitive contributions. ACS Appl Mater Interfaces 10(39):33097–33104. https://doi.org/10.1021/acsami.8b10110
83. Zhao J-Y, Wang R, Wang S, Lv Y-R, Xu H, Zang S-Q (2019) Metal–organic framework-derived Co9S8 embedded in N, O and S-tridoped carbon nanomaterials as an efficient oxygen bifunctional electrocatalyst. J Mater Chem A 7(13):7389–7395. https://doi.org/10.1039/C8TA12116H
84. Yu X-Y, Yu L, Wu HB, Lou XW (2015) Formation of nickel sulfide nanoframes from metal-organic frameworks with enhanced pseudocapacitive and electrocatalytic properties. Angew Chem 54(18):5331–5335. https://doi.org/10.1002/anie.201500267
85. Dong S, Li C, Ge X, Li Z, Miao X, Yin L (2017) ZnS-Sb_2S_3@C core-double shell polyhedron structure derived from metal-organic framework as anodes for high performance sodium ion batteries. ACS Nano 11(6):6474–6482. https://doi.org/10.1021/acsnano.7b03321
86. Xia X, Wang L, Sui N, Colvin VL, Yu WW (2020) Recent progress in transition metal selenide electrocatalysts for water splitting. Nanoscale 12(23):12249–12262. https://doi.org/10.1039/D0NR02939D
87. Luo M, Yu H, Hu F, Liu T, Cheng X, Zheng R, Bai Y, Shui M, Shu J (2020) Metal selenides for high performance sodium ion batteries. Chem Eng J 380:122557. https://doi.org/10.1016/j.cej.2019.122557
88. Yuan J, Liu W, Zhang X, Zhang Y, Yang W, Lai W, Li X, Zhang J, Li X (2020) MOF derived ZnSe–$FeSe_2$/RGO Nanocomposites with enhanced sodium/potassium storage. J Power Sources 455:227937. https://doi.org/10.1016/j.jpowsour.2020.227937
89. Etteieb S, Magdouli S, Zolfaghari M, Brar S (2020) Monitoring and analysis of selenium as an emerging contaminant in mining industry: a critical review. Sci Total Environ 698:134339. https://doi.org/10.1016/j.scitotenv.2019.134339
90. Yang X, Wang S, Yu DYW, Rogach AL (2019) Direct conversion of metal-organic frameworks into selenium/selenide/carbon composites with high sodium storage capacity. Nano Energy 58:392–398. https://doi.org/10.1016/j.nanoen.2019.01.064
91. Wang H, Li J, Li K, Lin Y, Chen J, Gao L, Nicolosi V, Xiao X, Lee J-M (2021) Transition metal nitrides for electrochemical energy applications. Chem Soc Rev. https://doi.org/10.1039/D0CS00415D
92. Feng X, Wang H, Bo X, Guo L (2019) Bimetal-organic framework-derived porous rodlike cobalt/nickel nitride for all-pH value electrochemical hydrogen evolution. ACS Appl Mater Interfaces 11(8):8018–8024. https://doi.org/10.1021/acsami.8b21369
93. Hu S, Wang S, Feng C, Wu H, Zhang J, Mei H (2020) Novel MOF-derived nickel nitride as high-performance bifunctional electrocatalysts for hydrogen evolution and urea oxidation. ACS Sustain Chem Eng 8(19):7414–7422. https://doi.org/10.1021/acssuschemeng.0c01450
94. Liu X, Zang W, Guan C, Zhang L, Qian Y, Elshahawy AM, Zhao D, Pennycook SJ, Wang J (2018) Ni-doped cobalt-cobalt nitride heterostructure arrays for high-power supercapacitors. ACS Energy Lett 3(10):2462–2469. https://doi.org/10.1021/acsenergylett.8b01393
95. Lai J, Huang B, Chao Y, Chen X, Guo S (2019) Strongly coupled nickel-cobalt nitrides/carbon hybrid nanocages with Pt-like activity for hydrogen evolution catalysis. Adv Mater 31(2):1805541. https://doi.org/10.1002/adma.201805541
96. Chen Z, Ha Y, Liu Y, Wang H, Yang H, Xu H, Li Y, Wu R (2018) In situ formation of cobalt nitrides/graphitic carbon composites as efficient bifunctional electrocatalysts for overall water splitting. ACS Appl Mater Interfaces 10(8):7134–7144. https://doi.org/10.1021/acsami.7b18858
97. Kang BK, Im SY, Lee J, Kwag SH, Kwon SB, Tiruneh S, Kim M-J, Kim JH, Yang WS, Lim B, Yoon DH (2019) In-situ formation of MOF derived mesoporous Co_3N/amorphous N-doped carbon nanocubes as an efficient electrocatalytic oxygen evolution reaction. Nano Res 12(7):1605–1611. https://doi.org/10.1007/s12274-019-2399-3

98. Hu L, Hu Y, Liu R, Mao Y, Balogun MS, Tong Y (2019) Co-based MOF-derived Co/CoN/Co_2P ternary composite embedded in N- and P-doped carbon as bifunctional nanocatalysts for efficient overall water splitting. Int J Hydrogen Energy 44(23):11402–11410. https://doi.org/10.1016/j.ijhydene.2019.03.157
99. Wang L-F, Qiu J-Z, Wu S-G, Chen Y-C, Li C-J, Li Q-W, Liu J-L, Tong M-L (2018) Humidity sensitive structural dynamics and solvatomagnetic effects in a 3D Co(II)-based coordination polymer. Inorg Chem 57(7):4070–4076. https://doi.org/10.1021/acs.inorgchem.8b00235
100. Lai S, Xu L, Liu H, Chen S, Cai R, Zhang L, Theis W, Sun J, Yang D, Zhao X (2019) Controllable synthesis of CoN_3 catalysts derived from Co/Zn-ZIF-67 for electrocatalytic oxygen reduction in acidic electrolytes. J Mater Chem A 7(38):21884–21891. https://doi.org/10.1039/C9TA08134H

Chapter 3
Batteries

Lin-Hai Pan, Hai-Yan He, Jian-Hua Wang, Xin Liu, Jia-Wei Qian, Jingwei Chen, and Li-Feng Chen

3.1 Introduction

In past decades, the energy crisis has gradually become a major issue due to the continuous economic development [1]. The excessive consumption of conventional fossil fuels has not only accelerated the depletion of non-renewable energy, but also caused serious environmental pollution [2]. Therefore, renewable energy systems, such as solar energy, wind energy, and ocean energy, are extensively explored to meet the energy demand in terms of economic and population growth in an environmentally friendly way [3]. Unfortunately, these energy storage systems are easily affected by external environment, and eventually fail in modulation of intermittent output power [4]. Based on this consideration, renewable energy systems with high stability and flexibility are further explored, in which rechargeable batteries have triggered intensive attention as reliable electrochemical energy storage (EES) systems in terms of efficient regulation of energy storage [5].

Currently, rechargeable lithium-ion batteries (LIBs) have been commercialized, and widely used in various electronic devices. However, the limited specific capacity of LIBs constructed with graphite anode and transition metal oxide cathode can no longer satisfy the demand of high energy density and long-duration stability of advanced electric equipments [6]. Hence, it is expected to focus on the exploration of electrode materials and new storage mechanisms in future, to develop LIBs with high energy density and long-cycling stability. For example, the usage of metallic lithium

L.-H. Pan · H.-Y. He · J.-H. Wang · X. Liu · J.-W. Qian · L.-F. Chen (✉)
Department of Thermal Science and Energy Engineering, Hefei National Laboratory for Physical Sciences at the Microscale, Department of Applied Chemistry, University of Science and Technology of China, Hefei 230026, Anhui, China
e-mail: chenlf@ustc.edu.cn

J. Chen
School of Materials Science and Engineering, Nanyang Technological University, Singapore 639798, Singapore

H. Pang (ed.), *Nano/Micro Metal-Organic Frameworks*,
https://doi.org/10.1007/978-981-16-4071-1_3

as a substitute of graphite greatly improves the energy density of the battery given the high specific capacity and low density of Li anode [7]. As a result, lithium-sulfur (Li–S) batteries, lithium-oxygen batteries (LOBs), and lithium-selenium batteries, directly using the lithium metal as anodes, exhibit huge potential in electric vehicles and smart grids [8–10]. Similar to LIBs, sodium-ion batteries (SIBs) with conventional carbon-based anode or sodium metal anode also attracted much attention in terms of low cost and high theoretical energy density [11]. Moreover, other advanced rechargeable batteries, including lithium-carbon dioxide battery, zinc/sodium-iodine ($Zn/Na\text{-}I_2$) battery, and redox flow batteries all exhibit promising merits for future energy storage systems [12–14]. However, a considerable gap between practical performances and theoretical values still persist in these batteries. Therefore, the rational structures and chemical compositions design of electrode materials is crucial for the practical application of these batteries.

Metallic organic frameworks (MOFs) are considered as a class of promising electrode materials for batteries owing to their large surface area, diverse structure, adjustable pore size and controllable chemical composition [15, 16]. Unfortunately, MOFs and MOF-based materials are still facing various challenges, such as poor electronic conductivity, low tap density, and irreversible structural destruction that hinder their practical utilization [17]. Comparatively, MOF derivatives, directly using MOFs as self-sacrificial templates, exhibits much promising potential in electrode materials given the abundant porous structures and better electrical conductivity provided by the interconnected carbon framework [18, 19]. In this review, it is focused on MOFs and MOF derivatives as electrode materials and separator membrane, and the advanced progress in various battery systems has been summarized. By discussing and analyzing the significant progress in different battery systems, not only the crucial advantages that MOFs and MOF derivatives in various battery systems have been appreciated, but also the potential issues have been recognized and possible solutions in energy storage have been proposed, eventually facilitating the application of MOF-based material in various energy storage fields.

3.2 MOFs for LIBs

LIBs are considered to be one of the significant breakthroughs in the field of EES during the past few decades. Despite the advantages of excellent stability, high reversible capacity and slight self-discharging, LIBs still hardly meet the increasing energy density requirements for high-end electronic devices. Therefore, more attention was focused on the design and modification of electrode materials to further improve the electrochemical performance of commercial LIBs. MOFs are emerging porous crystal materials, of which high specific surface area, variable chemical composition, and numerous active metal sites make MOFs promising electrode materials in conventional LIBs. Moreover, MOF composites and MOF derivatives also

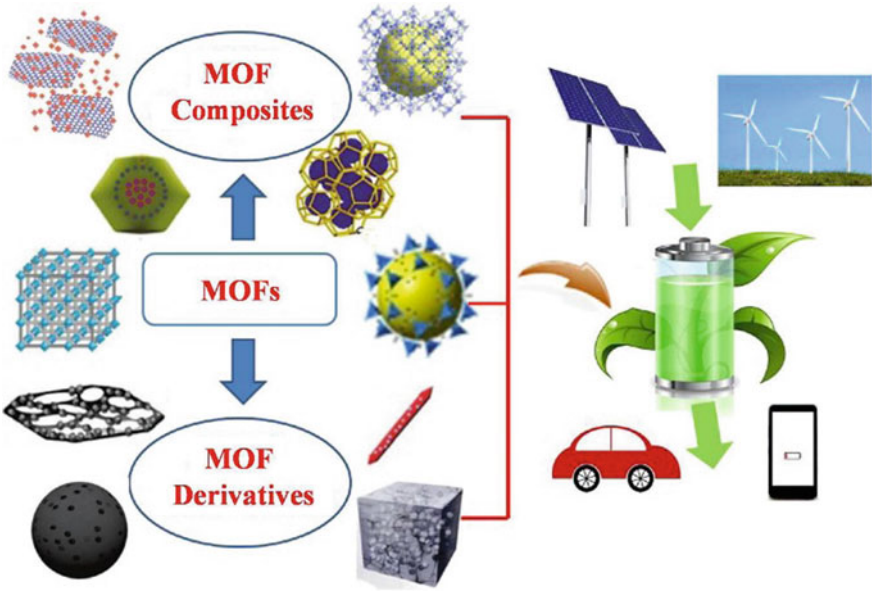

Fig. 3.1 MOF-related materials for LIBs in EES devices. Adapted with permission [20]. Copyright 2019, Elsevier B.V

have been widely used as electrode materials for LIBs in EES to overcome the problems of low capacity and poor cycle performance of LIBs, as shown in Fig. 3.1 [20].

3.2.1 Pristine MOFs as Anode Materials for LIBs

The electrochemical performance of batteries mainly depends on the electrode material. Compared to the traditional graphite anode, MOFs possess numerous advantages. Substitution of graphite with MOFs allows higher energy density and rate capability of LIBs. Chen and co-workers firstly synthesized the shape-controllable MOF-177 by a facile solvothermal route, which was employed as an anode of LIBs [21]. By analyzing the electrochemical performance, it was found that the MOF-177 electrode shows a low initial coulomb efficiency during the first cycle with charge/discharge capacity of 110 mAh g^{-1}/425 mAh g^{-1}. Despite fcharge/discharge capacities were cycles, the charge/discharge capacities are relatively low. In the second cycle, the discharge capacity is only 105 mAh g^{-1}, which is only one-fourth of discharge capacity in first cycle. The conversion and alloying reaction of lithium within MOF-117 electrode result in the capacity decay. The speculated reaction within the MOF-177 electrode could be expressed as follows:

$$Zn_4O(BTB)_2 \cdot (DEF)_m(H_2O)_n + e^- + Li^+ \rightarrow Zn + Li_2O \quad (3.1)$$

$$DEF + H_2O + e^- + Li^+ \rightarrow Li_2(DEF) + LiOH \quad (3.2)$$

$$Zn + Li^+ + e^- \leftrightarrow LiZn \quad (3.3)$$

Both transmission electron microscopy and X-ray photoelectron spectroscopy result reveal the irreversible damage occurred in the MOF-117 electrode after the conversion and alloying reaction, in which the formation of zinc metal during the discharge process seriously destroys the structure of MOF-117, and consequently leads to the capacity decay. Despite the non-ideal performance as anode material for LIBs, the investigation of MOF-117 is still of great significance to encourage more studies on MOFs as LIBs anodes. To improve the energy storage performance and reversible cycling of MOFs anodes and mitigate the irreversible structural destruction, Vittal and co-workers systematically studied the electrochemical performance of the as-prepared MOF for lithium storage by conversion reaction [22]. Among the synthesized three MOF materials: $Zn_3(HCOO)_6$, $Co_3(HCOO)_6$ and $Zn_{1.5}Co_{1.5}(HCOO)_6$, $Zn_3(HCOO)_6$ electrode exhibits the best electrochemical performance for lithium storage. For $Zn_3(HCOO)_6$ anode, the initial charge/discharge capacities were 693 mAh g^{-1}/1344 mAh g^{-1}. Although the initial Coulomb efficiency is not high, the capacity still can be stabilized at 560 mAh g^{-1} after 60 cycles. Similar to $Zn_3(HCOO)_6$ anode, the capacity of $Co_3(HCOO)_6$ and $Zn_{1.5}Co_{1.5}(HCOO)_6$ electrode also can be stabilized at 410 mAh g^{-1} and 510 mAh g^{-1} after 60 cycles, respectively. The excellent electrochemical performance is mainly attributed to the stable format frameworks and reversible conversion reaction during cycling. Both ex situ powder X-ray diffraction (PXRD) and Fourier transform infrared spectrometer (FTIR) indicated that the reaction between format MOFs with lithium leads to formation of lithium format instead of Li_2O during cycling. It is speculated that the reaction within the $Zn_3(HCOO)_6$ electrode could be expressed as follows:

$$Zn_3(HCOO)_6 + 6Li^+ + 6e^- \leftrightarrow 3Zn + 6HCOOLi \quad (3.4)$$

$$3Zn + 3Li^+ + 3e^- \leftrightarrow 3LiZn \quad (3.5)$$

Except for the above conversion type anodes, intercalation type anodes of MOFs were also further investigated. Ogihara and co-workers reported an excellent anode material, 2,6-naphthalene dicarboxylate dilithium, which is an intercalated MOF [23]. The intercalated MOF has an organic–inorganic layered structure, which can buffer the volume fluctuation in the intercalation process. As a result, the structure of intercalated MOF electrode remains intact, with limited volume change within 0.33% during cycling. Furthermore, the operating voltage of intercalated MOF is maintained at 0.8 V during reversible two-electron-transfer intercalation process, which is a desirable operating voltage range of anodes for high voltage bipolar LIBs.

3.2.2 MOF Composites and MOF-Derived Materials as Anodes for LIBs

At present, there are still many limitations in using pristine MOFs as electrode materials for LIBs due to issues related to low electrical conductivity, limited reversible capability, and cycling stability. To overcome above drawbacks of pristine MOFs, more and more attention was focused on the MOF composites and MOF-derived materials.

3.2.2.1 MOF Composites

Formation of composites can combine the advantages of each component while avoiding the disadvantages of individual components, explaining the better electrochemical performance in MOF composites. Therefore, MOFs decorated with various nanoparticles were constructed and widely used as electrode materials for LIBs. At present, there are several methods to construct nanoparticle/MOF composite materials, such as direct synthesis, [24] chemical vapor deposition method, [25, 26] solid-state reaction, [27] and solvothermal method [28].

Recently, metal oxide composite anodes have been widely investigated in LIBs [29]. The composite composed of nanostructured metal oxides and multiwalled carbon nanotubes (MWCNTs) is one of the typical anode materials with improved electrochemical performance for LIBs. Wang and co-workers synthesized nanocomposites of MWCNTs/Co_3O_4 by a simple and scalable method [30]. In a typical synthetic procedure, MWCNTs/ZIF-67 was firstly prepared by the reaction of MWCNTs functionalized with strong acid, cobalt salt and 2-methylimidazolate under proper conditions. Then, MWCNTs/Co_3O_4 composite was obtained by further annealing of MWCNTs/ZIF-67, as presented in Fig. 3.2a. The MWCNTs/Co_3O_4 anode exhibited high specific capacity of 821 mAh g^{-1} within 40 cycles and 820 mAh g^{-1} within 60 cycles at a current density of 100 mA g^{-1}. Even after 100 cycles, the MWCNTs/Co_3O_4 anode can still maintain capacity of 813 mAh g^{-1}, as shown in Fig. 3.2b. In addition, the MWCNTs/Co_3O_4 anode also showed excellent rate capability, as shown in Fig. 3.2c. Even at a high current density of 1000 mA g^{-1}, the specific capacity of MWCNTs/Co_3O_4 anode can still reach 514 mAh g^{-1}. These outstanding electrochemical performances of MWCNTs/Co_3O_4 anode, such as high specific capacity, excellent rate capability, and long-cycling stability, are all attributed to the synergistic interaction between MWCNTs and Co_3O_4, in which MWCNTs with hierarchical porous structure provide high electrical conductivity and mechanical stability, and the active component of Co_3O_4 contributes to high specific capacity.

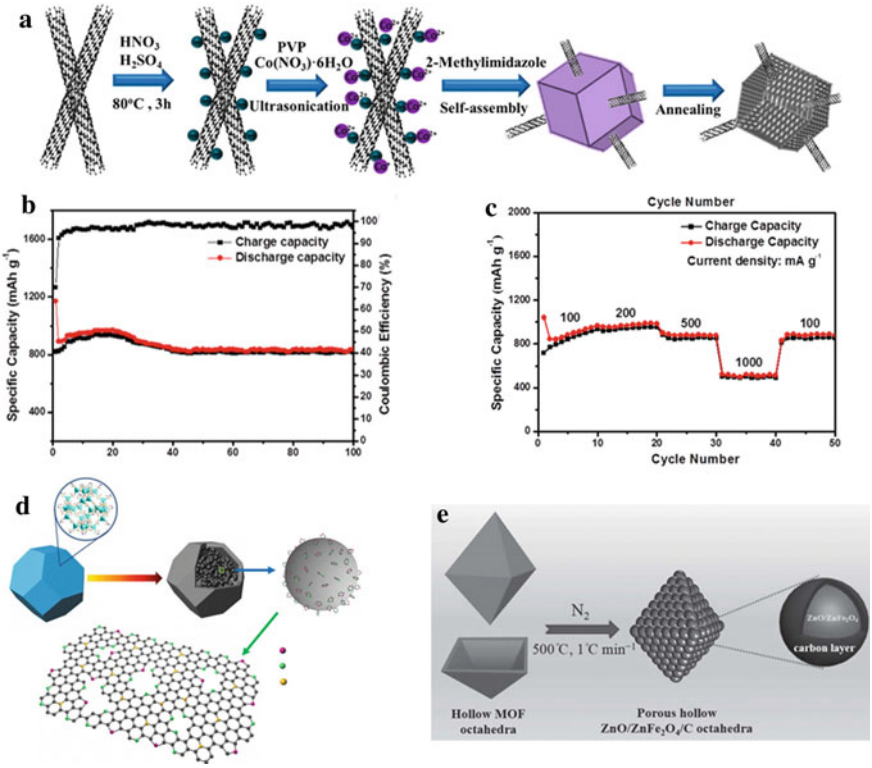

Fig. 3.2 **a** Schematic illustration of preparation process of MWCNTs/Co_3O_4. **b** Capacity and Coulombic efficiency vs. cycle number of the MWCNTs/Co_3O_4 at a current rate of 100 mA g^{-1} **c** Rate capability of the MWCNTs/Co_3O_4. **d** Schematic illustration of the synthesis procedure of N-doped graphene analogous particles and model of N-doping. **e** Schematic illustration of preparation process of ZnO/$ZnFe_2O_4$/C octahedra composite.**a-c**Adapted with permission [30]. Copyright 2015, American Chemical Society. **d** Adapted with permission [34]. Copyright 2014, Macmillan Publishers Limited. **e** Adapted with permission [35]. Copyright 2014, Macmillan Publishers Limited

3.2.2.2 MOF-Derived Materials

In recent years, more and more studies have shown that MOFs are effective precursors in fabrication of electrode materials for EES devices [17, 31, 32]. MOF-derived materials, such as MOF-derived metal oxides, MOF-derived carbon, and MOF-derived metal oxide/carbon composites, all have obviously improved electrochemical performance compared with the original MOF materials. Various MOF-derived materials could be fabricated according to the different structure and composition of pristine MOFs.

MOF-derived metal oxide anodes with high specific surface and hierarchical porous nanostructures can greatly improve the electrochemical performance of conventional LIBs due to more active sites for lithium-ions intercalation, huge buffer

space for volume fluctuation, and convenient paths for lithium-ions transport during cycling. Ogale and co-workers firstly reported that α-Fe_2O_3 nanospindles with excellent electrochemical performance were successfully synthesized by one-step pyrolysis of iron-based MOF [33]. The electrochemical tests of Li/α-Fe_2O_3 half-cell showed that the α-Fe_2O_3 anode possesses high reversible capacity and capacity retention. At a current density of 100 mA g^{-1}, the reversible capacity can arrive at 1024 mAh g^{-1}, and the capacity retention rate is over 90% after 40 cycles. In addition, Zheng and co-workers reported a high doping level N-doped MOF-derived carbon (N-C-800) using zeolitic imidazolate framework (ZIF-8) as precursors [34]. The prepared N-C-800 is N-doped graphene analogous particles after the carbonization of the nitrogen-containing ZIF-8 under nitrogen atmosphere at 800°C, in which the nitrogen content is up to 17.72 wt%, as shown in Fig. 3.2d. As anode of LIBs, N-C-800 electrode exhibits excellent electrochemical performance with reversible capacity of 2132 mAh g^{-1} at a current density of 100 mA g^{-1}. With current density increased to 5 A g^{-1}, the capacity is still stabilized at 785 mAh g^{-1}. Considering the advantages and disadvantages of MOF-derived metal oxides and MOF-derived carbon, in which MOF-derived metal oxides possess high specific capacity yet large volumetric changes while MOF-derived carbon framework owns high specific surface and electrical conductivity, synthesis of MOF-derived metal oxide/carbon composites is of significance to construct high-performance anodes of LIBs. The MOF-derived metal oxide/carbon composites can effectively alleviate the volume change during cycling while providing high specific capacity. Huang and co-workers reported a novel ZnO/$ZnFe_2O_4$/C octahedra composite with hollow interiors, which was fabricated by thermal treatment of the hollow MOF-5 octahedra under nitrogen atmosphere [35]. As shown in Fig. 3.2e, MOF-5 was used as the precursor and self-sacrificing template to prepare ZnO/$ZnFe_2O_4$/C composite electrode. The electrochemical test results showed that ZnO/$ZnFe_2O_4$/C anode achieved high specific capacity of 1390 mAh g^{-1} at a current density of 0.5A g^{-1} and 762 mAh g^{-1} even at 10A g^{-1}.

3.2.3 Pristine MOFs as Cathode Materials for LIBs

The capacity of cathode determines the capacity of the whole LIBs. Conventional cathode materials, such as $LiFePO_4$ and $LiCoO_2$, whose theoretical specific capacities are 170 mAh g^{-1} and 270 mAh g^{-1}, cannot meet the requirements of large-scale energy storage equipments. Moreover, the rate capability of LIBs also mainly depends on cathode materials. Therefore, various emerging cathode materials were explored in which MOFs are potential candidates due to their high specific surface, adjustable porous structure, and controllable chemical composition. Although MOFs possess many excellent properties, the insulating characteristic of MOFs heavily impedes electrochemical intercalation. In the beginning, some pristine MOFs were treated directly as electrode materials for energy storage, such as Ga-V phosphonate framework [36], and Zn-based MOF [21]. Tarascon and co-workers firstly used pristine MOFs ($Fe^{III}(OH)_{0.8}F_{0.2}(O_2CC_6H_4CO_2)$) (MIL-53(Fe)) as rechargeable cathode

successfully, in which 15 wt% carbon was added as conductive agents to improve the electrical conductivity of whole electrode, with lithium metal as a counter electrode [37]. The assembled batteries with pristine MOFs cathode and lithium metal anode displayed a low gravimetric and volumetric specific capacity of 75 mAh g^{-1} and 140 mAh L^{-1}, respectively. Despite the lower gravimetric and volumetric specific capacity, the mixed-valence MOFs were evidenced as possible cathode materials. Also, Serre and co-workers synthesized another kind of MOFs cathode material — MIL-68(Fe) [38]. Compared to the previously reported MIL-53(Fe), the attainable capacity of MIL-68(Fe) electrode is only 30 mAh g^{-1} in this work. The obvious difference between MIL-68(Fe) and MIL-53(Fe) demonstrated that the aperture and flexible or rigid properties of framework played an important role in the electrochemical performance. Meng and co-workers firstly reported MIL-101(Fe) MOF and investigated the electrochemical performance as cathode [39]. Compared to above-mentioned MIL-53 and MIL-68, the synthesis procedure of MIL-101 is more environmentally friendly needless of hydrofluoric acid. Notably, the metal iron center of MIL-101(Fe) is activated electrochemically, and the reversible conversion takes place between Fe^{2+} and Fe^{3+}. Despite the reversible conversion mechanism between Fe^{2+} and Fe^{3+}, there is obvious capacity decay with cycling due to the failure of Fe^{2+} oxidation to Fe^{3+}. Recently, Chen and co-workers synthesized a new conductive $Cu_3(HHTP)_2$ MOF, and investigated the relevant electrochemical performance as LIBs cathode [40]. Impressively, $Cu_3(HHTP)_2$ MOF exhibits high reversible capacity of ~95 mAh g^{-1} at 1C during cycling, which is extremely close to the theoretical specific capacity of 95.61 mAh g^{-1}. The comparison between the theoretical specific capacity and practical specific capacity shows that the intercalation ratio of lithium to copper MOF is almost 100%, which is much higher than of MIL-53(Fe) (Li:Fe, 62%) and MIL-101(Fe) (Li:Fe, 71%). Furthermore, $Cu_3(HHTP)_2$ cathode also exhibit outstanding rate capability given the improved electrical conductivity and porous structure. As shown in Fig. 3.3a, during the initial 20 cycles, the $Cu_3(HHTP)_2$ electrode is in the activation stage and gradually reaches the maximum capacity of 95 mAh g^{-1}. Expectedly, with the increase of current densities, the specific capacity of the electrode decreases correspondingly. The specific capacity of the $Cu_3(HHTP)_2$ electrode reaches the lowest value of 85 mAh g^{-1} at 20C. When the current density was reduced back to1C, the capacity of the electrode is restored to 89 mAh g^{-1}. Next, Fig. 3.3b shows the capacity retention of $Cu_3(HHTP)_2$ electrode at various current densities within 500 cycles. By comparing the specific capacity and capacity retention (%) at different rates, two interesting phenomena can be observed. i) The maximum capacity of the activated $Cu_3(HHTP)_2$ electrode is almost unchanged at different rates. ii) the capacity retention of $Cu_3(HHTP)_2$ electrode shows a competitive advantage at high rate. After 500 cycles, the capacity retention is 85% at 20 C, while the capacity retention is only 40% at 0.5 C. Through the electrochemical properties and chemical analysis, Chen and co-workers gave the explanation for the excellent rate capability of the $Cu_3(HHTP)_2$ electrode as following: i) the high conductivity of $Cu_3(HHTP)_2$ electrode realizing more efficient transport of lithium ions; ii) the porous layered structure achieving more efficient intercalation and desertion of lithium ion during cycling.

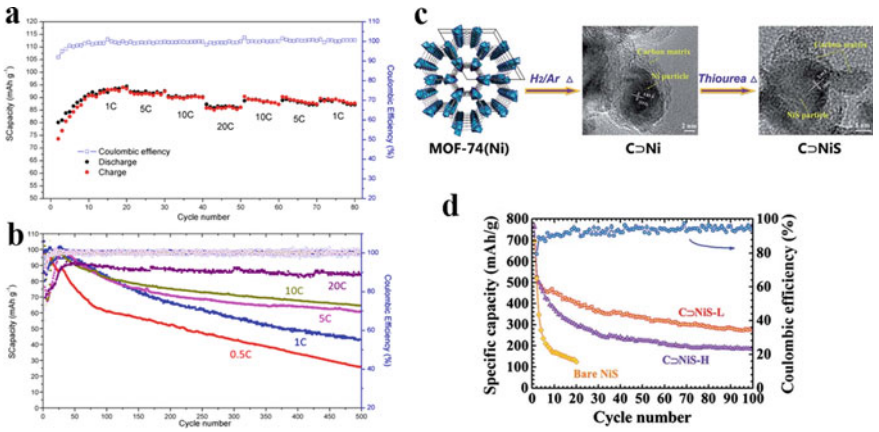

Fig. 3.3 **a** The rate capability at different current rates of the $Cu_3(HHTP)_2$ electrode. **b** At different current rates from 0.5 C to 20 C, the cycling performance of $Cu_3(HHTP)_2$ electrode within 500 cycles. **c** Schematic illustration of the synthesis of C ⊃ Ni and C ⊃ NiS. **d** Cycle performances of bare NiS and C ⊃ NiS cathode at 60 mA g^{-1}. **a, b** Adapted with permission [40]. Copyright 2019, Elsevier B.V. **c, d** Adapted with permission [41]. Copyright 2014, the Royal Society of Chemistry

3.2.4 MOF Composites and MOF-Derived Materials as Cathode for LIBs

The electrochemical performance of MOF composites and MOF-derived materials is superior to pristine MOFs given the enhancement of electrical conductivity and optimization of structural components. Therefore, MOF composites and derivatives were widely used as cathode materials for LIBs. Wang and co-workers reported that C ⊃ NiS, in which the β-NiS nanoparticles were uniformly dispersed in porous carbon matrix, was successfully prepared by the calcination of MOF-74(Ni) under H_2/Ar atmosphere, and subsequent chemical reaction with thiourea under Ar atmosphere (Fig. 3.3c) [41]. Benefiting from the highly dispersed structure of NiS in carbon matrix, the agglomeration and volume fluctuation are effectively prevented during cycling. Interestingly, the presence of NiS particles also improves the wettability and conductivity of carbon substrate, further enhancing the electrochemical performance of batteries. Resultantly, C ⊃ NiS cathode displayed excellent electrochemical performance that the reversible capacity reaches 300 mAh g^{-1} at a current density of 60 mA g^{-1} after 100 cycles, which is much higher than the bare NiS electrode (Fig. 3.3d). Subsequently, a novel cathode material (HCSP ⊂ GCC) was reported by Yu and co-workers in 2016 [42]. HCSP ⊂ GCC, as a new kind of MOF-derived materials, is composed of graphitic carbon nanocages and hollow cobalt sulfide nanoparticles, which is synthesized simply via a top-down route with Co-based zeolitic imidazolate framework (ZIF-67) as template at room temperature. When employed as a cathode of LIBs, the HCSP ⊂ GCC exhibits excellent electrochemical performance with energy density reaching 707 Wh kg^{-1}, much superior to other

conventional cathodes ($LiMn_2O_4$ ~ 500Wh kg^{-1}, $LiCoO_2$ ~ 540Wh kg^{-1}, $LiFePO_4$ ~ 500Wh kg^{-1}, $LiNi_{0.5}Mn_{1.5}O_4$ ~ 650Wh kg^{-1}) [43, 44]. As shown in Fig. 3.4a, the almost overlapped CV curves within initial 3 cycles reveal the excellent reversibility of the HCSP ⊂ GCC cathode. The discharge curves exhibit two plateaus, which is in line with the two characteristic peaks in CV curves (Fig. 3.4b). As presented in Fig. 3.4c-e, the HCSP ⊂ GCC cathode possesses excellent rate capability that the reversible capabilities reach 536, 489, 438, 393, 345, and 278 $mAhg^{-1}$ at 0.2, 0.5, 1, 2, 5, and 10 C, respectively, within the working voltage range of 1.0–3.0 V.

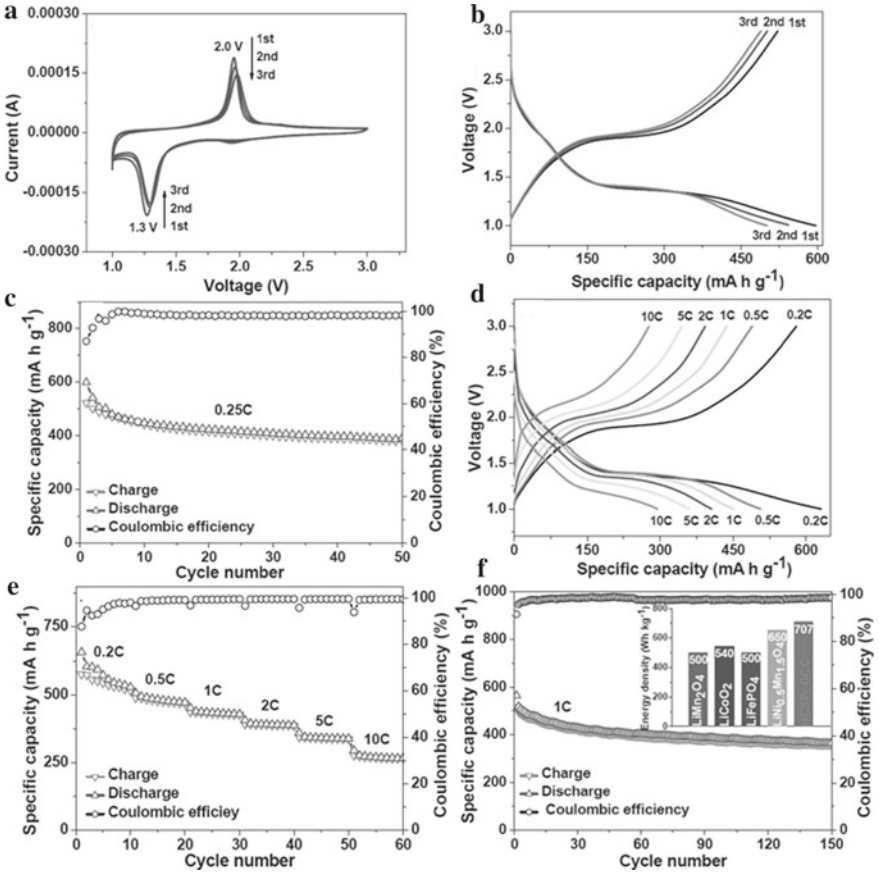

Fig. 3.4 Electrochemical performances of HCSP ⊂ GCC cathode. **a** CV curves. **b** charge and discharge curves at 0.25 C. **c** Cycling performances at 0.25 C. **d** Charge and discharge curves at 0.2–10 C. **e** Rate capability at 0.2–10 C rate. **f** Long-cycling performances at 1 C. Adapted with permission [42]. Copyright 2014, WILEY–VCH Verlag GmbH & Co. KGaA, Weinheim

3.3 MOFs for Li–S Batteries

In conventional LIBs, the charging and discharging of the battery is achieved through the lithium-ion intercalation mechanism. However, due to the restriction of the material structure, the number of lithium ions inserted in the electrode is limited, which greatly affects the energy density of batteries. Moreover, high cost of electrode also hinders their further application.{Goodenough, 2010 #186} [2]. Based on these considerations, elemental sulfur, the secondary product of the petroleum industry, has attracted much attention due to its abundance, low cost, and low toxicity [9]. Li–S batteries are one of the most promising energy storage systems given the high theoretical energy density (2567 Wh kg^{-1}), low cost, and environmental friendliness [45]. Despite the numerous advantages, the commercialization of Li–S batteries is still facing various challenges. On the one hand, poor conductivity of elemental sulfur and the shuttle behavior of polysulfide result in the irreversible loss of sulfur active component. On the other hand, the shuttle effect of polysulfides also causes the corrosion of lithium metal, further weakening the stability of the anode interface [46]. These adverse factors both result in low Coulombic efficiency and poor cycling stability. Therefore, much attention has been focused on the solutions for the poor conductivity of elemental sulfur and the shuttle effect of polysulfide in Li–S batteries. In recent years, research on advanced electrode materials and multifunctional separators has accelerated the development of Li–S batteries. Especially, porous MOF materials, composed of metal ions and organic ligands, have been widely studied in Li–S batteries due to the large specific surface, adjustable porosity, and numerous metal active sites [47].

3.3.1 Cathode in Li–S Batteries

The complex electrochemical reaction process and non-conductive physical properties of sulfur cathode determine that the major challenge in the progress of Li–S batteries lie in the cathode materials. In order to realize the practical application of Li–S batteries, it is essential to enhance the conductivity of the cathode materials, so as to improve the utilization of the active component and rate capability of batteries [48]. Furthermore, the suppression of polysulfide is also of great significance to decrease the irreversible capacity loss to improve the cycling stability of batteries. MOFs, with large specific surface area, controllable pore structure and abundant metal active site, are widely used in Li–S batteries. However, most of the MOF materials have poor electrical conductivity given the presence of organic ligands, causing the inferior electron conduction. Hence, generally MOF carbonization or adding conductive additives were adopted to improve the conductivity. Unfortunately, these methods virtually destroy the ordered structure of MOFs, and thereby weaken the electrochemical performance of batteries. As a consequence, the design

of MOFs with high intrinsic electrical conductivity is an important direction for the development of Li–S batteries in the future [49].

Jin and co-workers created a super-stretch cathode using an integrated porous 3D gel, which is consisted of a highly elastic fluorinated polymer matrix, a polar sulfur reservoir, and a conductive network of cross-linked multiwalled carbon nanotubes (MWCNT) [50]. As shown in Fig. 3.5a, the Co@NCNP/NCNT composite, which is synthesized by the pyrolysis process of the scalable zeolite imidazolate framework (ZIF-67) precursor under H_2/Ar atmosphere, was prepared as polar sulfur reservoirs to improve the redox kinetics and simultaneously suppress the shuttle effect of polysulfides. Both the high specific surface area of 281 m^2 g^{-1} and hierarchical pores of Co@NCNP/NCNT composites are beneficial for the accommodation of sulfur species and migration of lithium ions. Figure 3.5b showed that Zang and co-workers have fabricated dual heteroatom (N and P) doped porous carbon materials (NPMOF),

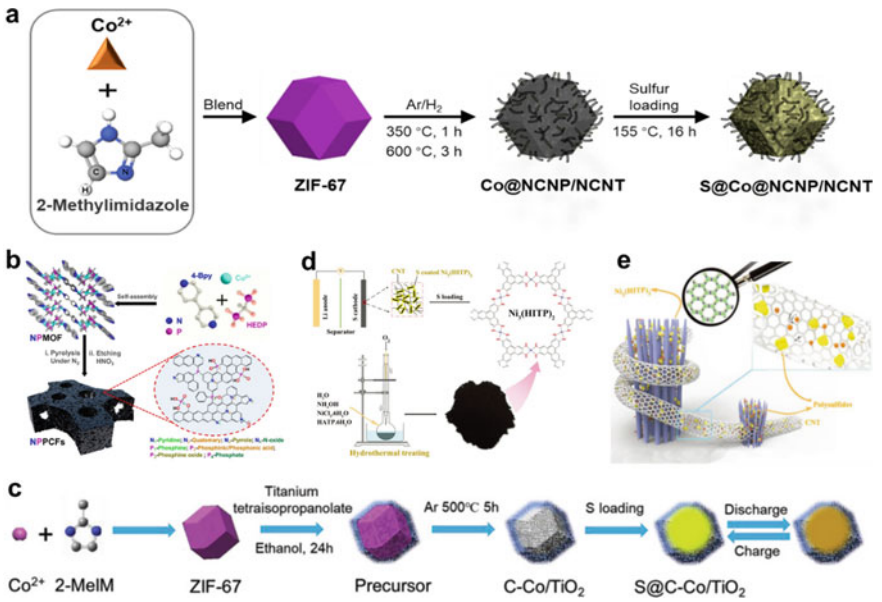

Fig. 3.5 **a** Schematic illustration of the preparation process of S@Co@NCNP/NCNT. Reproduced with permission [50]. Copyright 2020 Elsevier Ltd. **b** Schematic illustration for preparation of NPPCFs from the single-source NPMOF combined with mixed N- and P-containing ligands. Bottom right: types of nitrogen- and phosphorus-containing functional groups in NPPCFs. Reproduced with permission [51]. Copyright 2019 American Chemical Society. **c** Schematic of the synthesis of the S@C-Co/TiO_2 polyhedra. Reproduced with permission [52]. Copyright 2019 WILEY–VCH Verlag GmbH & Co. KGaA, Weinheim. **d** Schematic diagram of the synthesis of $Ni_3(HITP)_2$ and its application in Li–S batteries. **e** Schematic diagram of the synergistic effects of $Ni_3(HITP)_2$ and CNTs on the electrochemical performance in Li–S batteries. Inset of the magnifier is the crystalline structure of $Ni_3(HITP)_2$. **d, e** Reproduced with permission [53]. Copyright 2019 WILEY–VCH Verlag GmbH & Co. KGaA, Weinheim

which was synthesized simply through copper salt with 1-hydroxyethylidene-1,1-diphos-phonic acid (HEDP) and bipyridine [51]. Both the strong coordinated ability of HEDP ligand and the synergistic coordination of metal ions of mixed ligands are beneficial for the rapid generation of MOF. The Li–S batteries assembled by the S@NPPCF cathode through the melt-diffusion method and the pristine lithium foil anode maintained high Coulombic efficiency of 98%, which was attributed to the N, P-doped porous carbon framework that decreases the loss of sulfur cathode, and thereby high Coulombic efficiency and long lifespan. Ma and co-workers prepared a novel sulfur host material, in which TiO_2 with strong binding energy was uniformly dispersed in Co-decorated carbon polyhedrons (C-Co/TiO_2) through the pyrolyzation of Ti-doped ZIF-67 in Fig. 3.5c [52]. The multifunctional structure in the C-Co/TiO_2 framework simultaneously realizes the suppression of shuttle behavior due to the strong chemical trapping of TiO_2, and fast electron transport provided by carbon conductive networks for polysulfides conversion. Consequently, the S@C-Co/TiO_2 cathode shows a highly improved cycling stability and delivers an excellent discharge specific capacity of 466.3 and 383.8 mAh g^{-1} at 1 and 3 C, respectively. By designing a multifunctional structure, the cathode material simultaneously possesses the advantages of excellent conductive network, abundant chemical active sites, and widely interconnected ion channels, so as to achieve the better confinement and capture of polysulfides.

Despite the improvement of electrochemical performance in Li–S batteries after introducing the MOFs in sulfur cathode, there are still various adverse factors restricting the further improvement of electrochemical performance. Among these negative factors, poor electrical conductivity is one of the most fatal issues, which extremely limits the utilization of elemental sulfur, and thus restricts the large-scale application of MOFs on sulfur composite cathode [54]. Whereupon, the carbonization of MOFs or addition of conductive additives were generally adopted to improve the poor electronic conductivity. However, none of the two approaches is optimal. These methods virtually destroy the ordered structure of MOF materials and increase experimental complexity. Therefore, the design of MOF materials with high intrinsic electrical conductivity is of great significance for the improvement of electrochemical performance in Li–S batteries. Han and co-workers firstly employ a MOF of graphene analogue with high intrinsic electrical conductivity to realize the immobilization and conversion of polysulfide as shown in Fig. 3.5d [53]. In this work, the combination of physical constraint provided by the abundant distribution of micro- and mesopores, and chemical conversion of various active sites, such as nickel, oxygen, and nitrogen, both suppress the shuttle effect of polysulfide. Interestingly, a conductive framework consisting of carbon nanotubes (CNTs) with long-range conductivity was further employed to enhance the electron and ion conductivity of the cathode to further improve the electrochemical performance based on the characteristics of medium- and short-range conductivity of $Ni_3(HITP)_2$ (Fig. 3.5e). Compared with conventional MOF materials, metal ions with plane coordination and two-dimensional layered MOF with conjugated ligands have higher electrical conductivity. As a result, the electrical conductivity of $Ni_3(HITP)_2$ reaches 200 S m^{-1}, even higher than that of some carbon materials. However, carbon matrix will

encapsulate many central ions in MOF-derived carbon framework, causing limited active sites exposure to adsorb and convert polysulfides.

3.3.2 Separator in Li–S Batteries

The commercial separator is employed to avoid the internal short circuit through isolating the cathode and anode, while allowing free transport of ions [55]. Polysulfides easily pass through the separator from sulfur cathode to lithium anode, and further corrode lithium metals. A simple and effective method is to employ a functional membrane to prevent the polysulfide from escaping through the separator to protect the lithium anode. There are some strategies reported, including using free-standing functional microporous ion-sieving membranes and separator with functional modification, which have also been proved to be effective in suppressing the shuttle of polysulfide, and improving the Coulombic efficiency and cycling stability of batteries [56]. Presently, porous carbon materials, especially two-dimension carbon matrix, such as graphene, are extensively explored for the ion-sieving membranes and functional separators. Restricted by the high cost, these special carbon materials have not actually shown great advantages in terms of ion-sieving membranes and separators. Inspired by the discovery of MOFs in adsorption, separation, and catalysis, MOF materials with large specific surface area, tunable pore structure, and uniformly dispersed catalytic sites, exhibited a promising prospect in ion-sieving membranes and separators of Li–S batteries [57].

As shown in illustration in Fig. 3.6a, Li and co-workers fabricated a systematic MOF-based composite separator, in which the CNTs are closer to the cathode, and MOFs face to anode [58]. These MOF materials mainly include Y-FTZB, ZIF-7, ZIF-8, and HKUST-1 in this work. The conductive CNTs layer improves the utilization of active materials and simultaneously trap dissolved polysulfides, and the MOF-based layer inhibits the shuttle effect of polysulfides. Among these MOF-based separators, Y-FTZB-based separator looks denser compared to others. The battery with the Y-FTZB-based separator delivers a high discharge capacity of 1480 mAh g^{-1} at 0.1C and a capacity retention of 50.6% after 300 cycles (Fig. 3.6a), which is superior to other MOF-based separators. In addition, Cu^{2+} from HKUST-1 may have chemical side reactions with lithium and sulfur, a suitable voltage range should be adjusted in terms of charge and discharge, which is essential to reduce the degradation of MOFs and other side reactions. Their results show that the structural stability and stacking morphology of MOF particles are more important than the size of the internal cavity.

Wang and co-workers synthesized a cerium-based MOF and then combined it with CNTs to form Ce-MOF/CNT composite, which was served as modified layer for separator, as shown in Fig. 3.6b [59]. The design of composite modification layer not only realizes efficient catalysis and conversion of polysulfide into shorter chains, but also improves the utilization of sulfur given the enhancement of electrical conductivity associated with the usage of the CNTs. As a result, the battery

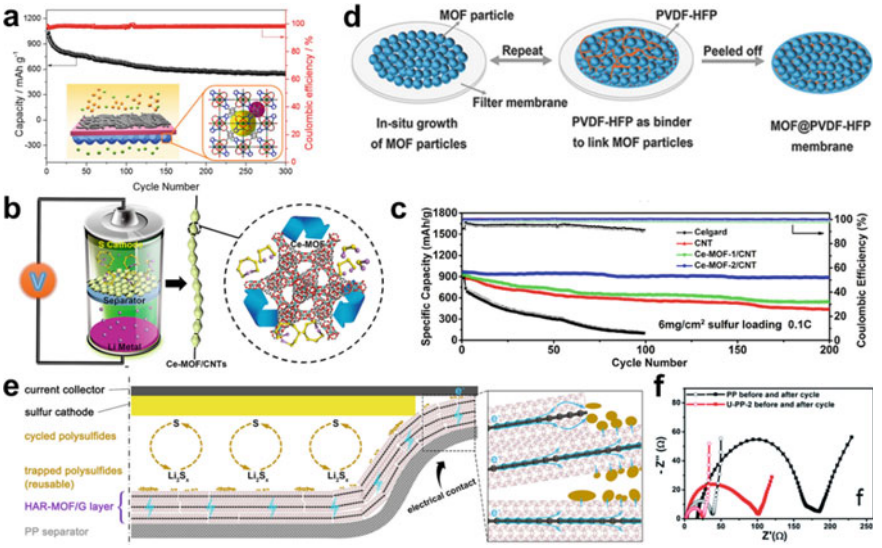

Fig. 3.6 **a** Cyclic performance of the Li–S batteries with this MOF-based composite separator at 0.1C for 300 cycles. The illustration shows MOF-based composite separator for Li–S battery. Reproduced with permission [58]. Copyright 2017 American Chemical Society. **b** Scheme of MOFs/CNT composites with catalysis of the conversion of polysulfides as the separator coating materials for Li–S battery. **c** Cyclic performance of the Li–S batteries with different separator at 0.1 C with the high sulfur loading for 200 cycles (6.0 mg cm^{-2} sulfur loading). **b, c** Reproduced with permission [59]. Copyright 2019 American Chemical Society. **d** Schematic illustration for fabricating a flexible MOF@PVDF-HFP membrane. Reproduced with permission [60]. Copyright 2018 WILEY–VCH Verlag GmbH & Co. KGaA, Weinheim. **e** Schematic illustration of the LiPSs shuttling inhibition and trapped LIPSs reutilization mechanisms of the ZIF-67/G nanosheet membranes. The magnified schematic shows the electrons transfer to potentially trapped polysulfides. Reproduced with permission [61]. Copyright American Chemical Society. **f**. EIS measurements before and after cycling for LSBs with U-PP-2 and PP separators. Reproduced with permission [62]. Copyright The Royal Society of Chemistry 2020

assembled by the as-prepared Ce-MOF/CNT composite separator exhibited excellent electrochemical performance, in which the capacity retention is 89.2% after 200 cycles even at a high sulfur loading of 6 mg cm^{-2} (Fig. 3.6c). Zhou and coworkers reported that a MOF membrane (MOF@PVDF-HFP) with good flexibility was synthesized using HKUST-1 nanoparticles as the basic component and PVDF-HFP as the binder through simple vacuum filtration (Fig. 3.6d) [60]. The highly uniform MOF particles improve the uniformity of lithium flux, which fundamentally inhibits the lithium dendrites growth. Resultantly, Li//Li symmetric battery with MOF@PVDF-HFP separator exhibits excellent interfacial stability during continuous lithium deposition/stripping processes even at ultra-high current densities of 10 mA cm^{-2}. In addition, due to the small pore size of MOF nanoparticles, the MOF@PVDF-HFP separator displays as an effective barrier to suppress the shuttle effect of polysulfide, realizing the ultra-long-cycling lifetime and ultra-low-capacity

attenuation of Li–S batteries. The high discharge capacity (1269 mAh g^{-1}) and cycling stability (936 mAh g^{-1} after 200 cycles) of the Li–S soft-pack battery with a high sulfur loading (5.8 mg cm^{-2}) in various bending states demonstrate the potential of the MOF@PVDF-HFP separator in developing of practical EES.

Similar to the functional separator, MOF-based ion-sieve membranes also improve the stability of Li–S batteries. However, the battery with MOF-based ion-sieve membranes actually still suffers from short-living and the capacity significantly decays 25–40% within 300–600 cycles [58, 60], which were mainly ascribed to the following three aspects: (i) formation of interconnected mesoporosity given the MOF grains with a quasi-spherical shape renders the polysulfide to pass through the membrane; (ii) defects, such as cracks, dislocation, in the grain boundary of the membranes allows the escape of polysulfide through the membrane; (iii) the weak mechanical robustness results in the formation of large cracks [63]. Tricoli and co-workers designed a Janus membrane with conductive/insulating layers [61]. Fig. 3.6e shows that the conductive layer close to the cathode is made of high-aspect-ratio MOF/graphene nanosheets, in which the dense and continuous filling of MOF almost eliminate the formation of mesopores, so as to prevent the shuttle of polysulfides, and avoid the loss of sulfur. The insulating layer close to anode is a commercial PP separator, which not only provides a mechanical support for the conductive layer, but also simultaneously acts as a protective layer to avoid short circuit and improves the safety of batteries. As a result, the battery with Janus membranes has superior long-term cycling stability with 75.3% capacity retention for 1700 cycles at a high sulfur loading of 3.5 mg cm^{-2}. Jiang and co-workers fabricated a mechanically and chemically stable Zr-MOF (UiO-66) membrane as a composite separator for Li–S batteries by a facile filtration method [62]. The polar functional groups in MOF, e.g., carboxyl, and hydroxyl groups, improve the wettability between the composite separator and electrolyte, which greatly promotes the transport of lithium ions and reduces the interface impedance (Fig. 3.6f). Significantly, the combination of the ion-sieving effect and the physical and chemical adsorption inhibited the shuttle effect of polysulfides without hampering the migration of lithium ions. Different from the pristine separator, the battery with UiO-66 separator exhibited a high capacity of 955.8 mAh g^{-1}, which was much superior to pristine separator of 289.2 mAh g^{-1}. In addition, the cycling stability and capacity retention were both improved benefiting from the UiO-66 membrane, in which the discharge capacity can reach 964.1 mAh g^{-1} at 0.5C and evenly decays only 0.08% per cycle.

3.4 MOFs and MOF-Derived Materials for LOBs

3.4.1 Pristine MOFs for LOBs

3.4.1.1 Cathode in LOBs

MOFs are frequently used cathode catalysts in LOBs, in which porous structure and regular channels not only improve the oxygen diffusion, but also provide enough space to accommodate discharge products (e.g., Li_2O_2) [64]. Furthermore, adjustable chemical functionalities and open metal sites can greatly promote redox reactions, and thereby accelerate the decomposition of discharge products to avoid the blockage of gas channels [65].

Li and co-workers [66] selected five pristine MOFs as oxygen cathode materials, and further explored the correlation between structure and electrochemical performance of MOFs in LOBs (Fig. 3.7a). Benefiting from accessible open metal centers and porous frameworks, oxygen enrichment behaviors are easily fulfilled. Consequently, the Mn-MOF-74 electrode shows a primary discharge capacity of 9420 mA h g^{-1} under 1 atm of oxygen, four times higher than the MOF-free oxygen electrode. Chen and co-workers [67] demonstrated that Ni-MOFs can be displayed as a high-powered cathode catalyst for rechargeable LOBs. The 3D micro-nano channels, open catalytic sites and large specific surface not only realize free diffusion for oxygen, but also provide enough contact between electrolyte and active metal sites to promote the ORR/OER process (Fig. 3.7b). Hence, the prepared Ni-MOFs cathode shows a high specific capacity of 9000 mA h g^{-1}, and a stable cycling of 170 cycles without obvious voltage drop. The obtained high specific capacity and cycling stability were mainly attributed to the formation of nanofiber-like Li_2O_2, and the subsequent efficient decomposition in ORR process. Both of these works demonstrate the potential value of pristine MOFs in LOBs with reversible electrochemical ORR/OER process.

A further enhancement was realized by using a bimetallic MOF material. The researchers synthesized bimetallic MnCo-MOF-74 cathode catalyst by a simple hydrothermal reaction, and subsequently explored the electrochemical performance in LOBs using this bimetallic MOF as cathode [68]. Compared to monometallic Mn-MOF-74 and Co-MOF-74, the MnCo-MOF-74 exhibited better catalytic activity and oxygen evolution reactions. Benefiting from the porous channels of the MnCo-MOF-74, as well as the abundant active metal clusters composed of Mn and Co, the MnCo-MOF-74 cathode realizes a high discharge capacity of 11,150 mA h g^{-1} at a current density of 200 mA g^{-1}, which is superior to both Mn-MOF-74 and Co-MOF-74 cathode (Fig. 3.7c). This work confirmed that the synergistic interaction of Mn and Co metal clusters obviously improves the discharge capacity and reversibility, further expanding the application of MOFs in LOBs.

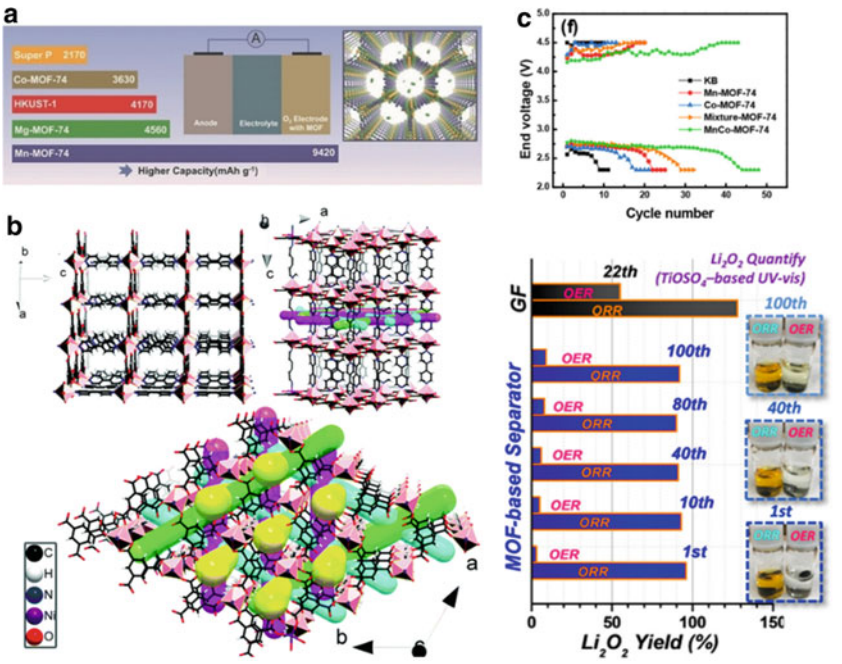

Fig. 3.7 **a** Rate capacities of LOBs for MOFs and related materials. Reproduced with permission [66]. Copyright 2014, WILEY–VCH. **b** Crystal structures of Ni-MOFs along the c axis, perpendicular to the c axis and along the b axis. The red, green, and blue rods stand for three cross linking channels, which are equal to each other. The yellow rods stand for channels along the c axis. Reproduced with permission [67]. Copyright 2015, the Royal Society of Chemistry. **c** End voltage vs. cycle number of the electrodes. Reproduced with permission [68]. Copyright 2018, American Chemical Society. **d** Li_2O_2 yields on discharged/charged cathodes harvested from various cycles. The inset presents the related photos of $TiOSO_4$-based titration solutions. Reproduced with permission [69]. Copyright 2018, American Chemical Society

3.4.1.2 Separator in LOBs

It is known that the separator is not an active component in the battery. However, the separator plays an irreplaceable role of separating the cathode and anode to avoid the internal short circuits, while achieving the free migration of lithium ions between cathode and anode. Therefore, the selection of separator is crucial for the electrochemical performance and lifespan of batteries. In past decades, MOFs have been investigated as separators due to the adjustable channels and controllable chemical functionalities. Especially, the specific channels within MOFs can realize the selective transport for specific ions or solvent molecule. Hence, it is feasible to design the pore size or chemical functionalities within MOFs based on the actual demands.

Zhou and co-workers [69] reported the MOF-modified separators to suppress the shuttling of soluble catalysts, improving the cycling stability and Coulombic efficiency of batteries. The selected HKUST-1@Celgard separators possess a smaller

pore aperture than those of soluble catalysts, and thereby restrain the diffusion of catalysts to lithium anode (Fig. 3.7d). The suppression of shuttling behavior prevents the erosion of lithium metal and optimizes the performance of LOBs. Consequently, the battery with MOF-modified separator displayed a high specific capacity, low overpotential, and long lifespan. The use of the specific pore structure in the MOFs to achieve selective transport of ions also provided the insight for the design of artificial interface.

3.4.1.3 Oxygen Diffusion Membrane in LOBs

In practical LOBs, moisture and carbon dioxide in air atmosphere seriously affect the performance and lifetime of LOBs. Inspired by the utilization of MOFs for gas separation, researchers tried to use MOFs as an oxygen-selective membrane to protect electrodes from corrosion in semi-open system to achieve the ultimate goal of real lithium-air batteries.

Lu and co-works [70] prepared a mixed matrix membrane (MMM), in which polydopamine-coated MOF crystals CAU-1-NH_2 were introduced into a PMMA matrix. Interestingly, the obtained MMM exhibits high oxygen permeability, high capture capability of carbon dioxide, and superior hydrophobic properties due to the multifunctional groups of -NH_2, -OH and -C = O in CAU-1-NH_2 and PMMA. Resultantly, the LOBs assembled by MMM had significantly improved cycling stability from 7 to 66 cycles with a capacity limit of 450 mA h g^{-1} at 450 mA g^{-1} under 30% relative humidity. However, the adsorption of carbon dioxide within MMM inevitably increased the weight of matrix membrane and decreased the energy density of batteries. Hence, the search for MOF-based oxygen-selective membrane should be focused on the efficient oxygen permeability without obvious adsorption for other irrelevant gases.

3.4.2 MOF-Derived Materials for LOBs

The direct utilization of MOFs was usually impeded by their low electrical conductivity and poor structure stability, resulting in undesirable energy efficiency, and cycling stability. Therefore, MOFs are usually used as self-sacrificial templates to generate various nanostructured electrode materials for LOBs, such as MOF-derived metal, MOF-derived metal oxides, and other MOF-derived materials. The periodic arrangement of active metal centers and organic linkers within MOFs make it successful to realize homogeneously distribution of catalytic sites when using MOFs as precursors. Compared to pristine MOFs, MOF-derived materials hold more promises as electrode materials thanks to the improved structure stability and electrical conductivity.

3.4.2.1 MOF-Derived Metal in LOBs

As we all know, transition metals have excellent catalytic performance for discharge products in lithium-air batteries. Therefore, it is a common method to disperse transition metal nanoparticles in a 3D conductive framework to construct oxygen cathode. However, the severe agglomeration leads to poor dispersion of metal nanoparticles in the conductive framework, which seriously affects its catalytic performance in LOBs. The usage of MOFs, as precursors, to construct MOF-derived metal electrodes can easily solve the problem of nanoparticle agglomeration. Wang and co-workers [71] reported a self-standing catalyst architecture with hierarchically porous carbon framework decorated with Co nanoparticles by simple 3D-printing, and subsequent thermal treatment of Co-MOF (Fig. 3.8a). The prepared carbon framework with Co nanoparticles (3DP-NC-Co) serves as a porous conducting matrix due to the excellent conductivity and mechanical stability. The conductivity of 3DP-NC-Co is about 2.2×10^3 S m^{-1}, which is extremely advantageous for the diffusion of oxygen

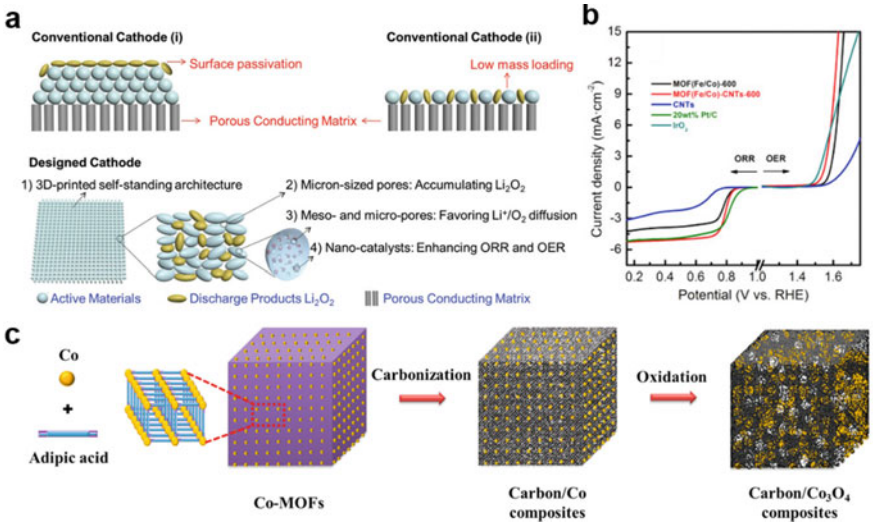

Fig. 3.8 **a** Comparison of three schematic Li-O_2 cathodes for Li_2O_2 deposition. The cathode structure exhibits the following characteristics: **1** Crack-free self-standing architecture of densely packed carbon nanoflakes with good conductivity that acts as a conducting matrix and thereby increases the practical specific energy. **2** Micron-sized pores formed between aligned Co-MOF-derived carbon flakes that accumulate Li_2O_2 particles to prevent the surface passivation. **3** Meso- and micropores developed within carbon flakes that facilitate the Li^+/O_2 diffusion. **4** Nanocatalysts that effectively boost oxygen reduction reaction (ORR) and oxygen evaluation reaction (OER). Reproduced with permission [71]. Copyright 2018, WILEY–VCH. **b** ORR and OER RDE voltammograms for the applied samples. Reproduced with permission [72]. Copyright 2017, Elsevier. **c** Schematic illustration of the formation procedure of the carbon/Co_3O_4composites via post two thermal treatments. Reproduced with permission [73]. Copyright 2017, Elsevier

and lithium ions. Most impressively, abundant meso- and micropores within Co-MOF-derived carbon flakes realized high-efficiency deposition and decomposition of Li_2O_2, which is ascribed to the trapping of insulating Li_2O_2 within the pores and the presence of Co electrocatalysts. Consequently, 3DP-NC-Co cathode achieved a high discharge capacity of 1124 mA h g^{-1}, which is superior to both RP-NC-Co and CP-NC-Co electrodes. Furthermore, lower overpotential and enlarged cycling lifespan also demonstrated the advantages of 3DP-NC-Co as a cathode electrocatalyst. This work proposed a new perspective in the large-scale synthesis of MOF-derived metal cathode in LOBs.

Compared with single transition metal electrocatalysts, bimetallic electrocatalysts have better electrochemical performance due to the synergistic effect of multiple active metal clusters. Therefore, bimetallic MOFs as self-sacrificing precursors to prepare MOF-derived metal material were widely investigated in LOBs. Chen et al. [72] synthesized FeCo alloy core@nitrogen-doped carbon shell nanoparticles/CNTs composite as bifunctional electrocatalysts for OER/ORR process. After the pyrolysis of FeCo-MOF at 600 °C, the resulting electrocatalyst with a core-shell structure affords remarkable bifunctional electrocatalytic activity with a slight △E gap of 0.79 V in alkaline electrolyte condition (Fig. 3.8b). Moreover, LOBs assembled by as-prepared composite cathode exhibited a high discharge/charge specific capacity of 5000 mAh g^{-1} at a constant current density of 100 mA g^{-1}, and excellent cycle stability of 40 cycles.

3.4.2.2 MOF-Derived Metal Oxides in LOBs

The features of chemical and mechanical stability with high ORR/OER electrocatalytic activity make metal oxides promising cathode catalysts in LOBs, such as MnO_2, Co_3O_4, and RuO_2. However, low electrical conductivity, large volume fluctuation, and inevitable particle agglomeration seriously affect the electrochemical behavior, such as electrode pulverization, capacity decay, and poor cycling stability. To alleviate these issues, an effective method was proposed using MOF as a sacrificial template to synthesize metal oxides@carbon composite. The carbon framework derived from MOFs can effectively improve the electronic conductivity and inhibit the volume variation during charging/discharging process, and the in situ generated metal oxide can be uniformly dispersed in the carbon framework to avoid agglomeration. Resultantly, MOF-derived metal oxides exhibited a bright application prospects in LOBs.

MOF-derived porous carbon/Co_3O_4 composite was synthesized via post-thermal treatment and applied in cathode for rechargeable LOBs. The cobalt-containing MOFs were selected as a sacrificial template to realize uniform distribution of Co_3O_4 nanoparticles [73] in the carbon framework, improving the electronic conductivity and alleviating the particle agglomeration of pure Co_3O_4 (Fig. 3.8c). Benefiting from high electrical conductivity, low volume change, and uniform distribution of Co_3O_4, the MOF-derived porous carbon/Co_3O_4 composite displayed a

high reversible capacity of 9850 mA h g^{-1} at a current density of 100 mA g^{-1} and excellent cycling stability of 320 cycles. Furthermore, Zhang and co-workers [74] successfully synthesized porous cobalt-manganese oxide by using nanocube-like MOFs as the precursor, and applied it as oxygen cathode electrocatalyst for LOBs. The LOB assembled by as-prepared MOF-derived porous cobalt-manganese oxide shows stable Coulombic efficiency of 95%, and high capacity retention under various current densities. The superior electrochemical performance of MOF-derived porous cobalt-manganese oxide could be ascribed to the synergistic electrocatalytic activity of cobalt-manganese oxide and favorable channels within carbon framework.

3.4.2.3 Other MOF-Derived Materials in LOBs

Except for the MOF-derived metal and metal oxides, there are still other MOF derivatives, such as MOF-derived carbides, nitrides, and sulfides. These MOF-derived materials also showed great potential in oxygen cathode due to adequate active sites and porous structure. Yan and co-workers [75] prepared nitrogen-doped porous molybdenum carbide electrode using Mo-based MOFs as the precursor. The micro-sized molybdenum carbide rods are composed of numerous nanocrystals, in which the interpenetrating mesoporous and macroporous channels not only offer sufficient exposure of active sites for the electrochemical reaction, but also provide abundant sites for the nucleation and deposition of discharge product. Among the two prepared molybdenum carbides, the α-MoC_{1-x} electrode exhibits improved electrochemical performance given the smaller charge transfer resistance and remarkable oxygen adsorption capability. Resultantly, α-MoC_{1-x} cathode possesses a superior discharge capacity of more than 20,000 mA h g^{-1} and cycling stability of 100 cycles. Amine and co-workers [76] used MOF as the precursor to successfully synthesize biphasic N-doped heterostructural cobalt nitride incorporating few layers of N-doped graphene, and applied it as oxygen cathode electrocatalyst in LOBs. The synthetic multiple-capsule porous electrode affords sufficient room to accommodate the discharge product on one hand and ensure the efficient oxygen diffusion to improve electrocatalytic activity on the other hand. The combination of nitrogen-doping defect in graphene and the sufficient exposure of Co-N surface afford stronger interaction between BND-Co@G-MCH and the discharge product of Li_2O_2, and eventually exhibited significantly improved electrocatalytic performance. Peng and co-workers [77] designed Co_9S_8@carbon porous nanocages as a bifunctional catalyst by using ZIF-67 as the precursor. The high electrocatalytic activity of Co_9S_8 and porous conductive carbon nanocages both improve oxygen reduction/evolution reactions, realizing a high energy efficiency of 72.7% and an enlarged lifespan of 110 cycles at a current density of 100 mA g^{-1}.

Summary

The high porosity, diverse structures, and controllable chemical compositions render MOFs and MOF derivatives promising materials in LOBs. Unfortunately, there are still many fundamental and technical issues that need to be addressed before realizing the practical application, such as limited Coulombic efficiency, energy density, and cycling stability. In the future, the application of MOFs and MOF-derived materials in LOBs are mainly focused on the cathode and separator. In terms of cathode, electronic conductivity and electrocatalytic efficiency should be further improved to meet the increasing requirements. Therefore, bimetallic MOFs and MOF derivatives exhibit more competitiveness in electronic conductivity and electrocatalytic efficiency. As for MOF-based separator, the controllable porosity and modifiable chemical composition can effectively suppress the diffusion of oxygen and soluble electrocatalyst to lithium anode side, and thereby reducing the degradation of metallic lithium. Hence, the rational design of channels and chemical composition within MOFs and MOF-derived materials are crucial for electrochemical performance of LOBs.

3.5 MOF-Derived Materials in Li-Se Batteries

In recent years, Li-Se batteries have attracted much attention due to its high energy density and low cost [78]. Selenium is one of the typical chalcogen elements and possesses various similar properties with sulfur. For example, Li-Se batteries (i.e., $16Li + Se_8 \leftrightarrow 8Li_2Se$) have similar reversible redox reactions as Li-S batteries (i.e., $16Li + S_8 \leftrightarrow 8Li_2S$) [79, 80]. Despite the lower specific capacity of Li-Se batteries (675 mAh g^{-1}) compared to Li-S batteries (1675 mAh g^{-1}), the volumetric energy density of Li-Se batteries (3253 mAh cm^{-3}) is comparable to Li-S batteries (3467 mAh cm^{-3}) [81, 82]. Impressively, as a metalloid element, selenium exhibits a considerable higher electrical conductivity of 1×10^{-3} S m^{-1} than that of sulfur (5×10^{-28} S m^{-1}), which promises a rapid electrochemical kinetics during lithiation and delithiation process [80, 83, 84]. However, restricted by the severe shuttle effect, the selenium cathode also suffers from rapid capacity decay and low Coulombic efficiency. In addition, the large volume fluctuation of Li-Se battery is also fatal to the electrode structure during the lithiation and delithiation processes, further deteriorating the electrochemical performance of batteries.

To acquire a better electrochemical performance for Li-Se battery, more attention should be focused on mitigating both shuttle effect of polyselenides and volume fluctuation of selenium electrode during cycling. Based on this consideration, various carbon materials were selected to construct carbon-selenium composites. Despite the advancements achieved by composites, it is still confronted with the low mass loading issue of selenium. In general, the loading capacity of selenium is less than 50 wt%, and consequently reduces the utilization of the cathode materials. In past decades, carbon-based materials derived from MOFs have attracted inspiring attention due to their large specific surface areas, unique porous structures and controllable chemical

components [85]. These MOF-derived carbon materials with unique pore structure are suitable as hosts for selenium confinement to alleviate the problems faced by selenium cathodes.

Li and co-workers [86] prepared a mesoporous carbon matrix (meso-C) derived from MOF-5 as cathode host to confine selenium, in which the selenium content reaches 48 wt%, accounting for half of the weight of the meso-C@Se composite. Benefiting from the intrinsic advantages of MOF-5 precursor, the meso-C possesses good electrical conductivity, high specific surface area and large pore volume. Consequently, the meso-C@Se composite cathode displays an initial discharge capacity of 641 mAh g^{-1} and retains 306.9 mAh g^{-1} after 100 cycles at 0.5 C. Li and co-workers [87] prepared Ni-MOF-derived hollow layered carbon spheres (MHPCS) by hydrothermal reaction, and subsequent carbonization treatment (Fig. 3.9b and c) Such Ni-MOF-derived hollow layered carbon spheres are composed of large number of interconnected mesoporous carbon bubbles with size of 10–20 nm. Finally, the MHPCS/Se composite was successfully obtained by combining MHPCS with selenium through melt-diffusion impregnation process (Fig. 3.9d-h). The synthesis

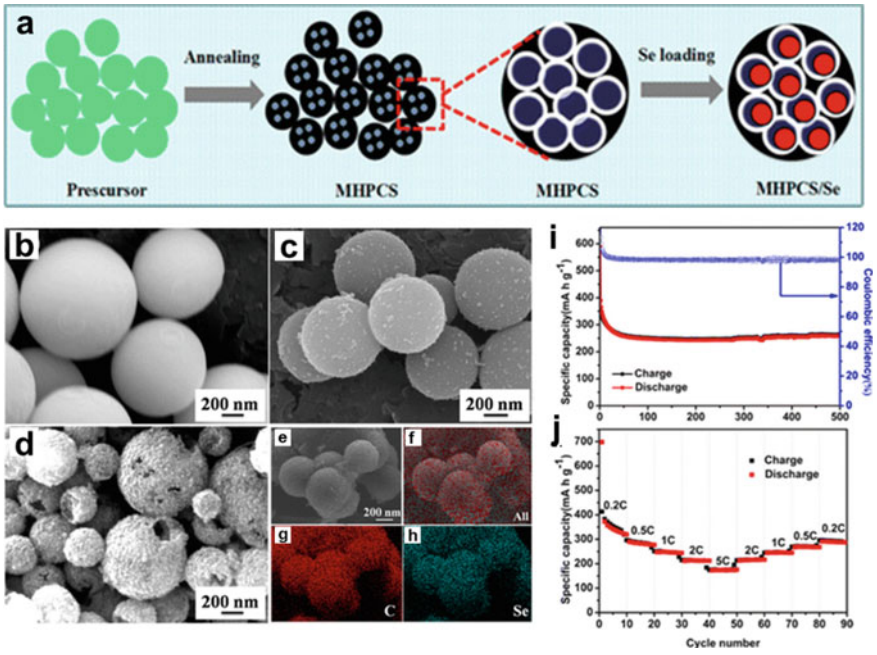

Fig. 3.9 **a** Schematic illustration of the synthesis process of MHPCS/Se composites. **b** SEM images of the sample Ni-MOFs, **c** MHPCS, and **d** MHPCS/Se composite, the EDX mappings of **g** C and **h** Se. **i** Cyclic performance and Coulombic efficiency of Li–Se batteries at 0.5 C. **j** Rate capability of MHPCS/Se composites. Reproduced with permission from Ref. [87], Copyright 2016, American Chemical Society

process of MHPCS/Se composites is shown in Fig. 3.9a. The combination of microporous and mesoporous structures in MHPCS can tightly confine selenium and provide additional buffer space to alleviate the volume change of selenium during charging and discharging process. As a result, MHPCS/Se cathode delivers a specific capacity of 588.2 mAh g^{-1} after 500 cycles at 0.5 C as shown in Fig. 3.9i, and the corresponding capacity decay is only 0.08% per cycle. Notably, the battery assembled by MHPCS/Se cathode displayed an ultra-high cycling stability, and retains the specific capacity of 200 mAh g^{-1} after 1000 cycles at 1 C. Besides excellent cycle stability, the MHPCS/Se cathode also exhibits an impressive rate capability in Fig. 3.9j. Xu and co-workers [88] prepared mesoporous carbon (meso-C) derived from Ni-based MOF. The prepared meso-C@Se cathode exhibits an initial discharge capacity of 599.7 mAh g^{-1} and retains the specific capacity of 417 mAh g^{-1} after 100 cycles at 3 C with a Coulombic efficiency of 99.9%.

Further enhancement can be realized by using hierarchical carbon framework systems in Li-Se batteries. Xu and co-workers [89] designed a unique hierarchical porous carbon microcube (CMC) host derived from Zn/Ni-MOF-2 for the selenium confinement. The preparation of Se/CMCs composites is illustrated in Fig. 3.10a, the

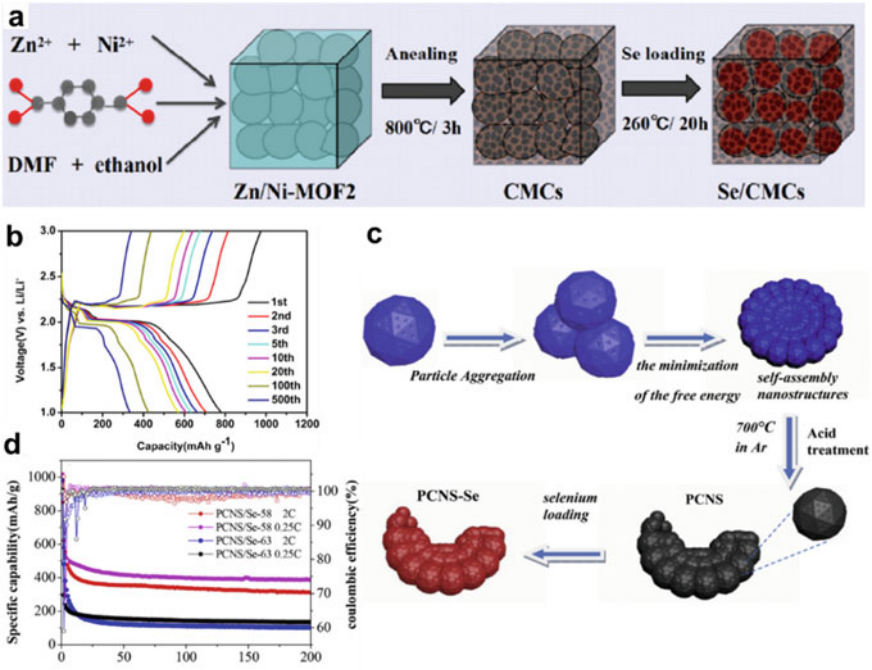

Fig. 3.10 **a** Schematic illustration of the preparation of Se/CMCs composites. **b** The discharge–charge profiles of Se/CMCs composite at 0.2 C. Reproduced with permission from Ref. [89], Copyright 2016, Elsevier. **c** Illustration of the synthesis route for the PCNS/Se composite. **d** Cycle performance of PCNS/Se-58 and PCNS/Se-63 at 2 C. Reproduced with permission from Ref. [91], Copyright 2019, Elsevier

porous carbon microcube was firstly prepared by thermal treatment of Zn/Ni-MOF-2, followed by acid-soaking process. The as-prepared porous carbon microcube with excellent conductivity, ultra-high specific surface area, and large pore volume greatly inhibit the dissolution of polyselenides and resultantly improve the utilization of selenium cathode. Therefore, CMC@Se cathode shows an initial discharge capacity of 780.4 mAh g^{-1}, with 425.2 mAh g^{-1} retained after 100 cycles at 0.2 C in Li-Se batteries (Fig. 3.10b). Zeng and co-workers [90] designed two-dimensional ultrathin carbon nanosheets (UCNS) derived from interconnected MOF. The ultrathin carbon nanosheet is obtained by further carbonization and acid wash of Al-MOF(SAM) prepared by in situ self-assembly strategy, with large specific surface area and hierarchical porous structure. Thanks to the unique hierarchical structure nanosheets, which was composed of large number of two-dimensional sub-units stacked in parallel, the volume expansion was alleviated with simultaneously improved utilization of active materials. Finally, the UCNS@Se composite cathode was obtained by encapsulating selenium into the UCNS host, the preparation of Se/CMCs composites is schemed in Fig. 3.10c. The battery assembled by UCNS@Se composite cathode displays a reversible capacity of 347.3 mAh g^{-1} after 240 cycles at 2 C (Fig. 3.10d). Later, Zeng and co-workers [91] designed hierarchically porous carbon nanosheets with surface morphology similar to fish scales, which were prepared by using self-assembled MOF (SAF) as template and carbon source. The fish-scale carbon nanosheets derived from SAF (PCNS) have a large specific surface area and a well-defined nanostructure, which endows enough space for the selenium loading, and provides stable electron and ion transfer channels. Besides, the fish-scale carbon nanosheets were also displayed as powerful adsorbent, maintaining the stability of lithium polyselenates during the charge and discharge process. Eventually, the PCNS@Se cathode was obtained by encapsulating selenium into PCNS, in which the selenium takes up 58 wt % of total PCNS@Se cathode. Benefiting from the hierarchically porous design, the PCNS@Se cathode exhibits a reversible discharge capacity of 311.8 mAh g^{-1} after 200 cycles at 2 C, and the Coulombic efficiency maintains 99% after 1000 cycles.

Heteroatom doping, such as nitrogen, oxygen, and sulfur, significantly improves the chemical affinity to polyselenides [92]. Hence, the employment of carbon doped with different heteroatoms as hosts to inhibit the shuttle effect of polyselenides is regarded as an effective strategy to improve the electrochemical performance. Yin and co-workers [93] used Al-MOF as a sacrifice template to synthesize a nitrogen-doped carbon sponge (NCS) with abundant micropores and mesopores via high temperature carbonization under Ar and NH_3 flow. The nitrogen-doped carbon sponge is composed of interconnected carbon layers with a size of 0.4–0.55 nm and mesopores between carbon layers as shown in Fig. 3.11a and c. By means of melting-diffusion-permeation process, selenium is firmly confined in the micropores of the carbon framework of NCS@Se composite as shown in Fig. 3.11b and d. The micropores and mesopores in the carbon layer fix dispersed selenium and buffer the volume change of Se during delithiation–lithiation processes, respectively. Besides, nitrogen-doping facilitates the electron conduction in carbon matrix and further promotes the rapid transfer of charges. Resultantly, NCS@Se composite cathode delivers a reversible

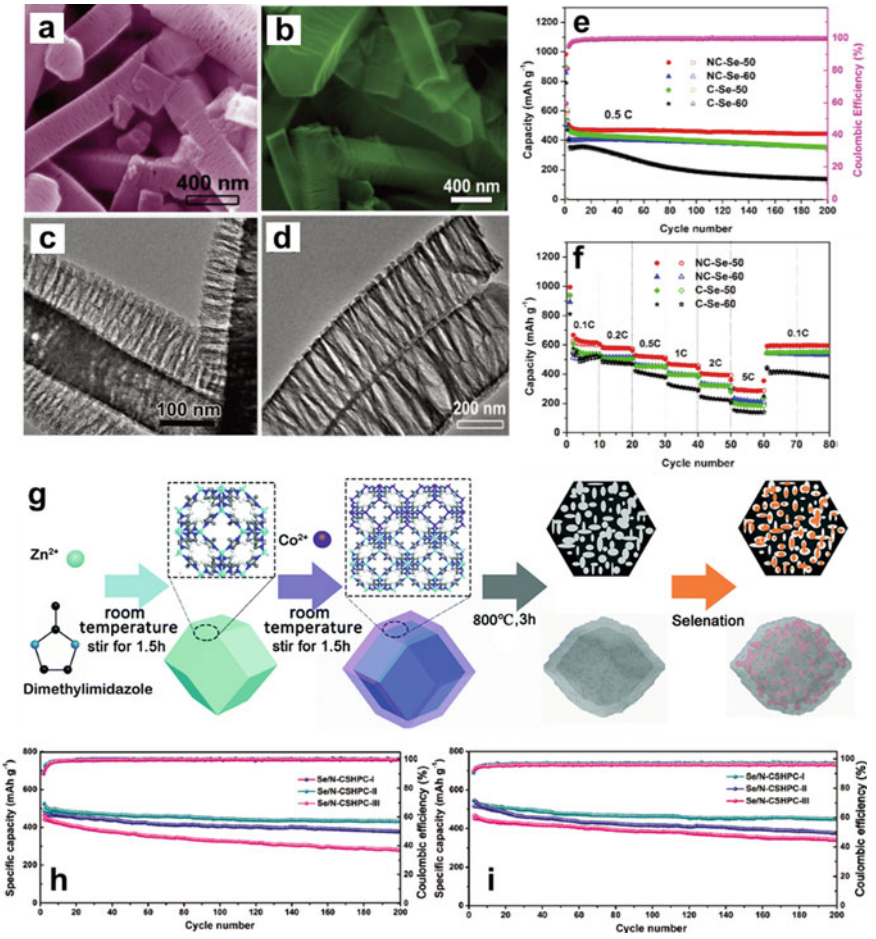

Fig. 3.11 **a** FESEM image, **c** TEM image of Al-MOF-derived NCS materials. **b** FESEM image, **d** TEM image of the NCS/Se-50 composites. **e** Cycling performances of NCS/Se and CS/Se composites at 0.5C, and pink circles show the Coulombic efficiency of NCS/Se-50. **f** Rate capabilities of NCS/Se and CS/Se composites. Reproduced with permission from Ref. [93], Copyright 2015, Royal Society of Chemistry. **g** Schematic illustration of the synthesis of the Se/N-CSHPC composite. **h** The cycling performances of the Se/N-CSHPC-I, Se/N-CSHPC-II, and Se/N-CSHPC-III electrodes at 0.5 C and **i** 1.0 C. Reproduced with permission from Ref. [94], Copyright 2019, Royal Society of Chemistry

capacity of 443.2 mAh g^{-1} after 200 cycles at 0.5 C (Fig. 3.11e), and the Coulombic efficiency maintains ~ 99.9%. Enlarging the rate to 5 C as shown in Fig. 3.11f, the NCS@Se composite cathode still delivers a capacity of 286.6 mAh g^{-1}. Also, Su and co-workers [94] reported a MOF-derived nitrogen-doped core-shell hierarchical porous carbon (N-CSHPC). The N-CSHPC was obtained after the carbonization of

the core–shell ZIF-8@ZIF-67 precursor, with interconnected mesoporous and micropores structures. Noteworthily, the mesopores emerged at the core–shell interface, and the micropores were located on the ZIF-8-derived core and ZIF-67-derived shell after the pyrolyzation of core-shell ZIF-8@ZIF-67 precursor. As shown in Fig. 3.11g, the N-CSHPC@Se nanocomposites were prepared by permeating selenium into N-CSHPC. The content of selenium exceeded 60%. This hierarchical porous structure is effective in fixing selenium and polyselenides to prevent them from escaping from the pores and alleviate the volume fluctuation during cycling. In addition, in situ nitrogen-doping both improves the electrical conductivity of cathode and provides a strong chemical adsorption to Li_2Se. As a result, the N-CSHPC@Se cathode shows a reversible capacity of 555 mAh g^{-1} after 150 cycles at 0.2 C and 462 mAh g^{-1} after 200 cycles at 0.5 C and 432 mAh g^{-1} after 200 cycles at 1 C (Fig. 3.11h and i).

The transition metal and heteroatoms co-doped carbon further immobilize polyselenides through strong chemical interaction, and enhance the conversion of polyselenides, thus improving the electrochemical performance. He and co-workers [95] used ZIF-67 to prepare cobalt and nitrogen co-doped three-dimensional porous graphitic carbon (C-Co-N), which was employed as the Lewis base matrix to accommodate selenium. The synthetic process for C-Co-N/Se is shown in Fig. 3.12a. The C-Co-N derived from ZIF-67 has a unique structure and abundant micropores and mesopores (Fig. 3.12b). Meanwhile, co-doping of cobalt and nitrogen further improves the conductivity of C-Co-N, and provides efficient channels for electron and ion conduction. In addition, the employment of C-Co-N also decreases the dissolution of polyselenides and suppresses volume expansion during cycling. Noteworthy, the selenium loading in C-Co-N@Se (Fig. 3.12c and d) reaches 76.5 wt%, which is far higher compared to reported carbon-based materials. Consequently, C-Co-N@Se composite cathode delivers a high capacity of 672.3 mAh g^{-1} at 0.1 C as shown in Fig. 3.12e, maintaining reversible capacity of 574.2 mAh g^{-1} at 1 C after 200 cycles, with an impressive rate capability as shown in Fig. 3.12f.

Recently, conductive polymer coatings have been designed as a protective barrier to restrict the migration of polyselenides to the anode. Through the design of conductive polymer coatings, the polyselenides are well confined in the carbon matrix, achieving the prohibited shuttle effect, and thus enhanced cycling stability. Tang and co-workers [96] used Zr-MOFs as a precursor to synthesize a novel UIO-67@Se@PANI composite, the synthesis process of the UIO-67@Se@PANI composite are presented in Fig. 3.12g. The prepared UIO-67@Se@PANI composite shows a sandwich-like structure, in which selenium was highly dispersed in the UIO-67 matrix, and polyaniline layer was uniformly coated on the surface of carbon matrix. Herein, the polyaniline layer on the surface of UIO-67@Se prevents the dissolution of polyselenides and simultaneously improves the conductivity of the cathode, resulting in better electrochemical stability. Combining the advantages of various components, UIO-67@Se@PANI composite cathode delivers a high specific capacity of 248.3 mAh g^{-1} at 1 C (1 C = 675 mA g^{-1}) after 100 cycles. In particular, due to the excellent transfer of electron and ion within composite, the UIO-67@Se@PANI cathode exhibited a desirable rate capability, and displayed a reversible capacity of 203.1 mAh g^{-1} and 167.6 mAh g^{-1} after 100 cycles even at high rates of 2 C and 5 C.

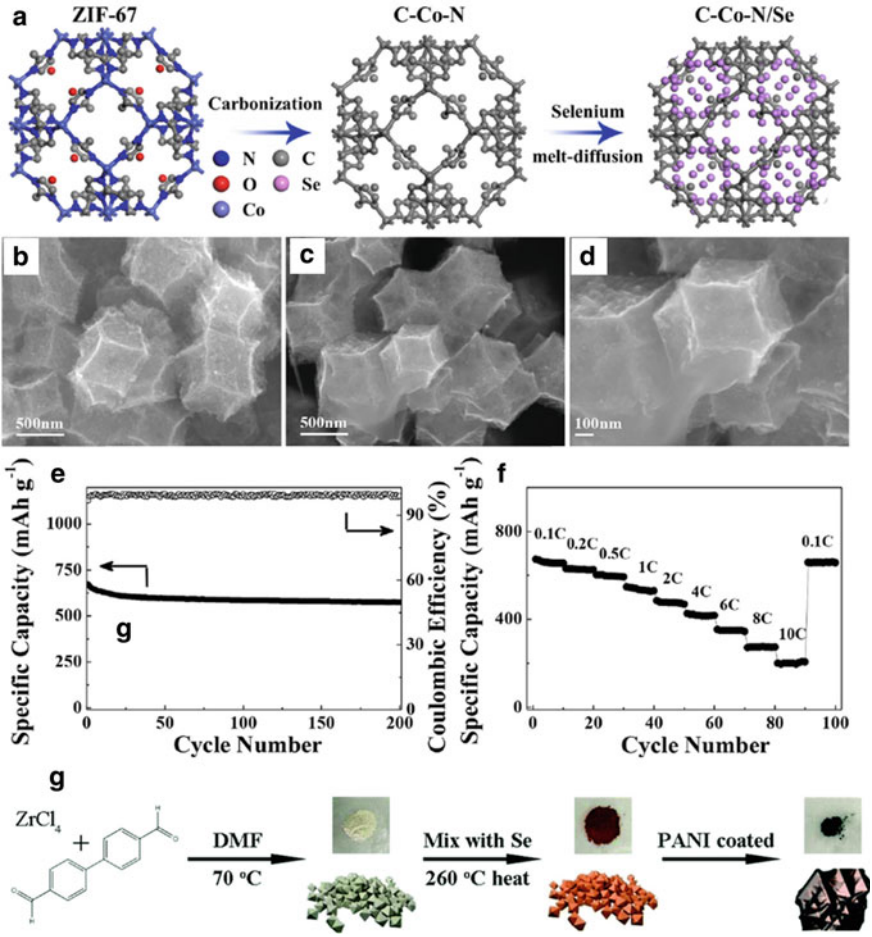

Fig. 3.12 **a** Schematic illustration of the synthetic process for C-Co-N/Se. SEM images of **b** C-Co-N and **c, d** C-Co-N/Se composites. **e** Cycling stability of the C-Co-N/Se cathodes at 0.1C for 200 cycles. **f** Rate performances at various C-rates of the C-Co-N/Se cathodes. Reproduced with permission from Ref. [95], Copyright 2017, Elsevier. **g** Illustration of the synthesis process of the UIO-67@Se@PANI composite. Reproduced with permission from Ref. [96], Copyright 2019, Royal Society of Chemistry

3.6 MOFs for SIBs

Sodium, which has similar physical and chemical properties to lithium, is rich in sources and low in cost, so the development of SIBs has been widely concerned [97, 98]. Therefore, the design of a stable and high-performance sodium storage material is of great significance to practical application of SIBs. Compared with lithium ions, sodium ions have a larger radius, which requires the electrode material with

large interlayer spacing for sodium-ion intercalation. MOFs, especially prussian blue analogues (PBAs) with framework configuration and large interstitial sites endow facile insertion and extraction of sodium ions during charge and discharge process, which makes MOFs as promising electrode materials in SIBs [99]. Furthermore, MOFs are also promising to be applied in separators and solid electrolytes through chemical compositions alteration or pore structure control [100]. In this section, a brief overview of MOFs and MOF-derived materials as electrodes, separators and solid electrolytes in SIBs are summarized. Despite that considerable progress has been made in recent years, the utility of MOFs and MOF-derivates in rechargeable SIBs is still an emerging research topic. By discussing the development of MOFs and MOF-derivates in SIBs, a basic guidance and future prospects are provided.

3.6.1 MOFs and MOF Derivatives as Electrode Materials

MOFs, especially PBAs with frame structure and large interstitial sites, are suitable for insertion/extraction of sodium ions during cycling. Therefore, various MOF materials are widely used as electrode materials in SIBs. Wang and co-workers [101] firstly investigated and used conductive conjugated coordination polymers (CCPs) as cathode for SIBs. The redox states variation during the electrochemical process verified the chemical structure of Ni-TTO in CCPs, in which the Ni-TTO can be transformed into Ni-ETT after the reduction and sodiation (Fig. 3.13a). As a result, the battery with CCPs cathode delivers a high capacity of 155 mA h g^{-1}, and 84% of

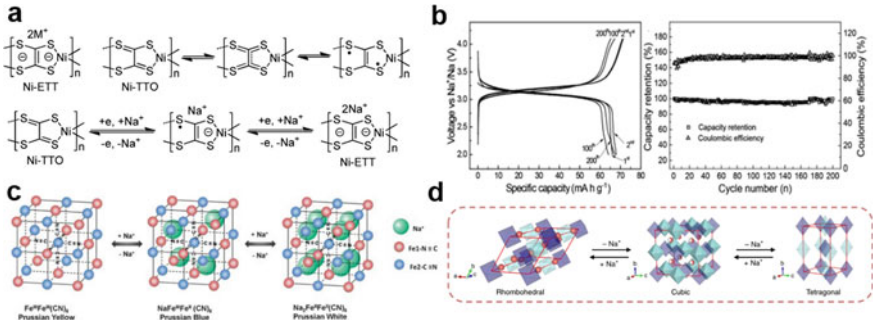

Fig. 3.13 **a** The proposed conversion mechanism of Ni-ETT and Ni-TTO, through a redox reaction. Reproduced with permission [101]. Copyright 2016 the Royal Society of Chemistry. Electrochemical characterization of NiFe-PBA. **b** Galvanostatic charge/discharge voltage profiles cycled at a current density of 20 mAg^{-1} and Cycling performance of the NiFe-PBA cycled at 20 mA g^{-1} between the voltage limits of 2.0 and 4.1 V (vs. Na^+/Na). Triangles show the corresponding Coulombic efficiencies. Reproduced with permission [103]. Copyright 2013, The Royal Society of Chemistry. **c** Redox mechanism of $FeFe(CN)_6$. Reproduced with permission [104]. Copyright 2015, The Royal Society of Chemistry. **d** Schematic three-phase evolutions during cycling of rhombohedral PB-S3. Reproduced with permission [106]. Copyright 2020, Springer Nature

the capacity was maintained even at 30C with a content of active materials as high as 80%. Notably, the prepared CCPs cathode possesses excellent rate capability due to the high conductivity of 30 S cm^{-1} and the high sodium-ion diffusion coefficient of 10^{-9} cm^2 s^{-1}. This work introduces the CCPs into the cathode of SIBs, and investigates the internal transformation mechanism during cycling, which pays the way for the design of various CCPs in other multifunctional electrochemical applications.

PBAs as perovskite face-centered cubic structures with large arrays are also a member of metal organic frameworks, which has attracted significant interest as cathode materials of rechargeable SIBs given their open-framework structure and excellent cycling stability in electrolytes. However, the investigation of PBAs is usually hindered by the low practical specific capacity, and thereby weakens its application potential. Hence, the improvement of specific capacity of PBAs is of great importance in SIBs. Xiang and co-workers [102] synthesized nanostructured $Na_2Co_{0.8}Ni_{0.2}[Fe(CN)_6]$ composite, and explored the reaction mechanism by combining ex situ X-ray diffraction, FTIR spectroscopy, and Raman spectroscopy. This work shows that through the reversible chemical reaction of the Co^{3+}/Co^{2+} and Fe^{3+}/Fe^{2+} redox pairs, the $Na_2Co_{0.8}Ni_{0.2}[Fe(CN)_6]$ composite has undergone the initial structural transformation from the rhombohedral phase to the cubic phase, and the solid solution mechanism in a wide potential range. It is found that the battery with $Na_2Co_{0.8}Ni_{0.2}[Fe(CN)_6]$ composite delivers a high reversible capacity of 116.4 mAh g^{-1} and a working potential of 0.67 V. Based on above calculation, the battery with $Na_2Co_{0.8}Ni_{0.2}[Fe(CN)_6]$ cathode and $NaTi_2(PO_4)_3$ anode achieves a high theoretical specific energy of 171 Wh kg^{-1} in aqueous SIBs. In addition, $Na_2Co_{0.8}Ni_{0.2}[Fe(CN)_6]$ cathode also displayed excellent cycling stability with a capacity retention of 88% after continuous charging/discharging for 100 cycles. Guo and co-workers [103] used a facile wet-chemical synthetic method to prepare NiFe-PBA as cathode material for SIBs. Interestingly, the change of the lattice parameter within the NiFe-PBA cathode is less than 1% even after continuous charging/discharging for 200 cycles. The lower volume fluctuation retains the structural stability and preserves effective transport paths for ions and electrons during cycling. The "zero-strain" characteristics of NiFe-PBA endow outstanding cycling stability with a capacity retention of 99.7% and Coulombic efficiency of nearly 100% after 200 cycles (Fig. 3.13b). Despite the natural advantage of PBAs in SIBs in terms of framework structure and large interstitial sites, there are still many issues to be resolved. Yang and co-workers [104] verified that improving the purity and crystallinity of PBAs can further enhance the electrochemical performance. In this work, single crystal $Fe^{III}Fe^{III}(CN)_6$ nanoparticles were synthesized as a model to improve the cycling performance of SIBs (Fig. 3.13c). As expected, single crystal $FeFe(CN)_6$ nanoparticles cathode achieves a reversible capacity of 120 mAh g^{-1} and maintains a Coulombic efficiency of 100%. Moreover, $FeFe(CN)_6$ nanoparticles cathode also displayed excellent cycling stability, with 87% capacity retention for more than 500 cycles at 20 C. This study demonstrates the relationship between electrochemical performance and structure of PBAs, such as purity and crystallinity, and also provides new perspectives to design high-performance SIBs. Ma and co-workers [105] prepared a coordinated water free micro-cubic PB by electron exchange between PB and graphene oxide (GO), which was used as

cathode material for SIBs. Interestingly, in a pure PB electrode, only part of the redox sites contributes to the insertion/expulsion of sodium ions, whereas nearly all the redox sites in RGOPC3 cathode responded to the insertion/exaction of sodium ions. As a result, the RGOPC3 cathode delivers a high specific capacity of 163.3 mAh g^{-1}, superior to pure PB electrode with 131.2 mAh g^{-1} at 30 mA g^{-1}. Additionally, the RGOPC3 cathode also exhibited excellent long-cycling stability and rate capability, with a specific capacity of 112 mAh g^{-1} at 800 mA g^{-1}, and the capacity retention reached 91.9% after continuous cycling for 500 cycles. This work demonstrated the relationship between the coordinated water and low-spin Fe sites, and also provided design principles for other similar materials in SIBs. Iron-based PB analogues are favored as sodium-ion cathode materials in terms of low cost and convenient preparation. Chou and co-workers [106] prepared the PBA of sodium-rich MOF structure by co-precipitation method as cathode for sodium-ion storage. The as-synthesized PBA cathode has undergone a three-phase transformation of prismatic, cubic, and tetragonal during charge and discharge process (Fig. 3.13d). It is the reversible variation of structure during cycling that endows $Na_{2-x}FeFe(CN)_6$ with excellent cycling stability. The prepared cathode material exhibits outstanding electrochemical performance with specific capacity of 70 mAh g^{-1} at a current density of 2000 mA g^{-1} and maintains a high retention of 71% after 500 cycles.

Generally, metals, such as bismuth, antimony, and tin are employed as the anode of SIBs. The insertion of sodium ions into the metal lattice generated large volume change, resulting in the destruction of the electrode materials. There are some solutions to solve the intractable issue, such as reducing the particle size of the active component or using alloys to minimize the volume change during cycling [107, 108]. Deng and co-workers [109] used MOF-836 as a precursor to synthesize Bi-Sb alloys by nanoscale laser metallurgy method. The space distribution and uniformity of alloys are precisely controlled given the atomically dispersed behavior within MOF. Benefiting from the uniform particle sizes and distribution, the nanosized $Bi_{0.70}Sb_{0.30}$ alloys exhibited a high specific capacity of 259.8 mAh g^{-1} at 200 mA g^{-1} after 500 cycles, and outstanding cycling stability with a capacity loss of merely 0.055% per cycle. Liang and co-workers [110] designed a carbon fiber supported binder-free electrode, which was composed of bismuth and carbon composite. The high specific surface of carbon fiber guarantees the uniform distribution of MOF arrays to eliminate the serious agglomeration (Fig. 3.14a). The active bismuth nanodots confined in arrays alleviate the volume fluctuation during cycling. Additionally, abundant active sites provided by N-doped carbon arrays accelerate the sodium storage kinetics, and thereby contributes extra specific capacity. At a current density of 50 mA g^{-1}, the synthesized anode delivers a specific capacity of 630 mAh g^{-1} during cycling, with a high Coulombic efficiency of 99.7%. Nickel sulfide was regarded as a promising anode material in SIBs given the low cost and high theoretical capacity. However, it still suffers from poor electrical conductivity and huge volume expansion during charging and discharging process, and finally results in poor cycling stability and rate capability. Bu and co-workers [111] prepared the composite of Ni_3S_2 nanoparticles and N-doped carbon nanosheets (Ni_3S_2@C), in which Ni_3S_2 nanoparticles were evenly embedded in N-doped carbon nanosheets (Fig. 3.14b). Compared to

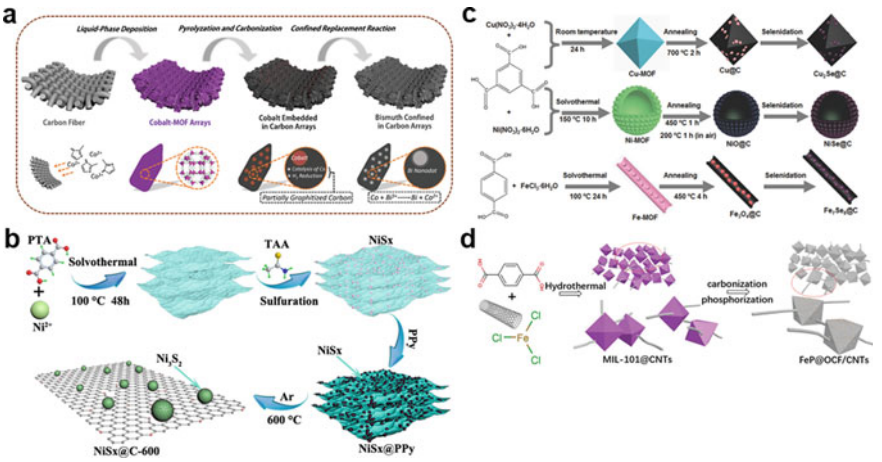

Fig. 3.14 **a** Schematic illustration of the synthesis of bismuth nanodots confined in carbon arrays. Reproduced with permission [110]. Copyright 2019, WILEY–VCH. **b** Schematic diagram of the fabrication of NiS_x@C-600. Reproduced with permission [111]. Copyright 2019, Elsevier. **c** Schematic illustration for the fabrication of uniform MOF-derived Cu_2Se@C porous octahedra, NiSe@C hollow microspheres, and peapod-like Fe_7Se_8@C nanorods as excellent anode materials for Na-ion batteries. Reproduced with permission [112]. Copyright 2018, WILEY–VCH. **d** Schematic diagram for the synthesis of FeP@OCF. Reproduced with permission [113]. Copyright 2020, WILEY–VCH

pure nickel sulfide, the design of Ni_3S_2@C shows the following three advantages: i) the coating of PPy guarantees formation of Ni_3S_2 nanoparticles with small sizes after thermal treatment process to shorten the transport path of the sodium ions; ii) the N-doped carbon shell improves the electrical conductivity of electrode, and thus increases the electrochemical capacity; iii) the carbon shell effectively alleviates the volume fluctuation during cycling and minimizes the degradation of electrode. Resultantly, NiS_x@C-600 delivers a superior discharge capacity of 432.8 mAh g^{-1} at 0.2 A g^{-1} for 100 cycles. Additionally, NiS_x@C-600 anode also displayed an impressive rate capacity of 371.6 mAh g^{-1} even at 6.4 A g^{-1} given the convenient transport path of electrons connected by N-doped carbon nanosheets. Hu and co-workers [112] designed a in situ carbon-encapsulated selenides by a MOF-derived selenization strategy, which was applied as a sodium-ion battery anode (Fig. 3.14c). The micro- and nanostructured selenides exhibited excellent rate capability and cycling stability. As a result, the as-prepared peapod-like Fe_7Se_8@C nanorods show a high specific capacity of 218 mAh g^{-1} after 500 cycles even at a high current density of 3 A g^{-1}. Similarly, the prepared porous NiSe@C spheres also delivers an ultrahigh cycling stability of 160 mA h g^{-1} at a current density of 3 A g^{-1} after 2000 cycles. This MOF-derived selenization strategy is a commonly used strategy to prepare carbon@selenide composites to construct high-performance SIB anodes. Zhao and co-workers [113] synthesized a novel architecture, in which FeP quantum dots are confined in P-doped 3D carbon framework (FeP@OCF) (Fig. 3.14d). This

unique structure design endows FeP@OCF with simultaneously enhanced diffusion-controlled and surface-controlled capacities, which enables a better electrochemical performance compared to pure FeP. Consequently, the FeP@OCF electrode displayed a better reversible capacity of 674 mAh g^{-1} at 0.1 A g^{-1}, and an impressive rate capability of 262 mAh g^{-1} even at 20 A g^{-1}. Furthermore, full cells using $Na_3V_2(PO_4)_3$ as cathodes and FeP@OCF as anodes deliver a high energy density of 185 Wh kg^{-1}, which emphasized the superiority of FeP@OCF to most reported transition metal phosphides anodes.

It is noted that vast diversity of metal ions and organic ligands make MOFs a promising precursor in energy storage materials. Goodenough and co-workers [114] used electrospinning technology to evenly distribute Co and Zn bimetallic ions into the polyacrylonitrile fiber to form a multifunctional composite fiber, and then put the composite fiber into an ethanol solution containing dimethylimidazole to in suit grow ZIF-67 and ZIF-8 composite layer (Fig. 3.15a). It is worth noting that this is a kinetic self-limiting reaction, in which the BMZIF layer formed during the reaction prevents the dimethylimidazole and metal ions from further reaction, and eventually forming PAN/$Zn(Ac)_2$/$Co(Ac)_2$@BMZIF core–shell composite fiber. After the calcination process, the ZIF-8 in the outer layer of BMZIF was transformed into porous nitrogen-doped amorphous carbon material, and a small amount of Co derived from ZIF-67 played as catalysts to further improve the graphitization degree of carbon materials. Additionally, the acid washing process enabled dissolution of metal particles, and thereby forming the N-doped porous carbon material. When employed as

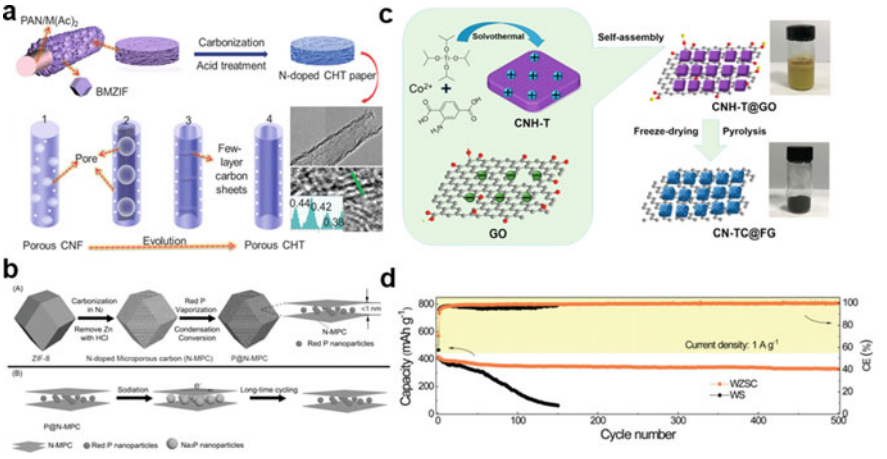

Fig. 3.15 **a** Schematic Illustration of the Synthesis of a Series of 1D Nanocarbons from Porous N-Doped CNFs to CHTs with Enlarged Graphene Interlayer Spacing Reproduced with permission [114]. Copyright 2017, Elsevier. **b** Schematic illustration of the preparation process. Reproduced with permission [115]. Copyright 2017, WILEY–VCH. **c** Schematic of the synthesis procedures of the CN-TC@FG. Reproduced with permission [116]. Copyright 2018, Elsevier. **d** Cycle performance of the WS_2 and WS_{2-x}/ZnS@C at the current density of 1 A g^{-1}. Reproduced with permission [117]. Copyright 2020, WILEY–VCH

the anode of SIBs, the prepared carbon material exhibited excellent rate capability and cycling stability, with a cycling lifespan up to 10,000 cycles. Given the high theoretical specific capacity of Na_3P (2596 mAh g^{-1}) and appropriate working voltage ($\approx$ 0.45 V vs. Na/Na^+), red phosphorus is regarded as a promising anode of SIBs. However, considering the poor conductivity and large volume variation of red phosphorus during cycling, the conductive carbon matrixes were designed to confine the red phosphorus to construct composite anode. Yu and co-workers [115] demonstrate a rational design to improve sodium storage performance by confining red phosphorus to MOF-derived N-doped microporous carbon matrix (P@N-MPC) (Fig. 3.15b). Due to the novel structure design, numerous micropores within N-doped porous carbon matrix facilitate the rapid transport of electrolyte ions, as well as enhance the electrical conductivity of encapsulated red phosphorus. Additionally, porous carbon matrix alleviates the volume fluctuation during continuous cycling. The battery with P@N-MPC anode delivers a high reversible specific capacity of 600 mAh g^{-1} at 0.15 A g^{-1}. Benefiting from the abundant pores, P@N-MPC also exhibits improved rate capability with 450 mAh g^{-1} at 1 A g^{-1} after 1000 cycles and an extremely low capacity loss of 0.02% per cycle. Sun and co-workers [116] employed multifunctional Co-doped amine-functionalized Ti-MOFs precursors to fabricate TiO_2-based anode (Fig. 3.15c). The usage of Co-doped amine-functionalized Ti-MOFs precursor can allow simultaneous incorporation of cobalt, nitrogen double-doping, and confinement of ultrafine TiO_2 nanoparticles in mesoporous carbon matrix. Interestingly, precursors with positive charges are spontaneously attached with graphene nanosheets, and subsequently self-assemble into a 3D carbon framework. The 3D conductive frameworks and convenient transport channels improve both electron conduction and sodium-ions transport. The unique structure design endows TiO_2-based anode with a high reversible capacity of 174 mA h g^{-1} at 6 C for 5000 cycles, 121 mA h g^{-1} at 15 C for 10,000 cycles, and 100 mA h g^{-1} at 30 C for 3000 cycles. Wu and co-workers [117] reported a novel structure design, in which uniform ZIF-8 layer was firstly grown in situ on the surface of the WS_2 nanorods, and then a bimetallic sulfide composite with a coaxial carbon coating layer was formed after the calcination. Given the better electronegativity of Zn compared to W, metallic Zn tends to combine with S, and eventually induces the generation of WS_2/ZnS heterostructure and simultaneously forms sulfur-rich vacancies in WS_2. The sulfur vacancies generated in the WS_2 crystal not only provide more reactive sites for sodium storage, but also induce excess electrons around W atoms, which are considered as negative charge centers, and thereby accelerating the rapid diffusion of sodium ions. When used as the anode of SIBs, the WS_2-X/ZnS/C anode exhibited excellent electrochemical performance with a reversible rate capacity of 170.8 mAh g^{-1} over 5000 cycles at 5A g^{-1}. A further enlargement of practical application was realized by assembling full cells using WS_2-X/ZnS/C as anode and P_2-$Na_{2/3}Ni_{1/3}Mn_{1/3}O_2$ as cathode. Similar to half cells, the full cell also delivers a high rate capacity of 84.9 mAh g^{-1} over 500 cycles at 1A g^{-1} and maintains coulombic efficiency near 100% (Fig. 3.15d).

The employment of MOF materials as carbon framework precursors fully takes advantage of the ultra-high surface area and satisfactory porosity. It is these unique

characteristics that endow MOFs and MOF derivatives without large deformation and volume expansion during continuous cycling. While emphasizing the advantages of MOFs, more attention should be focused on the challenges posed by high specific surface area and porosity. For example, high specific surface area and porosity enlarge the contact area between electrode and electrolyte, increase the side reactions, and eventually result in a poor initial Coulombic efficiency and lower volume energy density, which is not conducive to practical application.

3.6.2 MOFs as Separators

The sodium metal is the holy grail anode of the development of SIBs to deliver high energy density. However, uneven solid electrolyte interphase induces the growth of sodium dendrite and serious side reactions, and finally results in poor electrochemical performance. The poor interfacial stability is mainly ascribed to the uneven distribution of sodium ions, and subsequent disordered sodium deposition [118]. Therefore, the uniform sodium deposition can be achieved by regulating the distribution of sodium ions on the electrode surface so as to improve the electrochemical performance of batteries. Considering the uniform pore distribution and adjustable porosity, MOFs were always explored as separator to regulate the transport of sodium ions during charge and discharge process [119]. Recently, Kang and co-workers [120] designed and manufactured a new type of MOF-gel film as the separator for rechargeable organic battery (Fig. 3.16a). The sol-gel method used in this work realized the anisotropic growth of metal ions with organic ligands and the in situ self-assembly to form MOF-gel (Fig. 3.16b). Compared with conventional separator, the new type of MOF-gel separator constructed entirely of MOF material possesses a smoother surface and no obvious voids, which can further improve the selection and separation efficiency (Fig. 3.16c). The design of permselective MOF separator enables a long-life cycling, increasing the cycle numbers from 200 to 2000 cycles.

3.6.3 MOFs as Solid-State Electrolyte

For traditional electrolytes, narrow electrochemical window and flammability had serious impacts on electrochemical performance and safety of batteries. Hence, solid electrolytes with high electrochemical and mechanical stability, and strong flame retardancy has received more and more attention [121]. Despite the above advantages of solid electrolytes, there still exist some serious challenges, such as low conductivity and poor interface contact between electrode and electrolyte. Emerging porous materials, such as MOFs with high specific surface area and porosity, allows various charged substances to be loaded in the pores, thereby enhancing ionic conductivity. Dinca and co-workers [122] utilized Cu_2Cl_2BTDD and NaSCN to synthesize Na[Cu_2Cl_2(SCN)BTDD]•9(PC) as the solid-state electrolyte. Abundant

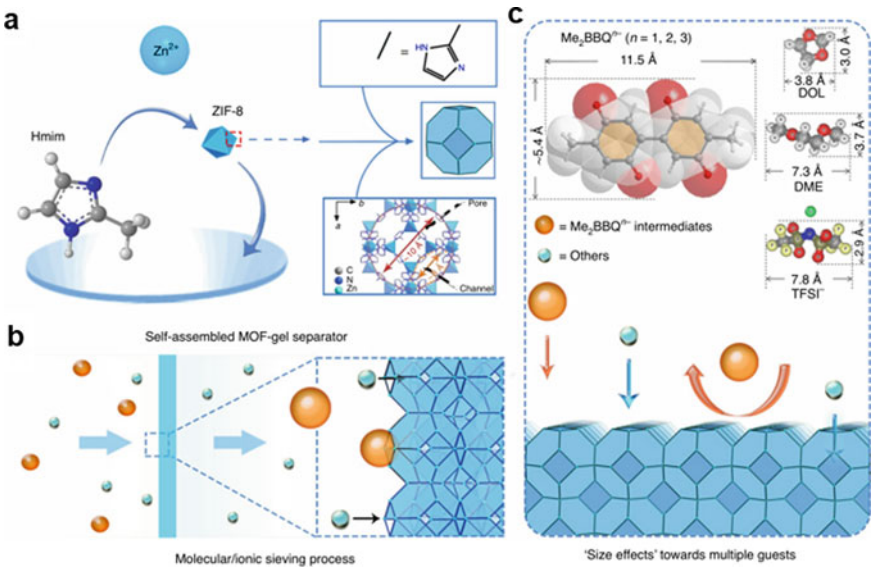

Fig. 3.16 **a** Schematic showing the self-assembly of microporous MOF-gel separators (ZIF-8). **b** Schematic illustrating the molecular and ionic sieving process of the MOF-gel separator. **c** Optimized geometries of Me_2BBQ^{n-} (n = 1, 2, 3) redox intermediates using DFT calculation. The intrinsic channel size between adjacent MOF cavities is smaller than that of $Li_pnIMe_2BBQ^{n-}$ redox intermediates but larger than that of other solvents or salts. The specific "size effects" ensure excellent permselectivity of the MOF-gel separators toward multiple guests. Hmim, 2-methylimidazole Reproduced with permission [120]. Copyright 2020, Springer Nature

anion sites within the prepared solid electrolyte accelerate the transport of cation, and thereby enhance the ionic conductivity. As a result, the sodium-ion conductivity of as-prepared solid electrolyte reaches 1×10^{-5} S cm^{-1}. The prepared MOF has high density and uniform distribution of binding sites for cation and anion, which systematically improve the ion conductivity to obtain a high-efficiency solid electrolyte.

3.7 MOF-Derived Materials in Sodium-Selenium Batteries

In recent years, with the rapid development of alkali metal batteries, especially the lithium-chalcogen batteries system, the current low energy density of commercial LIBs is expected to be boosted. Sodium-selenium (Na-Se) batteries, as a member of alkaline chalcogen batteries, have also received extensive attention. Like Li-Se batteries, Na-Se batteries also have issues of shuttle effect of polyselenides, large volume expansion, and poor electrical conductivity of selenium electrodes [123]. Therefore, the main approach to improve the electrochemical performance of Na-Se

batteries is to restrict the shuttle effect, alleviate the volume variation, and enhance the conductivity of selenium electrode. However, compared to Li-Se batteries, Na-Se batteries face a more severe challenge, namely the sluggish kinetics issue, especially when the seleniun content in the cathode exceed 50 wt%, which will severely limit the electrochemical performance of Na-Se batteries [124]. In addition, given the larger radius of sodium ion compared to lithium ion, the volume fluctuation during charging and discharging process in Na-Se batteries is particularly more serious. Therefore, there is more demand for carbon matrix in Na-Se batteries, which not only guarantees sufficient architectural stability, but also provides enough channels for ion migration and a larger space to alleviate volume expansion. In recent years, various carbon matrix materials are designed to accommodate selenium and improve the electrochemical performance of selenium electrodes, in which MOF-derived carbon matrix is a good choice because of the diversity and unique structure, and controllable chemical composition.

Adoption of N-doped porous carbon matrix is a common method to improve the electrochemical performance of alkali metal–chalcogen battery systems. Xu and co-workers [125] prepared nitrogen-doped porous carbon polyhedrons (NPCPs) by facile synthesis and thermal treatment of ZIF-67. The preparation processes of Se/NPCPs composite are displayed in Fig. 3.17a. Such a NPCPs host possesses large number of mesopores, high specific surface area and large pore volume, with unique porous structure that enables selenium to be firmly confined in the mesopores through the melting-diffusion process. The hollow structure within NPCPs can not only provide a continuous electron transmission path, but also buffer volume variation during cycling. In addition, compared with the preparation of other porous carbon matrix, NPCP does not require the KOH activation to form more pores. By encapsulating selenium into mesoporous carbon derived from ZIF-67, the Se/NPCP composite cathode is formed and subsequently assembled into Na-Se battery. Benefiting from the efficient confinement of selenium within the NPCPs, Na-Se battery with Se/NPCP composite cathode delivers a discharge capacity of 161.4 mAh g^{-1} after 1000 cycles at 2 C as shown in Fig. 3.17b. Furthermore, unique pore structure and excellent conductivity both accelerate the transport of ion and electron, the Se/NPCP cathode displayed an outstanding rate capability of 351.6 mAh g^{-1} and 307.8 mAh g^{-1} at 0.5 and 2 C, respectively, with a high Coulombic efficiency of 99.7% (Fig. 3.17c).

The employment of a hierarchical carbon framework system in Na-Se batteries is another way to enhance electrochemical performance. Xu and co-workers [126] developed carbon/selenium composites as cathodes for Na-Se batteries by impregnating selenium in metal–organic complex derived hierarchical porous carbon (Se-HPC) via a melt-infusion method, the preparation process for Se-HPC composite are displayed in Fig. 3.17d. Xu's team synthesized and reported the metal–organic complex of Cd-PPD (p-phenylenediamine), which is also a kind of MOF material, for the first time. After annealing, a hierarchical porous carbon (HPC) was obtained without metal residue. The prepared HPC cathode presents a three-dimensional layout of open architecture with obvious hollow structure, which are composed of

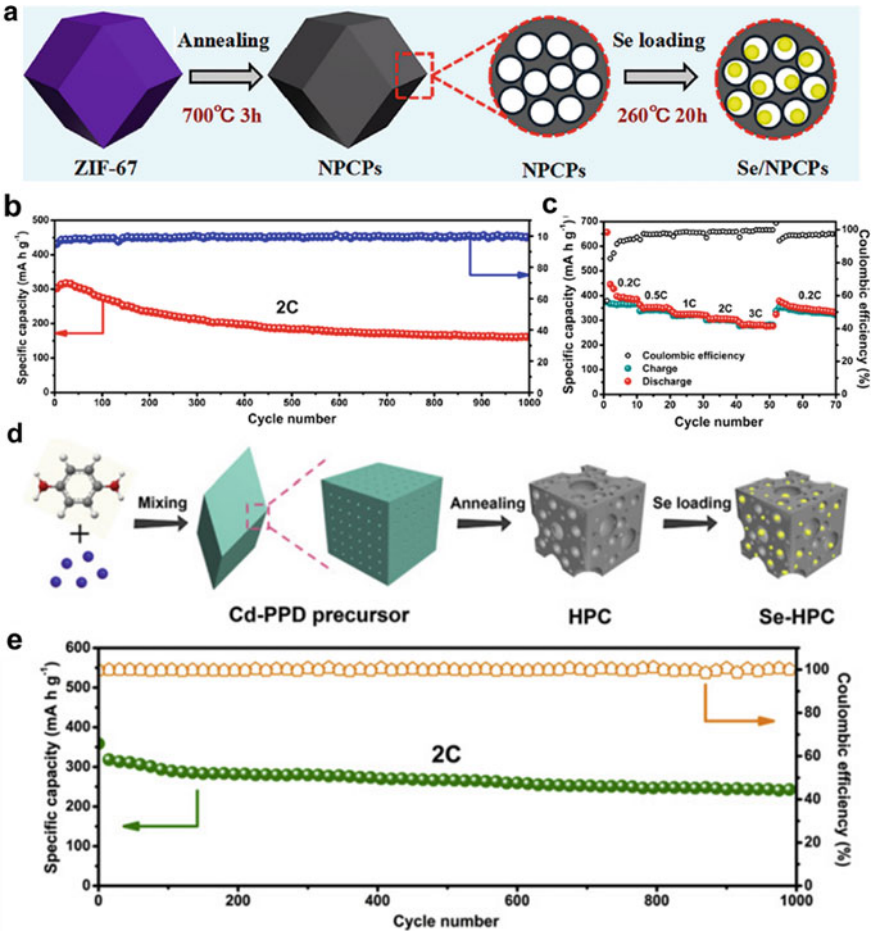

Fig. 3.17 **a** Schematic diagram of the preparation process of Se/NPCPs composite. **b** Cycling performance and Coulombic efficiency of Se/NPCPs composite electrode at 2 C. **c** Rate capability of Se/NPCPs composite. Reproduced with permission from Ref. [125], Copyright 2017, American Chemical Society. **d** Schematic illustration of synthesis process of Se-HPC composite. **e** Cycling performance and Coulombic efficiency of Se-HPC composite at 2 C. Reproduced with permission from Ref. [126], Copyright 2018, Elsevier

abundant micropores and mesopores, with large pore volume and specific surface area. After uniformly loading selenium into the entire carbon matrix, the Se-HCP electrode with a selenium loading of 56% exhibits a reversible capacity of 243 mAh g^{-1} over 1000 cycles at 2 C, with a capacity decay of 0.04% per cycle (shown in Fig. 3.17e). Moreover, the combination of micropore and mesopore facilitates the migration of ions, and thus delivers rate capabilities of 330 mAh g^{-1} and 260 mAh g^{-1} at 1 and 5 C, respectively. Also, Su and co-workers [127] designed a hierarchically radial-structured microporous carbon (HRMC) with N-doped (N-HRMC) (shown

in Fig. 3.18c) material as a host to anchor selenium clusters for Na-Se batteries, the schematic diagram of the preparation process of Se@N-HRMC is presented in Fig. 3.18a. The N-HRMC was firstly obtained by carbonizing the precursor of a zinc-glutamate (Zn-Glu) (shown in Fig. 3.18b), eliminating the zinc component while forming the conductive carbon matrix, and then doping in situ by pyrolysis without templates and activation process. Then, the Se@N-HRMC composite as shown in Fig. 3.18d was prepared by mixing N-HRMC with selenium powder and further thermal treatment with a high selenium content up to 62 wt%. The narrow (0.5 nm) pores and the formation of C-Se and C-O-Se bonding in Se@N-HRMC cathode have a strong confinement on Na_2Se to avoid the shuttle effect, minimizing the loss of active component and the effect on the sodium anode. Besides, in situ N-doping within the carbon matrix leads to large number of defects, which further enhances the electrical conductivity and chemical adsorption of polyselenides. Similar to other routine carbon matrix, the porous structure within the N-HRMC host can alleviate the volume change during charge and discharge process, improving the structure stability of electrode. Consequently, the Se@N-HRMC cathode exhibited a reversible capacity of 612 mAh g^{-1} after 200 cycles at 0.2 C as shown in Fig. 3.18e, and presents good rate performance in Fig. 3.18f and outstanding long-term cycling performance in Fig. 3.18g.

Doping with high nitrogen content is another way to improve the reversible sodium storage performance. Yu and co-workers [128] impregnated selenium in ZIF-8 derived N-doped microporous carbon polyhedrons (Se@N-MCPs) by melt infiltration to prepare the composite cathode for Na-Se batteries, in which the content of nitrogen reaches 12.88 wt%. The relevant preparation process for Se@N-MCPs cathode was shown in Fig. 3.19a. The unique structure of carbon framework realizes the sufficient confinement of selenium in N-doped microporous carbon polyhedrons (N-MCPs), and thereby suppresses the shuttle effect of polyselenides. Furthermore, high nitrogen-doping improves the electrochemical activity and rate capability by establishing highly conductive electron channels in the electrode. Resultantly, the Se@N-MCPs cathode delivers a high discharge capacity of 612 mAh g^{-1} after 100 cycles at 0.1 A g^{-1} (Fig. 3.19b), and 496 mAh g^{-1} at a higher current density of 5 A g^{-1} (Fig. 3.19c). The Se@N-MCPs cathode also displayed a better cycling stability of 500 cycles with only 0.049% capacity decay per cycle (Fig. 3.19d). Despite the advanced progress of MOF materials in Na-Se batteries, there are still many issues left to be further resolved.

3.8 MOFs and MOF Derivatives for Other Metal-Air Battery

Rechargeable metal-air battery is considered to be the most promising EES device in terms of higher energy density given the adequate supply of external air. However,

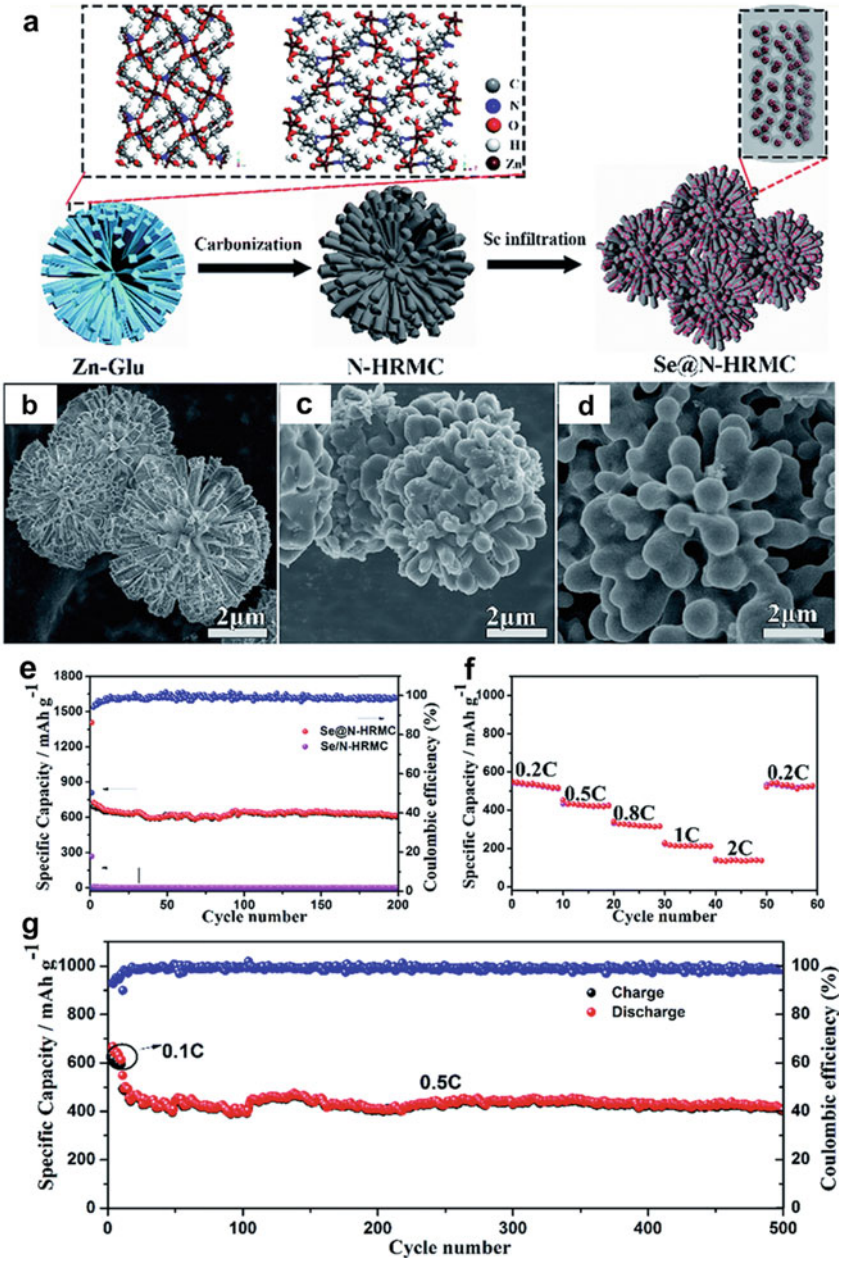

Fig. 3.18 **a** Schematic illustration of the synthesis process of Se@N-HRMC. The insets in (**a**) for Zn-Glu show the 2 × 2 × 2 supercell along *Z*- and *X*-axes, respectively. The inset for Se@N-HRMC shows the Se clusters inside. SEM image of **b** Zn-Glu, **c** N-HRMC and **d** Se@NHRMC. **e** Cycling performance of the Se@N-HRMC and Se/N-HRMC cathodes at 0.2 C. **f** Rate capabilities of the Se@N-HRMC cathode. **g** Long-term cycling performance of Se@N-HRMC electrodes at 0.5C. Reproduced with permission from Ref. [127], Copyright 2018, Royal Society of Chemistry

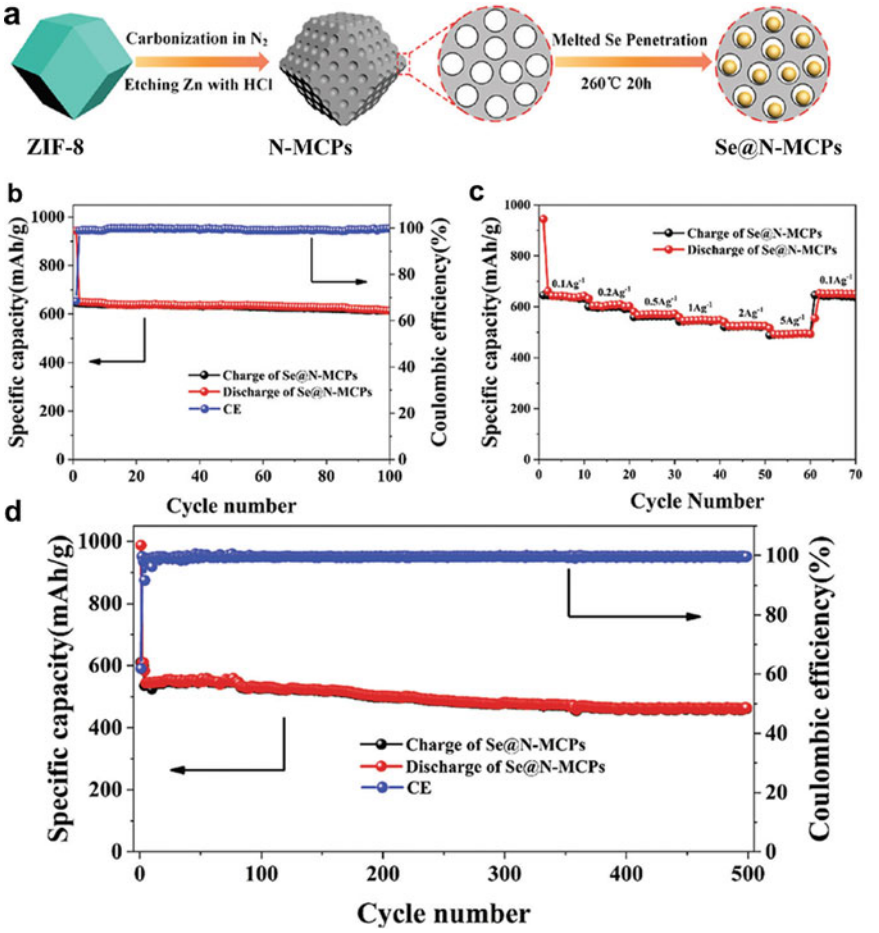

Fig. 3.19 **a** Schematic illustration of the preparation process for Se@N-MCPs. **b** Cycling performances of the Se@N-MCP electrodes at a current density of 0.1 A g^{-1} and the corresponding CE during cycling. **c** Rate capability of the Se@N-MCP electrodes at various current densities. **d** Long-term cycling performance of the Se@N-MCP electrodes at a current density of 1 A g^{-1}. Reproduced with permission from Ref. [128]. Copyright 2018, Royal Society of Chemistry and Chinese Chemical Society

the practical application of rechargeable metal-air batteries still faces several challenges, such as insufficient power density, low Coulombic efficiency, and poor cycling stability. Therefore, it is urgent to solve these troublesome issues, and eventually realize the commercialization of metal-air batteries.

Benefiting from large specific surface, tunable pore size and controllable chemical composition, MOFs and MOF derivatives were widely investigated in metal-air batteries, such as sodium-air battery, potassium-air battery, zinc-air battery, magnesium-air battery, and aluminum-air battery. Among these metal-air batteries,

sodium-air battery and potassium-air battery are all sensitive to water and carbon dioxide in the atmosphere. Therefore, metal-air batteries with these anode metals usually work under pure oxygen and are also called metal-oxygen batteries. By discussing the progress of MOFs and MOF derivatives in metal-air battery, some design principles and corresponding improvements that dominate the electrochemical behaviors are outlined.

3.8.1 MOF Derivatives for Sodium-Air Battery

Similar to lithium-air batteries, sodium-air batteries were also regarded as promising energy storage systems in terms of high energy density, low cost, and low environmental impact. Surprisingly, the specific electrochemical and catalytic mechanisms in sodium-air battery that are different from lithium-air batteries were discovered despite the similar physical and chemical properties between lithium and sodium elements. Unlike lithium ions with a small radius, sodium ions with a larger radius can easily combine with super-oxygen ion to form a stable superoxide discharge product. Therefore, it is crucial to both realize the accommodation and catalytic decomposition of discharge product within conductive carbon frameworks in charge and discharge process.

Lei and co-workers reported a MOF-derived N-doped carbon nanotubes (MOF-NCNTs), which was employed as electrocatalysts for sodium-air batteries [129]. The prepared MOF-NCNTs cathode displayed better electrochemical performance compared to commercial Pt/C electrode in terms of electrocatalytic activity and stability for the ORR and OER process (Fig. 3.20a).The battery assembled by MOF-NCNTs cathode exhibited a low voltage gap of 0.30 V at a current density of 0.1 mA cm^{-2}, which is superior to commercial Pt/C (0.50 V), RuO_2 (0.50 V), Co-CNTs (0.67 V), NCNTs (0.77 V), MWNTs (0.90 V), and carbon paper (1.18 V), as shown in Fig. 3.20b. Furthermore, the average discharge plateau and energy efficiency in MOF-NCNTs battery was 2.81 V and 87% after 35 cycles. These outstanding electrochemical performances were mainly assigned to the synergistic effect of the nitrogen-doping and confined Co nanoparticles in scaffold, in which N dopants and confined Co nanoparticles can provide abundant catalytic sites and accelerate electron transfer for the ORR and OER process. Furthermore, the defect provided by hollow carbon frameworks in nitrogen-doped carbon nanotubes also improves the adsorption of oxygen, further enhancing the mass transport. Both the facilitated mass transport and electron conduction enhanced the catalytic activity.

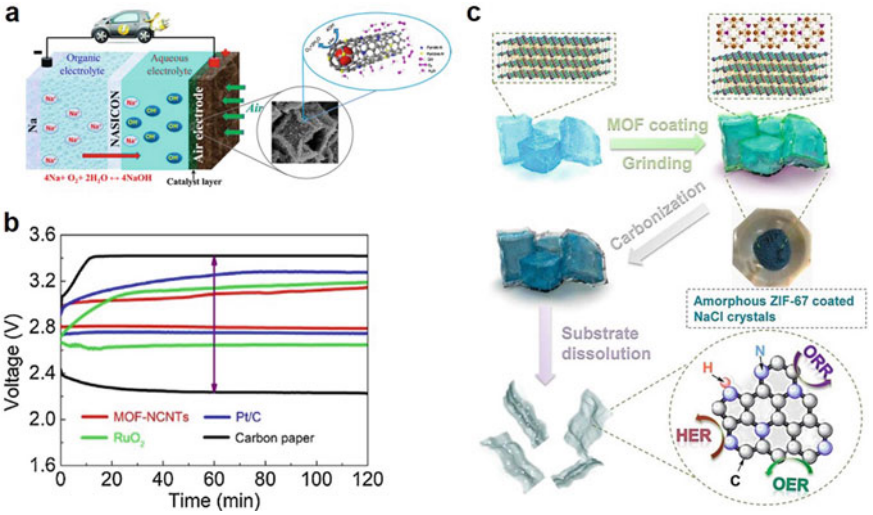

Fig. 3.20 **a** Schematic illustration of a typical hybrid sodium-air battery and the ORR and OER process at the surface of Co confined in MOF-NCNTs. **b** Charge-discharge curves of hybrid sodium-air batteries using MOF-NCNTS, Pt/C, RuO_2, and carbon paper catalysts at a current density of 0.1 mA·cm^{-2}. **c** Schematic illustration of the preparation process of MNG. **a, b** Adapted with permission [129]. Copyright 2018, Elsevier B.V. (c) Adapted with permission [131]. Copyright 2018, American Chemical Society

3.8.2 MOF Derivatives for Zinc-Air Battery

Zinc-air battery has many advantages, such as safety, abundant raw materials, and high energy density, and is very suitable to be used as power source for electric vehicles. However, the energy efficiency and cycling lifespan of zinc-air battery is still far lower than that of commercial LIBs, which is mainly related to the poor reversibility of zinc metal in alkaline electrolyte, and the electrocatalytic activity of dual-function air cathode. As an important component of zinc-air battery, bifunctional air cathode has always been the focus of study, in which the stable and efficient bifunctional catalysts are equipped on one hand, and suitable construction of electrode to ensure the enough supply of oxygen on the other hand. Noble metal catalysts have high catalytic activity but with a high cost. As a result, non-noble metal catalysts were further developed, in which MOF derivatives show unique advantages in air cathode of Zinc-air battery.

Manthiram and co-workers prepared a pair of MOF-derived catalysts for efficient oxygen reduction reaction and oxygen evolution reaction process [130]. The combination of doped carbons originated from pristine ZIF and a sacrificial tellurium template successfully resulted in formation of mixed-metal doped porous carbon nanotubes, which was named as CoFeZn@pCNT. The prepared CoFeZn@pCNT displays an outstanding catalytic activity for oxygen reduction reaction with a half-way oxygen reduction reaction potential of 0.87 V. Moreover, the oxygen evolution

reaction catalysts were prepared by combining Co, Fe, and Ni into ZIF-67, and followed by a simple sulfurization treatment. The obtained FeCoNi-S@ZIF catalyst displayed an excellent catalytic activity for oxygen evolution reaction with potential of 1.65 V vs. reverse hydrogen electrode. Yang and co-workers synthesized sheet-like mesoporous nitrogen-doped graphene (MNG) derived from amorphous MOFs [131]. Interestingly, the MNG catalyst derived from amorphous MOFs exhibited better catalytic activity than that of nitrogen-doped carbon (MNC) derived from highly crystallized MOFs, which is mainly related to the higher electronic conductivity, graphitization degree, and high specific surface. As a result, the battery assembled by MNG displayed a better electrocatalytic performance compared with as-prepared MNC catalysts and conventional platinum group metal catalysts (Fig. 3.20b).

3.9 Other Advanced Batteries

3.9.1 MOFs and MOF Derivatives for Lithium-Carbon Dioxide Batteries

Lithium-carbon dioxide batteries(Li-CO_2)are an emerging and attractive energy storage system, with an energy density seven times that of conventional LIBs. However, the development of Li-CO_2 batteries are hindered by several serious issues, such as the difficulty in decomposition of discharge product (Li_2CO_3), and the capture of high concentrations of CO_2 from atmospheric environment [132]. Therefore, it is of great significance to figure out the electrochemical mechanisms of Li_2CO_3 formation and decomposition as well as search for new functional materials to capture high concentrations of CO_2 form air. Benefiting from the efficient CO_2 capture and electrochemical catalysis given the porous structure and monodispersed active metal cluster, MOFs have shown great application potential in Li-CO_2 batteries (Fig. 3.21). Wang and co-workers [133] firstly investigated the performance of eight kinds of MOFs (Mn_2(dobdc), Mn(bdc), Co_2(dobdc), Ni_2(dobdc), Cu(bdc), Fe(bdc), $Mn(C_2H_2N_3)_2$, and $Mn(HCOO)_2$) in Li-CO_2 batteries (Fig. 3.22a). Thanks to high capture capability for CO_2 and numerous monodispersed active metal sites for the decomposition of Li_2CO_3, Mn_2(dobdc) porous catalyst electrode displays a remarkable discharge capacity of 18,022 mAh g^{-1} at a current density of 50 mA g^{-1} (Fig. 3.22b). Moreover, $Mn(HCOO)_2$ porous electrode alleviates the charge overpotential and maintains a low value of 4 V even at a high current density of 200 mA g^{-1} (Fig. 3.22c). In this work, the electrochemistry of MOF electrodes in Li-CO_2 batteries was investigated through various characterizations, and the findings pave the way to improve the reversibility and energy efficiency of Li-CO_2 batteries.

Except for the pristine MOFs, MOF derivatives are also regarded as promising materials in emerging Li-CO_2 batteries. Wang and co-workers [134] used GO-wrapped MOFs as precursor to prepare graphene-interconnected N-doped 3D carbon framework with ultrafine MnO nanoparticles (MnO@NC-G) for Li-CO_2

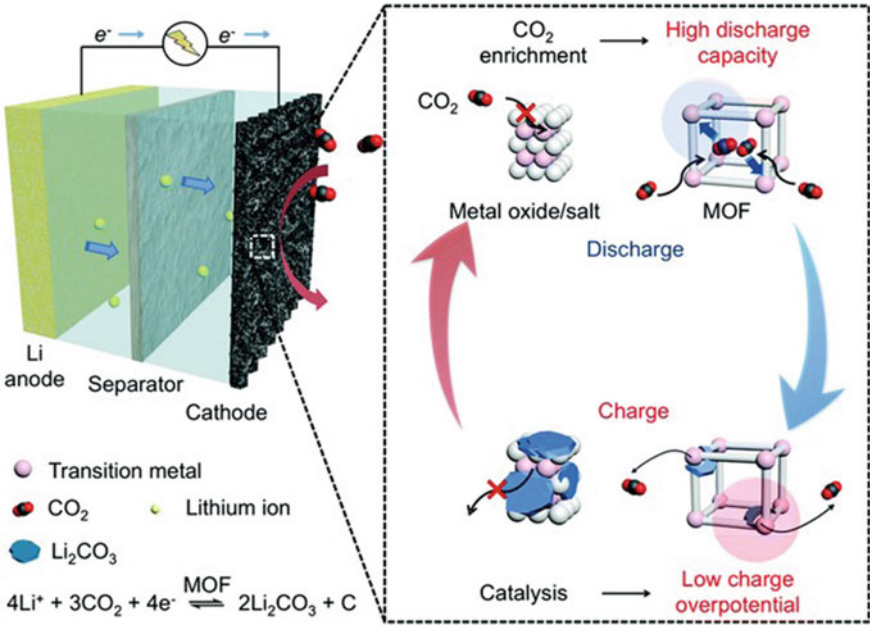

Fig. 3.21 Scheme of the advantages of Li-CO_2 battery equipped with MOF-based porous CO_2 electrode. Adapted with permission [133]. Copyright 2018, the Royal Society of Chemistry

batteries (Fig. 3.23a). With combination of high catalytic activity originated from homodisperse Mn (II) species and fast electron transport of nitrogen-doped carbon frameworks and 2D graphene nanosheet (Fig. 3.23b), the battery assembled by MnO@NC-G electrode exhibited excellent electrochemical performance compared to other Mn(II)-based cathodes. The prepared MnO@NC-G electrode enables a high discharge capacity of 25,021 mAh g^{-1} with a Coulombic efficiency of 95.6%, low voltage hysteresis of 0.88 V at a current density of 50 mA g^{-1}, and ultra-long-cycling lifespan over 200 cycles. This work provided new insight to synthesize highly efficient electrocatalysts for Li-CO_2 batteries.

The design of MOFs and MOF derivatives in Li-CO_2 batteries should be focused on the following three key aspects in future: i) uniformly dispersed catalytic species to ensure enough contact between active metal catalyst and discharge product. ii) an excellent electrical conductivity to guarantee the fast electron transport. iii) high strength of interconnected framework for accommodation of discharge products to avoid the blockage of cathode gas channel. These design guidelines will promote the development of MOFs and MOF derivatives in improving the electrochemical performance of Li-CO_2 batteries.

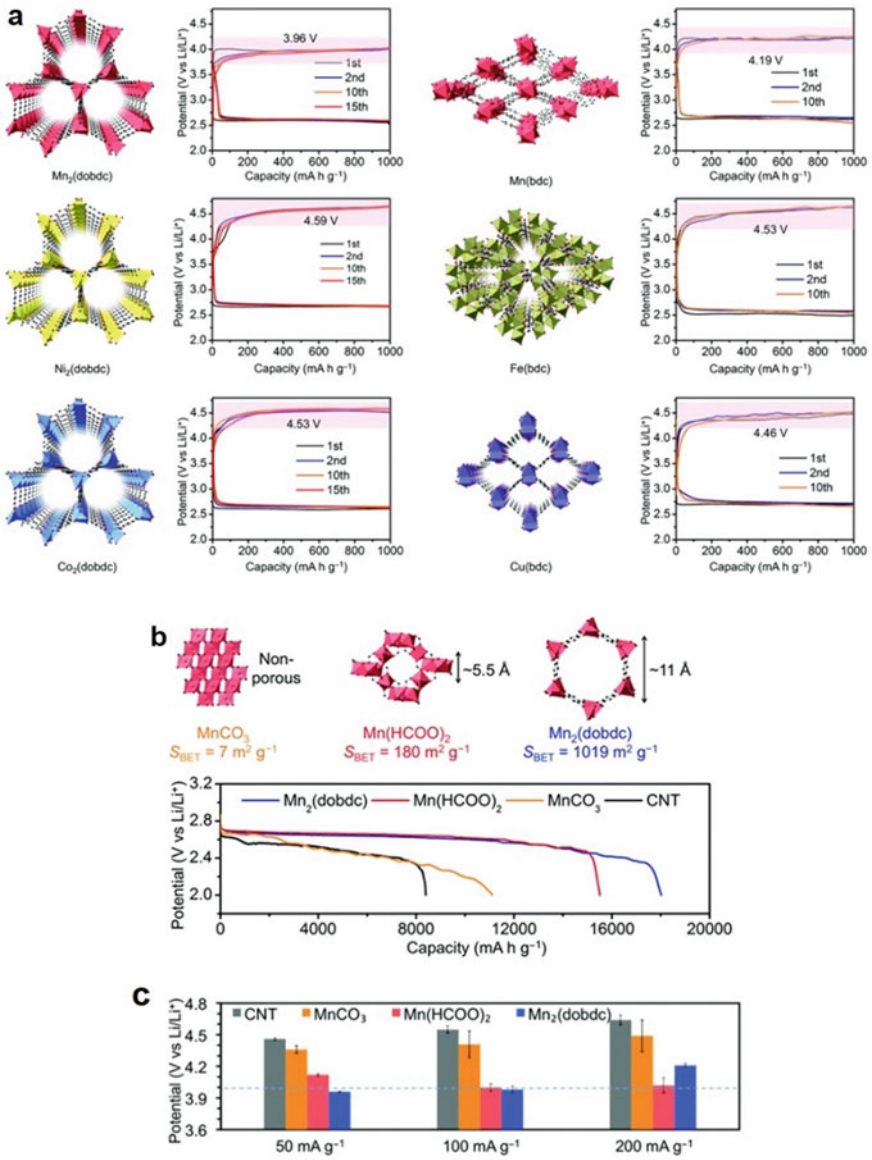

Fig. 3.22 **a** Crystal structures and discharge-charge voltage curves at 50 mA g^{-1} with a capacity of 1000 mA h g^{-1} of various MOF-based porous CO_2 electrode. **b** Crystal structures of $MnCO_3$, $Mn(HCOO)_2$ and Mn_2(dobdc) porous electrodes along certain directions, and discharge curves at 50 mA g^{-1} with a cut-off voltage of 2.0 V. **c** Average charge potentials of various CO_2 porous electrodes at different current densities. Adapted with permission [133]. Copyright 2018, the Royal Society of Chemistry

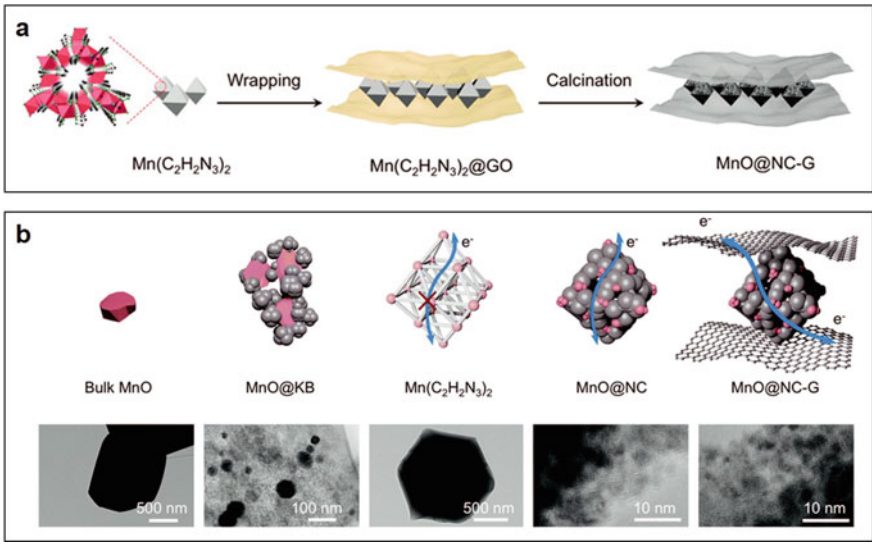

Fig. 3.23 **a** Synthetic technological process of MnO@NC-G. **b** The structural advantages of MnO@NC-G compared to other Mn(II) catalysts and corresponding TEM images. Adapted with permission [134]. Copyright 2019, the Royal Society of Chemistry

3.9.2 MOFs for Zn/Na-I_2 Batteries

Rechargeable water-based zinc-iodine (Zn-I_2) batteries are considered to be one of the strong competitors for the next generation energy storage systems in terms of the low cost and high safety. Unfortunately, the shuttle effect inside the Zn-I_2 batteries leads to the rapid capacity decay and low Coulombic efficiency during cycling, which seriously hinders its future commercialization [135]. Therefore, the suppression of shuttle effect of I_3^- within electrolyte is crucial for the development of Zn-I_2 batteries. Zhou and co-workers [136] exploited a MOF as an ionic sieve membrane to simultaneously solve the shuttle effect and side reactions on the Zn anode. The bare Zn foil is vulnerable to the water and iodine species within electrolyte during cycling, and thereby limiting the electrochemical performance and lifespan. The employment of multifunctional MOF membrane significantly inhibits the shuttling of I_3^- and alleviates side reaction on the Zn foil surface, minimizing the corrosion of zinc anode during cycling (Fig. 8.4a, c). Most impressively, presence of regular channels within MOFs leads to unique electrolyte structure by regulating the electrolyte solvation structure. As a result, Zn-I_2 batteries realize ultra-long lifespan of 6000 cycles, with high capacity retention of 84.6%, and high Coulombic efficiency of 99.65% (Fig. 3.24b). This work systematically reveals the nature of Zn anode corrosion, and proposes an effective strategy to develop high-performance and long-life aqueous Zn-I_2 batteries.

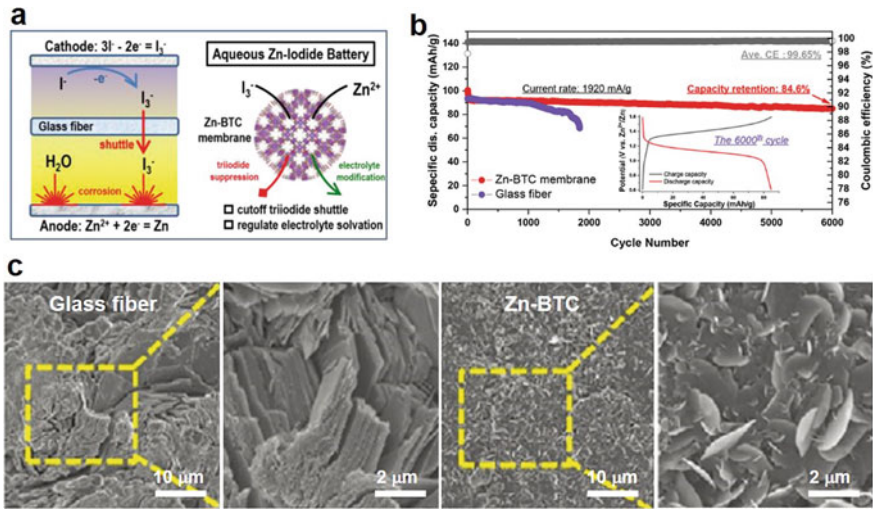

Fig. 3.24 **a** Schematic illustration of Zn-I_2 batteries with GF and Zn-BTC separator. **b** Cycling stability of Zn-I_2 batteries at current density of 1920 mA g^{-1} with GF and Zn-BTC separator. **c** SEM images of Zn anode after 20 cycles with GF and Zn-BTC separator. Adapted with permission [136]. Copyright 2020, Wiley–VCH GmbH

Similar to Zn-I_2 batteries, the development of Na-I_2 batteries is also severely impeded by their poor cycling stability due to the high solubility of polyiodide in electrolyte. Hence, a lot of efforts have been devoted to improving the electrochemical performance of batteries by inhibiting the shuttle effect of polyiodide. In order to suppress the polyiodide dissolution in Na-I_2 batteries, Feng and co-workers [137] reported an atomic modulation metal-bis(dihydroxy) species in a fully conjugated phthalocyanine copper MOF (PcCu-MOFs) (Fig. 3.25a). The characterization and theoretical calculation reveal that the square planar Fe-O_4 species in phthalocyanine copper MOF tends to combine with polyiodide to suppress the dissolution of polyiodide in electrolyte (Fig. 3.25b). As a result, the composite cathode consisting of Fe_2-O_8-PcCu and I_2 exhibited a stable capacity of 150 mAh g^{-1} after 3200 cycles (Fig. 3.25c). Additionally, the Fe_2–O_8–PcCu/I_2 composite cathodes also operate effectively in other metal-I_2 batteries, which provide a universal strategy for the design of high-performance metal-I_2 batteries.

3.9.3 MOFs for Organic Redox Flow Batteries

Redox flow battery (RFB) is a new type of rechargeable EES device, in which oxidation and reduction of two soluble electroactive components realized the reversible conversion between chemical energy and electrical energy. It is worth noting that RFBs are not only capable of being employed as energy storage devices for solar

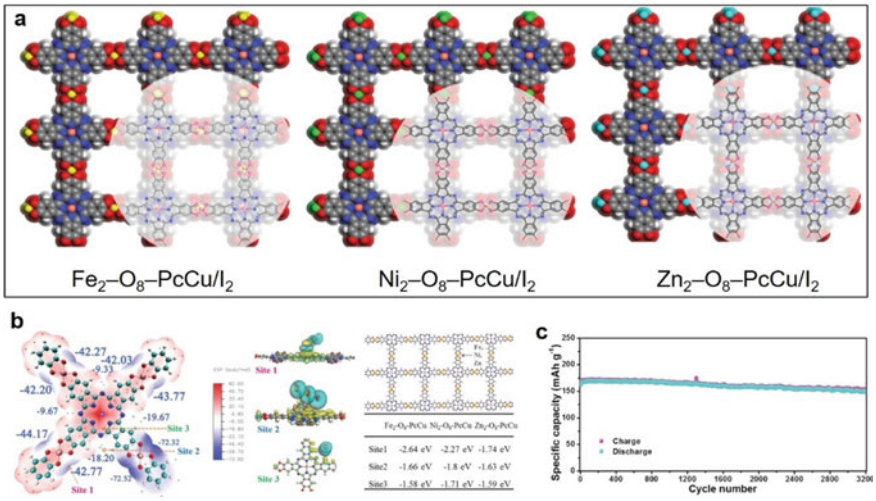

Fig. 3.25 **a** Schematic modeling and chemical structures of layered conjugated PcCu-MOFs. **b** First-principles calculations of suppressing polyiodide shuttle effect and promoting electrochemical kinetics of conversion reaction. **c** The cycling stability of Fe_2-O_8-PcCu/I_2 electrodes at 1.5 A g^{-1}. Adapted with permission [137]. Copyright 2019, WILEY–VCH Verlag GmbH & Co. KGaA, Weinheim

and wind power generation processes, but are also commonly used for power grid peak shaving to improve grid stability and security. RFBs are sometimes considered as an electrochemical regenerative fuel cell, since the electroactive components are not retained within electrodes, but stored in external containers in the form of two soluble redox couples to generate electricity (Fig. 3.26). Taking advantage of this key feature, RFBs have better durability compared to other conventional energy storage devices, since electrodes can be free of structural damage caused by repeated insertion/removal of active species during charge and discharge process [138]. To date, numerous aqueous and organic RFB systems have been successfully developed, in which organic RFB systems have attracted considerable attention due to wider operating potential window, and the consequent improvement of energy density. However, organic active species are soluble in nonaqueous electrolytes, and eventually leads to serious shuttle effects and irreversible capacity loss. Therefore, it is important to search for functional materials to alleviate the shuttle effects and irreversible loss of active materials.

Liu and co-workers [139] prepared two kinds of MOFs, as active catalysts, in a high energy density zinc-polyiodide liquid flow battery. Two nanoporous MOFs, MIL-125-NH_2 and UiO-66-CH_3, with high specific areas, accelerate the I_3^-/I^- redox reaction after deposition onto the surfaces of graphite felt. Consequently, the flow battery with MOF-modified graphite felts served as a cathode exhibited higher energy efficiency than the pristine graphite felts, increasing energy efficiency by 6.4% and 2.7%, respectively. Notably, UiO-66-CH_3 electrode is more chemically stable than MIL-125-NH_2 electrode in this work and thereby realized better cycling stability.

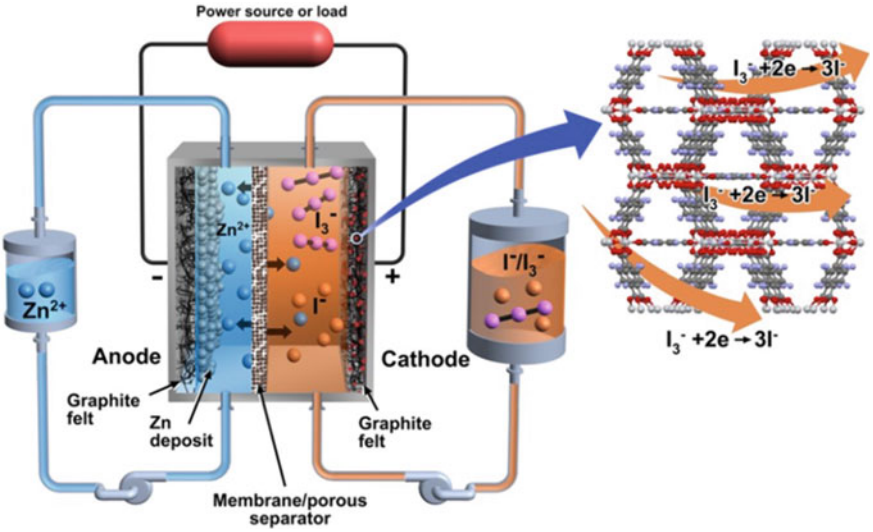

Fig. 3.26 Schematic of the zinc-polyiodide redox flow battery. Adapted with permission [139]. Copyright 2016, American Chemical Society

3.9.4 MOFs for Liquid Anode Batteries

It is known that the adverse effects of dendrite growth can be effectively eliminated by using liquid metal instead of bulk metal in alkali metal batteries. However, liquid anode batteries prevalently operate under high temperatures to realize desired wettability between the liquid metals and electrolyte. Consequently, the elevated operating temperature generally aggravates the corrosion of active components, and even results in severe safety hazards. To obtain a better electrochemical performance, the concept of alkali-based liquid anode was firstly proposed and investigated. The metal-based composite liquid electrode eliminates the issue of dendrite growth on one hand, and realizes efficient operation at a moderate temperature on the other hand [119]. Zhou and co-workers construct an organic oxygen battery with lithium-based liquid anode, MOF separator and oxygen cathode (Fig. 3.27a) [140]. The organic-lithium liquid anode was prepared by dissolving lithium metal with equal molar ratio in 1, 2-dimethoxy ethane biphenyls, in which electrons are transferred from lithium atoms to biphenyl molecules to form biphenyl-lithium complexes (Bp-Li, Fig. 3.27b). Interestingly, H_2O was dropped onto Bp-Li complex, and the reaction process was relatively mild without obvious explosion or bubble generation, which made Bp-Li complex a promising safety candidate for lithium-based liquid anode. Furthermore, a MOF-based composite was selected as separator, composed of ZIF-7 with high thermal and chemical stability, and polymer adhesive. It is found that the ZIF-7 separator can effectively prevent the migration of Bp-Li to the cathode by

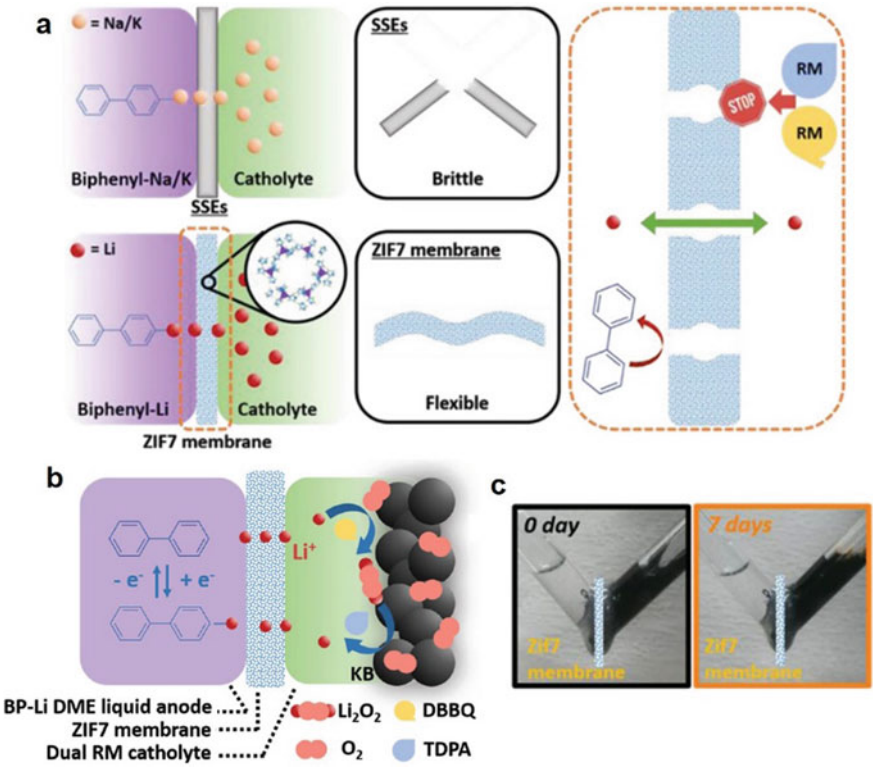

Fig. 3.27 **a** Schematic diagram of the difference between the previous report of biphenyl-Na/K liquid anode with solid-state electrolytes and biphenyl-Li liquid anode with a ZIF-7 separator in this work. **b** The schematic illustration of the organic oxygen battery with Bp-Li liquid anode, dual RM assisted KB cathode, and ZIF-7 separator. **c** Digital photos of the permeation device in the beginning and after 7 days. Adapted with permission [140]. Copyright 2020, WILEY–VCH Verlag GmbH & Co. KGaA, Weinheim

penetration test (Fig. 3.27c). Finally, the assembled batteries showed excellent rate capability, long-cycling lifespan, and low overpotential.

3.9.5 MOFs and MOF Derivatives for Fuel Cell

High catalytic performance with the lowest platinum content is crucial for the reduction of the cost in fuel cells. However, the catalyst is either easy to run off or exhibits poor stability under ultra-low platinum-loading. Therefore, achieving high catalytic activity under low platinum-loading condition has become a major obstacle in the development of fuel cells.

Liu and co-workers reported the Co-based MOF supported PtCo alloy nanocatalyst, in which the content of platinum was about 2.7–2.8 wt% [141]. The synergistic catalysis between platinum-cobalt core-shell nanoparticles on the catalytic substrate without platinum group metals displays excellent electrochemical performance under both high voltage and high current fields. Theoretical calculation shows that the interaction between platinum-cobalt nanoparticles and platinum group metal-free sites significantly improves ORR activity and durability (Fig. 3.28). Consequently, two catalysts realized ORR mass activities of 1.08 A mg_{Pt}^{-1} and 1.77 A mg_{Pt}^{-1} and maintained 64% and 15% of initial values after 30,000 cycles in the assembled fuel cell. This work successfully achieved stable ORR activity under low Pt-loading conditions and provides more ideas for cost reduction and efficiency improvement in fuel cells. Liu and co-workers realized bifunctional ORR and OER activity by introducing lattice-strained noble metal-free MOFs (Fig. 3.29a) [142]. It was observed for the first time that superoxide *OOH as a key intermediate product appeared at Ni^{4+} sites during both the oxygen reduction reaction and oxygen evolution reaction processes, revealing a four-electron mechanistic pathway (Fig. 3.29b). As a result, the prepared lattice-strained NiFe MOFs display mass activities of 500 A g_{metal}^{-1} at a half-wave potential of 0.83 V for the oxygen reduction reaction and 2000 A g_{metal}^{-1} at an overpotential of 0.30 V for the oxygen evolution reaction, 50–100 times higher than the pristine NiFe MOFs. Moreover, lattice-strained NiFe MOFs retain ~ 97% catalytic activity of ORR/OER reaction after 200 h at 100–200 mA cm^{-2}.

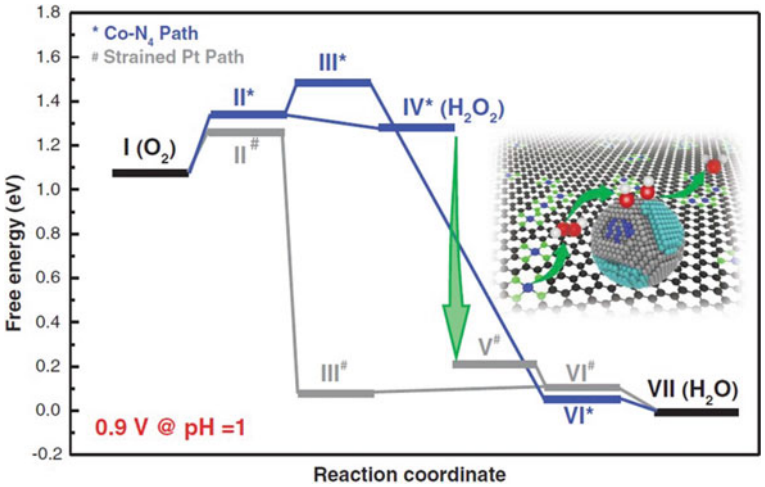

Fig. 3.28 Free-energy diagram of the ORR pathways. Adapted with permission [141]. Copyright 2018, The Authors, some rights reserved; exclusive licensee American Association for the Advancement of Science

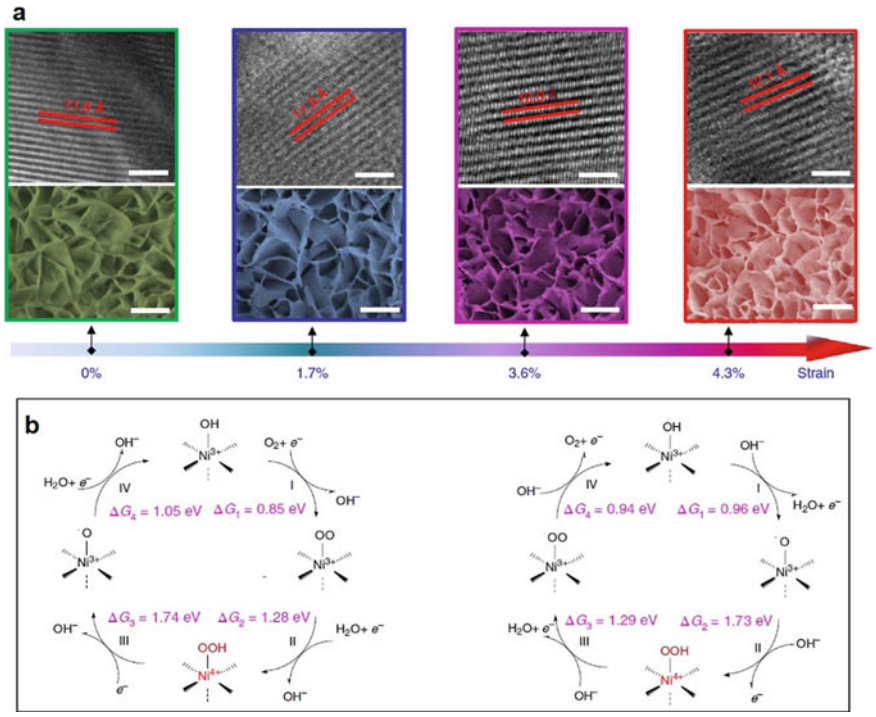

Fig. 3.29 **a** Structural characterizations of different lattice-strained MOFs. **b** Proposed ORR and OER catalytic mechanisms for the lattice-strained MOFs. Adapted with permission [142]. Copyright 2019, The Author(s), under exclusive license to Springer Nature

Summary

In this review, we have systematically summarized the significant progress of MOFs and MOF derivatives for emerging batteries and elaborated the opportunity and challenges in future development. The wide adoption of MOFs as electrode materials in rechargeable batteries still faces various challenges, such as poor electrical conductivity and structural instability, despite the various advantages of high specific area, diverse structure, and controllable chemical composition. In comparison, MOF derivatives, including MOF-derived metal, metal oxides, carbides, nitrides, and sulfides, show great promise as electrode materials for those emerging batteries. Nevertheless, many of them are also limited by low Coulombic efficiency and cyclic instability. Furthermore, the employment of MOFs and MOF derivatives generally involves costly and complicated fabrication process, and eventually restrict their large-scale applications in practical batteries. Hence, when designing MOF-based electrode materials, the various parameters in the battery, such as energy density, cycling stability, and preparation cost must be fully considered, to search for suitable MOFs and MOF-derived materials, and finally realize optimal electrochemical performance.

References

1. Chu S, Cui Y, Liu N (2016) The path towards sustainable energy. Nat Mater 16:16–22. https://doi.org/10.1038/nmat4834
2. Goodenough JB, Kim Y (2010) Challenges for rechargeable Li batteries. Chem Mater 22:587–603. https://doi.org/10.1021/cm901452z
3. Stamenkovic VR, Strmcnik D, Lopes PP, Markovic NM (2016) Energy and fuels from electrochemical interfaces. Nat Mater 16:57–69. https://doi.org/10.1038/nmat4738
4. Montoya JH, Seitz LC, Chakthranont P, Vojvodic A, Jaramillo TF, Norskov JK (2016) Materials for solar fuels and chemicals. Nat Mater 16:70–81. https://doi.org/10.1038/nmat4778
5. Tikekar MD, Choudhury S, Tu Z, Archer LA (2016) Design principles for electrolytes and interfaces for stable lithium-metal batteries. Nat Energy 1:16114. https://doi.org/10.1038/nenergy.2016.114
6. Gao X, Zhou Y-N, Han D, Zhou J, Zhou D, Tang W, Goodenough J B (2020) Thermodynamic understanding of Li-Dendrite formation. Joule 4:1864–1879. https://doi.org/10.1016/j.joule.2020.06.016
7. Liu B, Zhang J-G, Xu W (2018) Advancing lithium metal batteries. Joule 2:833–845. https://doi.org/10.1016/j.joule.2018.03.008
8. Jin J, Tian X, Srikanth N, Kong LB, Zhou K (2017) Advances and challenges of nanostructured electrodes for Li–Se batteries. J Mater Chem A 5:10110–10126. https://doi.org/10.1039/C7TA01384A
9. Manthiram A, Fu Y, Chung S-H, Zu C, Su Y-S (2014) Rechargeable Lithium-Sulfur batteries. Chem Rev 114:11751–11787. https://doi.org/10.1021/cr500062v
10. Shu C, Wang J, Long J, Liu H-K, Dou S-X (2019) Understanding the reaction chemistry during charging in aprotic lithium-oxygen batteries: existing problems and solutions. Adv Mater 31:1804587. https://doi.org/10.1002/adma.201804587
11. Sun B, Xiong P, Maitra U, Langsdorf D, Yan K, Wang C, Janek J, Schröder D, Wang G (2020) Design strategies to enable the efficient use of sodium metal anodes in high-energy batteries. Adv Mater 32:1903891. https://doi.org/10.1002/adma.201903891
12. Kwabi DG, Ji Y, Aziz MJ (2020) Electrolyte lifetime in aqueous organic redox flow batteries: a critical review. Chem Rev 120:6467–6489. https://doi.org/10.1021/acs.chemrev.9b00599
13. Li X, Yang S, Feng N, He P, Zhou H (2016) Progress in research on Li-CO_2 batteries: Mechanism, catalyst and performance. Chinese J Catal 37:1016–1024. https://doi.org/10.1016/S1872-2067(15)61125-1
14. Ma L, Ying Y, Chen S, Huang Z, Li X, Huang H, Zhi C (2020) Electrocatalytic iodine reduction reaction enabled by aqueous zinc-iodine battery with improved power and energy densities. Angew Chem Int Ed 59:2–10. https://doi.org/10.1002/anie.202014447
15. Morozan A, Jaouen F (2012) Metal organic frameworks for electrochemical applications. Energy Environ Sci 5:9269. https://doi.org/10.1039/c2ee22989g
16. Liu S, Zhang C, Sun Y, Chen Q, He L, Zhang K, Zhang J, Liu B, Chen L-F (2020) Design of metal-organic framework-based photocatalysts for hydrogen generation. Coord Chem Rev 413:213266. https://doi.org/10.1016/j.ccr.2020.213266
17. Wu H B, Lou X W (2017) Metal-organic frameworks and their derived materials for electrochemical energy storage and conversion: promises and challenges. Sci Adv 3:eaap9252. https://doi.org/10.1126/sciadv.aap9252
18. Chen L-F, Xu Q (2017) Converting MOFs into amination catalysts. Science 358:304–305. https://doi.org/10.1126/science.aap8004
19. Chen L-F, Hou C-C, Zou L, Kitta M, Xu Q (2020) Uniformly bimetal-decorated holey carbon nanorods derived from metal-organic framework for efficient hydrogen evolution. Sci Bull https://doi.org/10.1016/j.scib.2020.06.022
20. Zhang L, Liu H, Shi W, Cheng P (2019) Synthesis strategies and potential applications of metal-organic frameworks for electrode materials for rechargeable lithium ion batteries. Coord Chem Rev 388:293–309. https://doi.org/10.1016/j.ccr.2019.02.030

21. Li X, Cheng F, Zhang S, Chen J (2006) Shape-controlled synthesis and lithium-storage study of metal-organic frameworks Zn_4O(1,3,5-benzenetribenzoate)$_2$. J Power Sources 160:542–547. https://doi.org/10.1016/j.jpowsour.2006.01.015
22. Saravanan K, Nagarathinam M, Balaya P, Vittal JJ (2010) Lithium storage in a metal organic framework with diamondoid topology-a case study on metal formates. J Mater Chem 20:8329–8335. https://doi.org/10.1039/c0jm01671c
23. Ogihara N, Yasuda T, Kishida Y, Ohsuna T, Miyamoto K, Ohba N (2014) Organic dicarboxylate negative electrode materials with remarkably small strain for high-voltage bipolar batteries. Angew Chem Int Ed 53:11467–11472. https://doi.org/10.1002/anie.201405139
24. Wei T, Zhang M, Wu P, Tang Y-J, Li S-L, Shen F-C, Wang X-L, Zhou X-P, Lan Y-Q (2017) POM-based metal-organic framework/reduced graphene oxide nanocomposites with hybrid behavior of battery-supercapacitor for superior lithium storage. Nano Energy 34:205–214. https://doi.org/10.1016/j.nanoen.2017.02.028
25. Hermes S, Schroter MK, Schmid R, Khodeir L, Muhler M, Tissler A, Fischer RW, Fischer RA (2005) Metal@MOF: loading of highly porous coordination polymers host lattices by metal organic chemical vapor deposition. Angew Chem Int Ed 44:6237–6241. https://doi.org/10.1002/anie.200462515
26. Zhang H, Deng Q, Zhou A, Liu X, Li J (2014) Porous $Li_2C_8H_4O_4$ coated with N-doped carbon by using CVD as an anode material for Li-ion batteries. J Mater Chem A 2:5696–5702. https://doi.org/10.1039/C3TA14720G
27. Han Y, Qi P, Feng X, Li S, Fu X, Li H, Chen Y, Zhou J, Li X, Wang B (2015) In situ growth of MOFs on the surface of si nanoparticles for highly efficient lithium storage: Si@MOF nanocomposites as anode materials for lithium-ion batteries. ACS Appl Mater Interfaces 7:2178–2182. https://doi.org/10.1021/am5081937
28. Qiao Q-Q, Li G-R, Wang Y-L, Gao X-P (2016) To enhance the capacity of Li-rich layered oxides by surface modification with metal–organic frameworks (MOFs) as cathodes for advanced lithium-ion batteries. J Mater Chem A 4:4440–4447. https://doi.org/10.1039/c6ta00882h
29. Hou Y, Li J, Wen Z, Cui S, Yuan C, Chen J (2015) Co_3O_4 nanoparticles embedded in nitrogen-doped porous carbon dodecahedrons with enhanced electrochemical properties for lithium storage and water splitting. Nano Energy 12:1–8. https://doi.org/10.1016/j.nanoen.2014.11.043
30. Huang G, Zhang F, Du X, Qin Y, Yin D, Wang L (2015) Metal organic frameworks route to in situ insertion of multiwalled carbon nanotubes in Co_3O_4 polyhedra as anode materials for Lithium-Ion batteries. ACS Nano 9:1592–1599. https://doi.org/10.1021/nn506252u
31. Xia W, Mahmood A, Zou R, Xu Q (2015) Metal–organic frameworks and their derived nanostructures for electrochemical energy storage and conversion. Energy Environ Sci 8:1837–1866. https://doi.org/10.1039/c5ee00762c
32. Zheng S, Li X, Yan B, Hu Q, Xu Y, Xiao X, Xue H, Pang H (2017) Transition-metal (Fe, Co, Ni) based metal-organic frameworks for electrochemical energy storage. Adv Energy Mater 7:1602733. https://doi.org/10.1002/aenm.201602733
33. Banerjee A, Aravindan V, Bhatnagar S, Mhamane D, Madhavi S, Ogale S (2013) Superior lithium storage properties of α-Fe_2O_3 nano-assembled spindles. Nano energy 2:890–896. https://doi.org/10.1016/j.nanoen.2013.03.006
34. Zheng F, Yang Y, Chen Q (2014) High lithium anodic performance of highly nitrogen-doped porous carbon prepared from a metal-organic framework. Nat Commun 5:5261. https://doi.org/10.1038/ncomms6261
35. Zou F, Hu X, Li Z, Qie L, Hu C, Zeng R, Jiang Y, Huang Y (2014) MOF-derived porous ZnO/$ZnFe_2O_4$/C Octahedra with hollow interiors for high-rate lithium-ion batteries. Adv Mater 26:6622–6628. https://doi.org/10.1002/adma.201402322
36. Cheng C-Y, Fu S-J, Yang C-J, Chen W-H, Lin K-J, Lee G-H, Wang Y (2003) NCHU-3: a crystalline inorganic-organic hybrid molecular sieve with extra-large cages. Angew Chem Int Ed 42:1937–1940. https://doi.org/10.1002/anie.200250544

37. Férey G, Millange F, Morcrette M, Serre C, Doublet M-L, Grenèche J-M, Tarascon J-M (2007) Mixed-Valence Li/Fe-based metal-organic frameworks with both reversible redox and sorption properties. Angew Chem Int Ed 46:3259–3263. https://doi.org/10.1002/anie.200605163
38. Fateeva A, Horcajada P, Devic T, Serre C, Marrot J, Grenèche J-M, Morcrette M, Tarascon J-M, Maurin G, Férey G (2010) Synthesis, structure, characterization, and redox properties of the porous MIL-68(Fe) solid. Eur J Inorg Chem 2010:3789–3794. https://doi.org/10.1002/ejic.201000486
39. Shin J, Kim M, Cirera J, Chen S, Halder GJ, Yersak TA, Paesani F, Cohen SM, Meng YS (2015) MIL-101(Fe) as a lithium-ion battery electrode material: a relaxation and intercalation mechanism during lithium insertion. J Mater Chem A 3:4738–4744. https://doi.org/10.1039/C4TA06694D
40. Gu S, Bai Z, Majumder S, Huang B, Chen G (2019) Conductive metal-organic framework with redox metal center as cathode for high rate performance lithium ion battery. J Power Sources 429:22–29. https://doi.org/10.1016/j.jpowsour.2019.04.087
41. Wang Z, Li X, Yang Y, Cui Y, Pan H, Wang Z, Chen B, Qian G (2014) Highly dispersed β-NiS nanoparticles in porous carbon matrices by a template metal–organic framework method for lithium-ion cathode. J Mater Chem A 2:7912–7916. https://doi.org/10.1039/C4TA00367E
42. Liu J, Wu C, Xiao D, Kopold P, Gu L, van Aken P A, Maier J, Yu Y (2016) MOF-Derived hollow Co_9S_8 nanoparticles embedded in graphitic carbon nanocages with superior Li-Ion storage. Small 12:2354–2364. https://doi.org/10.1002/smll.201503821
43. Choi N-S, Chen Z, Freunberger S A, Ji X, Sun Y-K, Amine K, Yushin G, Nazar L F, Cho J, Bruce P G (2012) Challenges facing lithium batteries and electrical double-layer capacitors. Angew Chem Int Ed 51:9994–10024. https://doi.org/10.1002/anie.201201429
44. Xiao J, Chen X, Sushko P V, Sushko M L, Kovarik L, Feng J, Deng Z, Zheng J, Graff G L, Nie Z, Choi D, Liu J, Zhang J-G, Whittingham M S (2012) High-performance $LiNi_{0.5}Mn_{1.5}O_4$ spinel controlled by Mn^{3+} concentration and site disorder. Adv Mater 24:2109–2116. https://doi.org/10.1002/adma.201104767
45. Bruce PG, Freunberger SA, Hardwick LJ, Tarascon J-M (2012) Li-O_2 and Li-S batteries with high energy storage. Nat Mater 11:19–29. https://doi.org/10.1038/nmat3191
46. Choi N-S, Chen Z, Freunberger SA, Ji X, Sun Y-K, Amine K, Yushin G, Nazar LF, Cho J, Bruce PG (2012) Challenges facing lithium batteries and electrical double-layer capacitors. Angew Chem Int Ed 51:9994–10024. https://doi.org/10.1002/anie.201201429
47. Zheng Y, Zheng S, Xue H, Pang H (2019) Metal-organic frameworks for lithium–sulfur batteries. J Mater Chem A 7:3469–3491. https://doi.org/10.1039/c8ta11075a
48. Xu J, Lawson T, Fan H, Su D, Wang G (2018) Updated metal compounds (MOFs, S, OH, N, C) used as cathode materials for lithium-sulfur batteries. Adv Energy Mater 8:1702607. https://doi.org/10.1002/aenm.201702607
49. Xia W, Mahmood A, Zou R, Xu Q (2015) Metal–organic frameworks and their derived nanostructures for electrochemical energy storage and conversion. Energy Environ Science 8:1837–1866. https://doi.org/10.1039/c5ee00762c
50. Yan W, Wei J, Chen T, Duan L, Wang L, Xue X, Chen R, Kong W, Lin H, Li C, Jin Z (2021) Superstretchable, thermostable and ultrahigh-loading lithium-sulfur batteries based on nanostructural gel cathodes and gel electrolytes. Nano Energy 80:105510. https://doi.org/10.1016/j.nanoen.2020.105510
51. Wang R, Mi J-S, Dong X-Y, Liu X-F, Lv Y-R, Du J, Zhao J-Y, Zang S-Q (2019) Creating a polar surface in carbon frameworks from single-source metal-organic frameworks for advanced CO_2 uptake and lithium–sulfur batteries. Chem Mater 31:4258–4266. https://doi.org/10.1021/acs.chemmater.9b01264
52. Liu R, Liu Z, Liu W, Liu Y, Lin X, Li Y, Li P, Huang Z, Feng X, Yu L, Wang D, Ma Y, Huang W (2019) TiO_2 and Co nanoparticle-decorated carbon polyhedra as efficient sulfur host for high-performance Lithium-Sulfur batteries. Small 15:e1804533. https://doi.org/10.1002/smll.201804533

53. Cai D, Lu M, Li L, Cao J, Chen D, Tu H, Li J, Han W (2019) A Highly conductive MOF of graphene analogue $Ni_3(HITP)_2$ as a sulfur host for high-performance Lithium-Sulfur batteries. Small 15:1902605. https://doi.org/10.1002/smll.201902605
54. Cao X, Tan C, Sindoro M, Zhang H (2017) Hybrid micro-/nano-structures derived from metal–organic frameworks: preparation and applications in energy storage and conversion. Chem Soc Rev 46:2660–2677. https://doi.org/10.1039/c6cs00426a
55. Arora P, Zhang Z (2004) Battery separators. Chem Rev 104:4419–4462. https://doi.org/10.1021/cr020738u
56. Huang J-Q, Zhang Q, Wei F (2015) Multi-functional separator/interlayer system for high-stable lithium-sulfur batteries: progress and prospects. Energy Storage Mater 1:127–145. https://doi.org/10.1016/j.ensm.2015.09.008
57. Bai S, Liu X, Zhu K, Wu S, Zhou H (2016) Metal-organic framework-based separator for lithium–sulfur batteries. Nat Energy 1:16094. https://doi.org/10.1038/nenergy.2016.94
58. Li M, Wan Y, Huang J-K, Assen AH, Hsiung C-E, Jiang H, Han Y, Eddaoudi M, Lai Z, Ming J, Li L-J (2017) Metal-organic framework-based separators for enhancing Li–S battery stability: mechanism of mitigating polysulfide diffusion. ACS Energy Lett 2:2362–2367. https://doi.org/10.1021/acsenergylett.7b00692
59. Hong X, Song C, Yang Y, Tan H, Li G, Cai Y, Wang H (2019) Cerium based metal-organic frameworks as an efficient separator coating catalyzing the conversion of polysulfides for high performance lithium-sulfur batteries. ACS Nano 13:1923–1931. https://doi.org/10.1021/acsnano.8b08155
60. He Y, Chang Z, Wu S, Qiao Y, Bai S, Jiang K, He P, Zhou H (2018) Simultaneously inhibiting lithium dendrites growth and polysulfides shuttle by a flexible MOF-based membrane in Li-S batteries. Adv Energy Mater 8:1802130. https://doi.org/10.1002/aenm.201802130
61. Liu B, Taheri M, Torres JF, Fusco Z, Lu T, Liu Y, Tsuzuki T, Yu G, Tricoli A (2020) Janus conductive/insulating microporous ion-sieving membranes for stable Li-S batteries. ACS Nano 14:13852–13864. https://doi.org/10.1021/acsnano.0c06221
62. Han J, Gao S, Wang R, Wang K, Jiang M, Yan J, Jin Q, Jiang K (2020) Investigation of the mechanism of metal–organic frameworks preventing polysulfide shuttling from the perspective of composition and structure. J Mater Chem A 8:6661–6669. https://doi.org/10.1039/d0ta00533a
63. Denny MS, Kalaj M, Bentz KC, Cohen SM (2018) Multicomponent metal-organic framework membranes for advanced functional composites. Chem Sci 9:8842–8849. https://doi.org/10.1039/c8sc02356e
64. McCloskey BD, Burke CM, Nichols JE, Renfrew SE (2015) Mechanistic insights for the development of Li-O_2 battery materials: addressing Li_2O_2 conductivity limitations and electrolyte and cathode instabilities. Chem Commun 51:12701–12715. https://doi.org/10.1039/c5cc04620c
65. Girishkumar G, McCloskey B, Luntz AC, Swanson S, Wilcke W (2010) Lithium−Air battery: promise and challenges. J Phys Chem A 1:2193–2203. https://doi.org/10.1021/jz1005384
66. Wu D, Guo Z, Yin X, Pang Q, Tu B, Zhang L, Wang YG, Li Q (2014) Metal-organic frameworks as cathode materials for Li-O_2 batteries. Adv Mater 26:3258–3262. https://doi.org/10.1002/adma.201305492
67. Hu X, Zhu Z, Cheng F, Tao Z, Chen J (2015) Micro-nano structured Ni-MOFs as high-performance cathode catalyst for rechargeable Li-O_2 batteries. Nanoscale 7:11833–11840. https://doi.org/10.1039/c5nr02487k
68. Kim SH, Lee YJ, Kim DH, Lee YJ (2018) Bimetallic metal-organic frameworks as efficient cathode catalysts for Li-O_2 batteries. ACS Appl Mater Interfaces 10:660–667. https://doi.org/10.1021/acsami.7b15499
69. Qiao Y, He Y, Wu S, Jiang K, Li X, Guo S, He P, Zhou H (2018) MOF-based separator in an Li-O_2 battery: an effective strategy to restrain the shuttling of dual redox mediators. ACS Energy Lett 3:463–468. https://doi.org/10.1021/acsenergylett.8b00014
70. Cao L, Lv F, Liu Y, Wang W, Huo Y, Fu X, Sun R, Lu Z (2015) A high performance O_2 selective membrane based on CAU-1-NH_2@polydopamine and the PMMA polymer for Li-air batteries. Chem Commun 51:4364–4367. https://doi.org/10.1039/c4cc09281c

71. Lyu Z, Lim GJH, Guo R, Kou Z, Wang T, Guan C, Ding J, Chen W, Wang J (2019) 3D-printed MOF-derived hierarchically porous frameworks for practical high-energy density Li-O_2 batteries. Adv Funct Mater 29:1806658. https://doi.org/10.1002/adfm.201806658
72. Wang H, Yin F, Lv P, Fan T, He X, Chen B (2017) Metal–organic-framework-derived FeCo alloy core@nitrogen-doped carbon shell nanoparticles anchored on carbon nanotubes for rechargeable Li-O_2 battery. Int Int J Hydrog Energy 42:2127–2133. https://doi.org/10.1016/j.ijhydene.2016.11.118
73. Song MJ, Kim IT, Kim YB, Kim J, Shin MW (2017) Metal-organic frameworks-derived porous carbon/Co_3O_4 composites for rechargeable lithium-oxygen batteries. Electrochim Acta 230:73–80. https://doi.org/10.1016/j.electacta.2017.01.121
74. Zhang J, Wang L, Xu L, Ge X, Zhao X, Lai M, Liu Z, Chen W (2015) Porous cobalt-manganese oxide nanocubes derived from metal organic frameworks as a cathode catalyst for rechargeable Li-O_2 batteries. Nanoscale 7:720–726. https://doi.org/10.1039/c4nr05865h
75. Yu H, Dinh KN, Sun Y, Fan H, Wang Y, Jing Y, Li S, Srinivasan M, Yan Q (2018) Performance-improved Li-O_2 batteries by tailoring the phases of Mo_xC porous nanorods as an efficient cathode. Nanoscale 10:14877–14884. https://doi.org/10.1039/c8nr04319a
76. Tan G, Chong L, Amine R, Lu J, Liu C, Yuan Y, Wen J, He K, Bi X, Guo Y, Wang HH, Shahbazian-Yassar R, Al Hallaj S, Miller DJ, Liu D, Amine K (2017) Toward highly efficient electrocatalyst for Li-O_2 batteries using biphasic N-Doping Cobalt@Graphene multiple-capsule heterostructures. Nano Lett 17:2959–2966. https://doi.org/10.1021/acs.nanolett.7b00207
77. Dou Y, Lian R, Zhang Y, Zhao Y, Chen G, Wei Y, Peng Z (2018) Co_9S_8@carbon porous nanocages derived from a metal-organic framework: a highly efficient bifunctional catalyst for aprotic Li-O_2 batteries. J Mater Chem A 6:8595–8603. https://doi.org/10.1039/c8ta01913d
78. Lee S, Lee H, Ha N, Lee J T, Jung J, Eom K (2020) In Batteria electrochemical polymerization to form a protective conducting layer on Se/C cathodes for high-performance Li-Se batteries. Adv Funct Mater 30:2000028. https://doi.org/10.1002/adfm.202000028
79. Li Y-J, Fan J-M, Zheng M-S, Dong Q-F (2016) A novel synergistic composite with multi-functional effects for high-performance Li-S batteries. Energy Environ Science 9:1998–2004. https://doi.org/10.1039/C6EE00104A
80. Fan H, Zheng Z, Zhao L, Li W, Wang J, Dai M, Zhao Y, Xiao J, Wang G, Ding X, Xiao H, Li J, Wu Y, Zhang Y (2019) Extending cycle life of Mg/S battery by activation of Mg Anode/Electrolyte interface through an LiCl-assisted $MgCl_2$ solubilization mechanism. Adv Funct Mater 30:1909370. https://doi.org/10.1002/adfm.201909370
81. Li Z, Wu HB, Lou XW (2016) Rational designs and engineering of hollow micro-/nanostructures as sulfur hosts for advanced lithium-sulfur batteries. Energy Environ Sci 9:3061–3070. https://doi.org/10.1039/C6EE02364A
82. Zeng L-C, Li W-H, Jiang Y, Yu Y (2017) Recent progress in Li-S and Li-Se batteries. Rare Met 36:339–364. https://doi.org/10.1007/s12598-017-0891-z
83. Li X, Liang J, Li X, Wang C, Luo J, Li R, Sun X (2018) High-performance all-solid-state Li-Se batteries induced by sulfide electrolytes. Energy Environ Sci 11:2828–2832. https://doi.org/10.1039/C8EE01621F
84. Zhang B, Zhang Y, Li J, Liu J, Huo X, Kang F (2020) In situ growth of metal-organic framework-derived $CoTe_2$ nanoparticles@nitrogen-doped porous carbon polyhedral composites as novel cathodes for rechargeable aluminum-ion batteries. J Mater Chem A 8:5535–5545. https://doi.org/10.1039/d0ta00674b
85. Li C, Liu L, Kang J, Xiao Y, Feng Y, Cao F-F, Zhang H (2020) Pristine MOF and COF materials for advanced batteries. Energy Storage Mater 31:115–134. https://doi.org/10.1016/j.ensm.2020.06.005
86. Lai Y, Gan Y, Zhang Z, Chen W, Li J (2014) Metal-organic frameworks-derived mesoporous carbon for high performance lithium-selenium battery. Electrochim Acta 146:134–141. https://doi.org/10.1016/j.electacta.2014.09.045

87. Liu T, Dai C, Jia M, Liu D, Bao S, Jiang J, Xu M, Li CM (2016) Selenium embedded in metal-organic framework derived hollow hierarchical porous carbon spheres for advanced lithium-selenium batteries. ACS Appl Mater Interfaces 8:16063–16070. https://doi.org/10.1021/acsami.6b04060
88. Liu T, Zhang Y, Hou J, Lu S, Jiang J, Xu M (2015) High performance mesoporous C@Se composite cathodes derived from Ni-based MOFs for Li-Se batteries. RSC Adv 5:84038–84043. https://doi.org/10.1039/c5ra14979g
89. Liu T, Jia M, Zhang Y, Han J, Li Y, Bao S, Liu D, Jiang J, Xu M (2017) Confined selenium within metal-organic frameworks derived porous carbon microcubes as cathode for rechargeable lithium–selenium batteries. J Power Sources 341:53–59. https://doi.org/10.1016/j.jpowsour.2016.11.099
90. Jin W-W, Li H-J, Zou J-Z, Inguva S, Zhang Q, Zeng S-Z, Xu G-Z, Zeng X-R (2019) 2D ultrathin carbon nanosheets derived from interconnected Al-MOF as excellent hosts to anchor selenium for Li-Se battery. Mater Lett 252:211–214. https://doi.org/10.1016/j.matlet.2019.05.131
91. Jin W-W, Li H-J, Zou J-Z, Inguva S, Zhang Q, Zeng S-Z, Xu G-Z, Zeng X-R (2020) Metal organic framework-derived carbon nanosheets with fish-scale surface morphology as cathode materials for lithium–selenium batteries. J Alloys Csssompd. 820. https://doi.org/10.1016/j.jallcom.2019.153084
92. Gu X, Xin L, Li Y, Dong F, Fu M, Hou Y (2018) Highly Reversible Li-Se Batteries with Ultra-Lightweight N S-Codoped Graphene Blocking Layer. Nano-Micro Lett 10:59. https://doi.org/10.1007/s40820-018-0213-5
93. Li Z, Yin L (2015) MOF-derived, N-doped, hierarchically porous carbon sponges as immobilizers to confine selenium as cathodes for Li-Se batteries with superior storage capacity and perfect cycling stability. Nanoscale 7:9597–9606. https://doi.org/10.1039/c5nr00903k
94. Song J-P, Wu L, Dong W-D, Li C-F, Chen L-H, Dai X, Li C, Chen H, Zou W, Yu W-B, Hu Z-Y, Liu J, Wang H-E, Li Y, Su B-L (2019) MOF-derived nitrogen-doped core-shell hierarchical porous carbon confining selenium for advanced lithium-selenium batteries. Nanoscale 11:6970–6981. https://doi.org/10.1039/c9nr00924h
95. He J, Lv W, Chen Y, Xiong J, Wen K, Xu C, Zhang W, Li Y, Qin W, He W (2017) Three-dimensional hierarchical C-Co-N/Se derived from metal-organic framework as superior cathode for Li-Se batteries. J Power Sources 363:103–109. https://doi.org/10.1016/j.jpowsour.2017.07.065
96. Ye W, Wang K, Yin W, Chai W, Rui Y, Tang B (2019) A novel Zr-MOF-based and polyaniline-coated UIO-67@Se@PANI composite cathode for lithium-selenium batteries. Dalton Trans 48:10191–10198. https://doi.org/10.1039/c9dt01961h
97. Jang-Yeon Hwang S-T M a Y-K S (2017) Sodium-ion batteries: present and future. Chem Soc Rev 3529-3614. https://doi.org/10.1039/c6cs00776g
98. Lee M, Hong J, Lopez J, Sun Y, Feng D, Lim K, Chueh WC, Toney MF, Cui Y, Bao Z (2017) High-performance sodium-organic battery by realizing four-sodium storage in disodium rhodizonate. Nat Energy 2:861–868. https://doi.org/10.1038/s41560-017-0014-y
99. Ye Z, Wang F, Jia C, Shao Z (2018) Biomass-based O, N-codoped activated carbon aerogels with ultramicropores for supercapacitors. J Mater Sci 53:12374–12387. https://doi.org/10.1007/s10853-018-2487-x
100. Mohamed Eddaoudi JK, Rosi N, Vodak D, Wachter J, O'Keeffe M, Yaghi OM (2002) Systematic design of pore size and functionality in isoreticular MOFs and their application in methane storage. Science 295:469–472
101. Wu Y, Chen Y, Tang M, Zhu S, Jiang C, Zhuo S, Wang C (2019) A highly conductive conjugated coordination polymer for fast-charge sodium-ion batteries: reconsidering its structures. Chem Commun 55:10856–10859. https://doi.org/10.1039/c9cc05679c
102. Luo D, Lei P, Tian G, Huang Y, Ren X, Xiang X (2020) Insight into electrochemical properties and reaction mechanism of a cobalt-rich prussian blue analogue cathode in a $NaSO_3CF_3$ electrolyte for aqueous sodium-ion batteries. J Phys Chem C 124:5958–5965. https://doi.org/10.1021/acs.jpcc.9b11758

103. You Y, Wu X-L, Yin Y-X, Guo Y-G (2013) A zero-strain insertion cathode material of nickel ferricyanide for sodium-ion batteries. J Mater Chem A 1:14061–14065. https://doi.org/10.1039/c3ta13223d
104. Wu X, Deng W, Qian J, Cao Y, Ai X, Yang H (2013) Single-crystal $FeFe(CN)_6$ nanoparticles: a high capacity and high rate cathode for Na-ion batteries. J Mater Chem A 1:10130–10134. https://doi.org/10.1039/c3ta12036h
105. Yang D, Xu J, Liao X-Z, Wang H, He Y-S, Ma Z-F (2015) Prussian blue without coordinated water as a superior cathode for sodium-ion batteries. Chem Commun 51:8181–8184. https://doi.org/10.1039/c5cc01180a
106. Wang W, Gang Y, Hu Z, Yan Z, Li W, Li Y, Gu QF, Wang Z, Chou SL, Liu HK, Dou SX (2020) Reversible structural evolution of sodium-rich rhombohedral Prussian blue for sodium-ion batteries. Nat Commun 11:980. https://doi.org/10.1038/s41467-020-14444-4
107. Kim Y, Kim Y, Park Y, Jo YN, Kim YJ, Choi NS, Lee KT (2015) SnSe alloy as a promising anode material for Na-ion batteries. Chem Commun 51:50–53. https://doi.org/10.1039/c4cc06106c
108. Park GD, Lee JH, Kang YC (2016) Superior Na-ion storage properties of high aspect ratio SnSe nanoplates prepared by a spray pyrolysis process. Nanoscale 8:11889–11896. https://doi.org/10.1039/c6nr02983c
109. Zhang W, Yan W, Jiang H, Wang C, Zhou Y, Ke F, Cong H, Deng H (2019) Uniform Bi–Sb alloy nanoparticles synthesized from MOFs by laser metallurgy for sodium-ion batteries. ACS Sustain Chem Eng 8:335–342. https://doi.org/10.1021/acssuschemeng.9b05474
110. Zhang Y, Su Q, Xu W, Cao G, Wang Y, Pan A, Liang S (2019) A confined replacement synthesis of bismuth nanodots in MOF derived carbon arrays as binder-free anodes for sodium-ion batteries. Adv Sci 6:1900162. https://doi.org/10.1002/advs.201900162
111. Shuang W, Huang H, Kong L, Zhong M, Li A, Wang D, Xu Y, Bu X-H (2019) Nitrogen-doped carbon shell-confined Ni_3S_2 composite nanosheets derived from Ni-MOF for high performance sodium-ion battery anodes. Nano Energy 62:154–163. https://doi.org/10.1016/j.nanoen.2019.05.030
112. Xu X, Liu J, Liu J, Ouyang L, Hu R, Wang H, Yang L, Zhu M (2018) A general metal-organic framework (MOF)-derived selenidation strategy for in situ carbon-encapsulated metal selenides as high-rate anodes for na-ion batteries. Adv Funct Mater 28:1707573. https://doi.org/10.1002/adfm.201707573
113. Shi S, Sun C, Yin X, Shen L, Shi Q, Zhao K, Zhao Y, Zhang J (2020) FeP quantum dots confined in carbon-nanotube-grafted P-doped carbon octahedra for high-rate sodium storage and full-cell applications. Adv Funct Mater 30:1909283. https://doi.org/10.1002/adfm.201909283
114. Chen Y, Li X, Park K, Lu W, Wang C, Xue W, Yang F, Zhou J, Suo L, Lin T, Huang H, Li J, Goodenough JB (2017) Nitrogen-doped carbon for sodium-ion battery anode by self-etching and graphitization of bimetallic MOF-based composite. Chem 3:152–163. https://doi.org/10.1016/j.chempr.2017.05.021
115. Li W, Hu S, Luo X, Li Z, Sun X, Li M, Liu F, Yu Y (2017) Confined amorphous red phosphorus in MOF-derived N-doped microporous carbon as a superior anode for sodium-ion battery. Adv Mater 29:1605820. https://doi.org/10.1002/adma.201605820
116. Xu H, Liu Y, Qiang T, Qin L, Chen J, Zhang P, Zhang Y, Zhang W, Tian W, Sun Z (2019) Boosting sodium storage properties of titanium dioxide by a multiscale design based on MOF-derived strategy. Energy Storage Mater 17:126–135. https://doi.org/10.1016/j.ensm.2018.07.023
117. Wu Q, Yao Z, Zhou X, Xu J, Cao F, Li C (2020) Built-in catalysis in confined nanoreactors for high-loading Li-S Batteries. ACS Nano 14:3365–3377. https://doi.org/10.1021/acsnano.9b09231
118. D. I. Iermakova R D, M. R. Palac´ ın, A. Ponrouch, (2015) On the comparative stability of Li and Na metal anode interfaces in conventional alkyl carbonate electrolytes. J Electrochem Soc 162:7060–7066. https://doi.org/10.1149/2.0091513jes

119. He Y, Qiao Y, Chang Z, Zhou H (2019) The potential of electrolyte filled MOF membranes as ionic sieves in rechargeable batteries. Energy Environ Sci 12:2327–2344. https://doi.org/10.1039/c8ee03651a
120. Bai S, Kim B, Kim C, Tamwattana O, Park H, Kim J, Lee D, Kang K (2020) Permselective metal-organic framework gel membrane enables long-life cycling of rechargeable organic batteries. Nat Nanotechnol 4944. https://doi.org/10.1038/s41565-020-00788-x
121. Ji X, Hou S, Wang P, He X, Piao N, Chen J, Fan X, Wang C (2020) Solid-state electrolyte design for lithium dendrite suppression. Adv Mater 32. https://doi.org/10.1002/adma.202002741
122. Park SS, Tulchinsky Y, Dinca M (2017) Single-Ion Li^+, Na^+, and Mg^{2+} solid electrolytes supported by a mesoporous anionic Cu-azolate metal-organic framework. J Am Chem Soc 139:13260–13263. https://doi.org/10.1021/jacs.7b06197
123. Yuan H, Liu T, Liu Y, Nai J, Wang Y, Zhang W, Tao X (2019) A review of biomass materials for advanced lithium-sulfur batteries. Chem Sci 10:7484–7495. https://doi.org/10.1039/c9sc02743b
124. Zhao X, Yin L, Zhang T, Zhang M, Fang Z, Wang C, Wei Y, Chen G, Zhang D, Sun Z, Li F (2018) Heteroatoms dual-doped hierarchical porous carbon-selenium composite for durable Li-Se and Na-Se batteries. Nano Energy 49:137–146. https://doi.org/10.1016/j.nanoen.2018.04.045
125. Xu Q, Liu T, Li Y, Hu L, Dai C, Zhang Y, Li Y, Liu D, Xu M (2017) Selenium encapsulated into metal-organic frameworks derived N-doped porous carbon polyhedrons as cathode for Na-Se batteries. ACS Appl Mater Interfaces 9:41339–41346. https://doi.org/10.1021/acsami.7b14380
126. Xu Q, Liu H, Du W, Zhan R, Hu L, Bao S, Dai C, Liu F, Xu M (2018) Metal-organic complex derived hierarchical porous carbon as host matrix for rechargeable Na-Se batteries. Electrochim Acta 276:21–27. https://doi.org/10.1016/j.electacta.2018.04.164
127. Dong W, Chen H, Xia F, Yu W, Song J, Wu S, Deng Z, Hu Z-Y, Hasan T, Li Y, Wang H, Chen L, Su B-L (2018) Selenium clusters in Zn-glutamate MOF derived nitrogen-doped hierarchically radial-structured microporous carbon for advanced rechargeable Na-Se batteries. J Mater Chem A 6:22790–22797. https://doi.org/10.1039/c8ta07662f
128. Li S, Yang H, Xu R, Jiang Y, Gong Y, Gu L, Yu Y (2018) Selenium embedded in MOF-derived N-doped microporous carbon polyhedrons as a high performance cathode for sodium-selenium batteries. Mater Chem Front 2:1574–1582. https://doi.org/10.1039/c8qm00177d
129. Wu Y, Qiu X, Liang F, Zhang Q, Koo A, Dai Y, Lei Y, Sun X (2019) A metal-organic framework-derived bifunctional catalyst for hybrid sodium-air batteries. Appl Catal B Environ 241:407–414. https://doi.org/10.1016/j.apcatb.2018.09.063
130. Agarwal S, Yu X, Manthiram A (2020) A pair of metal organic framework (MOF)-derived oxygen reduction reaction (ORR) and oxygen evolution reaction (OER) catalysts for zinc-air batteries. Mater Today Energy 16:100405. https://doi.org/10.1016/j.mtener.2020.100405
131. Niu W, Yang Y (2018) Amorphous MOF introduced N-Doped graphene: an efficient and versatile electrocatalyst for zinc-air battery and water splitting. ACS Appl Energy Mater 1:2440–2445. https://doi.org/10.1021/acsaem.8b00594
132. Baek K, Jeon WC, Woo S, Kim JC, Lee JG, An K, Kwak SK, Kang SJ (2020) Synergistic effect of quinary molten salts and ruthenium catalyst for high-power-density lithium-carbon dioxide cell. Nat Commun 11:456. https://doi.org/10.1038/s41467-019-14121-1
133. Li S, Dong Y, Zhou J, Liu Y, Wang J, Gao X, Han Y, Qi P, Wang B (2018) Carbon dioxide in the cage: manganese metal-organic frameworks for high performance CO_2 electrodes in Li-CO_2 batteries. Energy Environ Sci 11:1318–1325. https://doi.org/10.1039/c8ee00415c
134. Li S, Liu Y, Zhou J, Hong S, Dong Y, Wang J, Gao X, Qi P, Han Y, Wang B (2019) Monodispersed MnO nanoparticles in graphene-an interconnected N-doped 3D carbon framework as a highly efficient gas cathode in Li-CO_2 batteries. Energy Environ Sci 12:1046–1054. https://doi.org/10.1039/c8ee03283a
135. Pan H, Li B, Mei D, Nie Z, Shao Y, Li G, Li XS, Han KS, Mueller KT, Sprenkle V, Liu J (2017) Controlling solid-liquid conversion reactions for a highly reversible aqueous zinc-iodine battery. ACS Energy Lett 2:2674–2680. https://doi.org/10.1021/acsenergylett.7b00851

136. Yang H, Qiao Y, Chang Z, Deng H, He P, Zhou H (2020) A metal-organic framework as a multifunctional ionic sieve membrane for long-life aqueous zinc-iodide batteries. Adv Mater 32:2004240. https://doi.org/10.1002/adma.202004240
137. Wang F, Liu Z, Yang C, Zhong H, Nam G, Zhang P, Dong R, Wu Y, Cho J, Zhang J, Feng X (2020) Fully conjugated phthalocyanine copper metal-organic frameworks for sodium-iodine batteries with long-time-cycling durability. Adv Mater 32. https://doi.org/10.1002/adma.201905361
138. Jian QP, Wu MC, Jiang HR, Lin YK, Zhao TS (2021) A trifunctional electrolyte for high-performance zinc-iodine flow batteries. J Power Sources 484. https://doi.org/10.1016/j.jpowsour.2020.229238
139. Li B, Liu J, Nie Z, Wang W, Reed D, Liu J, McGrail P, Sprenkle V (2016) Metal-organic frameworks as highly active electrocatalysts for high-energy density, aqueous zinc-polyiodide redox flow batteries. Nano Lett 16:4335–4340. https://doi.org/10.1021/acs.nanolett.6b01426
140. Deng H, Chang Z, Qiu F, Qiao Y, Yang H, He P, Zhou H (2020) A safe organic oxygen battery built with li-based liquid anode and MOFs separator. Adv Energy Mater 10:1903953. https://doi.org/10.1002/aenm.201903953
141. Chong L, Wen J, Kubal J, Sen FG, Zou J, Greeley J, Chan M, Barkholtz H, Ding W, Liu D-J (2018) Ultralow-loading platinum-cobalt fuel cell catalysts derived from imidazolate frameworks. Science 362:1276–1281. https://doi.org/10.1126/science.aau0630
142. Cheng W, Zhao X, Su H, Tang F, Che W, Zhang H, Liu Q (2019) Lattice-strained metal-organic-framework arrays for bifunctional oxygen electrocatalysis. Nat Energy 4:115–122. https://doi.org/10.1038/s41560-018-0308-8

Chapter 4
Supercapacitors

Jianan Zhang, Xiaoyu Zhang, Dongping Xue, Huicong Xia, and Su Jiang

4.1 Introduction

With the rapid development of modern economy, coal, oil, diesel, and other non-renewable energy resources are increasingly in short supply. At the same time, the use of these energies causes PM2.5, haze, greenhouse effect, and other environmental problems. To solve these urgent environmental problems, the development of renewable and clean energy has become a feasible way [1–5]. Electrochemical energy storage systems, such as fuel cells, supercapacitors (SCs), and second-generation lithium batteries, show great promise in harnessing new energy sources such as solar and wind power. Therefore, the research of electrochemical energy conversion and storage system is urgent [6–8]. Among them, SCs has good cycle stability, high power density, and good electrochemical reversibility, so it has great application potential in portable electronic products, standby power storage, electric vehicles and so on [9–13]. SCs have been widely used in the national economy, science and technology, and daily life. It has an important impact on alleviating energy and environmental crisis and improving people's living standards. What's more, it has become a new field of research and public attention [14–23]. Since the performance of SCs is mainly determined by its electrode materials, the research of high-performance materials has already been the focus of attention in this field.

J. Zhang (✉) · X. Zhang · D. Xue · H. Xia · S. Jiang
College of Materials Science and Engineering, Zhengzhou University, Zhengzhou 450001, P. R. China
e-mail: zjn@zzu.edu.cn

X. Zhang
e-mail: zhangxiaoyu0321@163.com

D. Xue
e-mail: xdongping1231@126.com

S. Jiang
e-mail: jiangszzu@163.com

H. Pang (ed.), *Nano/Micro Metal-Organic Frameworks*,
https://doi.org/10.1007/978-981-16-4071-1_4

Metal–organic frameworks (MOFs) are a new kind of porous crystalline materials constructed in three-dimensional (3D) space with metal ions/clusters and organic bridging ligands as ligands [24]. Over the past few years, MOFs have attracted a lot of attention and are now one of the most rapidly growing areas of research. To date, there are more than 20,000 MOFs with different compositions, crystal structures, and morphologies been reported [25]. MOFs have great potential in SCs due to their customizable structure and function, high porosity, and large internal surface area. In this section, original MOF and MOF-derived materials are mainly discussed as electrode materials for SCs.

4.2 Pristine MOF for Supercapacitors

The use of pristine MOF materials as electrodes for supercapacitor (SC) has been the subject of much attention due to their great surface area and intrinsic redox properties. In this context, many metal ions such as Ni, Fe, Co, Mn, Cu, Zn, Ce, V, Cr, Al, Zr, and organic linkers like big families of terephthalic acids, imidazolates, and carboxylic acids, various types of bipyridine, benzoic acids, and phenylene have been employed in the production of pure MOFs for such application. Common good organic linkers are 1,4-benzenedicarboxylic acid (1,4-H_2bdc), 2-methylimidazole, 2,3,6,7,10,11-hexahydroxytriphenylene (HHTP), etc., as shown in Fig. 4.1. Worthwhile mentioning, that most of these kinds of ligands show weak

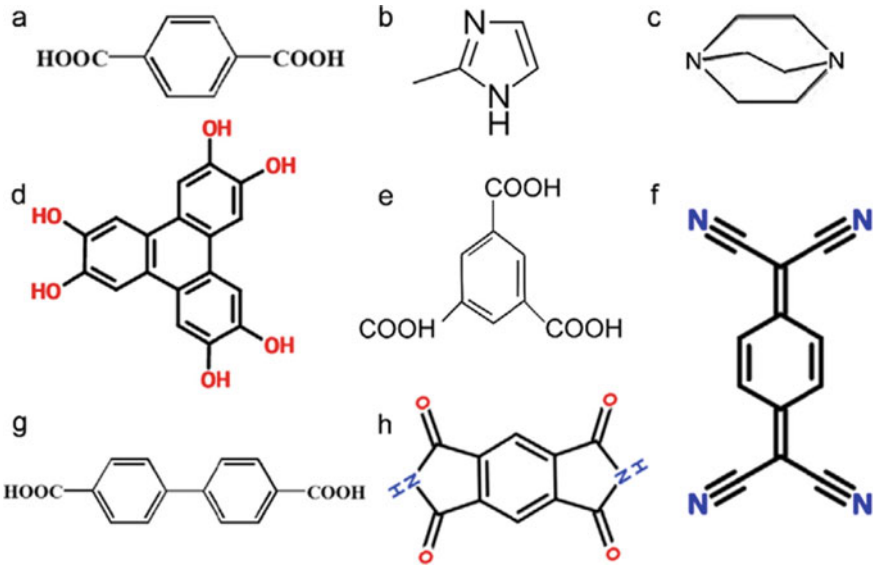

Fig. 4.1 Schematic representation of 1,4-H_2bdc (**a**), $C_4H_6N_2$ (**b**), $C_6H_{12}N_2$ (**c**), $C_{18}H_{12}O_6$ (**d**), H_3BTC (**e**), $C_{12}H_4N_4$ (**f**), 4,4'-H_2bpc (**g**) and $C_{10}H_4O_4N_2$ (**h**)

electron-withdrawing property which leads to act as a redox center. However, the direct application of MOFs as SC electrode materials is mainly faced with poor conductivity and mechanical/chemical stability. Besides, short cycle life at higher rates due to the increase in resistance and inadequate faradaic redox reactions at higher current densities as well as low electrode surface area, resulting in a small contact area between the electrolyte and the electrode material. In SCs, the use of MOFs has only been widely reported by researchers in recent years.

Early trials to use pristine MOFs as electrode materials for SCs have been reported via Díaz and co-workers [26]. Co_8-MOF-5 was selected to be combined with polytetrafluoroethylene and carbon black to construct electrode. Result exhibited a very low capacitance value of 0.3 F g^{-1}, which might be restricted via specific MOF and electrolyte. Meanwhile, Lee et al. explored Co-MOF as a promising material for SCs and opened the door to further research various MOFs as an electrode material [27]. The Co-MOF as electrode materials demonstrated capacitance of 206.76 F g^{-1} and good pseudocapacitor behavior (7.18 Wh kg^{-1}). In addition, three similar carboxylic acids with different molecular lengths were utilized as organic ligands to synthesize different morphology and pore sizes of Co-MOFs have been reported by Lee and co-workers [28]. Among the three Co-MOFs, the longer linkers have larger surface areas and larger pores. According to the surface area and pore diameter, the specific capacitance, power density, and energy density of the three Co-MOFs electrodes were detected to be ranging from 131.8 to 179.2 F g^{-1}; from 3.88 to 5.64 kW kg^{-1}; and from 20.7 to 31.4 Wh kg^{-1}, respectively. To achieve electrode materials with higher capacitance for SCs from two-dimensional (2D) layered MOFs, Liu and co-workers reported the syntheses of a 2D Co-MOF (Co-LMOF, $\{[Co(Hmt)(tfbdc)(H_2O)_2]\cdot(H_2O)_2\}_n$; $H_2tfbdc = 2,3,5,6$-tetrafluoroterephthalic acid; Hmt = hexamethylenetetramine) and its electrochemical performances as the electrode materials of SCs and found that Co-LMOF showed considerably high specific capacitance (1978 F g^{-1}) and can also retain 94.3% of the original capacitance over 2000 cycles [29]. Meanwhile, another Co-MOF material with conductive networks frames and a layer structure was synthesized via Wei and co-workers [30]. This material delivered a remarkable capacitance of 2564 F g^{-1} and can keep at 95.8% after 3000 cycles. In addition, Zheng et al. prepared ultra-thin 2D Co-MOF nanosheets and detected its supercapacitive behaviors [31]. Result showed and it achieved 1159 F g^{-1}, which might originate from the short ion diffusion length. Abazari et al. reported a novel Co-based MOF, (NH_2-TMU-53, $[Co(2\text{-}ATA)_2(4\text{-}bpdb)_4]_n$; 2-ATA = 2-aminoter ephthalic acid, 4-bpdb = N,N-bis-pyridin-4-ylmethylene-hydra zine) and evaluated its supercapacitive performance. It presented an upper capacitance, as well as good cycling stability (92.03% after 6000 cycles). When assembled asymmetric supercapacitor (ASC) device from NH_2-TMU-53 and AC, it delivered the high power and energy density [32].

As mentioned above, Co-based MOF can be applied in SCs as electrode materials. For SCs, Ni-MOFs as supercapacitive electrode materials are also very common. Liao et al. successfully prepared a series of Ni-MOF for electrochemical SCs by mixing isonicotinic acid and nickel nitrate in N, N-dimethylformamide (DMF) at 140°C for 96 h in a high-pressure tank [33]. Electrochemical test results showed

good capacitance performance (634 F g^{-1} at 5 mV s^{-1}) and cycle stability (84% for 2000 cycles). Kang and colleagues studied a novel pseudocapacitor material Ni-MOF, $Ni_3(BTc)_2{\cdot}12H_2O$ [34]. The experimental results show that Ni-MOF has excellent performance of 726 F^{-1} pseudocapacity and excellent cycling stability. However, Yang and colleagues obtained layered nanostructured Ni-MOF by mixing terephthalic acid (PTA) and nickel chloride in DMF at 120 °C for different times [35]. The material exhibits high capacitance at 0.5 A g^{-1} (1127 F g^{-1}) and cycle stability (90% after 3000 cycles). This excellent electrochemical performance is due to the inherent properties of Ni-MOF, such as preferred exposure surfaces and layered structures. Qu and co-workers successfully prepared novel, nickel-based, pillared MOFs of similar topology using 9,10-anthracenedicarboxylic acid (ADC), 2,3,5,6-tetramethyl-1,4-benzenedicarboxylic acid (TM), 1,4-naphthalene-dicarboxylic acid (NDC) as carboxylate ligands, and 1,4-diazabicyclo[2.2.2]-octane (DABCO) as pillar ligands [36]. As the electrode material of SCs, DMOF capacitor shows excellent electrochemical performance. Compare with the other two, Ni-DMOF-ADC had better cycling stability (98% after 16,000 cycles). Sheberla et al. reported $Ni_3(HiTP)_2$ (Ni_3(2,3,6,7,10,11-hexaamine triphenyl)$_2$) with high conductivity as the sole electrode material for double-layer electrical capacitors (EDLCs) [37]. As shown in Fig. 4.2h, $Ni_3(HITP)_2$ is composed of stacked π-conjugated two-dimensional layers, which are penetrated by one-dimensional cylindrical channel with a diameter of about 1.5 nm. The surface area normalized capacitance of $Ni_3(HITP)_2$ is up to about 18 μF cm^{-2}, which is higher than that of other carbon materials except porous graphene (Fig. 4.2j). As shown in Fig. 4.2i, the $Ni_3(HiTP)_2$ electrode shows high reliability in 10,000 cycles with a capacitance retention rate greater than 90%. Therefore, highly conductive porous MOF ($Ni_3(HiTP)_2$) is a promising active electrode material for EDLC. In addition to the above results, other Ni-MOFs used as SCS electrode materials have also been reported [38, 39].

Apart from Co- and Ni-based MOFs, other MOFs utilized in SCs have also been reported. Three Fe-based MOFs (MIL-88(Fe), MIL-53(Fe), and MIL-100(Fe)) synthesized by campagnol and co-workers was used as electrode materials for SCs [40]. They showed the effects of pellet thickness, pore size, and cations of different sizes on performance. Experimental results display that MIL-100 (Fe) has better performance than that of a combination of carbon and nanotubes in the same solution. However, the dissolution of the reduction process strongly limits the cycle stability of the electrode.

In addition, Choi et al. constructed a coin-type supercapacitor (SC) device based on nMOFs electrodes [41]. A series of 23 MOF compounds were successfully synthesized and examined with various organic ligands and central metal ions, including MOF-74 structures (multi-metallic metal oxide mixing units and 1D pores), zirconium (IV) MOF of different lengths and shapes of links and nanocrystalline sizes, MOF-5 structures (with multiple mixing functions and three-dimensional pores) and MOF containing metal units of different nucleity. In particular, a zirconium based MOF (nMOF-867, $Zr_6O_4(OH)_4$(2,2'-bipyridine-5,5'-dicarboxylate)$_6$) exhibited abnormally high volume and area-specific capacitances (0.64 F $cm_{stack}{}^{-3}$ and 5.09 mF $cm_{areal}{}^{-2}$) and its performance can also maintain at least 10,000 cycles

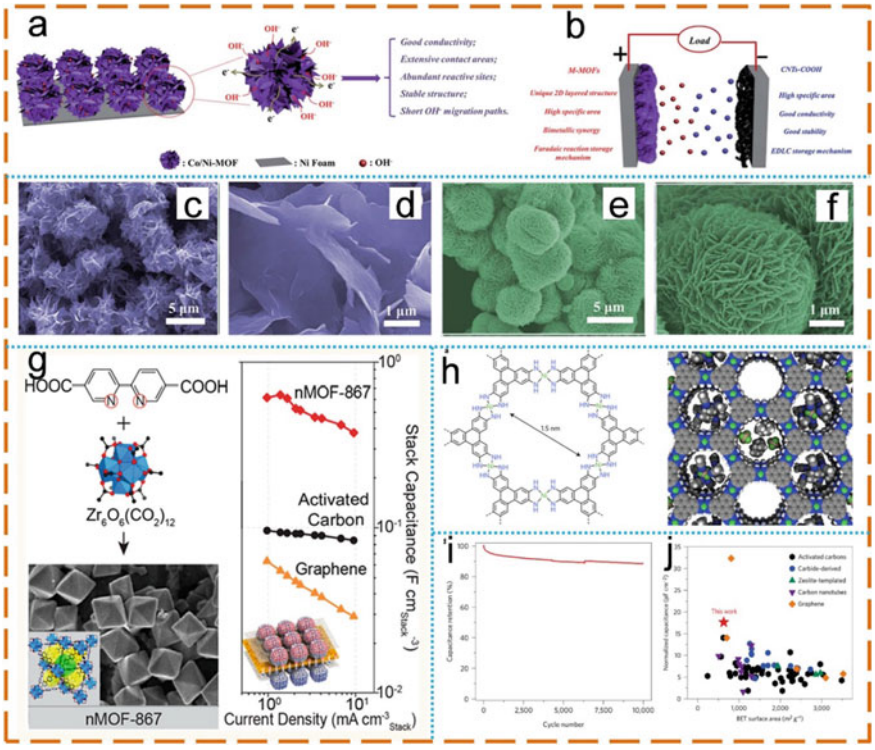

Fig. 4.2 **a** Schematic diagram of ion and charge transfer in the Co/Ni-MOF electrode. **b** An abstract illustration of hybrid supercapacitors. **c, d** SEM images of the as-synthesized Co/Ni-MOF and **e,f** Zn/Ni-MOF. **g** Structure of MOF-867 and the construction and performance of the nMOF SCs. **h** Structural schematics of $Ni_3(HITP)_2$. **i** Capacitance retention under repeated cycling at 2 A g^{-1} for 10,000 cycle. **j** Comparison of areal capacitances among various EDLC materials. **a–f** Reprinted with permission from Ref. [42]. Copyright 2016, The Royal Society of Chemistry. **g** Reprinted with permission from Ref. [41]. Copyright 2014, American Chemical Society. **h–j** Reprinted with permission from Ref. [37]. Copyright 2016, Nature

(Fig. 4.2g). In order to improve the electrical conductivity of MOFs, Jiao et al. successfully obtained mixed MOFs (M-MOFs) by partially replacing Ni^{2+} in Ni-MOF with Co^{2+} or Zn^{2+} [42]. According to the SEM images of Co/Ni-MOF and Zn/Ni-MOF (Fig. 4.2c-f), it can be clearly observed that Co/Ni-MOF flower-like structures are composed of many nanosheets (average thickness of 30 nm) and the morphology of Zn/Ni-MOF is similar to that of Co/Ni-MOF. As a battery-type electrode material, M-MOFs have a unique two-dimensional layered structure (Fig. 4.2b), which can provide enough space for OH^- insertion and disinsertion (Faraday Reaction). This special hybrid SC combines the advantages of capacitive and Faraday reactions to improve the power density and energy density. Compared with Ni-MOF, 2D M-MOF shows excellent electrochemical performance. M-MOF has excellent electrochemical properties for the following reasons. First, as shown in Fig. 4.2a, the

flower-like M-MOF structure, as the conduction pathway and backbone, provides a strong support for the structural integrity and efficient charge transfer of the faraday reaction. In addition to broadening the application of MOFs, their research could open up new ways to bridge the performance gap between batteries and SCs.

4.3 MOF-Derived Materials for Supercapacitors

In recent years, in addition to directly use pure MOFs, more and more researchers have used MOFs as a sacrificial template to prepare highly controllable nanostructured materials and apply them to electrochemistry [24]. Some recent reports have shown that pure MOF has problems such as low conductivity, poor electrolyte ion transport performance, and low conversion efficiency, which limit its application in energy storage. Compared with pure MOFs materials, MOF-derived materials have superiority in electrochemical energy storage. MOF is a highly porous crystalline material that can be transformed into the desired product through a one-step calcination process, which promotes the fact that MOF is used for the development of nanostructured materials, which enhances their practical applications on pilot and industrial scales. Due to these advantages, MOF materials have been successfully used to develop porous carbon, metal compounds, and composite materials (M/MO@C) [43]. In this section, the application of MOF-derived materials in supercapacitors is reviewed.

4.3.1 MOF-Derived Porous Carbon Materials for Supercapacitors

As a common electrode material, carbon materials have the characteristics of high electrical conductivity, low thermal expansion coefficient, and low density, and have been widely used in the field of electrochemical energy storage. However, the storage capacity of conventional carbon materials is small, so it is difficult to increase power density and energy density. Recently, the preparation of carbon materials with microporous, mesoporous, and macroporous structures using MOF precursors as templates has attracted widespread attention. This is mainly because the preparation of porous carbon materials largely maintains the specific surface area of the precursor MOF. The uniform distribution of the pore size of the carbon material and the effective contact of the electrolyte help it improve the electrochemical performance of the supercapacitor.

Without adding any other precursors, the porous carbon material obtained by directly carbonizing the MOF will have excellent electrochemical performance when used in supercapacitors.

Three-dimensional porous carbon materials are favored by many scientific researchers due to their simple preparation process. Amali et al. used the ultrasonic method to prepare the microporous framework ZIF-8, and assembled the microporous particles into medium/large pores as the secondary structure [44]. After simple carbonization, ZIF-8 forms a three-dimensional layered porous carbon framework with micropores, mesopores, and macropores, and has excellent supercapacitor electrode performance (Fig. 4.3a–c). Similarly, Torad et al. used cobalt-containing zeolite imidazole framework 67 (ZIF-67) to directly carbonize highly graphitized three-dimensional NPCs [45]. Their NPCs have high specific surface area, large pore volume, and inherent electrical conductivity. It is expected to become a high-efficiency electrode for high-performance supercapacitors. Compared with the previous carbon-based double-layer capacitors, the maximum specific capacitance obtained by using this NPC as the electrode material of the supercapacitor is very high. Salunkhe et al. designed a new type of symmetrical supercapacitor based on NPC by directly carbonizing zinc-based MOF without controlling the reaction conditions to synthesize two NPCs with different particle sizes [46]. The results show that the NPC material has excellent electrochemical properties, and the maximum specific capacitance in 1 M H_2SO_4 electrolyte is 251 $F{\cdot}g^{-1}$. Research shows that these high-efficiency electrodes have good capacitance, high stability, and good rate capability. As the electrode material of supercapacitors, carbon derived from Al-PCP has ideal capacitor performance. Porous carbon polyhedron and other materials are used as different electrodes to synthesize supercapacitors to obtain better electrochemical performance. Yi et al. constructed an asymmetric supercapacitor based on the core–shell structure of porous carbon materials derived from MOF and CNT@NiO composite materials [47]. The main component of the anode material is polyhedral porous carbon obtained by carbonizing ZIF-8 at a high temperature of 1000 °C. This kind of porous carbon has uniform pore size, no large defects on the surface, and large specific surface area (1980 $m^2\ g^{-1}$), which is very helpful

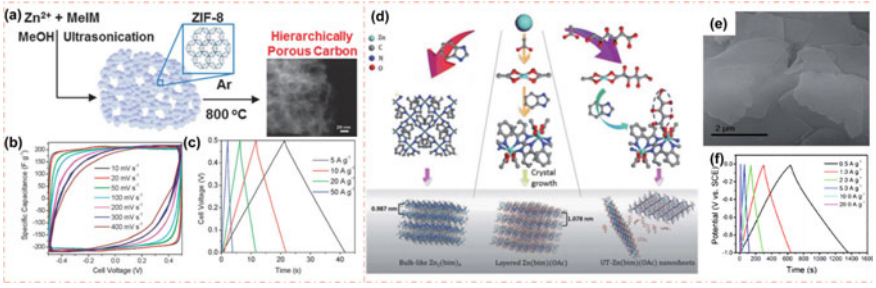

Fig. 4.3 **a** Schematic illustration for the preparation of hierarchically porous carbon from an assembly of ZIF-8 particles. **b** Cyclic voltammograms at different sweep rates of AS-ZC-800 for an electrochemical capacitor in 1.0 M H_2SO_4 electrolyte. **c** galvano static charge–discharge curves at high current densities. **d** Schematic illustrations of the synthesis of $Zn_2(bim)_4$, Zn(bim)(OAc), and UT-Zn(bim)(OAc). **e** SEM image of the UT-Zn(bim)(OAc) nanosheets. **f** Galvanostatic charge–discharge profiles of the UT-CNS electrode at different current densities

to improve the energy storage performance of combined supercapacitors. The electrochemical test results show that at a certain current density, the electrode made of porous carbon has a high specific capacitance. The charge and discharge test of asymmetric supercapacitors of CNT@NiO composite and porous carbon showed that the power density and energy density are both high within a certain voltage range. In addition, asymmetric supercapacitors also have excellent cycle stability. This is due to the synergy between porous carbon and CNT@NiO, which makes asymmetric supercapacitors have high energy density and power density as well as good cycle stability. In addition to pure porous carbon, N-doped porous carbon also has excellent performance when applied to electrode materials of supercapacitors. N doping not only introduces pseudocapacitance, but also improves surface wettability, making it easier for electrolyte ions to enter the electrode material, thereby increasing capacitance. Too much N will cause the conductivity to decrease, so it is necessary to explore a suitable synthesis method to control the nitrogen content within a reasonable range. Nune et al. used N-containing isoreticular metal–organic framework (IRMOF-3) as a template to prepare a series of N-doped carbon materials with different structures, and by adjusting the carbonization temperature, the nitrogen content and porosity can be changed [48]. For a carbonization temperature of 950 °C, N-doped porous carbon has an extremely high capacitance of 239 $F{\cdot}g^{-1}$. In contrast, similar N-free carbons have a low capacitance of 24 $F{\cdot}g^{-1}$, which indicates the importance of nitrogen dopants in the charge storage process. Since it is easy to produce small amounts of N-doped porous carbon, this route can be extended. N-doped carbon materials synthesized from MOF-8 have low electrical conductivity due to their high nitrogen content. Due to graphitization, the nitrogen content and specific surface area of porous carbon prepared by ZIF-67 are reduced. On this basis, Yamauchi et al. used a seed method to grow ZIF-67 on the surface of ZIF-8 to prepare ZIF-8@ZIF-67 core–shell composites, and then heat-treated them in flowing nitrogen to obtain N-doped carbon (NC) is the core of carbon nanotubes, graphitic carbon (GC) is the shell, and nanopore NC@GC composites have a core–shell structure [49]. The research results show that the specific surface area of the obtained composite carbon material is 127 m^2g^{-1}, the nitrogen content is moderate, and the pore structure distribution ranges from micropores to mesopores. At the same time, NC@GC electrode has excellent electrochemical performance. When tested at a higher current density of 2 $A{\cdot}g^{-1}$, the capacitance value is as high as 270 $F{\cdot}g^{-1}$, which is due to the synergy of NC's high nitrogen content and highly graphitized GC. The researchers also found that gaps of different sizes in carbon materials can be connected to each other, resulting in a relatively large specific surface area, which can promote the transport of electrolyte ions.

However, the three-dimensional porous carbon material has a small specific surface area and low pore utilization rate, which easily causes slow electrochemical capacitors and electrochemical catalytic reaction kinetics and poor long-term stability, which limits its application in the field of electrochemical energy storage. In contrast, two-dimensional porous carbon materials have the advantages of ultrathin morphology, large specific surface area, high aspect ratio, continuous layering,

etc., so they have better electrochemical performance when applied to supercapacitors. Yan et al. directly carbonized Al-PCP to obtain a two-dimensional porous carbon material with a higher BET surface area [50]. Similarly, nitrogen doping can also be used to change the electrochemical properties of two-dimensional porous carbon materials. Zhao et al. reported a low-cost, bottom-up synthesis of ultra-thin Zn(bim)(OAc) MOF nanosheets and their derived N-doped porous ultra-thin (2.5–0.8 nm) carbon nanosheets (UT-CNS) synthesis method, and applied it to supercapacitors, to study it [51]. The capacitance of UT-CNS at high current density is higher than that of most of the reported electrode carbon materials of MOF supercapacitors (Fig. 4.3d–f).

Sometimes, porous carbon materials obtained by indirect carbonization can also obtain better performance. In the indirect carbonization process, first, an external carbon source (such as furan alcohol, ethylenediamine, tetraethyl chloride, and phenolic resin) is penetrated into the pores of the MOF by impregnation or gas phase methods and then carbonized in an inert atmosphere. Zhang et al. prepared a series of ZIF-derived porous carbon materials by co-carbonizing ZIF-7 with carbon sources such as glucose, ethylene glycol, glycerol, and furfuryl alcohol [52]. The results show that the ZIF-7/glucose composite carbon L-950 as an electrode for electrochemical capacitors exhibits ultra-high specific capacitance under alkaline conditions and has good stability. In addition, no conductive agent (such as acetylene black) is needed in the preparation process of the working electrode, which not only reduces the preparation cost, but also benefits the stability and performance. Jiang et al. used zeolite-like metal–organic framework as the precursor and template, and furfuryl alcohol as the precursor to prepare porous carbon materials with very high surface area (3405 $m^2 \cdot g^{-1}$, BET method) for electric double-layer capacitors [53]. The electrode material has high hydrogen storage capacity (2.77% by weight at 77 K and 1 atm) and good electrochemical performance.

In contrast, because the use of MOF as a template and carbon source for direct carbonization does not require an additional carbon source, but only involves a simple calcination step, and the carbon content in MOF is higher, so it is simpler and more practical in industrial-scale preparation.

The above research shows that MOF is an excellent template for preparing porous carbon materials. Due to its ultra-thin morphology and large specific surface area, the two-dimensional structure of carbon materials can obtain excellent electrochemical performance when applied to electrode materials of supercapacitors. The conductivity of the electrode material will affect the capacitance, and the balance between porosity and graphitization is also an important factor affecting electrochemical performance. In addition, additives, carbonization temperature, and treatment methods all affect the porosity or conductivity of the carbon material. In addition, in the process of synthesizing MOF, introducing heteroatoms or other templates on the ligand is also a way to increase the capacitance of the capacitor. This method can effectively improve the surface wettability of carbon materials while providing additional redox reaction centers.

4.3.2 MOF-Derived Metal Compounds Materials for Supercapacitors

Metal compounds store energy in the form of Faraday pseudocapacitors. At present, the metal compounds used in the field of supercapacitors mainly include metal oxides/hydroxides, metal sulfides, etc [54].

Metal oxides have attracted extensive attention from researchers due to their rich reserves, controllable morphology, reversible redox reaction, and higher theoretical specific capacitance. Among many metal oxides, Co_3O_4 electrode materials are considered to be ideal pseudocapacitance materials due to their excellent electrical conductivity, good chemical stability, and high specific capacitance.

Meng et al. used cobalt-based metal organic framework (Co-MOF) crystals to prepare porous Co_3O_4 materials through a solid phase conversion process (Fig. 4.4a) [55]. The results show that the prepared Co_3O_4 has crystallinity and clear porous properties (Fig. 4.4b). The electrochemical results showed that the porous Co_3O_4 particles exhibited a high specific capacitance of 150 $F{\cdot}g^{-1}$ at a current density of 1 $A{\cdot}g^{-1}$, and maintained a slightly higher capacitance after 3400 cycles, which can be attributed to Due to higher specific surface area and accessible channel structure characteristics (Fig. 4.4c–d). Therefore, the method is simple, controllable, and repeatable. Importantly, this specific solid-state thermal conversion strategy can be easily extended to prepare other porous metals and/or metal oxide nanomaterials with specific surface textures and morphologies. In addition to the solid-state conversion strategy, Co_3O_4 nanostructures can also be prepared by directly calcining the MOF precursor. Pang et al. synthesized dendritic Co_3O_4 nanostructures by calcining Co-8-hydroxyquinoline coordination structure [56]. As an electrode material for supercapacitors, they found that the nanostructured Co_3O_4 electrode has high specific capacitance and long cycle life. By adjusting the reaction conditions, porous carbon materials, and Co_3O_4 nanostructures can be synthesized simultaneously. Salunkhe et al. used ZIF-67 as a precursor to calcinate porous C and Co_3O_4 under different temperature conditions [57]. The characterization of structure and morphology showed that the porous carbon prepared by derivatization has a large specific surface area (350 m^2 g^{-1}); at the same time, the derivative Co_3O_4 has high purity without obvious carbon impurities, and the specific surface area can reach 148m^2 g^{-1}. The electrochemical performance test results of the electrodes composed of these two derivatives show that the specific capacitances of porous C and porous Co_3O_4 are 272 $F{\cdot}g^{-1}$ and 504 $F{\cdot}g^{-1}$, respectively, at a scanning speed of 5 $mV{\cdot}s^{-1}$. They further constructed an asymmetric supercapacitor based on two electrodes, and the asymmetric supercapacitor showed a higher energy density (15 $Wh{\cdot}kg^{-1}$) and power density (8000 $W{\cdot}kg^{-1}$). Moreover, after 2,000 charge–discharge cycle tests, asymmetric supercapacitors can still maintain high stability. On the one hand, the reason is that the porous Co_3O_4 has a larger porosity, which provides a better channel for ion transfer, so that the electrolyte can completely contact the electrode material. On the other hand, the good conductivity of porous carbon effectively improves the charge transfer speed of asymmetric supercapacitors.

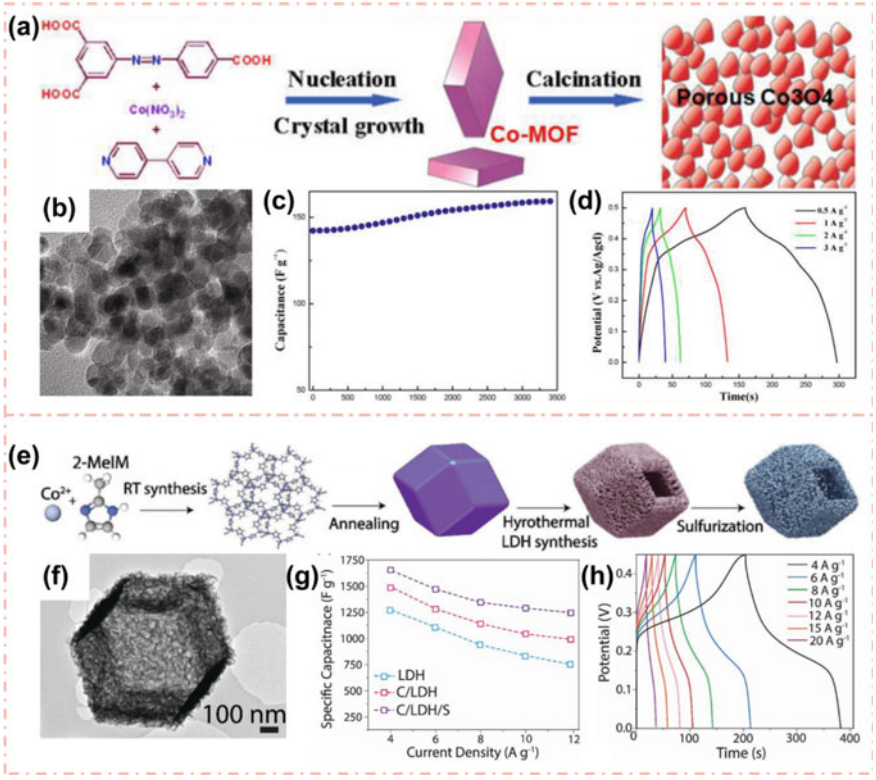

Fig. 4.4 **a** Schematic illustration of the formation process for porous Co_3O_4 aggregates. **b** HRTEM image of porous Co_3O_4 material. **c** Average specific capacitance versus cycle number of porous Co_3O_4 electrode at a galvanostatic charge/discharge current density 1 A g^{-1}. **d** Galvanostatic charge/discharge curves of porous Co_3O_4 electrode material at various charge/discharge current densities of 0.5, 1, 2, and 3 A g^{-1}, respectively, the potential window was ranged from 0 to 0.5 V. **e** Schematic illustration for the synthesis process of hollow NiCo-LDH/Co_9S_8 hybrid. **f** TEM images of C/LDH/S. **g** Specific capacitances as a function of current density. **h** charge–discharge profiles at various current densities for C/LDH/S

In addition to Co_3O_4, other metal oxides can also be applied to supercapacitors. For example, the use of manganese oxide as a supercapacitor electrode material can obtain good electrochemical performance. Maiti et al. reported that 1,3,5-benzoic acid manganese metal–organic framework (Mn-BTCMOF) formed a well-crystallized Mn_2O_3 mesoporous nanomaterial through simple heat treatment [58]. When tested as a pseudocapacitor electrode in a three-electrode configuration, a specific capacitance of 250 F·g^{-1} can be obtained at 0.2 A·g^{-1}. In addition, in order to prove its practicality, a two-electrode asymmetric supercapacitor pouch battery was assembled. It uses Mn_2O_3 as the positive electrode and commercially available activated carbon as the negative electrode. In the case of a power density of 1004 Wh·kg^{-1}, it shows an ultra-high energy of 147.4 Wh·kg^{-1}. The current work shows

the potential of the MOF-derived route, which can be used to obtain metal oxides with nanostructures required for high-performance electrochemical applications. In addition, cesium oxide has also been used in supercapacitor materials with similar good results. Maiti et al. reported the use of [Ce(1,3,5-BTC)(H_2O)$_6$] (1,3,5-BTC = 1,3,5 phenyl tricarboxylate) MOF as the sacrificial template [59]. This method is simple and convenient to synthesize CeO_2. At 0.2 A·g^{-1}, the pseudocapacitance of CeO_2 produced by MOF is 1204 F·g^{-1}, which far exceeds its theoretical capacitance (560 F·g^{-1}). This study shows that controllable nanostructures can potentially alleviate the low energy density and capacitance attenuation problems that plague current metal oxide electrostatic precipitators.

In recent years, metal sulfides have played an important role in energy storage fields such as solar cells, lithium-ion batteries, and supercapacitors. Compared with metal oxides and hydroxides, sulfides have lower electronegativity, rich redox reactions, and higher electrochemical activity. Recent studies have found that the MOF-derived metal sulfide nanostructure has a high specific surface area and a large number of pores, which is very helpful to improve the capacitance performance of supercapacitors.

Le et al. used MOF as a sacrificial template to prepare a layered core–shell hollow iron cobalt sulfide-cobalt sulfide nanoarray, which was supported on conductive nickel foam (Fe-Co-S/NF) (Fig. 4.4e) [60]. The etching/ion exchange reaction between Co-MOF and $FeSO_4$ and subsequent solvothermal vulcanization resulted in the formation of layered core–shell hollow nanostructures, in which $FeCo_2S_4$-nanosheets and shells were assembled on Co_3O_4 hollow nanoarrays (Fig. 4.4f). Due to its complex composition and unique structure, Fe-Co-S/NF has rich electroactive potential, shorter charge/ion diffusion path, rich redox reaction, and good structural robustness, which help to improve the super Electrochemical performance of capacitor electrodes. Therefore, the obtained Fe-Co-S/NF electrode has a specific capacitance of 2695 F·g^{-1} at 1 A·g^{-1}, and a capacitance retention rate of 69.8% at 10 A·g^{-1}. 84% of the life is maintained in 84 cycles. In addition, Fe-Co-S/NF and rGO were used as cathode and anode respectively to assemble asymmetric supercapacitors. The obtained equipment provides a high energy density of 43.6 Wh·kg^{-1} at a power density of 770 W·kg^{-1}, while still maintaining a capacity retention rate of 89.6% after 5000 cycles (Fig. 4.4g–h). The strong electrochemical performance shows that Fe-Co-S/NF can be used as a promising electrode material in high-performance supercapacitor applications. Yilmaz et al. reported the in-situ quasi-crystal transformation of the hollow rhombohedral dodecahedron template derived from MOF and the interlayer metal sulfide (NiCo-LDH/NiCo-LDH/ Co_9S_8) system construction [61]. The intergranular metal sulfide (Co_9S_8) in LDH provides the best interface for mixed components and material stability. The NiCo-LDH/Co_9S_8 hybrid system together provides an ideal porous structure, rich redox chemicals, and high conductivity matrix. This leads to a significant improvement in its complementary electrocatalytic hydrogen release and supercapacitor energy storage performance. This work established the potential of MOF-derived SC scaffolds in the design of new hybrid inorganic-inorganic functional materials for electrochemical applications and other fields.

These outstanding research results all show that MOF can be used as a template for preparing metal compounds, and these metal compounds have good electrochemical performance when used in supercapacitor electrodes. In order to make the actual capacitance as close to the theoretical capacitance as possible in the application process, the surface area of the MOF should be as large as possible. Therefore, metal compounds derived from MOF have become popular materials due to their suitable ion transport channels and large contact area.

4.3.3 MOF-Derived Metal Metal/metal Compounds and Carbon Materials for Supercapacitors

Different types of electrode materials have different characteristics. Carbon-based materials have good electrical conductivity, but their specific capacitance is relatively small. Metals and their compounds have higher theoretical capacity, but their conductivity is poor. In order to obtain better electrochemical performance, it is necessary to use the advantages of different materials to make up for their respective defects, so that composite materials came into being. In short, a composite material is a material with new characteristics, which combines two or more materials with different characteristics through physical or chemical methods. The composite material can not only maintain the advantages of a single electrode material, but also can compensate for its own defects through the composite material, thereby achieving the purpose of improving electrochemical performance. The advantages of nanomaterials with a hybrid electrode structure composed of graphene sheets and inorganic substances include: (1) Effectively improve the electrical connectivity between the various electroactive materials, and shorten the ion transport path through the electrolyte path; (2) Two-phase The dense mixing makes them have a synergistic effect, which greatly improves the overall electrochemical performance.

Recent studies have found that MOF-derived metal and carbon composite materials can be used in supercapacitors. Metal has good conductivity and capacitance, while carbon material has ordered holes and conductivity. These characteristics give MOF specific functions to improve the electrochemical performance of supercapacitors. Wen et al. synthesized Ni-MOF@CNT composite material by a two-step method and applied it in the field of electrochemical energy storage. The results show that when the current density is 0.5 $A \cdot g^{-1}$, the specific capacitance of Ni-MOF@CNT reaches 1765 $F \cdot g^{-1}$ [62]. In addition, an asymmetric supercapacitor was constructed by combining Ni-MOF@CNT electrode and oxidized GO/CNT electrode. When the power density is 480 $W \cdot kg^{-1}$, its energy density can reach 36.6 $Wh \cdot kg^{-1}$. In addition, after 5000 charge and discharge tests, Ni-MOF@CNT still retains 95% of the capacitance. This is mainly due to the large amount of electrocatalytically active Ni metal ions exposed on the surface of the MOF itself, which facilitates the occurrence of redox reactions. At the same time, CNT can effectively improve the conductivity of the entire composite capacitor and accelerate the electron transfer

process, so that the composite capacitor exhibits excellent electrochemical performance. Lin et al. prepared a mixed material of CNT and Mn-MOF and used it as an electrode material for Mn-based supercapacitors. After adding CNT to Mn-MOF, the conductivity and specific capacitance are greatly improved [63]. This work has opened up a new direction for the development of manganese-based supercapacitor materials and provided an effective way to improve the capacitance performance of MOF materials. Some people also synthesize bimetal-loaded carbon nanosheets for use as electrode materials for supercapacitors. Because of the synergy between the bimetals and can change the electronic structure, the electrochemical properties of the material can be improved. Xia et al. used a solvothermal method to improve the conductivity and electrochemical activity of MOF materials by adjusting their morphology and composition [64]. The hollow structures of Ni/Co-MOF nanosheets and Ni-MOF nanosheets were assembled in supercapacitors for electrochemical performance optimization. The results show that in 1 M LiOH aqueous solution, the specific capacitance of Ni/Co-MOF nanosheets is 530.4 $F{\cdot}g^{-1}$ and the specific capacitance is 530.4 $F{\cdot}g^{-1}$, which is much higher than Ni-MOF (306.8 $F{\cdot}g^{-1}$) and ZIF-67 (168.3 $F{\cdot}g^{-1}$), has good rate and rate performance and has good cycle performance after 2000 cycles, and capacity degradation occurs. This work emphasizes the important role of adjusting Ni/Co-MOF two-dimensional nanosheets in accelerating electron and charge transport to optimize energy storage and conversion devices (Fig. 4.5a–d).

Compared with pure carbon, transition metal oxide as a redox-active electrode material provides higher energy density and specific capacitance, which depends on th65 and 1434.37 e reversible Faraday reaction at the interface, thus having higher

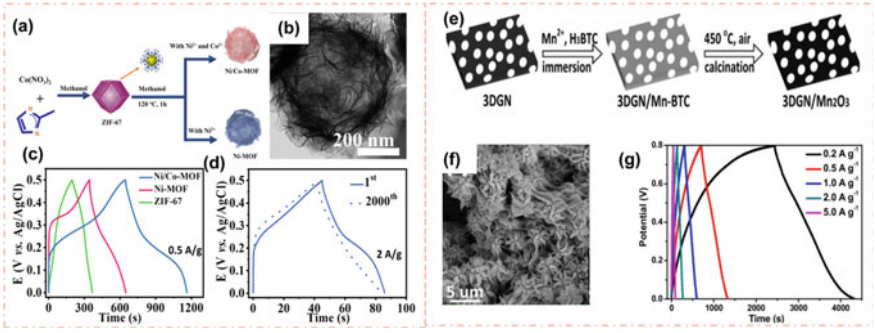

Fig. 4.5 **a** Schematic illustration of the synthesis of Ni/Co-MOF nanoflakes and Ni-MOF nanoflakes. **b** TEM images of Ni/Co-MOF nanoflakes. **c** Galvanostatic charge–discharge curves comparison of Ni/Co-MOF nanoflakes, ZIF-67, and Ni/Co-MOF nanoflakes at various current densities in 1 M LiOH solution. **d** Galvanostatic charge–discharge curves of Ni/Co-MOF nanoflake supercapacitor before and after 2000 cycles measured at 2 A g^{-1}. e Schematic illustration for the fabrication of 3DGN/Mn_2O_3. **f** High magnifications SEM image of 3DGN/Mn_2O_3. **g** GCD curves of the electrodes of Mn-BTC, Mn_2O_3, 3DGN/Mn-BTC and 3DGN/Mn_2O_3 at 0.2 A g^{-1}; **h** Specific capacitance as a function of the current density of the electrodes of Mn-BTC, Mn_2O_3, 3DGN/Mn-BTC and 3DGN/Mn_2O_3

energy density and specific capacitance, but pure transition metal The inherent high resistance and poor cycle stability of oxides greatly reduce their overall effectiveness. Therefore, the combination of pseudocapacitance materials and carbon-based conductive materials as electrodes has been widely used to realize high-efficiency supercapacitor devices to compensate for the inherent defects of metal oxides, increase overall energy density, and promote cycle stability.

Meng et al. reported a porous Fe_3O_4/carbon composite supercapacitor electrode material with excellent temperature resistance and long-term cycle stability [65]. Due to the poor annealing effect of the MOF template, the Fe-MOF template is easy to calcinate in one step. The template is composed of porous Fe_3O_4 nanoparticles and carbon, so the preparation of the material can be easily controlled. When this material is used as an electrode, it has excellent long-term cycle stability to temperature changes, which may be due to the porous structure and good conductivity of the composite material. This work provides a new method to prepare porous carbon/metal oxide electrodes derived from MOF with excellent conductivity and good capacitance characteristics. Ji et al. proposed a simple strategy to construct three-dimensional graphene networks (3DGN) and metal–organic materials, using MOF-derived metal oxide composites as free-standing electrodes for supercapacitors for the first time (Fig. 4.5e) [66]. The manganese-based MOF is first grown in situ on the 3DGN substrate by a simple solution immersion method, and then subjected to high-temperature treatment to form a 3DGN decorated by Mn_2O_3 with a flower-like stacked nanowire morphology (Fig. 4.5f). The designed 3DGN/Mn_2O_3 electrode material has ultra-high specific capacitance and excellent long-cycle stability, and will not decay after 1800 charge and discharge cycles (Fig. 4.5g). The excellent electrochemical performance is derived from the synergistic effect of the high conductivity and large surface area of 3DGN and the excellent pseudocapacitance activity of Mn_2O_3 nanowires. The results indicate that 3DGN/MOF-derived metal oxide composite materials are promising and effective binder-free electrode materials for high-performance supercapacitors. Jayakumar et al. prepared highly optimized mixed oxides of nickel and cobalt from the zeolite imidazole framework [67]. The mixed oxide is further used to produce a nickel–cobalt mixed oxide/graphene 3D hydrogel composite material to enhance electrochemical performance through a continuous and porous graphene conductive network. The electrode made of GNi:Co = 1:1 successfully obtained a higher specific capacitance of 2870.8 $F{\cdot}g^{-1}$ at 1 $A{\cdot}g^{-1}$, and also showed a capacitance retention rate of 81% after 5000 cycles. Thereby greatly improving the cycle stability. An asymmetric supercapacitor was also assembled using pure graphene 3D hydrogel as the negative electrode and GNi:Co = 1:1 as the positive electrode. With a 1.5 V potential window and a binder-free electrode, the capacitor can provide a high specific energy density of 50.2 $Wh{\cdot}kg^{-1}$ at a high power density of 750 W kg^{-1}. This may be due to the synergy between Co, Ni, and C and the electronic effects that increase the electrochemical performance. Xu et al. used GO/MOF as the precursor and obtained a variety of rGO/MOF-derived aerogels through a two-step calcination method [68]. The porous metal oxide composite material prepared by this method has the following advantages: on the one hand, the presence of graphene can effectively prevent the agglomeration of MOF and its derived

porous metal oxide; on the other hand, the material has the high metal oxide properties. The specific capacitance performance has the high conductivity of graphene. At a current density of 1 A g^{-1}, its specific capacitance is as high as 869.2 F·g^{-1}, and there is no significant drop in performance after 5000 cycles. In addition, they found that the method can be used to prepare various graphene/MOF-derived metal oxide composite materials, such as rGO/ZnO, rGO/CuO, rGO/NiO/Ni, and rGO/Co_3O_4. This work provides a new and effective method to prepare MOF-derived porous composites using GO/MOF composites as precursors. Javed et al. report a convenient hydrothermal method for growing mesopore 2D Zn-Cobalt nanosheets directly at low temperatures on flexible carbon substrates (Zn-Co–O@CC) with an average thickness of 45 nm (Fig. 4.6a–b) [69]. The Zn-Co–O@CC electrode showed high capacitance of 1750, 1573.65, and 1434.37 F·g^{-1} in the neutral aqueous electrolyte LiCl, NaCl, and KCl at current densities of 1.5 A·g^{-1} and KCl, respectively. In up to 5000 cycles, it has excellent performance at high current densities and has good cycle stability (>94%) (Fig. 4.6c). In addition, highly flexible asymmetric supercapacitor devices have been fabricated using Zn-Co–O@CC as the positive electrode and NPC@CC (Zn-Co–O@CC//NPC@CC) as the negative electrode. Asymmetric supercapacitors can operate under a large potential window of 0.0–2.0 V, and provide an ultra-high energy density of 117.92 W h kg^{-1} and a power density of 1490.4 W kg^{-1}, showing excellent energy storage performance. The cycle stability after 5000 charge/discharge cycles is 94%. These results provide valuable insights for the preparation of asymmetric supercapacitors for high-efficiency energy storage devices using bimetal oxide and MOF-derived carbon. Metal oxide has attracted much attention due to its high theoretical capacitance, wide working potential range, low cost, natural abundance, and environmental friendliness, but the conductivity and ion diffusivity of simple metal oxide electrodes will lead to low specific capacitance. And the performance is poor. The multiplication performance of supercapacitors hinders its application. Zhou et al. reported a simple and cost-effective method to directly grow MIL-88-Fe-derived-Fe_2O_3@C on oxidized carbon nanotube fibers (S-Fe_2O_3@C/ OCNTF) [70]. The S-α-Fe_2O_3@C/OCNTF electrode has a high area capacitance of 1232.4 mF·cm^{-2} at a current density of 2 mA·cm^{-2}, and a considerable power ratio and capacitance retention rate at a current density of 20 mA·cm^{-2}. And it matches well with the Na-MnO_2 NSs/CNTF cathode of CNTF-doped MnO_2 nanosheets. Electrochemical test results show that the asymmetric supercapacitor S-α-Fe_2O_3@C/OCNTF//$NaMnO_2$NSs/CNTF has a high specific capacitance of 201.3 mF·cm^{-2} and an excellent energy density of 135.3 Wh·cm^{-2}. Therefore, the MIL-88-Fe-MOF derivative S-Fe_2O_3@C will become a promising anode for the next generation of wearable asymmetric supercapacitors.

In addition to metal oxides, other metal compounds (such as metal sulfides) and carbon composite materials can also exhibit excellent electrochemical performance. Qu et al. successfully synthesized a hierarchical porous hybrid electrode composed of R-NiS and rGO [71]. The electrode was directly sulfided with MOF-74/rGO hybrid material. When tested in supercapacitors, the R-NiS/rGO hybrid electrode has higher specific capacitance, excellent rate capability, and good cycle life, which is far

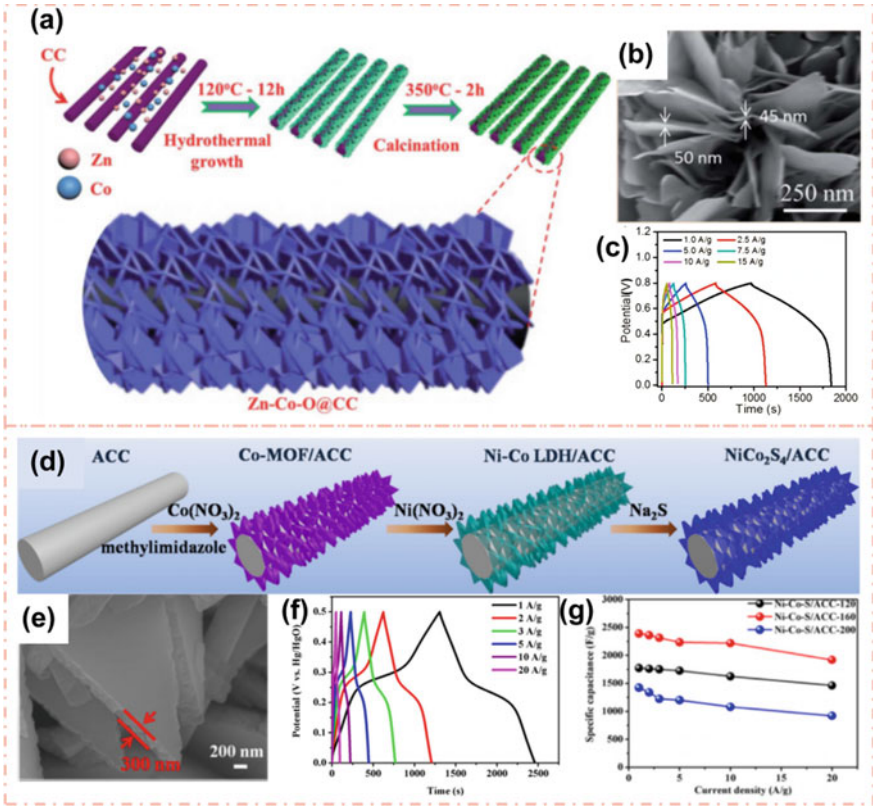

Fig. 4.6 **a** Schematic illustration of the strategy to directly grow the bimetallic nanosheets (Zn-Co–O@CC) on a flexible conductive carbon cloth substrate with a short-term post-annealing treatment at 350 °C in an oxygen atmosphere. **b** High-resolution FESEM images and the average thickness of nanosheets is about 47.5 nm as indicated. **c** Charge/discharge curves of the Zn-Co–O@CC electrode recorded at various current densities ranging from 1 to 15 A g^{-1}. **d** Schematic illustration for the synthesis of MOF-derived ultra-thin $NiCo_2S_4$ nanoarrays on electrochemical activated carbon cloth. **e** High magnification SEM images of Co-MOF/ACC. **f** GCD curves at different current densities of Ni-Co-S/ACC-160. **g** Specific capacitances calculate from GCD curves of all the Ni-Co-S electrodes, respectively

superior to other nickel-sulfur-based electrodes previously reported. The improvement of electrochemical performance is mainly attributed to the edge enrichment of (101) and (110) active sites of R-NiS/rGO hybrid materials. Through experimental measurement and DFT-based calculations, they have an effect on the OH in 2 M KOH electrolyte very strong affinity. In addition, especially when coupled with the capacitive electrode C/NG-A to construct a hybrid supercapacitor with R-NiS/RGO/electrolyte/C/NG-A, the hybrid device exhibits a very high energy density and power density. The developed layered porous hybrid electrode manufacturing method is suitable for the manufacture of other high-performance electrodes for

various energy storage and conversion devices. Zhao et al. demonstrated the rational design and preparation of hollow and ultra-thin nickel cobalt sulfide nanocrystals (Ni-Co-S/ACC) for flexible hybrid supercapacitors on electrochemically activated carbon cloth, where Ni-Co-S nanosheets are extracted from the metal–organic framework by etching/ion exchange method (Fig. 4.6d) [72]. The Ni-Co-S/ACC electrode can provide very high specific capacitance at a current density of 1 $A \cdot g^{-1}$ and has good rate performance. The enhanced electrochemical performance should be attributed to the hollow and ultra-thin structure of electrochemically activated carbon cloth and Ni-Co-S nanosheets, resulting in hydrophilicity, good electrical conductivity, and abundant redox active sites (Fig. 4.6e). When Ni-Co-S/ACC is used as the positive electrode of a flexible hybrid supercapacitor and activated carbon is used as the negative electrode, it shows a high energy density of 30.1 W $h \cdot Kg^{-1}$ and excellent cycling at a power density of 800.2 $W \cdot Kg^{-1}$ stability (Fig. 4.6g–h). In addition, the excellent flexibility and wear resistance of hybrid supercapacitors can predict its application prospects in high-performance wearable energy storage devices.

Finally, this section will provide some personal insights into the future direction of this attractive research field. We hope that this article can summarize groundbreaking research and promote new developments based on MOF and MOFs-derived materials.

References

1. Lindley D (2010) Smart grids: the energy storage problem. Nature 463:18–20. https://doi.org/10.1038/463018a
2. Liu C, Li F, Ma L-P, Cheng H-M (2010) Advanced materials for energy storage. Adv Mater 22:E28–E62. https://doi.org/10.1002/adma.200903328
3. Chu S, Majumdar A (2012) Opportunities and challenges for a sustainable energy future. Nature 488:294–303. https://doi.org/10.1038/nature11475
4. Chen M, Li W, Shen X, Diao G (2014) Fabrication of core-shell α-Fe 2 O 3 @ Li 4 Ti 5 O 12 composite and its application in the lithium ion batteries. ACS Appl Mater Interfaces 6:4514–4523. https://doi.org/10.1021/am500294m
5. Zeng Y, Yu M, Meng Y, Fang P, Lu X, Tong Y (2016) Iron-based supercapacitor electrodes: advances and challenges. Adv Energy Mater 44:1601053. https://doi.org/10.1002/aenm.201601053
6. Liu J, Zheng M, Shi X, Zeng H, Xia H (2016) Amorphous FeOOH quantum dots assembled mesoporous film anchored on graphene nanosheets with superior electrochemical performance for supercapacitors. Adv Funct Mater 26:919–930. https://doi.org/10.1002/adfm.201504019
7. Li Y, Xu J, Feng T, Yao Q, Xie J, Xia H (2017) Fe2O3 nanoneedles on ultrafine nickel nanotube arrays as efficient anode for high-performance asymmetric supercapacitors. Adv Funct Mater 27:1606728. https://doi.org/10.1002/adfm.201606728
8. Zhang C, Yin H, Han M, Dai Z, Pang H, Zheng Y, Lan Y-Q, Bao J, Zhu J (2014) Two-dimensional tin selenide nanostructures for flexible all-solid-state supercapacitors. ACS Nano 8:3761–3770. https://doi.org/10.1021/nn5004315
9. Yu M, Cheng X, Zeng Y, Wang Z, Tong Y, Lu X, Yang S (2016) Dual-doped molybdenum trioxide nanowires: a bifunctional anode for fiber-shaped asymmetric supercapacitors and microbial fuel cells. Angew Chemie 128:6874–6878. https://doi.org/10.1002/ange.201602631

10. Yu M, Lin D, Feng H, Zeng Y, Tong Y, Lu X (2017) Boosting the energy density of carbon-based aqueous supercapacitors by optimizing the surface charge. Angew Chemie Int Ed 56:5454–5459. https://doi.org/10.1002/anie.201701737
11. Zeng Y, Lin Z, Meng Y, Wang Y, Yu M, Lu X, Tong Y (2016) Flexible ultrafast aqueous rechargeable Ni//Bi battery based on highly durable single-crystalline bismuth nanostructured anode. Adv Mater 28:9188–9195. https://doi.org/10.1002/adma.201603304
12. Jabeen N, Xia Q, Savilov SV, Aldoshin SM, Yu Y, Xia H (2016) Enhanced pseudocapacitive performance of ?-MnO2 by cation preinsertion. ACS Appl Mater Interfaces 8:33732–33740. https://doi.org/10.1021/acsami.6b12518
13. Hu X, Shao W, Hang X, Zhang X, Zhu W, Xie Y (2016) Superior electrical conductivity in hydrogenated layered ternary chalcogenide nanosheets for flexible all-solid-state supercapacitors. Angew Chemie 128:5827–5832. https://doi.org/10.1002/ange.201600029
14. Simon P, Gogotsi Y (2008) Materials for electrochemical capacitors. Nat Mater 7:845–854. https://doi.org/10.1038/nmat2297
15. Chalk SG, Miller JF (2006) Key challenges and recent progress in batteries, fuel cells, and hydrogen storage for clean energy systems. J Power Sources 159:73–80. https://doi.org/10.1016/j.jpowsour.2006.04.058
16. Zhang Q, Uchaker E, Candelaria SL, Cao G (2013) Nanomaterials for energy conversion and storage. Chem Soc Rev 42:3127. https://doi.org/10.1039/c3cs00009e
17. Whittingham MS (2008) Materials challenges facing electrical energy storage. MRS Bull 33:411–419. https://doi.org/10.1557/mrs2008.82
18. Li X-C, Zhang Y, Wang C-Y, Wan Y, Lai W-Y, Pang H, Huang W (2017) Redox-active triazatruxene-based conjugated microporous polymers for high-performance supercapacitors. Chem Sci 8:2959–2965. https://doi.org/10.1039/C6SC05532J
19. Fan L, Tang L, Gong H, Yao Z, Guo R (2012) Carbon-nanoparticles encapsulated in hollow nickel oxides for supercapacitor application. J Mater Chem 22:16376–16381. https://doi.org/10.1039/c2jm32241b
20. Tong J, Zhang H, Gu J, Li L, Ma C, Zhao J, Wang C (2016) Poly(ethylene glycol)-block-poly(propylene glycol)-block-poly(ethylene glycol)-assisted synthesis of graphene/polyaniline composites as high-performance supercapacitor electrodes. J Mater Sci 51:1966–1977. https://doi.org/10.1007/s10853-015-9506-y
21. Zhang J, Sun B, Ahn H-J, Wang C, Wang G (2013) Conducting polymer-doped polyprrrole as an effective cathode catalyst for Li-O2 batteries. Mater Res Bull 48:4979–4983. https://doi.org/10.1016/j.materresbull.2013.04.050
22. Yu M, Wang Z, Hou C, Wang Z, Liang C, Zhao C, Tong Y, Lu X, Yang S (2017) Nitrogen-doped Co3O4 mesoporous nanowire arrays as an additive-free air-cathode for flexible solid-state zinc-air batteries. Adv Mater 29:1602868. https://doi.org/10.1002/adma.201602868
23. Liu C, Zhao S, Lu Y, Chang Y, Xu D, Wang Q, Dai Z, Bao J, Han M (2017) 3D porous nanoarchitectures derived from SnS/S-Doped graphene hybrid nanosheets for flexible all-solid-state supercapacitors. Small 13:1603494. https://doi.org/10.1002/smll.201603494
24. Sun J-K, Xu Q (2014) Functional materials derived from open framework templates/precursors: synthesis and applications. Energy Environ Sci 7:2071. https://doi.org/10.1039/c4ee00517a
25. Cao X, Tan C, Sindoro M, Zhang H (2017) Hybrid micro-/nano-structures derived from metal–organic frameworks: preparation and applications in energy storage and conversion. Chem Soc Rev 46:2660–2677. https://doi.org/10.1039/C6CS00426A
26. Díaz R, Orcajo MG, Botas JA, Calleja G, Palma J (2012) Co8-MOF-5 as electrode for supercapacitors. Mater Lett 68:126–128. https://doi.org/10.1016/j.matlet.2011.10.046
27. Lee DY, Yoon SJ, Shrestha NK, Lee S-H, Ahn H, Han S-H (2012) Unusual energy storage and charge retention in Co-based metal–organic-frameworks. Microporous Mesoporous Mater 153:163–165. https://doi.org/10.1016/j.micromeso.2011.12.040
28. Lee DY, Shinde DV, Kim E-K, Lee W, Oh I-W, Shrestha NK, Lee JK, Han S-H (2013) Supercapacitive property of metal–organic-frameworks with different pore dimensions and morphology. Microporous Mesoporous Mater 171:53–57. https://doi.org/10.1016/j.micromeso.2012.12.039

29. Liu X, Shi C, Zhai C, Cheng M, Liu Q, Wang G (2016) Cobalt-based layered metal-organic framework as an ultrahigh capacity supercapacitor electrode material. ACS Appl Mater Interfaces 8:4585–4591. https://doi.org/10.1021/acsami.5b10781
30. Yang J, Ma Z, Gao W, Wei M (2017) Layered structural co-based MOF with conductive network frames as a new supercapacitor electrode. Chem-A Eur J 23:631–636. https://doi.org/10.1002/chem.201604071
31. Zheng Y, Zheng S, Xu Y, Xue H, Liu C, Pang H (2019) Ultrathin two-dimensional cobalt-organic frameworks nanosheets for electrochemical energy storage. Chem Eng J 373:1319–1328. https://doi.org/10.1016/j.cej.2019.05.145
32. Abazari R, Sanati S, Morsali A, Slawin AL, Carpenter-Warren C (2019) Dual-purpose 3D pillared metal-organic framework with excellent properties for catalysis of oxidative desulfurization and energy storage in asymmetric supercapacitor. ACS Appl Mater Interfaces 11:14759–14773. https://doi.org/10.1021/acsami.9b00415
33. Liao C, Zuo Y, Zhang W, Zhao J, Tang B, Tang A, Sun Y, Xu J (2013) Electrochemical performance of metal-organic framework synthesized by a solvothermal method for supercapacitors. Russ J Electrochem 49:983–986. https://doi.org/10.1134/S1023193512080113
34. Kang L, Sun S-X, Kong L-B, Lang J-W, Luo Y-C (2014) Investigating metal-organic framework as a new pseudo-capacitive material for supercapacitors. Chinese Chem Lett 25:957–961. https://doi.org/10.1016/j.cclet.2014.05.032
35. Yang J, Xiong P, Zheng C, Qiu H, Wei M (2014) Metal–organic frameworks: a new promising class of materials for a high performance supercapacitor electrode. J Mater Chem A 2:16640–16644. https://doi.org/10.1039/C4TA04140B
36. Qu C, Jiao Y, Zhao B, Chen D, Zou R, Walton KS, Liu M (2016) Nickel-based pillared MOFs for high-performance supercapacitors: Design, synthesis and stability study. Nano Energy 26:66–73. https://doi.org/10.1016/j.nanoen.2016.04.003
37. Sheberla D, Bachman JC, Elias JS, Sun C-J, Shao-Horn Y, Dincă M (2016) Conductive MOF electrodes for stable supercapacitors with high areal capacitance. Nat Mater 1:1–6. https://doi.org/10.1038/nmat4766
38. Xu J, Yang C, Xue Y, Wang C, Cao J, Chen Z (2016) Facile synthesis of novel metal-organic nickel hydroxide nanorods for high performance supercapacitor. Electrochim Acta 211:595–602. https://doi.org/10.1016/j.electacta.2016.06.090
39. Yan Y, Gu P, Zheng S, Zheng M, Pang H, Xue H (2016) Facile synthesis of an accordion-like Ni-MOF superstructure for high-performance flexible supercapacitors. J Mater Chem A 4:19078–19085. https://doi.org/10.1039/C6TA08331E
40. Campagnol N, Romero-Vara R, Deleu W, Stappers L, Binnemans K, De Vos DE, Fransaer J (2014) A Hybrid Supercapacitor based on Porous Carbon and the Metal-Organic Framework MIL-100(Fe). ChemElectroChem 1:1182–1188. https://doi.org/10.1002/celc.201402022
41. Choi KM, Jeong HM, Park JH, Zhang Y, Kang JK (2014) Supercapacitors of Nanocrystalline Metal À Organic Frameworks. ACS Nano 8:7451–7457. https://doi.org/10.1021/nn5027092
42. Jiao Y, Pei J, Chen D, Yan C, Hu Y, Zhang Q, Chen G (2017) Mixed-metallic MOF based electrode materials for high performance hybrid supercapacitors. J Mater Chem A 00:1–9. https://doi.org/10.1039/C6TA09805C
43. Moon HR, Lim DW, Suh MP (2013) Fabrication of metal nanoparticles in metal-organic frameworks. Chem Soc Rev 42:1807–1824. https://doi.org/10.1039/C2CS35320B
44. Amali AJ, Sun J-K, Xu Q (2014) From assembled metal-organic framework nanoparticles to hierarchically porous carbon for electrochemical energy storage. Chem Commun 50:1519–1522. https://doi.org/10.1039/C3CC48112C
45. Torad NL, Salunkhe R, Li Y, Hamoudi H, Imura M, Sakka Y, Hu C-C, Yamauchi Y (2014) Electric double-layer capacitors based on highly graphitized nanoporous carbons derived from ZIF-67. Chem Eur J 20:7895–7900. https://doi.org/10.1002/chem.201400089
46. Salunkhe RR, Kamachi Y, Torad N, Hwang SM, Dou SX, Kim JH, Yamauchi Y (2014) Fabrication of symmetric supercapacitors based on MOF-derived nanoporous carbons. J Mater Chem A 2:19848–19854. https://doi.org/10.1039/C4TA04277H

47. Yi H, Wang H, Jing Y, Peng T, Wang X (2015) Asymmetric supercapacitors based on carbon nanotubes@NiO ultrathin nanosheets core-shell composites and MOF-derived porous carbon polyhedrons with super-long cycle life. J Power Sources 285:281–290. https://doi.org/10.1016/J.JPOWSOUR.2015.03.106
48. Jeon J-W, Sharma R, Meduri P, Arey B, Schaef H, Lutkenhaus J, Lemmon J, Thallapally P, Nandasiri M, McGrail BP, Nune S (2014) In situ one-step synthesis of hierarchical nitrogen-doped porous carbon for high-performance supercapacitors. ACS Appl Mater Interfaces 6:7214–7222. https://doi.org/10.1021/am500339x
49. Tang J, Salunkhe R, Liu J, Torad N, Imura M, Furukawa S, Yamauchi Y (2015) Thermal conversion of core–shell metal–organic frameworks: a new method for selectively functionalized nanoporous hybrid carbon. J Am Chem Soc 137:1572–1580. https://doi.org/10.1021/ja511539a
50. Yan X, Li X, Yan Z, Komarneni S (2014) Porous carbons prepared by direct carbonization of MOFs for supercapacitors. Appl Surf Sci 308:306–310. https://doi.org/10.1016/j.apsusc.2014.04.160
51. Zhao K, Liu S, Ye G, Gan Q, Zhou Z, He Z (2018) High-yield bottom-up synthesis of 2D metal–organic frameworks and their derived ultrathin carbon nanosheets for energy storage. J Mater Chem A 6:2166–2175. https://doi.org/10.1039/C7TA06916B
52. Zhang P, Sun F, Shen Z, Cao D (2014) ZIF-derived porous carbon: a promising supercapacitor electrode material. J Mater Chem A 2:12873–12880. https://doi.org/10.1039/C4TA00475B
53. Jiang H-L, Liu B, Lan Y-Q, Kuratani K, Akita T, Shioyama H, Zong F, Xu Q (2011) From metal-organic framework to nanoporous carbon: toward a very high surface area and hydrogen uptake. J Am Chem Soc 133:11854–11857. http://pubs.acs.org/https://doi.org/10.1021/ja203184k
54. Du W, Wang X, Zhan J, Sun X, Kang L, Jiang F, Zhang X, Shao Q, Dong M, Liu H, Murugadoss V, Guo Z (2019) Biological cell template synthesis of nitrogen-doped porous hollow carbon spheres/MnO_2 composites for high-performance asymmetric supercapacitors. Electrochim Acta 296:907–915. https://doi.org/10.1016/j.electacta.2018.11.074
55. Meng F, Chen W, Zhao L, Xu W, Wang M, Liu Y, Zhang J, Wang W, Zhao D, Guo X (2013) Porous Co_3O_4 materials prepared by solid-state thermolysis of a novel Co-MOF crystal and their superior energy storage performances for supercapacitors. J Mater Chem A 1:7235–7241. https://doi.org/10.1039/C3TA11054K
56. Pang H, Gao F, Chen Q, Liu R, Lu Q (2012) Dendrite-like Co_3O_4 nanostructure and its applications in sensors, supercapacitors and catalysis. Dalton Trans 41:5862–5868. https://doi.org/10.1039/C2DT12494G
57. Salunkhe R, Tang J, Kamachi Y, Nakato T, Kim JH, Yamauchi Y (2015) Asymmetric supercapacitors using 3D nanoporous carbon and cobalt oxide electrodes synthesized from a single metal-organic framework. ACS Nano 9:6288–6296. https://doi.org/10.1021/acsnano.5b01790
58. Maiti S, Pramanik A, Mahanty S (2016) Electrochemical energy storage in Mn_2O_3 porous nanobars derived from morphology-conserved transformation of benzenetricarboxylate-bridged metal–organic framework. Cryst Eng Comm 18:450–461. https://doi.org/10.1039/C5CE01976A
59. Maiti S, Pramanik A, Mahanty S (2014) Extraordinarily high pseudocapacitance of metal organic framework derived nanostructured cerium oxide. Chem Commun (Camb) 50:11717–11720. https://doi.org/10.1039/C4CC05363J
60. Le K, Gao M, Liu W, Liu J, Wang Z, Wang F, Murugadoss V, Wu S, Ding T, Guo Z (2019) MOF-derived hierarchical core-shell hollow iron-cobalt sulfides nanoarrays on Ni foam with enhanced electrochemical properties for high energy density asymmetric supercapacitors. Electrochim Acta 323:134826. https://doi.org/10.1016/j.electacta.2019.134826
61. Yilmaz G, Yam KM, Zhang C, Fan HJ, Ho W (2017) In situ transformation of MOFs into layered double hydroxide embedded metal sulfides for improved electrocatalytic and supercapacitive performance. Adv Mater 29:1606814. https://doi.org/10.1002/adma.201606814
62. Wen P, Gong P, Sun J, Wang J, Yang S (2015) Design and synthesis of Ni-MOF/CNT composites and rGO/carbon nitride composites for an asymmetric supercapacitor with high energy and power density. J Mater Chem A 3:13874–13883. https://doi.org/10.1039/C5TA02461G

63. Zhang Y, Lin B, Sun Y, Zhang X, Yang H, Wang J (2015) Carbon nanotubes@metal-organic frameworks as Mn-based symmetrical supercapacitor electrodes for enhanced charge storage. RSC Adv 5:58100–58106. https://doi.org/10.1039/C5RA11597C
64. Xia H, Zhang J, Yang Z, Guo S, Guo S, Xu Q (2017) 2D MOF Nanoflake-assembled spherical microstructures for enhanced supercapacitor and electrocatalysis performances. Nanomicro Lett 9:43. https://doi.org/10.1007/S40820-017-0144-6
65. Meng W, Chen W, Zhao L, Huang Y, Zhu M, Huang Y, Fu Y, Geng F, Yu J, Chen X, Zhi C (2014) Porous Fe_3O_4/carbon composite electrode material prepared from metal-organic framework template and effect of temperature on its capacitance. Nano Energy 8:133–140. https://doi.org/10.1016/j.nanoen.2014.06.007
66. Ji D, Zhou H, Zhang J, Dan Y, Yuan H, Yang H, Yuan A (2016) Facile synthesis of a metal–organic framework-derived Mn_2O_3 nanowire coated three-dimensional graphene network for high-performance free-standing supercapacitor electrodes. J Mater Chem A 4:8283–8290. https://doi.org/10.1039/C6TA01377E
67. Jayakumar A, Antony R, Wang R, Lee J-M (2017) MOF-derived hollow cage Nix Co_3-xO_4 and their synergy with graphene for outstanding supercapacitors. Small 13:1603102. https://doi.org/10.1002/smll.201603102
68. Xu X, Shi W, Li P, Ye S, Ye C, Ye H, Lu T, Zheng A, Zhu J, Xu L, Zhong M, Cao X (2017) Facile fabrication of three-dimensional graphene and metal–organic framework composites and their derivatives for flexible all-solid-state supercapacitors. Chem Mater 29:6058–6065. https://doi.org/10.1021/acs.chemmater.7b01947
69. Javed MS, Shaheen N, Hussain S, Shaheen N, Hussain S, Li J, Shah SSA, Abbas Y, Ahmad MA, Raza R, Mai W (2019) An ultra-high energy density flexible asymmetric supercapacitor based on hierarchical fabric decorated with 2D bimetallic oxide nanosheets and MOF-derived porous carbon polyhedra. J Mater Chem A 7:946–957. https://doi.org/10.1039/C8TA08816K
70. Zhou Z, Zhang Q, Sun J, He B, Guo J, Li Q, Li C, Xie L, Yao Y (2018) Metal-organic framework derived spindle-like carbon incorporated α-Fe_2O_3 grown on carbon nanotube fiber as anodes for high-performance wearable asymmetric supercapacitors. ACS Nano 12:9333–9341. https://doi.org/10.1021/acsnano.8b04336
71. Qu C, Zhang L, Meng W, Liang Z, Zhu B, Dang D, Dai S, Zhao B, Tabassum H, Gao S, Zhang H, Guo W, Zhao R, Huang X, Liu M, Zou R (2018) MOF-derived α-NiS nanorods on graphene as an electrode for high-energy-density supercapacitors. J Mater Chem A 6:4003–4012. https://doi.org/10.1039/C7TA11100B
72. Zhao W, Zheng Y, Cui L, Jia D, Wei D, Zheng R, Barrow C, Yang W, Liu J (2019) MOF derived Ni-Co-S nanosheets on electrochemically activated carbon cloth via an etching/ion exchange method for wearable hybrid supercapacitors. Chem Eng J 371:461–469. https://doi.org/10.1016/j.cej.2019.04.070

Chapter 5
MOF-Derived Materials for Energy Conversion

Jianan Zhang, Su Jiang, Dongping Xue, and Xiaoyu Zhang

5.1 Introduction

The massive consumption of fossil fuels and the gradual deterioration of the environment force us to develop new renewable energy sources to solve the energy and environmental crisis in an eco-friendly way, and people have exert a lot of effort in several directions. On the one hand, many researches aim to promote the evolution of energy-available gases (such as hydrogen and oxygen) [1]. On the other hand, some gas (such as carbon dioxide), which aggravates environmental degradation, can be converted [2], adsorbed [3], and captured through some novel and scientific strategies [4–9]. Besides, clean and efficient batteries (e.g., fuel cells and metal–air batteries) are being developed constantly.

As we all know, noble metals or their oxides (Pt, Ru and RuO_2, IrO_2, etc.) are regarded as the most advanced catalysts for electrocatalytic reaction [10, 11]. However, due to the high price and low abundance, these catalysts are difficult to be applied in large-scale electrocatalytic industries. Therefore, people are committed to looking for alternative for noble metal-based catalysts for industrial applications of electrocatalyst. The design and synthesis of non-noble metal-based catalysts with high catalytic activity are obviously the best choice and have attracted more and more attention [12, 13]. As a new type of porous material, the metal–organic framework

J. Zhang (✉) · S. Jiang · D. Xue · X. Zhang
College of Materials Science and Engineering, Zhengzhou University, Zhengzhou 450001, PR China
e-mail: zjn@zzu.edu.cn

S. Jiang
e-mail: jiangszzu@163.com

D. Xue
e-mail: xdongping1231@126.com

X. Zhang
e-mail: zhangxiaoyu0321@163.com

H. Pang (ed.), *Nano/Micro Metal-Organic Frameworks*,
https://doi.org/10.1007/978-981-16-4071-1_5

(MOF) has received special attention in the past decades due to its unique physical and chemical properties and wide range of applications. MOF is a kind of organic–inorganic porous material composed of organic ligands and metal centers with crystalline morphology. It has the advantages of unique electronic structure, low coordination environment, quantum size effect, and metal–support interaction [4–6]. It has broad prospects for improving electrocatalytic activity, stability, and selectivity in the field of clean energy conversion and has been developed as new and efficient electrocatalyst materials used in multiple energy conversion reactions. A large number of studies have shown that metal single atoms, nanoparticles, metal alloys, metal compounds, metal-porous carbon hybrids, etc., that derived from MOFs have excellent catalytic activity and durability [1, 7]. Here, we summarized the current application and development of various MOF-derived electrocatalysts for overall water splitting, hydrogen evolution reaction (HER), oxygen evolution reaction (OER), oxygen reduction reaction (ORR), and carbon dioxide reduction reaction (CO_2RR). And the future of MOF derivatives in electrocatalysis field is prospected.

5.2 MOF-Derived Materials for Water Splitting

Water splitting has become a hot topic in the storage and conversion of renewable energy due to its non-polluting and sustainable advantages [8]. The hydrogen it produces is a promising clean energy. Generally, water splitting ($2H_2O \rightarrow 2H_2\uparrow + O_2\uparrow$) is divided into two half reactions, oxygen evolution reaction (OER) and hydrogen evolution reaction (HER). Under standard conditions, the theoretical cell voltage for water splitting is 1.23 V. However, since there are dynamic barriers in both HER and OER, a larger operating voltage is required [9], an effective electrocatalyst is needed to lower the energy barrier of the water splitting reaction. Based on the advantages of MOFs, many MOFs and their derivative materials are used for water splitting. For most MOF materials, stability in acidic or alkaline electrolytes is an important challenge, because MOF exposed to the electrolyte is easily decomposed, ligands are easily protonated in acid solutions, and in some cases metal ions may be converted to metal hydroxide in alkaline solutions gradually [14]. It is difficult for a catalyst to show excellent catalytic performance for HER and OER at the same time, and the sluggishness of OER will also restrict the smooth progress of the HER reaction. The poor electronic conductivity also hinders the further improvement of the catalytic performance of MOF and its derivatives. In addition, the mechanism by which MOFs-based materials are used in HER or OER is still unclear [7]. Therefore, there are still many obstacles and challenges in exploring the dual-function water splitting catalysts.

5.2.1 MOF-Derived Metal Nanoparticles and Clusters for Water Splitting

In the process of exploring catalysts for dual-functional reactions such as water splitting, metal nanoparticles have been extensively studied due to their unique and excellent catalytic performance [8]. However, the high surface energy of nanoparticles makes them easy to settle during the reaction process, which leads to inactivation. At the same time, many by-products produced during the reaction will poison the catalyst, resulting in a decrease in catalyst activity and reuse rate. Loading nanoparticles through porous materials as a catalytic platform is an effective way to solve the above problems. MOF, as a porous material that has been widely concerned in recent years, has also produced many research results in loading nanoparticles. Chen et al. reported the designed structure of Co-based MOF (ZIF-67) with in situ insertion of carbon nanotubes (CNTs) and used it as a template to prepare a hybrid of hollow Co nanoparticles (NPs)-encapsulated N-doped porous carbon nanoframes interlinked by CNTs (Fig. 5.1a and b) [15]. The resulting Co-NC/CNT hybrid continuous 3D network has highly exposed active sites and good electrical conductivity, and shows high dual-functional catalytic performance for rapid water splitting in alkaline solution. To afford a current density of 10 mA cm^{-2}, the voltage needed is only 1.625 V with this catalyst (Fig. 5.1c). The unique 3D network architecture composed of the carbon frame derived from ZIF-67 as joints and the CNT as the linkers can dramatically improve conductivity and mass/charge transfer. The large surface area and the insertion of CNTs ensure a large exposure of active sites and rapid transportation of electrolytes and products. Cobalt nanoparticles derived from MOF can achieve effective exposure and immobilization of active sites in this structure.

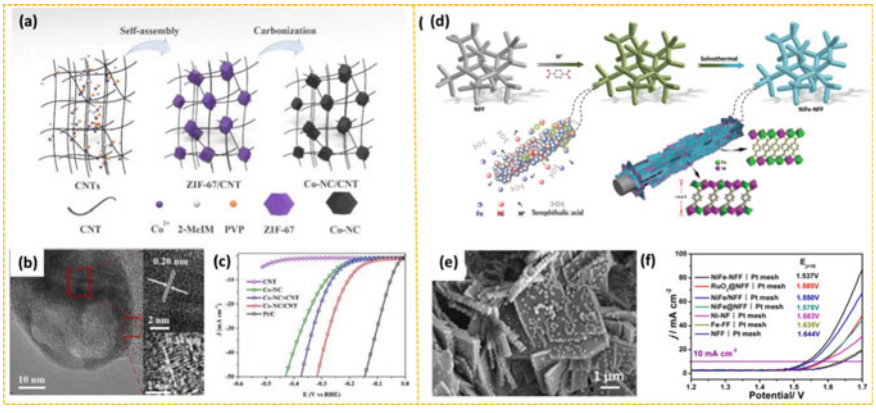

Fig. 5.1 **a** Schematic illustration of the synthesis of Co-NC/CNT. **b** HRTEM images of hollow Co NPs and the carbon layers, respectively. **c** HER polarization curves of Pt/C, Co-NC/CNT, Co-NC + CNT, Co-NC, and CNT in 1.0 M KOH. **d** Schematic representation for the formation of the NiFe-NFF electrode. **e** SEM images of NiFe-NFF. **f** LSV curves of overall water electrolysis for the two-electrode electrolyzers composed of the prepared anode electrocatalysts and a Pt mesh cathode

Researches on the water splitting catalysis based on cobalt nanoparticles in alkaline condition are mostly carried on the matrix of nitrogen-doped carbon materials [16]. N-doped carbon materials exist in the catalysts in different forms and structures, which are loaded and fix real metal sites in different ways as components of the catalyst. Ai et al. used the unique composition and structure of the cobalt-based zeolite imidazolate framework (ZIF-67) as a precursor to synthesize cobalt nanoparticles embedded in porous nitrogen-rich carbon (PNC/Co) [17]. The obtained PNC/Co can be used as a bifunctional catalyst for water splitting and has high activity to both HER and OER in a strong alkaline medium. In 1.0 M KOH electrolyte, PNC/Co requires only a small overpotential at a current density of 10 mA cm^{-2} and produces high Faraday efficiency for both HER and OER. When manufactured as an alkaline water electrolyzer, the dual-function PNC/Co can provide a water splitting current of 10 mA cm^{-2} at a battery voltage of 1.64 V.

Due to the special geometric structure and quantum effect of nanoclusters, it has special physical and chemical properties in light, electricity, magnetism, etc., which provides the possibility for its application in special fields. Because most or all of its metal atoms may be exposed to the surface and have a high surface atom ratio, the unique atomic stacking structure makes it have high surface activity, so it has an important application value in catalytic reactions. Transition metal catalysts have received widespread attention in the early stages of catalyst development, and the research on transition metal nanoclusters in the field of catalysis has also achieved remarkable results. The introduction of metal nanoclusters into the framework of MOFs will be a novel research direction. However, metal nanoclusters have insufficient stability, being surrounded by ligands and low synthesis yield. The loading of metal nanoclusters into MOFs to form composite materials and their application in the field of heterogeneous catalysis will face many challenges. In recent years, MOF-derived metal nanocluster catalysts are more inclined to study bimetallic clusters. Zhu and co-workers reported for the first time the semi-sacrificial template growth of a self-supporting MOF nanocomposite electrode, which is composed of ultra-thin nickel-rich Ni(Fe)-MOF nanosheets (which is synthesized from NiFe alloy foam) modified by ultra-small iron-rich Fe(Ni)-MOF clusters [18]. In this electrode, Fe(Ni)-MOF clusters are uniform, with a particle size of 2–5 nm, and the thickness of Ni(Fe)-MOF nanosheets is only 1.56 nm (Fig. 5.1d and e). When used directly as a self-supporting working electrode for the oxygen evolution reaction (OER), it can provide impressive electrocatalytic performance with overpotentials of 227 and 253 mV to reach the current density of 10 and 100 mA cm^{-2}, respectively, which is far better than the benchmark of RuO_2 and most of the most advanced non-precious metal catalysts (Fig. 5.1f). Further studies have shown that the combination of the unique nanostructure of the catalyst and the strong coupling effect between the active sites of Ni and Fe makes it have such excellent catalytic performance of this catalyst.

A large number of researches have been conducted on bimetallic catalysts based on iron and nickel, which has promoted the emergence of more novel and effective catalyst design strategies and methods. Lu et al. demonstrated a newly designed water-stable NH_2-MIL-88B (Fe_2Ni)-MOF, which is grown in situ on the surface of a highly conductive 3D macroporous nickel foam (NF), denoted as NFN-MOF/NF

[8]. The catalyst is an efficient dual-function electrocatalyst, which can achieve ultra-stable overall water splitting under high current density. NFN-MOF/NF achieved ultra-low overpotentials of 240 and 87 mV in 1 M KOH at a current density of 10 mA cm^{-2} for OER and HER, respectively. For total water splitting, only an ultra-low battery voltage of 1.56 V is needed to reach a current density of 10 mA cm^{-2}, which is better than the corresponding performance of the pairing of Pt/C on NF on the cathode and IrO_2 on NF on the anode. At the same time, the NFN-MOF/NF catalyst showed excellent stability, showing only a small chronopotential decay after 30 h at 500 mA cm^{-2}. The abundant active centers in MOF, bimetallic cluster $\{Fe_2Ni(\mu 3\text{-}O)(COO)_6(H_2O)_3\}$, the positive coupling effect between iron metal ion and Ni ion in MOF, and the synergistic effect between MOF and NF endowed the prepared catalyst with excellent catalytic performance.

Due to the small size of metal nanoclusters, it is easy to be oxidized in the electrochemical system, or aggregate and collapse to reduce the activity, so its electrochemical stability needs to be further improved. This is also a big challenge for the application of metal nanoclusters in the electrochemical field. The unique structure of MOF is beneficial to solve these problems. However, in terms of electrolysis of water splitting, there are few studies on whether MOF-derived metal nanoparticle catalysts or metal nanocluster catalysts are derived from MOFs. In all, there are still many unknown areas in this field that need to be explored.

5.2.2 *MOF-Derived Bimetallic Compounds for Water Splitting*

The metal atoms and organic ligands in the MOF are connected by coordination bonds to form periodic structural units. Due to their high surface area, mesoporous structure, and abundant organic ligands, they are an excellent precursor for producing electrocatalysts [19]. In recent years, in the field of catalysis and energy conversion, in addition to MOF-derived carbon materials, researches on MOF-derived metal compounds have also increased significantly.

MOF-derived synthesis methods are mainly used to synthesize single-metal phosphides, while the research on MOF-derived bimetallic phosphides is very limited [20]. MOF can mix different metal atoms in atomic-level periodic structural units through coordination bonds and should be an ideal precursor for the production of bimetallic phosphides. The synergistic effect and excellent electrocatalytic activity for water splitting of bimetal phosphides make it have great potential in this field. Liang et al. synthesized Ni_2P-CoP bimetallic phosphide through the low-temperature phosphating reaction of Ni-Co bimetallic organic frameworks (Ni-Co-MOFs), in which phthalic acid was used as an organic ligand to connect Ni and Co atoms (Fig. 5.2a and b) [21]. The Ni_2P-CoP catalyst showed an overpotential of 102 mV at 10 mA cm^{-2} of HER, while that of OER showed an overpotential of 320 mV at 10 mA cm^{-2}, which is better than most granular CoP and Ni_2P-based catalysts

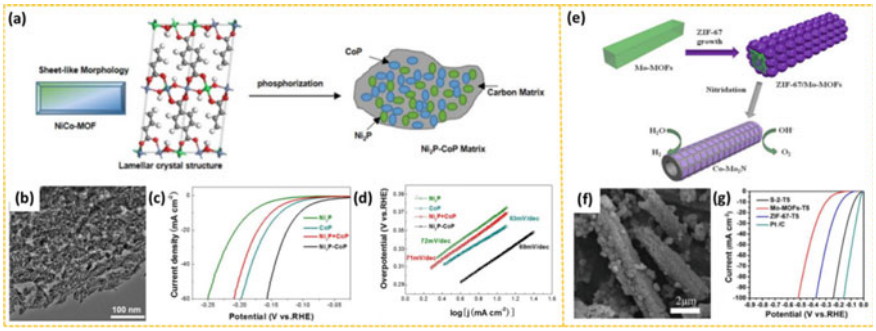

Fig. 5.2 **a** Schematic of the fabrication of Ni_2P–CoP matrix from Ni-Co–MOF. **b** TEM image and of Ni_2P–CoP derived from the phosphorization of Ni-Co–MOFs. **c** LSV polarization curves of Ni_2P, CoP, Ni_2P + CoP, and Ni_2P–CoP in 0.5 M H_2SO_4 electrolyte at a scan rate of 5 mVs^{-1}. **d** The corresponding Tafel plot of Ni_2P, CoP, Ni_2P + CoP, and Ni_2P–CoP in 0.1 M KOH electrolyte at a scan rate of 5 mV s^{-1}. **e** Schematic procedure for the synthesis of Co-Mo_2N hybrid. **f** The SEM image of ZIF-67/Mo-MOF. **g** Polarization curves for S-2-T5, Mo-MOFs-T5, ZIF-67-T5, and Pt/C in 1.0 M KOH with a scan rate of 5 mV s^{-1}

(Fig. 5.2c). In the obtained catalyst, Ni_2P and CoP particles have achieved nanoscale close mixing, forming many Ni_2P/CoP interfaces. Compared with monometallic phosphides, the strong synergistic effect in the bimetallic Ni-Co-P system gives HER and OER enhanced electrocatalytic activity (Fig. 5.2d).

When researchers use MOF-derived bimetallic compounds in the field of catalysis, direct metal conversion may not be able to effectively control the ratio of bimetals. The strategy of MOF plus MOF can rationally design the ratio of bimetals to a certain extent, which has attracted researchers' attention recently. Fu et al. reported the design of a Co-Mo_2N tube based on the "MOF plus MOF" strategy for effective electrocatalytic water splitting in 1 M KOH [22]. ZIF-67/Mo-MOF is obtained by solid solution phase assembly method. The effective combination is related to the similarity of the ligands in the two MOFs. After nitriding, ZIF-67 is converted to Co metal, and Mo-MOFs are converted to hollow Mo_2N, thereby providing a hollow Co-Mo_2N hybrid with a Co outer layer on the Mo_2N core (Fig. 5.2e and f). The ratio of Co and Mo in Co-Mo_2N can be easily adjusted, which provides an opportunity to obtain an optimized catalyst. Electrochemical tests show that the combination of Co and Mo_2N can greatly improve the HER performance of the material. At a current density of 10 mA cm^{-2}, the overpotential on Co-Mo_2N is only 76 mV, which is much lower than that of Mo-MOFs-derived Mo_2N corresponding to 296 mV and ZIF-67-derived Co-carbon corresponding to 180 mV. Compared with Mo_2N and Co, the hybrid also shows enhanced OER activity. Therefore, Co-Mo_2N can be used as the anode and cathode of the integral water splitting cell with overpotential (η) of 1.576 V. The increase in HER activity may be attributed to the close contact of Co and Mo_2N that optimizes the adsorption of reagents, the tubular structure which makes mass transfer easier, and Mo_2N with good conductivity which is conducive to

charge transport. These features are conducive to the improvement of water splitting catalytic activity.

In the field of catalysis for overall water splitting, researchers have obtained many MOF-derived catalysts, such as monometals, monometallic compounds, bimetallic alloys, and bimetallic compounds, through structural design, functional modification, and preparation of composite materials. And these catalysts exhibit excellent performance during the catalytic process. However, MOF-based catalysts for water splitting, especially single-atom, still lack satisfactory research results, and further use of the structural advantages and tunable characteristics of MOF to design and develop catalysts still faces challenges.

5.3 MOF-Derived Materials for HER

The study of hydrogen evolution reaction (HER) is very important in renewable energy technology and will determine the quality distribution of hydrogen-powered clean technology in the future. Electrolytic water splitting is an effective and environmentally friendly method of producing hydrogen. Electrocatalytic HER can be carried out in acidic (usually 0.5 M H_2SO_4 or $HClO_4$) and alkaline (usually 1 M KOH) electrolytes, but the reaction mechanism is different. The reaction processes of hydrogen evolution under different conditions are as follows:

Alkaline conditions:

$$2H_2O + 2e^- \rightarrow H_2 + 2OH^-$$

Acid conditions:

$$2H^+ + 2e^- \rightarrow H_2.$$

Under standard conditions, the theoretical electrolytic cell voltage for water splitting is 1.23 V. However, since kinetic barriers appear in both HER and OER, a larger working voltage is required to activate the reaction. The most important factor that causes high kinetic obstacles to water splitting is the instinctive catalytic activity of HER or OER catalysts. As a well-known HER high-efficiency catalyst, Pt has high current density and low Tafel slope in the HER[10]. However, its low abundance and high cost limit its application on an industrial scale. Therefore, while pursuing high catalytic performance under low platinum loading, researchers are also committed to finding non-noble metal-based HER catalysts.

The recent applications of pristine MOFs and their derivatives in various hydrogen production technologies have also attracted a large number of researchers' attention. MOF-based materials have unique advantages, such as high specific surface area, crystalline porous structure, and diverse and tunable chemical composition [5]. These advantages endow MOF-based materials very attractive function in the process of catalyzing hydrogen release by reducing the reaction potential and accelerating the reaction rate. MOF used as a HER catalyst mainly relies on the metal catalytic

active sites inside (Ni, Fe, Co, Mn, Mo, etc.) [23, 24]. In order to expose more electrocatalytic active sites, constructing nano-2D/3D MOF to increase its surface area is an effective way to enhance the performance of HER catalyst [25]. In this section, we will review the researches of MOF-derived metal single atoms, metals, alloys, and other transition metal compounds (oxides, nitrides, sulfides, phosphides, etc.) in this field.

5.3.1 MOF-Derived Metal Single Atoms for HER

Due to its almost 100% metal utilization rate, excellent catalytic performance, and good recyclability, single-atom catalysts have become a new field of catalysis related to energy conversion in recent years. Unsaturated coordination environment and unique electronic structure endow single-atom catalysts with excellent catalytic performance. MOF-derived materials usually inherit most of the characteristics of MOF and have the same advantages of high porosity and high metal loading as MOF, which is conducive to effective mass transfer and full exposure of active sites in the catalytic process. In addition, compared with other synthetic single-atom catalyst synthesis systems, the MOF-based synthesis strategy can easily achieve the uniform/precise metal doping at the atomic level and maintain the porosity in the catalyst, which will greatly improve catalytic activity of prepared catalysts. MOF-derived single-atom catalysts have received great attention in the past few years. With the help of the spatial separation of MOF, atomic-level catalytic sites at a certain distance between each metal center can be dispersed. During the pyrolysis process, the migration of metal atoms will be greatly inhibited, thereby obtaining a single-atom catalyst. However, although MOF-derived materials have great advantages in the preparation of single-atom catalysts, they are mostly used in carbon dioxide reduction reactions (CO_2RRs) and oxygen reduction reactions (ORRs). For water splitting and its two half reactions, HER and OER, related studies are very limited.

The framework derived from MOF can encapsulate catalytic sites and play an irreplaceable role in constructing highly efficient HER catalysts. As transition metals, tungsten and tungsten-based materials (WC_x, WN_x, WP_x, WS_x, etc.) are considered as attractive candidates to replace the noble metal Pt-based catalysts in electrocatalytic HER. However, the practical application of W-based HER electrocatalysts still faces various challenges. How to enhance its activity and long-term stability in the HER process is a bottleneck that is difficult to break in the research of W-based HER catalysts. Cheng et al. supported the single W atom catalyst on nitrogen-doped carbon (W-SAC) derived from a metal–organic framework (MOF), which can perform an efficient electrochemical hydrogen production reaction with high activity and excellent stability (Fig. 5.3a) [26]. High-angle circular dark-field scanning transmission electron microscopy (HAADF-STEM) and X-ray absorption fine structure (XAFS) spectroscopic analysis show that W species are dispersed atomically (Fig. 5.3b and c). In 0.1 M KOH solution, W-SAC shows a low overpotential of 85 mV at a current

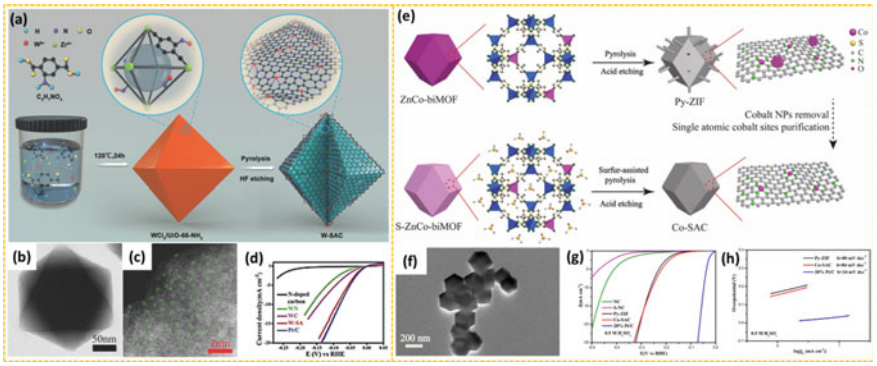

Fig. 5.3 **a** HAADF-STEM image of the W-SAC. **b** Tafel plots of the W-SA and other catalysts. **b–c** TEM characterizations of the W-SAC at different magnifications. **d** HER polarization curves for the W-SAC. The polarization curves were recorded at 5 mV s^{-1}. **e** Illustration of the coupled evolution of single-atom cobalt sites and metallic cobalt sites and their decoupling process. **f** The TEM images of Co-SAC. **g** The LSV curves of catalysts NC, S-NC, Py-ZIF, Co-SAC, and 20%Pt/C in nitrogen-saturated 0.5 M H_2SO_4. **h** The corresponding Tafel slopes of different catalysts in nitrogen-saturated 0.5 M H_2SO_4

density of 10 mA cm^{-2}, and the small Tafel slope at 53 mV dec^{-1} (Fig. 5.3d). The HER activity of W-SAC is almost equal to commercial Pt/C. Density functional theory (DFT) calculations indicate that $W_1N_1C_3$ anchored on the MOF-derived nitrogen-doped carbon framework may be the active site and plays an important role in enhancing HER performance. People have been committed to the research on the structure design of MOF-derived catalysts and metal site binding. However, the key catalytic process which dominates the catalytic performance related to the metal sites in the MOF-derived catalyst is still unclear. Chen et al. demonstrated the coupling evolution of single-atom cobalt sites and Co@CaN sites in the pyrolysis of Zn/Co bimetallic metal–organic framework (ZnCo-biMOF) (Fig. 5.3e and f) [27]. The removal of metal particles by the sulfur assistant site purification strategy does not cause a decrease in ORR and HER activity, indicating the main catalytic effect from atomic cobalt sites. The optimized catalyst exhibits excellent ORR and HER performance, which is close to the commercial 20% Pt/C catalyst under the same conditions (Fig. 5.3g and h).

5.3.2 MOF-Derived Metals and Alloys for HER

In the exploration of non-noble metal-based HER catalysts, transition metals (such as Ni, Co, W) have attracted attention due to their favorable electronic structure. A large number of transition metal materials have been designed as high-performance HER electrocatalysts in acidic, neutral, or alkaline media. MOF derivatives play a variety of roles in the process of constructing catalysts and further application for HER, such

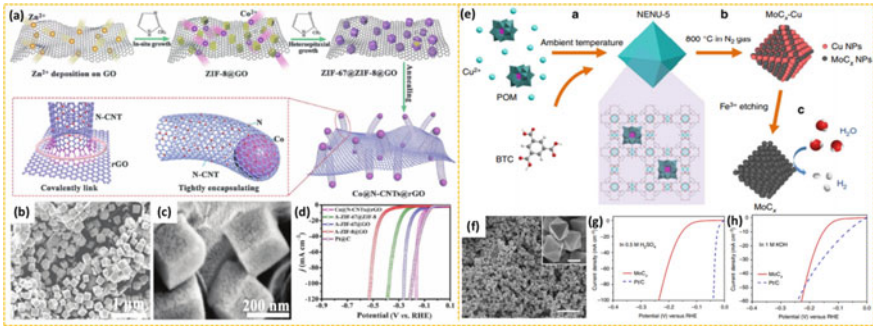

Fig. 5.4 **a** Synthetic procedure for the preparation of Co@N-CNTs@rGO hybrid composites. **b–c** TEM image of the representative ZIF-67@ZIF-8@GO composites. **d** LSV curves at the current density of 10 mA cm^{-2} of Co@N-CNTs@rGO, A-ZIF-8@GO, A-ZIF-67@GO, and A-ZIF-67@ZIF-8 electrodes. **e** Schematic illustration of the synthesis procedure for porous MoC_x nano-octahedrons. **f** FESEM image (inset: magnified image; scale bar, 500 nm) of the as-prepared NENU-5 nano-octahedrons; scale bar, 5 mm. **g** Polarization curve at 2 mV s^{-1} in 0.5 M H_2SO_4. **h** Polarization curve at 2 mV s^{-1} in 1.0 M KOH

as encapsulating catalytic sites and metal sites in their framework as grafted sites and as precursors for framework formation. Among MOF-derived metal catalysts, MOF mainly exists as a precursor that becomes a carbon matrix after pyrolysis. The morphology of the electrocatalyst can also be adjusted by the morphological design of the MOF precursor or the morphological evolution during/after pyrolysis. Fang and his co-workers used GO-coated core–shell (Co, Zn)-bimetallic ZIF as the precursor and produced the embedded in situ N-doped CNTs-grafted ultra-fine Co nanoparticles in graphene sheets by thermally inducing the reduction and carbonization of the ZIF-67@ZIF-8@GO precursor simultaneously (Fig. 5.4a–c) [28]. Due to the synergistic effect of the resulting catalyst, large surface area, and high porosity, Co@N-CNTs@rGO has highly exposed active sites and enhances diffusion kinetics and mass transfer. The electrochemical characterization proved that the composite material can reach 10 mA cm^{-2} at low potential of only 108 and 87 mV in 1 M KOH and 0.5 M H_2SO_4, respectively, which is far better than most reports of Co-based electrocatalyst in a wide pH range (Fig. 5.4d). MOF-derived metal catalysts usually face the problems of aggregation of metal particles, poor contact between the metal and the substrate, and insufficient exposure of active sites. In addition to the above-mentioned grafting, GO sheet wrapping, etc., it can also be solved by using MOF-derived matrix structure to restrict the catalytic species. Starting from a compound composed of a copper-based metal–organic framework host and a molybdenum-based polyoxometalate guest, Wu and his workers successfully prepared mesoporous molybdenum carbide nano-octahedra composed of ultra-fine nanocrystals [29]. This synthesis strategy relies on the in situ and limited carburization reaction between the organic ligand of MOF (or its derived carbon-based substance) and the guest polyoxometalate (POM) residing in the pores of the MOF host (Fig. 5.4e and f). The introduction of guest metal species as co-precursors into the MOF host can easily synthesize

early transition metal (such as Mo, W, and V) carbides. The carburizing process will be limited to the carbonaceous matrix derived from MOFs organic ligands, which effectively prevents the agglomeration and coalescence of the carbide nanocrystals generated in situ. Thanks to its porous, solid structure and ultra-fine primary nanocrystals, the prepared molybdenum carbide nano-octahedrons have excellent HER electrocatalytic activity under acidic and alkaline conditions (Fig. 5.4g and h).

The metal–organic framework with designable metal ion centers and organic ligands as a precursor provides a very promising opportunity for the one-step synthesis of alloy@carbon materials. By changing the metal ion center (such as Fe, Co, Ni, Cu) and designing organic ligands with different dopants (N, P, S atoms), various alloys covered with doped graphene layers are obtained from the MOF precursors, which may be a promising HER catalyst. Elements with CN groups as connections and transition metals (Fe, Co, Mn, etc.) as metal nodes, Prussian blue analogues (PBA) are rich in nitrogen and can be used as ideal precursors for non-noble metals to produce carbon with high nitrogen doping rate. Based on these findings, Yang et al. synthesized FeCo alloy nanoparticles by directly annealing MOFs nanoparticles in N_2, which were wrapped in a high nitrogen-doped (8.2%) graphene layer [30]. At 10 mA cm^{-2}, the synthesized catalyst showed a low initial overpotential (88 mV), and the overpotential was only 262 mV. In addition, due to the protection of the graphene layer, it has excellent long-term durability even after the 10,000th cycle. This kind of stability is rarely seen or reported in non-noble metal HER catalysts in acidic media. Density functional theory (DFT) calculations show that nitrogen dopants can provide adsorption sites for H*, and an appropriate increase in nitrogen will reduce the $\triangle G_{H^*}$ of HER. In addition, the unique structure of the MOF-derived metal and graphene composite material can also reduce $\triangle G_{H^*}$, thereby improving catalytic activity.

Obtaining MOF-derived carbon-based metal catalysts under suitable temperature and inert atmosphere is the current research hotspot of MOF derivatives in the field of catalysis. The simple synthesis method and good electron transfer ability make it possible that a large number of experiments and reasonable designs can be developed to obtain improved catalytic performance and stability. However, the true catalytic sites of MOF-derived metal-based catalysts have always been controversial, and people are still committed to the pursuit of the definite answer. For MOF-derived metal alloys applied to HER, due to the strong synergistic catalysis between metal nanoparticles, the catalytic activity of the reaction can be significantly improved. However, there are not many studies on MOF-derived metal alloys. And the type of the object of study, metal alloy nanoparticles, is limited. The main problems faced also exist in the efficiency and stability of the catalyst. It is crucial to improve the activity and durability of the catalyst further and increase the composition ratio control and design of the involved metals for future research in this field [31].

5.3.3 MOF-Derived Other Compounds for HER

In addition to rational and effective design of MOF-derived transition metal catalysts to improve performance, doping heteroatoms (P, S, Se or Te, etc.) to obtain phosphides or sulfides to adjust metal active sites and/or MOF-derived heteroatom–carbon hybrids are also an excellent strategy for the design and synthesis of excellent HER electrocatalysts [32]. Thanks to the diversity of MOF, MOF-derived nanomaterials can interact with ultra-fine catalytic particles or atoms anchored on a carbon matrix to synthesis metals and metals/metal oxides/hydroxides, carbides, chalcogenides, phosphides, nitride, phosphate, or their hybrid. Moreover, introducing heteroatoms into the carbon material to form a real catalytic substance is an important strategy for adjusting the electron density of the catalytic metal site to enhance the synergistic effect between the active substance and the heteroatom-doped carbon matrix. In addition to heteroatom doping, MOF-derived transition metal oxides are also widely used in the field of energy conversion. A large number of studies based on transition metal oxide catalysts have been reported for the reaction process of HER. Wei et al. prepared for the first time a new bifunctional catalyst NiO/Co_3O_4 concave microcubic (NCMC) derived from $Ni_3[Co(CN)_6]_2$ precursor. Under alkaline conditions, this catalyst shows excellent and effective catalytic performance for HER and OER [19]. First, uniform precursor $Ni_3[Co(CN)_6]_2$ microcubes were prepared by precipitation reaction at room temperature, and then the collected microcubes were gradually calcined in an air atmosphere to obtain NCMC. Finally, a hollow concave microcube composed of carbon-doped Ni-Co mixed metal oxide was prepared. To provide HER with a current density of 10 mA cm^{-2}, NCMC shows an overpotential of 169.5 mV and has good cycle stability. The excellent activity and stability of the catalyst is mainly attributed to the unique hollow structure, which can greatly improve the permeability of the electrolyte, which is conducive to the reaction kinetics process. The carbon introduced by the catalyst can improve the conductivity of NCMC, and it is also favorable to charge transfer of the HER process. Combining NiO and Co_3O_4 into a microcube may have a synergistic effect on water splitting and provide more active sites for the electrocatalytic process. In addition, the unique concave structure of the resulting NCMC catalyst can provide electrolytes with more contact area, thereby improving its catalytic activity. Although the HER performance achieved by this catalyst is inferior to that of the Pt/C catalyst, it is better than most non-noble metal and HER catalysts.

In recent years, transition metal phosphide (TMP) has a catalytic mechanism similar to hydrogenase, so it is regarded as a very promising type of HER catalyst. But for the reaction process of TMP for HER, hydrogen and TMP bind strongly. In addition, the final conversion to TMP requires high-temperature calcination, but this will damage the original MOF structure and cause agglomeration of metal centers. Therefore, people have extensively studied doping cations or anions as an effective strategy to transform its electronic structure and optimize the free energy of hydrogen adsorption (ΔG_{H^*}) to further enhance its HER performance. However, since it is difficult to control the type, amount, and dispersion of dopants, the methods that

have been reported often have limitations. Through reasonable design, the hybrid catalyst that combines TMP and MOF can not only have the best ΔG_{H^*}, but also use MOF to define a well-defined porous structure, both of which are beneficial to HER performance. Liu et al. reported a controlled partial phosphating process to create CoP species in Co-MOF, resulting in a CoP/Co-MOF hybrid nanostructured CoP/CoP/CoP with large electrochemically active surface area (ECSA) and high electrolyte/mass diffusion rate [33]. Co-MOF hybrids are synthesized on carbon fiber (CF) paper. These processes include the hydrothermal deposition of Co(OH)F, the reaction with imidazole vapor to convert Co(OH)F to Co-MOF, and the reaction with sodium hypophosphite to achieve partial phosphorylation (Fig. 5.5a and b). DFT calculations and experimental results show that the transfer of electrons from CoP to Co-MOF through the NP/N-Co bond can lead to the best adsorption energy of H_2O ($\Delta G_{H_2O^*}$) and hydrogen (ΔG_{H^*}). Together with Co-MOF's unique porous structure, above-mentioned advantages can significantly improve HER performance. In 1 M phosphate buffer solution (PBS, pH = 7.0), the overpotential is 49 mV at a current density of 10 mA cm^{-2}. The excellent catalytic performance surpasses almost all recorded electrocatalysts based on TMP and non-noble metals. In addition, when the current density is 10 mA cm^{-2}, the CoP/Co-MOF mixed solution and 1.0 M KOH and 0.5 M H_2SO_4 electrolyte show Pt-like catalytic performance of 27 and 34 mV, respectively (Fig. 5.5c).

Cobalt has the best HER catalytic performance as a transition metal, and the combination of its phosphide and other metal compounds may achieve better catalytic performance than the corresponding single-component catalyst. Luo et al. successfully prepared a new one-dimensional N-doped graphitic carbon-supported hybrid

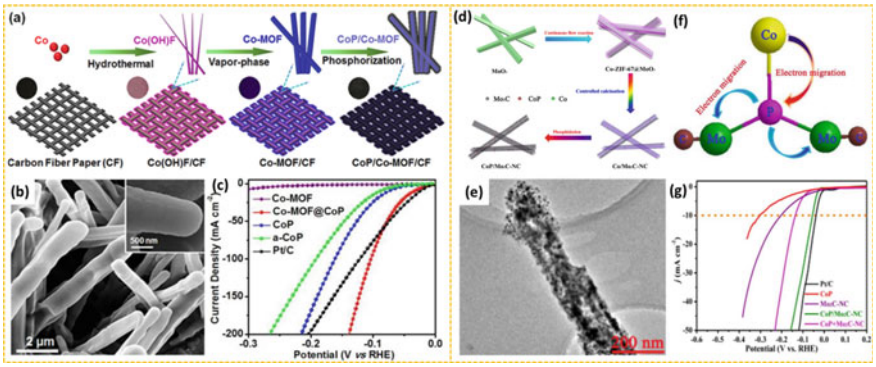

Fig. 5.5 **a** Schematic of the fabrication process of CoP/Co-MOF. **b** Scanning electron microscopy (SEM) image of CoP/Co-MOF. **c** LSV curves in 1 M KOH of Co-MOF, CoP/Co-MOF, CoP, a-CoP, and Pt/C. **d** Schematic illustration of the fabrication of the CoP/Mo_2C-NC. **e** TEM of CoP/Mo_2C-NC. **f** Schematic illustration of the electron immigration between CoP and Mo_2C. **g** HER polarization curves of the CoP/Mo_2C-NC, CoP + Mo_2C-NC, Mo_2C-NC, CoP, and the commercial Pt/C (20 wt %) in 0.5 M H_2SO_4 solution

electrocatalyst composed of Mo-based carbide and Co-based phosphide (CoP/Mo_2C-NC) (Fig. 5.5d and e) [34]. A simple continuous flow method and post-heat treatment process define the nanostructure and larger specific surface area. Due to the electronegativity between Co^{2+} and Mo^{x+}, a new Co–P–Mo chemical bond is formed between Co^{2+} and Mo^{x+} at the interface (Fig. 5.5f). The strong chemical coupling between CoP and Mo_2C triggers the migration of the cobalt electron cloud in CoP/Mo_2C-NC to Mo, which leads to the formation of a high valence state of Co^{3+} and a lower valence state of Mo (i.e., Mo^{2+}, Mo^{3+}). Providing abundant HER active sites, which in turn results into the optimization of hydrogen bonding and HER kinetics (Fig. 5.5g).

In addition to oxides and phosphides, other transition metal compound materials have been reported for the catalysis of HER. Among non-precious metal-based catalysts, Ni-based catalysts have been extensively studied by researchers. Among them, nickel nitride has been studied and found to have more active sites, and it has the potential for faster charge carrier transport and good catalytic performance. But its uncontrolled structure affects its further application and performance improvement in the field of catalysis. Mei et al. successfully synthesized nickel nitride on a novel MOF-derived nickel catalyst from nickel foam at different temperatures (300, 350, 400 °C) (denoted as C–T, T = 300, 350, 400) (Fig. 5.6a and b) [35]. Compared with other materials, C-350 is proved to have higher catalytic performance for HER, with a low overpotential of 47 mV at 10 mA cm^{-2} (Fig. 5.6c). In addition, the current density can be maintained for at least 24 h, showing its potential in practical applications. Transition metal selenide exhibits excellent electrochemical reaction performance due to its abundant redox active sites, larger effective specific surface area, and shorter ion diffusion path. A large number of studies have shown that transition metal selenides and their composites exhibit extremely high reactivity to water splitting electrocatalysis, which can be used for the preparation of clean hydrogen energy. Zhou et al. synthesized $CoSe_2$ nanoparticles embedded in defective carbon nanotubes ($CoSe_2$@DC) through the carbonization–oxidation–selenization process

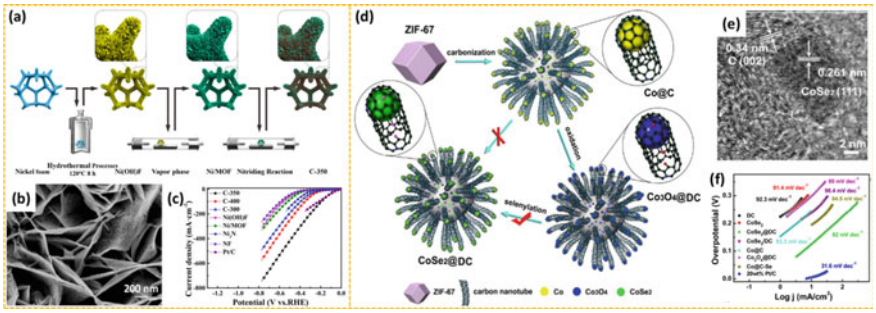

Fig. 5.6 **a** Schematic of C-350 preparation process. **b** SEM of C-350. **c** LSVs of C-350 in 1.0 M KOH, 1.0 M KOH with 0.5 M urea, and 0.5 M urea. LSV. **d** Schematic illustration of the synthetic procedure for $CoSe_2$ @DC. **e** TEM images of $CoSe_2$@DC. **f** The Tafel plots of DC, $CoSe_2$, $CoSe_2$/DC, $CoSe_2$@DC, and 20 wt% Pt/C

of cobalt-based MOFs (Fig. 5.6d and e) [36]. According to comparative experiments, the pre-oxidation treatment before the selenization process is a key step to introduce more and more defects into the carbon nanotubes, which promotes the reaction between Co@carbon and selenium and enhances the HER performance. The hierarchical structure composed of carbon nanotubes derived from Co-MOF results in a large electrochemical surface area and more HER active sites. In addition, $CoSe_2$ nanoparticles are partially embedded in defective carbon nanotubes. Therefore, on the one hand, the active sites of $CoSe_2$ nanoparticles can be exposed in the electrolyte and contribute to HER. On the other hand, the electronic density state of carbon is adjusted through nonmetal doping and transition metal compounds, which introduces the additional catalytic activity of the carbon shell. Thanks to the synergy between the $CoSe_2$ core and the defective carbon shell, the prepared $CoSe_2$@DC exhibits excellent HER activity with high current density and strong catalytic stability. The initial potential is only 40 mV vs RHE, and the Tafel slope is 82 mV dec^{-1} in 0.5 M H_2SO_4 (Fig. 5.6f).

The research of MOF and its derivatives as an electrocatalyst synthesis platform has promoted the emergence of various novel and highly active carbon-based electrocatalysts, such as defective carbon nanotubes, carbon nanosheets, and grafted structures. Based on the previous summary, we can find that MOF is mainly used as a precursor by pyrolysis in an inert atmosphere during the synthesis of products that can replace precious metal-based HER catalysts. During the pyrolysis process, the organic part of the MOF precursor is converted into carbon materials. At the same time, the metal part evaporates at high temperatures or remains in the carbon matrix in many possible forms, including atomically dispersed sites and metal-containing nanoparticles. By selecting a suitable MOF precursor, a carbon-based or metal-based active material for HER electrocatalysis can be obtained from the MOF-derived carbon-based material. In addition, the composition of the electrocatalyst can be further adjusted by introducing additional precursors or treatment after pyrolysis. The morphology of the electrocatalyst can also be adjusted by the morphological design of the MOF precursor or the morphological evolution during/after pyrolysis. Through these methods, most commonly used research active materials for ORR, OER, and HER electrocatalysis have been obtained from the pyrolysis of MOF. They have good morphology, can be used for electrocatalysis of gas escape, and show top performance.

Looking to the future, the development of MOF and its derivative materials for HER electrocatalysts is still in progress, with both opportunities and challenges. In order to realize the practical application of these electrocatalysts in energy devices, it is necessary to further reduce the overpotential and improve the stability. The following strategies can be considered to further improve the performance of MOF derivatives for HER catalysis: (1) In order to increase the exposed active sites, reasonable control can be used to reduce the particle size of the metal or metal compound on the MOF to nanometer or even atomic level. (2) The strategy of doping transition metals (such as Fe, Co, and Ni) and nonmetals (such as N, P, S, and Se) shows effective performance improvement, indicating that it has high research value. (3) Based on the study of bimetal or multimetal, MOF can find that the synergy between metal

elements and derivatives can reduce the HER energy barrier, thereby improving the electrocatalytic activity. However, the controllable synthesis of bimetal or multimetal MOF with adjacent different metal ions is still a challenge. (4) The low conductivity of MOF has always been a defect that hinders the improvement of its catalytic performance. Choosing a conductive organic linker with conjugated bonds to construct a conductive MOF and reducing carbon defect sites are two possible and effective ways to improve its conductivity.

5.4 MOF-Derived Materials for OER

As another half reaction of water splitting, oxygen evolution reaction (OER) has attracted widespread attention. High-efficiency electrocatalysis for oxygen evolution is very important for various energy-related processes. The reaction process of oxygen evolution reaction is as follows:

Alkaline condition:

$$4OH^- \rightarrow O_2 + 2H_2O + 4e^-$$

Acid condition:

$$2H_2O \rightarrow O_2 + 4H + + 4e^-$$

Since the four-electron–proton coupling reaction requires higher energy to decrease the kinetic barrier, higher energy is required to activate the reaction during the water splitting process, which affects the progress of HER. Therefore, high-efficiency electrocatalysts used in OER can greatly promote the development of energy conversion technology. RuO_2 and IrO_2 as noble metal-based electrocatalysts have been extensively researched and developed due to their high electrochemical activity for OER. However, resource shortage and high cost are the main obstacles to their practical application. Therefore, there is an urgent need to design and construct non-noble metal-based catalysts with abundant resource and high electrochemical performance [37]. In the way to achieve this goal, some progress has been made in the research of catalysts used under alkaline conditions. However, under acidic conditions, transition metals tend to lose outer electrons, resulting in higher overpotential and the poor stability, which make it difficult to approach the corresponding performance of ruthenium-based and iridium-based catalysts under acidic conditions. Therefore, the exploration of OER catalysts under acidic conditions is still a research hotspot [38].

The reports that have appeared also indicate that MOF and its derivatives also have excellent performance in the field of OER catalysis. However, the main problem lies in the poor stability of MOF in the catalytic process. In addition, most related studies will go through the process of pyrolyzing MOF crystals to obtain carbon-based materials. This step often faces a significant reduction of the surface area of the MOF. And the pore/channel structure may be also destroyed, which hinders the

entry of reactants. Therefore, the application of MOF and its derivative materials in OER still has much unknown area waiting to be explored. Due to the need to increase the OER reaction rate, the application of MOF derivatives in OER has attracted more attention than HER.

Similar to HER, the application of MOF derivatives in OER catalysis can also be divided into metal-derived carbon-based materials and metal compound materials (such as oxides, phosphides, and sulfides) [39]. Very few studies are devoted to obtaining MOF-derived single-atom catalysts. Therefore, this section mainly reviews the research progress of MOF derivatives for OER catalysis based on the first two categories.

5.4.1 MOF-Derived Atomically Dispersed Material for OER

The activity of the electrocatalyst strongly depends on the number of active sites, which can be increased by reducing the size of the electrocatalyst. Due to the atomic-level active sites, single-atom catalysts have attracted special attention. However, research related to MOF-derived single-atom materials for HER, OER, and water splitting is very scarce. Due to its superior catalytic performance compared with other transition metals, cobalt is often used as a research object earlier in the process of exploring related new fields. In the study of single-atom-level catalysts for cobalt and its compounds, obtaining atomic-level CoO_x catalysts is a huge challenge. The cobalt-based metal–organic framework (MOF) possesses atomically dispersed Co ions, which stimulates a possible way to partially convert these Co ions into active atomic-level CoO_x species on-site, while retaining the high porosity of MOF. Wang and his colleagues applied O_2 plasma to treat ZIF-67 to form atomic CoO_x species (CoO_x-ZIF) in situ in ZIFs as an effective OER electrocatalyst (Fig. 5.7a) [40]. The porous structure of MOF provides the possibility for O_2 plasma to activate atomically dispersed Co species (Fig. 5.7b). In addition, plasma is highly efficient for a rapid treatment, which would not severely destroy the overall structure of the MOF during treatment. The CoO_x species obtained in ZIF-67 shows advanced electrocatalytic performance for OER, and the coupling of CoO_x-ZIF with the conductive support produces better activity than RuO_2 (Fig. 5.7c).

Controlling the size of the catalyst at the atomic level is a very promising way to improve the performance of the catalyst. Although the research results of SAC catalysts have appeared in the field of OER, it should be realized that these studies are still at an initial stage [41]. And the OER performance of SACs is still lower than other advanced OER catalysts, such as metal (hydrogen) oxides, which is far from meeting the requirements of industrial applications. The main reasons for this situation may be the low loading of metals and the limited coordination environment. The unique atomic-level dispersion structure of MOF provides an excellent precursor for the on-site atomic-level catalyst formation of OER. Theoretically, MOF itself is a single-atom-dispersed metal ion, while the low conductivity and fewer electrocatalytic active sites of MOF limit their application in electrocatalysts. Therefore, the

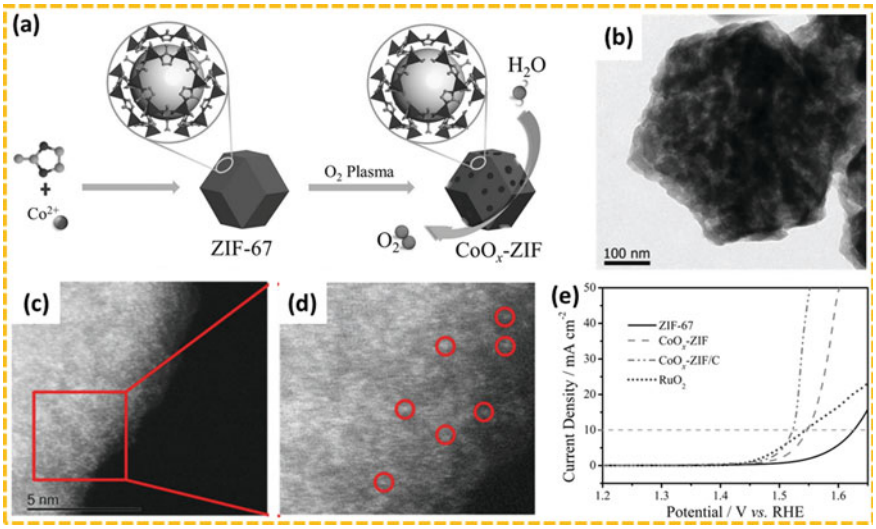

Fig. 5.7 **a** Preparation of CoO_x-ZIF. **b** TEM images of CoO_x-ZIF. **c** enlarged HAADF-STEM images of CoO_x-ZIF (the atoms of Co are marked by red circles). **d** LSV curves for OER on ZIF-67, CoO_x-ZIF, CoO_x-ZIF/C, and RuO_2

construction of uncoordinated metal sites is very important for the research of MOF derivatives in the field of single-atom electrocatalysis. In the research and exploration of MOF-derived atomically dispersed OER catalysts, broad prospects and unknown challenges coexist.

5.4.2 MOF-Derived Metal Materials for OER

Many transition metals have OER activity and are largely insoluble in alkaline electrolytes, for which efficient, alternative, homogeneous, and heterogeneous electrocatalysts have become a subject of intense focus. Due to their inherent characteristics, including large surface area, unique porosity, and tailorable functionality, MOFs with various types of catalytic sites can be used to construct homogeneous and heterogeneous catalysts. Although MOFs have abundant metal sites, few of them have been directly used for electrocatalysis due to their poor conductivity. It is reported that Ni-, Fe-, and Co-based MOFs are catalytically active for OER according to recent researches, while there is still much room for the MOFs with large sizes to improve their catalytic performances [42].

Cobalt-based MOF has obvious catalytic activity for OER, but the catalytic performance of large-size MOF still needs to be further improved. As an emerging kind of nanomaterial, ultra-thin 2D nanomaterials have been extensively studied by researchers. Therefore, in recent years, ultra-thin two-dimensional MOF nanosheets

have emerged as an attractive class of chemical and structural materials, but their applications in catalysis are very few. Xu and colleagues synthesized ultra-thin two-dimensional Co-MOF nanosheets from a mixed solution of Co^{2+} and phthalic acid (BDC) by a one-pot hydrothermal method (Fig. 5.8a and b) [43]. Due to its ultra-thin thickness and high accessibility of active sites exposed on the surface, two-dimensional Co-MOF nanosheets exhibit excellent electrocatalytic performance. Under alkaline conditions, the Tafel slope (74 mV dec^{-1}) of the ultra-thin two-dimensional Co-MOF nanosheet catalyst is lower than that of the micro–nano-Co-MOFs (94 mV dec^{-1}), and the bulk Co-MOFs (122 mV dec^{-1}) and RuO_2 (118 mV dec^{-1}), indicating that the ultra-thin 2D Co-MOF nanosheet catalyst has excellent OER kinetics. The obtained product exhibits excellent electrocatalytic activity for OER and has excellent and rapid electron/mass transfer capability. It only needs a low overpotential of about 263 mV to reach 10 mA cm^{-2} under alkaline conditions (Fig. 5.8c) and maintains good electrochemical stability within 12000 s, which is better than most previously reported catalysts based on MOF.

During the pyrolysis of MOF, carbon or an external reducing agent can reduce metal ions to metal or alloy nanoparticles, which is expected to provide excellent OER activity. Adjusting the type and proportion of metal ions in the MOF precursor can affect the composition of metal/alloy nanoparticles in the pyrolysis product. Unlike monometal-based MOF derivatives, metal atoms in metal/alloy nanoparticles with different compositions have different electronic structures, so MOF-derived bimetal and even multimetal-based catalytic materials exhibit different OER activities. Zou et al. prepared a Fe and Ni-based MOF (Fe_2Ni MOF) on nickel foam by a one-pot method. The MOF exhibited a loose nanosheet structure [44]. The interaction between the adsorbed OOH species and the transition metal 3d orbital is the key to determine the OER activity of transition metal-based materials. The bimetallic system accelerates the electron transfer between Fe^{3+} and Ni^{2+} through the oxygen of the ligand, thereby increasing the 3d orbital electron density of Ni. Fe_2Ni MOF

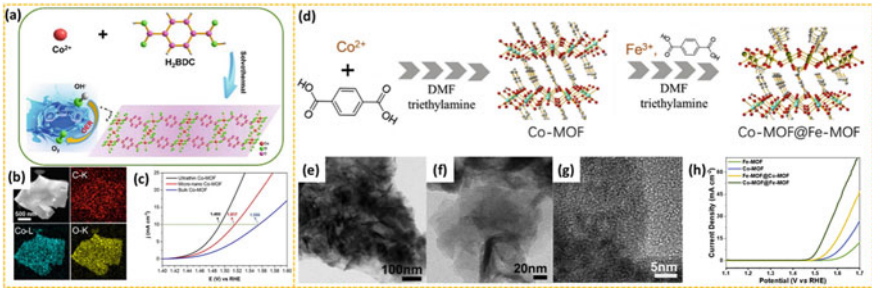

Fig. 5.8 **a** Schematic illustration of the synthesis of ultra-thin two-dimensional cobalt–organic framework (Co-MOF) nanosheet catalysts. **b** EDX elemental mapping images of C, Co, and O in the nanosheets. c Magnified polarization curves of ultra-thin 2D Co-MOF nanosheet, micro–nano-Co-MOF, and bulk Co-MOF materials. Comparative potentials at current densities of 10 mA cm^{-2}. **d** Schematic illustration for the synthesis of Co-MOF@Fe-MOF. **e**–**g** TEM images of Co-MOF@Fe-MOF. **h** LSV polarization curves toward OER in 1 M KOH with scanning rate of 5 mV s^{-1}

is different from other NiFe-MOFs. Firstly, the MOF is not just a mixture of Fe-MOF and Ni MOF, but a composite of Fe and Ni, so that electron transfer can be performed between Fe and Ni elements to improve OER activity. Secondly, the ligand of Fe_2Ni MOF is different from other NiFe-MOF, so it has a special morphology that can increase active sites. Finally, the success of the Fe_2Ni MOF/NF catalyst of the present invention is attributed to the synergy between MOF and NF. In particular, Fe_2Ni MOF/NF has better performance in OER compared with single-metal MOF materials (Fe-MOF/NF and Ni MOF/NF). It exhibits a low overpotential of 222 mV at a current density of 10 mA cm^{-2}, and the Tafel slope is 42.39 mV dec^{-1}.

In addition to bimetallic MOF composites, metal-based MOF hybrid systems can also exhibit excellent catalytic performance. It is generally believed that the high activity of IrO_2 and RuO_2 catalysts in OER is attributed to the moderate bonding of their intermediates, such as OH and O–O. By contrast, the adsorption energy of these intermediates on non-precious transition metals (e.g., Fe, Co, Ni) is too strong or too weak, making the catalytic activity of the catalyst relatively low. The coupling of iron and cobalt sites can adjust the bonding strength of these species on the metal sites, thereby obtaining enhanced OER activity. For FeCo-based bimetallic catalysts, Fe sites are the main catalytic active centers, while the main function of Co species is to provide a conductive network and synergistic effects of sites. Liu et al. used a step-by-step synthesis strategy to synthesize a hybrid MOF material composed of iron-based MOF and cobalt-based MOF, with graphene oxide nanosheets as an additive (Fig. 5.8d–g) [45]. The results show that the electrocatalytic activity of hybrid MOF materials for OER is higher than that of single-phase materials. The electrochemically inert Fe-MOF material on the surface of Co-MOF can significantly enhance the catalytic performance. In order to achieve a current density of 10 mA cm^{-2}, MOF based on mixed CoFe requires only 290 mV of overpotential in 1 M KOH (Fig. 5.8f) The catalytic activity can be maintained for a longer time, while the current density is only slightly reduced, indicating its good cycle stability. According to a series of characterization analysis, in the hybrid, the tightly packed Fe-MOF and Co-MOF nanosheets can expose more metal centers to achieve effective intermolecular synergistic interaction. The excellent OER activity of Co-MOF@Fe-MOF can also be attributed to the abundant formation of defects or voids during electrochemical activation to promote active site exposure. At the same time, the presence of graphene oxide nanosheets and carbon-based framework in MOF may also inhibit the agglomeration of active Co–Fe species.

Although many reported bimetal or multimetal MOF derivative catalytic materials exhibit certain advantages over single-metal catalysts, it is not just a simple hybridization or mixing of MOF-derived single-metal catalysts leads to better catalytic activity than that of the component of the MOF. Many factors, such as the ratio of the metal, the choice of the matrix, the form and structure of the catalyst, the synthesis method, and the solvent, will affect the activity of the non-monometallic catalyst [31].

5.4.3 MOF-Derived Other Compound Materials for OER

For certain metal-based active materials, including metal oxides, chalcogenides, nitrides, and phosphides, surface oxidation during OER can further enhance their OER activity. Due to the improved surface properties and electronic structure, TMP shows great OER catalytic activity. In general, TMP materials have lower electrical conductivity and smaller surface area, resulting in poor electrocatalytic performance. Generally speaking, under certain conditions, MOF-derived functional nanomaterials can retain part of the precursor characteristics with higher specific surface area and uniform element distribution. This inspired researchers to combine the favorable structure of MOF with TMP materials to construct effective catalysts. Some studies have used MOF materials as precursors to produce a series of TMP materials (CuP, CoP, NiP, FeP, NiFeP, etc.) for electrocatalysis. Xu et al. prepared Fe_3Co bimetallic MOFs with different compositions by a sodium hydroxide-assisted method. Through continuous carbonization and phosphorylation reactions, a series of MOF-derived multi-component products were synthesized (denoted as Fe_xCo_y-P/C) (Fig. 5.9a and b) [37]. Compared with the commercial RuO_2 catalyst, the obtained P-doped product has enhanced OER electrocatalytic performance in alkaline electrolyte (Fig. 5.9c). The characterization result proves that the Fe_xCo_y-P/C product made from Fe_xCo_y-P/C also shows a lower charge transfer resistance (the resistance of the charge transfer) R_{ct} than Fe_xCo_y/C product and the commercial RuO_2 catalyst, which is attributed to the increase in electronic conductivity in the presence of multi-component metal phosphides. In the process of preparing transition metal phosphides, the phosphating process uses an external phosphorus source, which is usually accompanied by the presence of toxic gas PH_3 and/or explosive white phosphorus, which is toxic and dangerous. Huang et al. [46] designed a novel and less toxic strategy for preparing TMP materials without adding external phosphorus sources. Appropriate P-containing ligands and transition metal salts were selected to synthesize a stable cage structure. And then with the P-containing MOF used as the precursor, 3D hollow barrel-shaped FeNiP/C-900 nanoparticles are easily obtained by $Fe(NO_3)_3$ etching and heat treatment (Fig. 5.9d). Furthermore, the bimetallic phosphide embedded in the carbon matrix is pyrolyzed at 900 °C (expressed as FeNiP/C-900), maintaining the shape of a hollow barrel precursor (Fig. 5.9e), having a high specific surface area, and exhibiting high efficiency. The OER electrocatalytic activity has a current density of 10 mA cm^{-2} at an overpotential of 229 mV. And the Tafel slope is only 74.5 mV dec^{-1} (Fig. 5.9f and g).

Transition metal oxides of MOF derivatives are the main research object in this field and have been widely used in energy conversion. Ma et al. prepared Co_3O_4 nanocrystals in an N-doped mesoporous graphitic carbon layer/multi-walled carbon nanotube (MWCNT) hybrid through the carbonization and subsequent oxidation process of a MOF based on carbon nanotubes (Fig. 5.10a and b) [47]. As a result, in an alkaline medium, the hybrid material catalyzes OER with an initial potential of 1.50 V (relative to the reversible hydrogen electrode) and an overpotential of only 320 mV to achieve a stable current density of at least 25 of 10 mA cm^{-2} (Fig. 5.10c).

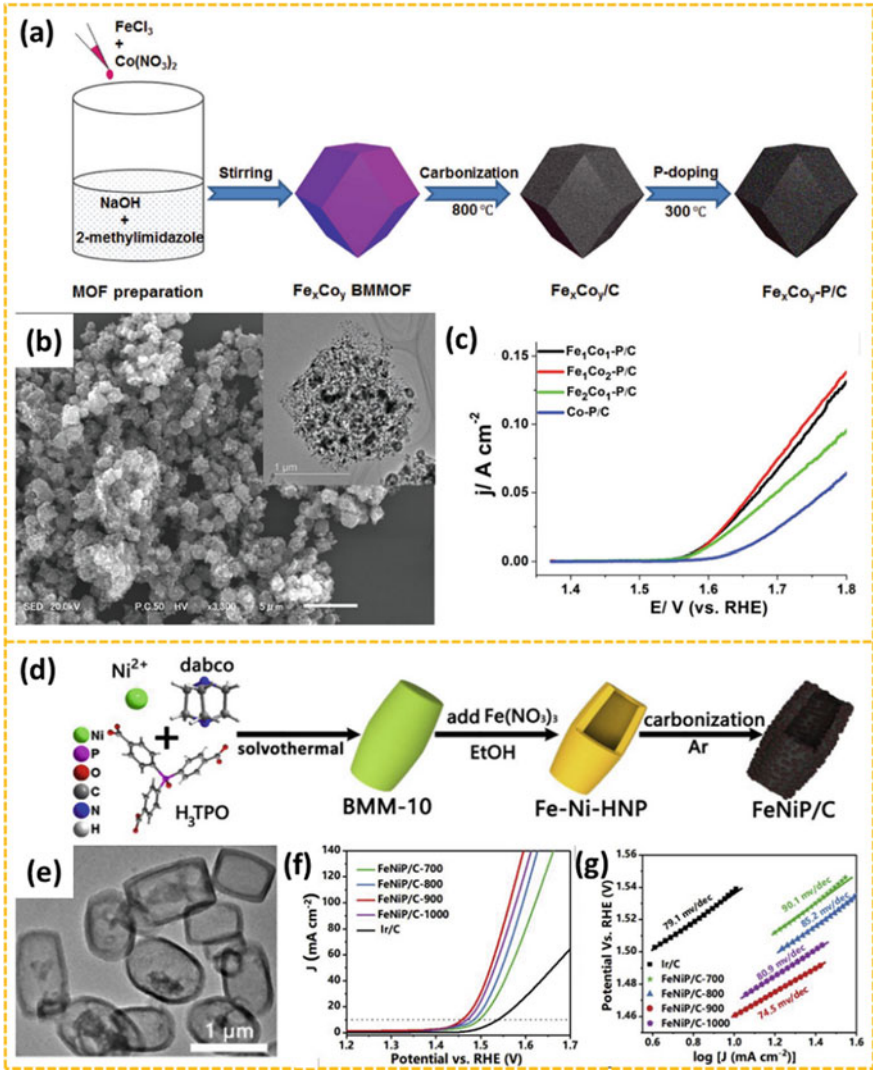

Fig. 5.9 **a** Synthetic process of the Fe_xCo_y-P/C. **b** SEM and TEM (inset) images of Fe_1Co_2-P/C. **c** LSV curves of the as-prepared Fe_xCo_y-P/C and CoP/C. **d** Schematic illustration of the synthesis of in situ MOF-derived bimetallic phosphide composite. **e** TEM images of Fe–Ni-HNP. **f** The OER polarization curves. **g** The corresponding Tafel plots at 1.0 V vs. scan rates of FeNiP/C-700, 800, 900, 1000 and Ir/C in 1.0 M KOH electrolyte

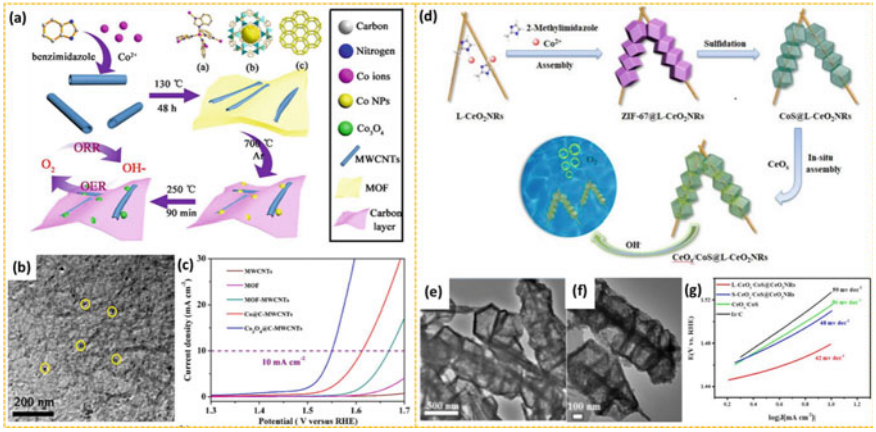

Fig. 5.10 **a** Schematic illustration on the synthesis of Co_3O_4@C-MWCNTs. **b** TEM image of Co_3O_4@C-MWCNTs. **c** LSV curves of MWCNTs, MOF, MOF-MWCNTs, Co@C-MWCNTs, and Co_3O_4@C-MWCNTs in an O_2-saturated 1.0 M KOH solution (scan rate 5 mV s^{-1}). **d** Fabrication of Ni_3 $[Co(CN)_6]_2$ microcubes and preparation of NCMC by heat treatment of the precursors at different temperatures. **e** The OER overpotentials of carbon paper, NCMC, and RuO_2 to achieve a current density of 10 mA·cm^{-2}. **f** Schematic illustration of the fabrication process of CeO_x/CoS@L-CeO_2NRs. **g** Schematic illustration of the synthesis of in situ MOF-derived bimetallic phosphide composite

Compared with oxides, metal sulfides have higher electrical conductivity, which are a new frontier in finding affordable, active, and stable OER catalysts. Recently, due to good catalytic performance, low cost, and structural stability, transition metal sulfides (TMS) have attracted great interest. In particular, S, which has high electronegativity in TMS, can extract electrons from transition metals and then can be used as an active site to stabilize reaction intermediates, thereby improving the efficiency of OER. Manthiram and his co-workers successfully prepared MOF-derived mixed metal sulfide catalyst (FeCoNi-S@ZIF) by combining cobalt, iron, and nickel into a MOF structure (ZIF-67) followed by a vulcanization process [48]. The onset potential to OER is about 1.56 V vs. RHE. Under the chronoamperometric test, the catalyst showed excellent stability. The study also found that through proper pretreatment and proper control of the synthesis temperature, the OER performance of the catalyst can be greatly improved, increasing the onset potential by approximately 100 mV (compared to RHE from 1.66 to 1.56 V).

Based on the extensive research on transition metal oxides and sulfides, people have also tried to combine the two to obtain hybrid catalytic materials with excellent catalytic performance. In the field of lattice strain engineering, MOF with unique dynamic characteristics becomes an ideal candidate material. Tang et al. stringed together a single CeO_x/CoS unit derived from MOF with CeO_2 nanorods (NRs) through an ingenious strategy of simultaneously engineering lattice strain and high-energy interface (Fig. 5.10d) [49]. The homologous long CeO_2 nanorods (L-CeO_2NRs) were selected as hard templates to induce the nucleation and growth of

the prototype zeolite imidazole salt skeleton ZIF-67. After that, ZIF-67 was used as a sacrificial template to produce CeO_x/CoS@L-CeO_2N with a core–shell hybrid nanostructure similar to the riboshell form. The wire penetrating nano-cage structure similar to candied haws can achieve strong coupling between adjacent CeO_x and CoS units, improve electrical conductivity, and facilitate material transport and corresponding synergistic effects (Fig. 5.10e and f). The interconnection between adjacent CeO_x/CoS cells causes lattice strain, which in turn forms a large number of lattice distortions and lattice defects. This series of effects brings more available active sites to this special structure. Characterization data indicate that the synthesized catalyst can effectively promote OER process. In an alkaline environment, it can effectively catalyze water oxidation, with a low onset potential of 238 mV (at a current density of 10 mA cm^{-2}) and a low Tafel slope of 42 mv dec^{-1} (Fig. 5.10g), and it has considerable operational stability. The multifunctional MOF derivative with the shape of Chinese candied haws inherits the advantages of the MOF-derived CeO_x/CoS hybrid. The function of this material can be compared with or even surpassed most reported cobalt-based electrocatalysts and commercialized Ir/C catalysts.

To sum up, MOF-derived metal-based carbon materials and metal compounds have been widely used in the catalytic process of OER. Among metal-based carbon materials, in addition to single metals, bimetal and mixed-metal-based carbon materials are constantly studied and show excellent catalytic activity and stability. It was found that other elements in metal compounds could bring more active sites. Through reasonable structural design, optimization of synthesis process, and crystal engineering to induce lattice strain and generate high-energy interfaces, many effective strategies have been developed for the preparation of functional MOF derivatives. However, researches on the OER reaction under alkaline conditions still make up the majority. The transition metal-based catalysts applied under acidic conditions still need to be studied to replace the noble metal-based RuO_2 and IrO_2 and obtain cost-effective catalysts for industrial-scale applications.

5.5 MOF-Derived Materials for ORR

The increasing energy consumption and environmental degradation around the world have aroused great interest in the research of using green and efficient electrochemical technology to develop sustainable energy conversion and storage systems. Fuel cells and metal–air batteries have become highly anticipated electrochemical energy conversion devices due to their high energy density, excellent energy conversion efficiency, and low fossil fuel dependence. The performance of fuel cells and metal–air batteries depends on the oxygen reduction reaction (ORR) on the cathode, but the reaction is very slow in kinetics, so ORR electrocatalysts are needed to accelerate.

The ideal oxygen reduction reaction should be that O_2 is fully reduced to H_2O, and no intermediate product H_2O_2 is produced, because H_2O_2 will cause serious oxidation and corrosion problems under the excitation of catalysts (including Pt). But in fact, for most catalysts, a mixture of $2e^-$ and $4e^-$ often occurs. Therefore,

the $4e^-$ reaction selectivity of the catalyst has also become an important indicator for evaluating the quality of ORR catalysts. Similar to HER, at present, Pt-based catalysts are still ORR catalysts with the highest activity, the lowest overpotential, and the highest $4e^-$ reaction selectivity. However, the current low-Pt catalysts still do not meet the standards for industrial application in terms of total Pt dosage and intrinsic activity, which hinders their large-scale application in fuel cells and metal–air batteries. In addition to high cost, Pt-based catalysts also have many problems such as easy poisoning, aggregation, and poor durability. Therefore, the development of high-activity, low-cost, and stable ORR catalysts is of great significance to the practical application of fuel cell technology [50].

MOF derivatives, especially MOF-derived porous carbon nanomaterials, have been extensively studied as ORR electrocatalysts to solve the difficult problem of industrial application of Pt-based catalysts. The surface area and porosity of MOF-derived NPC nanomaterials play an important role in their catalytic performance for ORR. The best ORR performance of catalysts derived from MOF precursors is usually obtained by optimizing the porosity and surface area of those derived catalysts [51].

5.5.1 MOF-Derived Nonmetallic Carbon-Based Materials for ORR

Since the doping of nonmetallic heteroatoms (especially nitrogen) can adjust the intrinsic characteristics of functional carbon materials, such as internal microstructure and composition, electronic characteristics, and surface and partial electrochemical characteristics, it always leads to a lower oxygen adsorption energy barrier and activates or significantly improves the electrocatalytic activity of ORR. Therefore, nonmetal-doped carbon-based electrocatalysts show a huge research prospect for the development of ORR. Researchers have observed that carbon catalysts containing nitrogen materials involving carbon nanotubes (CNTs), graphene, and hollow carbon spheres show good electrical conductivity and high selectivity to ORR and serve as excellent nonmetallic electrocatalysts for ORR. This can be attributed to the inherent electronic properties derived from the conjugation between the graphene π system and the nitrogen lone pair of electrons. So that the carbon-based material exhibits good catalytic activity, low overpotential, and good electrochemical properties. In recent years, more and more researchers have prepared nonmetal-heteroatom-doped carbon-based materials using MOF as a template, applied them to the electrocatalytic reaction of ORR, and obtained satisfactory results.

Zhu et al. developed a MOF (ZIF-8)-derived N-doped porous carbon (NPC) nanomaterial as a highly active ORR catalyst, which not only enhances the exposure activity of NPC through the KOH activation strategy, and the surface defects are enhanced due to the expansion of the holes (Fig. 5.11a) [52]. Experiments show that KOH activation not only enlarges the pore size of ZIF-8-derived NPC nanomaterials

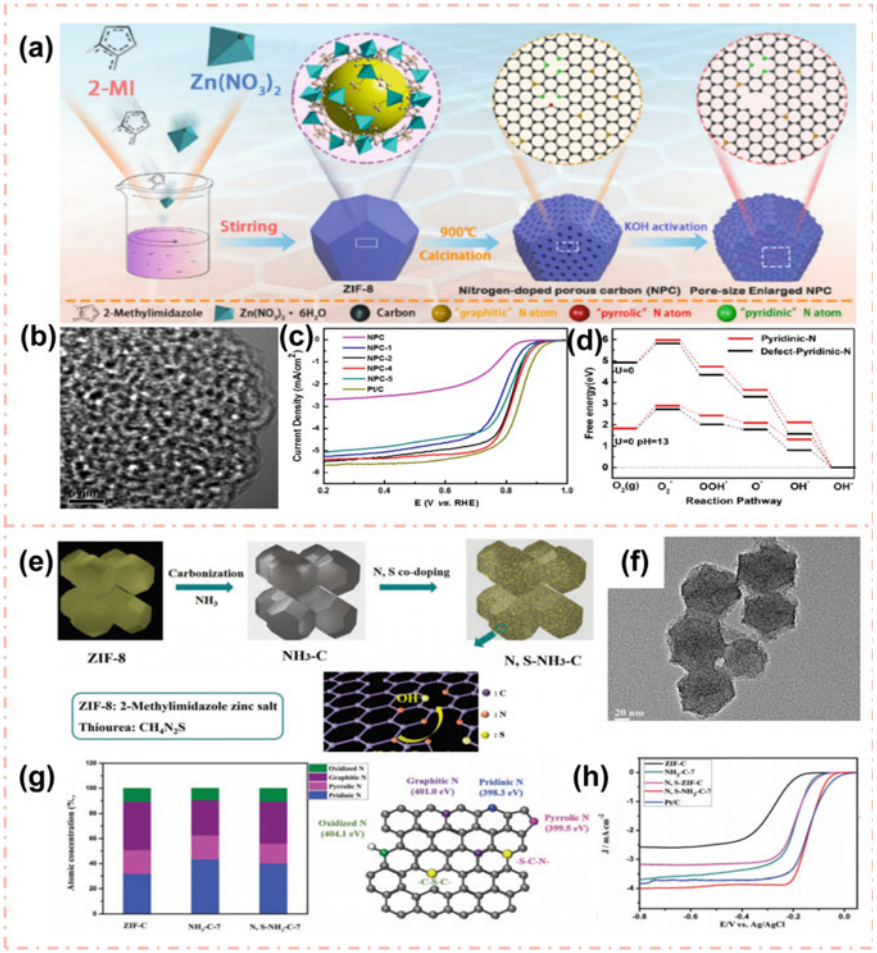

Fig. 5.11 **a** Schematic diagram of the synthesis of the pore size-enlarged NPC nanomaterials derived from ZIF-8 precursors. **b** High-resolution TEM images of the NPC-4 sample. **c** Linear sweep voltammograms of ZIF-8-derived NPC nanomaterial, KOH-activated ZIF-8-derived NPC nanomaterials, and Pt/C (20%) in O_2-saturated 0.1 M KOH solution at a scan rate of 10 mV·s $^{-1}$ with 1600 rpm. **d** Free energy of different N structures. **e** Schematic illustration of the fabrication of the N, S co-doped nano-carbon as the electrocatalyst toward ORR. The ZIF-8 precursor and thiourea are used as C/N and S precursors, respectively. **f** TEM image of N,S-NH_3-C-7. **g** Bar diagrams representing the atomic concentration of four kinds of nitrogen species (left); atomic structure of the N,S-doped nano-carbon with chemical bonding configurations of nitrogen and sulfur dopants (right). **h** Linear sweep voltammograms (LSVs) of ZIF-C (black), NH_3-C-7 (blue), N,S-NH_3-C-7 (red), and 20% Pt/C (cyan) in O_2-saturated 0.1 M KOH solution at 1600 rpm with a scan rate of 10 mV s^{-1} after background subtraction

and produces many mesopores, but also produces a large number of defects in NPC nanomaterials (Fig. 5.11b). MOF-derived NPC nanomaterials activated by 4 h in KOH (NPC-4) showed an activity of 0.257 mA cm^{-2} at 0.9 V vs. RHE, which is almost 10 times that of NPC nanomaterials (0.0265 mA cm^{-2}). Compared with the commercially available Pt/C, NPC-4 has comparable ORR activity, higher stability, and better tolerance to methanol. Moreover, compared with N-doped carbon, defective N-doped carbon is more beneficial to ORR, because the existence of defects will increase the O adsorption capacity and promote the ORR process (Fig. 5.11c and d).

When nitrogen is doped, other heteroatoms are added at the same time. Because nitrogen and other heteroatoms have a direct synergistic effect, they can jointly improve the electronic structure of the catalyst. Therefore, this co-doped carbon-based material can also be used as an electrocatalyst to improve the electrical conductivity and chemical properties of ORR. Sun et al. introduced the preparation of N and S co-doped nano-carbons derived from MOF precursors as electrocatalysts for ORR (Fig. 5.11e) [53]. The results show that the MOF-derived N, S co-doped nano-carbon has a higher specific surface area (2439.9 m^2 g^{-1}) and a porous structure (Fig. 5.11f). Importantly, compared with the commercially available Pt/C catalysts, the N and S co-doped nano-carbons exhibit higher catalytic activity for ORR, better long-term stability, and methanol tolerance. The calculation results show that the excellent electrochemical performance of nano-carbon co-doped with N and S is mainly due to the synergistic effect of N and S dopants. In addition, this work revealed for the first time that N, S coupled dopants in nano-carbon can produce active sites with higher ORR catalytic activity than separate N and S dopants (Fig. 5.11g and h).

The discovery of the relationship between structure and performance of nonmetallic heteroatom-doped/co-doped nano-carbon provides guidance for the design of high-performance electrocatalysts.

5.5.2 MOF-Derived Metal Single-Atom Dispersion Materials for ORR

Carbon-based catalysts with transition metals and nitrogen (M-Nx/C, M = Fe, Co, etc.) are one of the most promising alternatives to Pt-based catalysts. Because of its excellent ORR performance and rich ingredients, it has attracted widespread attention. It is generally believed that the high intrinsic activity (such as turnover frequency) of the active center in the M-Nx/C catalyst is mainly derived from the nitrogen coordinated single atom embedded in the carbon matrix, and its oxygen adsorption energy is close to optimization. In addition, the high specific surface area and good porous structure of M-Nx/C promote ORR performance by exposing a large number of active centers.

At present, Fe single atom is one of the single-atom catalysts most synthesized by researchers. Deng et al. reported a hollow carbon nanopolyhedral catalyst doped with N and a single Fe atom, which was prepared by pyrolyzing hollow ZIF-8 with iron

acetylacetonate and g-C_3N_4 [54]. The catalyst retains the polyhedral morphology of its precursor and only has the Fe-N_4 part promoted by g-C_3N_4 nitridation. The catalyst exhibits excellent ORR activity in both acidic and alkaline media. In addition, its ORR stability in acidic and alkaline media exceeds that of commercial Pt/C. Most notably, the catalyst exhibits ultra-high performance in H_2/O_2 proton exchange membrane fuel cells (PEMFCs). Lin et al. used an open framework platform with abundant chelating ligands to prepare a series of stable metal SAC [55]. The metal ions are first fixed on the active bipyridine site by post-synthesis modification and then undergo pyrolysis and acid leaching. Interestingly, it is found that each metal atom is coordinated to five N atoms, while the average coordination number reported previously is four. The prepared Fe SAC/N–C catalyst has excellent ORR activity (half-wave potential of 0.89 V), excellent stability, and good methanol tolerance. DFT calculation results show that the coordinated pyridine can well regulate the interaction strength of oxygen on Fe ions, thereby improving ORR activity. More importantly, it has been proven that this strategy can be successfully extended to the process of preparing other transition metal SACs, only by changing the metal precursor used in the metallization step.

When preparing atom-dispersed Fe–N-C catalysts, it is difficult to avoid the formation of iron clusters containing iron carbides (FexC/Fe) and the required carbon matrix containing dispersed FeNx sites. Therefore, an indeterminate amount of ORR occurs, making it difficult to maximize the catalytic efficiency. Therefore, Zhang et al. proposed to use sulfurization to improve the activity of FexC/Fe for ORR catalysis (Fig. 5.12a) [56]. In addition to its excellent activity in alkaline media, FeNC-S-FexC/Fe exhibits better ORR activity and durability in acidic media, its 0.821 V half-wave potential is better than commercial Pt/C catalysts (20%), and even after 10,000 cycles, its activity will not decay. Therefore, FeNC-S-FexC/Fe can be used as a high-performance ORR catalyst in zinc–air batteries. The FexC/Fe clusters and Fe-S and C–S–C bonds increase the original FeNx active centers (Fig. 5.12b–e). Similarly, Jin et al. prepared Fe, N, and S co-doped carbon matrix/carbon nanotube nanocomposites (Fe–N–S CNN) by pyrolysis of ZIF-8 impregnated with iron salts [57]. Benefiting from the synergistic effect of carbon matrix and nanotubes, abundant iron nitride, and thiophene-S active sites, Fe-NS CNN has excellent ORR performance, and the half-wave potential under alkaline conditions is 0.91 V vs. RHE. Under acidic conditions, it was 0.78 V vs. RHE, while commercial Pt/C catalysts were 0.85 V vs. RHE and 0.795 V vs. RHE, respectively.

In addition to Fe single atoms, Co single atoms can also be used in electrocatalysts to improve the electrochemical performance of ORR. Yin et al. reported a new strategy, which pyrolyzes the Zn/Co metal–organic framework at high temperature, evaporates Zn, and can achieve stable Co single atom on nitrogen-doped [58]. The obtained Co-Nx single center shows excellent ORR performance, its half-wave potential (0.881 V) is more positive than commercially available Pt/C (0.811 V) and most reported non-noble metal catalyst, and the metal loading exceeds 4 wt%. Surprisingly, the obtained Co-Nx single center shows excellent ORR performance, and its half-wave potential (0.881 V) is more positive than commercially available Pt/C (0.811 V) and most reported non-noble metal catalyst. The durability test shows

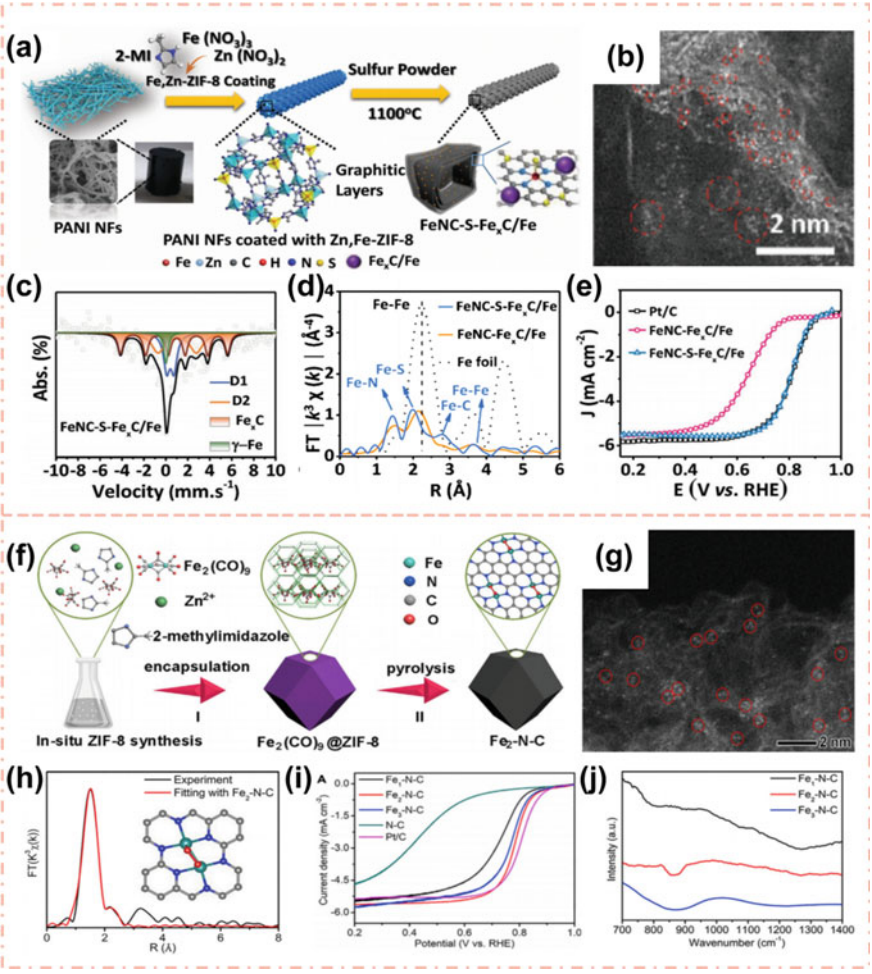

Fig. 5.12 **a** Synthesis scheme of the FeNC-S-FexC/Fe catalyst. **b** Atomically scaled HAADF-STEM image. **c** Room-temperature ^{57}Fe Mössbauer spectrum of FeNC-S-FexC/Fe. **d** FT of the EXAFS of FeNC-S-FexC/Fe. **e** LSV curves of ORR in O_2-saturated 0.1 M $HClO_4$ at 1600 rpm for different catalysts. **f** Schematic illustration for the two-step synthesis of Fe_2-N–C. **g** HAADF-STEM images of Fe_2-N–C. **h** The k_3-weighted Fourier transform experimental Fe K-edge EXAFS spectrum (black line) and the fitting curve (red line) of Fe_2-N–C. **i** ORR polarization curves in O_2-saturated 0.5 M H_2SO_4 solution at a sweep rate of 10 mV s^{-1} and rotation speed of 1,600 rpm. **j** LT-FTIR spectra after O_2 adsorption on Fe_1-N–C, Fe_2-N–C, and Fe_3-N–C at 140 K. The optimized adsorption configurations, adsorption energies (EO_2), and O–O bond lengths for O_2 molecules on Fe_1-N–C, Fe_2-N–C, and Fe_3-N–C

that the Co single atom exhibits excellent chemical and thermal stability during the electrocatalytic process, and can resist sintering at 900 °C. This discovery opens up a new procedure for conventional and practical synthesis of various materials with single atoms, which may help new discoveries at the atomic level in condensed matter materials.

Atom-dispersed transition metals are ideal for N-doped carbon catalysts in alkaline solutions, but they still have low activity and durability in acidic media. Xiong et al. reported a new strategy to precisely rotate the number of Fe atoms in clusters on N-doped carbon from the perspective of the oxygen adsorption configuration on the catalytic center and the substrate effect (Fig. 5.12f and g) [59]. Due to the adsorption of peroxygen-like oxygen and appropriate N species and content, Fe_2-NC has good acidic ORR activity. Compared with commercial Pt/C, the half-wave potential difference is only −20 mV, and it has good durability (Fig. 5.12h–j). These results show that the design of the catalyst, by precisely adjusting the number of Fe atoms in the cluster, can promote the understanding of the oxygen reduction mechanism and promote the commercialization of proton exchange membrane fuel cells.

Fe–N–C materials have been proven to be promising non-noble metal electrocatalysts for ORR, but their activity and durability in acidic electrolytes are still far from satisfactory. Jiang et al. prepared bimetallic (Fe, Ni)-nitrogen-doped carbon (FeNi-NC) by thermally blending Fe and Ni ZIF-8 [60]. The activity of $FeNi_{0.25}$-NC catalyst on ORR is equivalent to that of commercially available Pt/C catalyst. In particular, due to the excellent tolerance of Fe and Ni active sites to phosphate anions, $FeNi_{0.25}$-NC shows superior ORR activity in phosphorous acid electrolytes than commercially available Pt/C catalysts. Studies have shown that Ni plays a dual role in improving ORR activity and Fe–N–C stability. On the one hand, Ni–N and Fe–N partially synergize ORR, especially in high ORR overpotential regions; on the other hand, Ni acts as a catalyst during high-temperature carbonization to promote graphitization and improve the stability of FeNi-NC catalyst. This work provides an effective bimetallic strategy for adjusting the activity and stability of the ORR M–N–C catalyst in acid electrolytes.

5.5.3 MOF-Derived Other Metal Materials for ORR

Metal/metal compound nanoparticles show high activity for the catalytic process of ORR. However, the dissociation, migration, and aggregation of these nanoparticles always result in decreased activity and stability. Anchoring metal nanoparticles on the surface of the carbon substrate through structural defects and heteroatoms, or confining them in the cavities, is an effective method to solve these problems. MOFs are sacrificial agents and templates widely used in porous carbon materials. An obvious advantage of MOFs raw materials is that by simply replacing the organic ligands or metal centers of the composition, the composition of MOFs can be changed

to bind specific heteroatoms and metal species in situ. In addition, additional functional metals can be introduced by constructing multimetal center MOFs or confining metal ions to the cavities of MOFs.

Cui et al. adopted a simple strategy to limit the growth of MOFs in graphene aerogel (GA) and rationally designed and synthesized a new type of nitrogen-containing graphene aerogel–cobalt in the catalyst (Co–N-GA) (Fig. 5.13a) [61]. It is worth noting that Co–N-GA exhibits hierarchical porosity, involving micropores, mesopores, and macropores, and a high specific surface area (466.6 m^2 g^{-1}) (Fig. 5.13b). More importantly, thanks to the synergistic effect of layered porosity, high surface area, N-doped carbon, and internal metal Co, the catalyst Co–N-GA exhibits exceptionally excellent activity on ORR and has good stability (Fig. 5.13c). This strategy opens up a new platform to construct various hierarchical porous GA-based catalysts as superior electrocatalysts for energy storage and conversion technologies. Wang et al. developed a molten salt-assisted solid-state assembly strategy to prepare Fe/CoZn MOFs composites [62]. The subsequent carbonization of these MOFs produces Fe/Co-modified nitrogen-doped mesoporous carbons (Fe/Co-NCs). Inclined NCS has many advantages, such as a sheet structure with high porosity and tubular macropores (15 nm), N-doped carbon skeleton, and highly dispersed Fe/Co nanoparticles. Due to the existence of synergy between these structural advantages and active sites, Fe/Co-NC exhibits high activity on both ORR and HER. Among them, FeNC exhibits excellent ORR activity, has undergone a four-electron ORR process, and has a higher initial potential (0.963 V), half-wave potential (0.877 V vs. RHE), and excellent durability (95% current after 20000 s). The Co-NC exhibited high HER activity, with a current density of 10 mA cm^{-2} and a low overpotential of 242 mV. The remarkable ORR and HER performance is mainly attributed to the simultaneous binding of multiple active centers. For instance, nitrogen-based and metal species (Fe/Co) synergistically promote ORR and HER processes, and high porosity accelerates mass and electron transfer. Chen et al. synthesized a

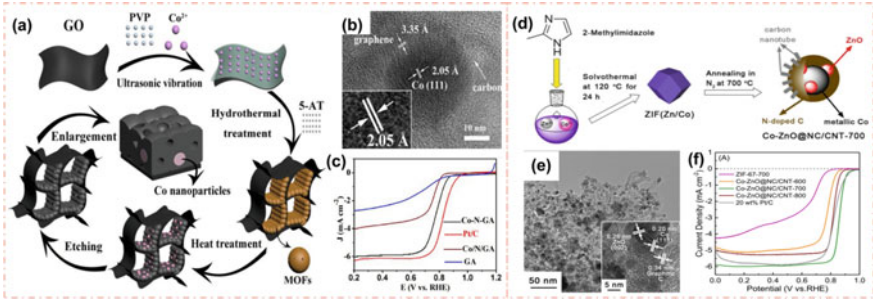

Fig. 5.13 **a** Illustration of the preparation procedure of Co–N-GA. **b** TEM of Co–N-GA. **c** ORR polarization curves at 10 mV s^{-1} under 1600 rpm. **d** Schematic illustration of the synthesis of Co-ZnO@NC/CNT-700. **e** SEM images of Co-ZnO@NC/CNT-700. **f** The specific capacitance of the electrodes as a function of current density. **g** The ORR LSV curves of Co-ZnO@NC/CNT-700 and 20 wt% Pt/C at 1600 rpm and the scan rate of 5 mv s^{-1}

series of metallic Co-ZnO (Co-ZnO@NC/CNTT) coated in N-doped carbon/carbon nanotubes by annealing bimetallic MOFs containing Co and Zn in N_2 atmosphere (Fig. 5.13d) [63]. In the hybrid, the metallic Co combines with ZnO and is wrapped by NC, while coral-like carbon nanotubes are grown from Co-ZnO@NC nanoparticles (Fig. 5.13e). When applied to ORR catalysis, Co-ZnO@NC/CNT-700 has a half-wave potential of ~ 0.86 V and a limiting current density of 5.98 mA cm^{-2}, even better than 20wt% Pt/C (Fig. 5.13f). In addition, this work also shows that the presence of ZnO is closely related to high ORR catalytic activity from two aspects. ZnO catalyzes the formation of the main active species for ORR: Co^0, Co^{2+}, pyridine, and graphitized N. ZnO promotes the growth of carbon nanotubes and micro-/mesoporous structures and improves the electrochemically active surface area and mass transfer in the ORR process.

Heteroatom-doped carbon materials can be used as high-efficiency ORR electrocatalysts, which are expected to replace noble metal electrocatalysts and are used in advanced electrochemical energy conversion systems, including proton exchange membrane fuel cells and metal–air batteries. The doping of different elements, the preparation of multi-dimensional structures, and the construction of layered pores have been widely used in well-designed ORR electrocatalysts. The preparation of MOF-derived heteroatom-doped carbon electrocatalysts usually has the advantages of mild reaction conditions, convenient operation, and low cost. In addition, due to the unique and adjustable structure of the MOF precursor, the obtained electrocatalyst has ultra-high specific surface area, layered pore structure, and high-density active centers with good dispersion, which will provide fast mass, and protons transfer and enhance the catalytic activity of ORR.

Carbon electrocatalysts doped with multiple heteroatoms can further improve the electrocatalytic activity of ORR, which can be attributed to the synergistic effect between various heteroatoms. These heteroatoms can produce larger asymmetric spins, and the charge density is optimized for the carbon skeleton. At the same time, adjust the porous size and structure to expose more active specific surface area, introduce heteroatoms to provide more active site centers, and prevent the aggregation of M-Nx sites to form uniformly dispersed high-density active sites, which is useful for improving ORR. The catalytic activity of the electrocatalyst is effective. In addition, the size is also closely related to the transport properties and electrocatalytic activity of ORR electrocatalysts. It has been proven that smaller electrocatalysts can provide more favorable quality and electron transfer processes. However, most of the synthesis routes of MOF-derived M-Nx-doped carbon-based catalysts involve high-temperature pyrolysis, which may produce two or more metal compound species at the same time, which is not conducive to determining the specificity of each species in catalysis effect. Therefore, this may be one of the key issues for the future improvement of MOF-derived metal-doped carbon catalysts. In addition, there are serious obstacles to the development of MOF-derived carbon catalysts; that is, they are prone to agglomeration, are difficult to grow on the substrate during high-temperature processing, and may become another research hotspot to improve ORR transmission kinetics and improve electrocatalytic activity. Based on the above review, in recent years, MOF-derived heteroatom-doped carbon electrocatalysts with

high-performance ORR have made many significant progresses, which is expected to create more innovations for carbon-based electrocatalysts in the future.

5.6 MOF-Derived Materials for CO_2RR

With the increasing consumption of fossil energy, CO_2 emissions increased significantly, which broke the balance of carbon cycle in nature, and led to the aggravation of greenhouse effect. This not only brings negative impact on the environment, but also is not conducive to the sustainable development of human society. If CO_2 can be recovered and converted into available resources, the above problems can be effectively solved and carbon recycling can be realized. In many ways of CO_2 conversion, electrocatalytic reduction has attracted extensive attention due to its simple experimental equipment, mild reaction conditions, and the use of renewable energy to provide electricity. However, CO_2 is a very stable thermodynamic gas (C = O, 806 kJ mol^{-1}), coupled with the fierce competitive reaction. Therefore, the conversion process is still facing great challenges. Thus, the key to the effective utilization of CO_2 reduction technology lies in the rational design and development of electrocatalysts with high activity, selectivity, and stability. In the early period of the electrocatalytic CO_2 reduction reaction (CO_2RR) research, the selection of electrocatalysts is mainly focused on bulk metals, especially noble metals such as Pt and Au [64]. However, the high cost, poor long-term stability, and low natural reserves of noble metals hinder their commercialization.

In recent years, it has been found that MOF-derived materials include heteroatom-doped carbon-based materials, transition metal single-atom dispersion materials, transition metal nanoparticles and oxides, among which the carbon-based materials doped by heteroatom and transition metal single-atom dispersion electrocatalyst can effectively reduce CO_2. In this section, MOF-derived nonmetallic carbon-based materials, metal single-atom dispersion materials, and other metal materials (including nanoparticles, oxides, and alloys) are introduced, and their performance and research status in the electrocatalytic reduction of CO_2 are described.

5.6.1 MOF-Derived Nonmetallic Carbon-Based Materials for CO_2RR

There are two main types of MOF-derived nonmetallic carbon-based materials, including intrinsic defect carbon materials and heteroatom-doped carbon materials. Heteroatom doping can optimize the electronic structure of carbon materials, redistribute the spin and charge density locally, and improve the surface adsorption/desorption behavior of intermediates [65–68]. In addition, the doping of heteroatoms can also stimulate the adjacent carbon atoms to improve the conductivity

of carbon materials, thus enhancing the overall electrocatalytic activity of carbon materials [69]. However, recently, Yao and Dai et al. have shown that the intrinsic carbon defect of pentagon has higher activity than that of carbon catalyst doped with N heteroatom [70]. The main reason is that with the deepening of research, it has been found that the proper design of intrinsic defects in the carbon skeleton can affect the overall charge state of undoped carbon nanomaterials, increase the density of active sites, and thus improve electrocatalytic performance [71, 72]. In particular, the existence of topological defects can effectively improve the catalytic performance of CO_2 reduction. In particular, the existence of topological defects can effectively improve the catalytic performance of CO_2 reduction. The main method to construct topological defects is nitrogen removal. Nitrogen removal is the process of carbon-based nanomaterials in the high-temperature treatment process, and the original N atoms are removed, forming edge or vacancy defects in the carbon skeleton. The resulting dangling bonds of some carbon atoms will be connected with each other, further forming topological defects [73]. This method can also limit the intense thermal motion of C atoms to avoid the recovery of the defective carbon skeleton formed. For example, Kang et al. synthesized a hierarchical porous carbon catalyst rich in topological defects (DHPC) by pyrolyzing ZnO NP@ZIF-8 (Fig. 5.14a–d) [74]. The mesoporous and carbon defect structure in DHPC improved its adsorption and activation capacity for CO_2. FE_{CO} can reach 99.5% at −0.5 V versus RHE in 0.5 M $KHCO_3$ electrolyte. The DFT calculation shows that pentagon defects can adsorb CO_2 spontaneously, and the barrier of DHPC electrocatalytic reduction of CO_2 to CO is lower than that of pyridine-n-doped catalyst, but it still reaches 0.33 eV. Moreover, the desorption of intermediate *CO on DHPC catalyst is also a spontaneous process (Fig. 5.14e–g). Therefore, MOF-derived intrinsic carbon defect engineering

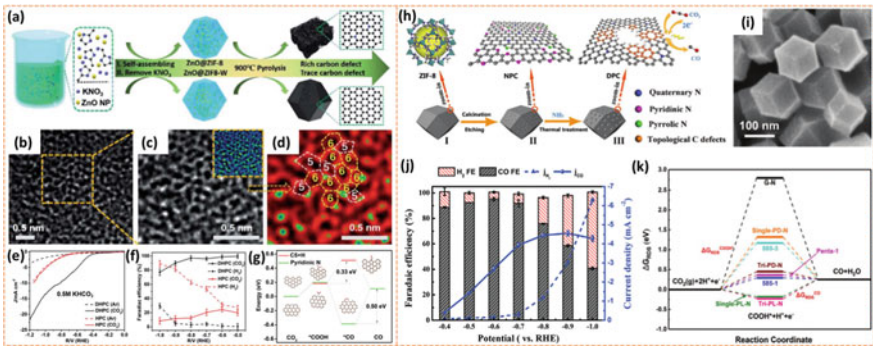

Fig. 5.14 **a** Synthetic process of DHPC and HPC. **b** High-resolution transmission electron microscopy (HRTEM) of DHPC. Magnification of one segment of the HRTEM image (**c** and **d**) after fast Fourier transformation (FFT) filtering. **e** LSV curves of DHPC and HPC in a 0.5 M $KHCO_3$ electrolyte. f Faradaic efficiencies of DHPC and HPC in 0.5 M $KHCO_3$ at various potentials. **g** Free energy diagram for CO_2 reduction to CO over different defect sites. **h** Schematic illustration of the synthetic route. **i** The FESEM image of DPC-NH3-950. **j** Faradaic efficiencies of CO (gray) and H_2 (red) and the partial current of CO on DPC-NH3-950. **k** The calculated free energy diagram for CO_2RR

is expected to become a new paradigm for improving the performance of ECR catalysts and provide guidance for improving and developing new carbon-based electrocatalysts. Chen et al. completely removed pyridinic-N and pyrrolic-N in N-rich porous carbon particles by NH_3-heat treatment to obtain a high-density topologically defective carbon catalyst (Fig. 5.14h and i) [75]. X-ray absorption near-edge structure (XANES) measurements confirmed that as the processing temperature increases, the N content decreases and the topological defect density continues to increase, and the catalytic performance of CO_2 reduction was also improved (Fig. 5.14j and k).

The catalytic performance of undoped carbon nanomaterials can be greatly improved by properly adjusting the intrinsic defects of carbon skeleton, and intrinsic defects will inevitably exist in the synthesized carbon nanomaterials. Therefore, combining various advanced characterization techniques and theoretical calculations, studying the effect of intrinsic carbon defects on the ECR performance of the catalyst is of great significance to obtain a more efficient and stable catalyst.

5.6.2 MOF-Derived Metal Single-Atom Dispersion Materials for CO_2RR

Atomic-level structure catalyst is a kind of catalyst with atomic scale and mainly refers to the metal/nonmetal active center on the support to disperse at atomic level without agglomeration. When the size of nanocrystals is constantly reduced to atomic clusters or single atoms, the energy-level structure and electronic structure of nanocrystals will change fundamentally, which makes them show different catalytic characteristics from nanomaterials, so they can show distinctive activity, selectivity, and stability in electrocatalytic CO_2RR [76–78]. It is well known that the surface free energy of metal single atoms is large, and it is easy to migrate and agglomerate in the process of pyrolysis synthesis [79]. Therefore, various strategies are used to prevent agglomeration, such as strategies of spatial confinement [80], coordination design [81], and defect engineering [82]. It is a simple and effective method to prevent atom agglomeration by using metal–organic frameworks to assist the construction of single-atom catalysts. The formed single-atom catalysts are mostly metal-N–C (M–N–C) materials, which is one of the most studied and most effective catalysts. Li et al. dispersed Ni ions on the surface of ZIF-8, heat-treated at a high temperature of 1000 °C, and Ni atoms replaced Zn and finally formed Ni–N active sites (Fig. 5.15a–c) [83]. The Ni monoatomic catalyst can effectively convert CO_2 to CO (FE > 70%) (Fig. 5.15d and e). The Faraday efficiency of Co single-atom catalyst constructed by similar method is as high as 94%, the current density is 18.1 mA cm^{-2} under 520 mv overpotential, and the TOF value of CO generation reaches 18,200 h^{-1} [84]. At the same time, the author found that Co atoms with less N coordination number have more unoccupied 3d orbitals, which is conducive to the adsorption of CO_2· intermediates, and increase the CO_2 reduction rate. Jiang et al. also reasonably constructed a series of single-atom catalysts (M1-N–C, M

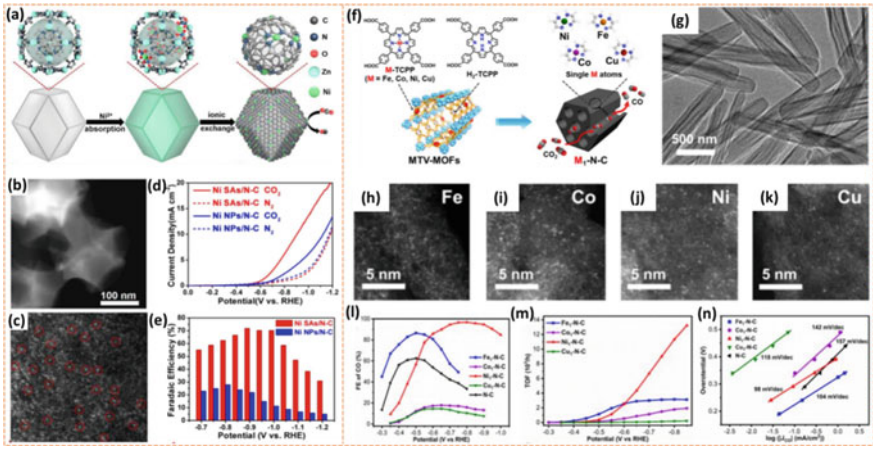

Fig. 5.15 **a** Scheme of the formation of Ni SAs/N–C. **b** HAADF-STEM images of Ni SAs/N–C. **c** Magnified HAADF-STEM images of Ni SAs/N–C. **d** LSV curves in the N_2-saturated (dotted line) or CO_2-saturated (solid line) 0.5 M $KHCO_3$ electrolyte at a scan rate of 10 mVs^{-1}. **e** FEs of CO of Ni SAs/N–C and Ni NPs/N–C at different applied potentials. **f** Illustration showing the general fabrication of single-atom M1-N–C catalysts based on MTV-MOFs for electrocatalytic CO_2 reduction. **g** Transmission electron microscopy (TEM) images of Ni1-N–C. The aberration-corrected HAADF-STEM images of (**h**) Fe1-N–C. **i** Co1-N–C. **j** Ni1-N–C. **k** Cu1-N–C. **l** FEs and (**m**) TOFs of M1-N-C for CO in pure CO_2-saturated 0.5 m $KHCO_3$. **n** Tafel plots of M1-N-C for CO_2RR

= Fe, Co, Ni, and Cu) with the same structure of porphyrin polymetallic organic frameworks, which have almost the same characteristics (particle size, surface area, porous structure) in Fig. 5.15f–k [85]. Under the condition of pure CO_2, Ni1-N–C with monoatomic Ni as the active center exhibited the most satisfactory CO_2RR performance with the highest co selectivity of 96.8%, followed by Fe1-N–C, then Co1-N–C, and Cu1-N–C (Fig. 5.15i–n). In view of the ultra-high selectivity of single-atom catalyst, researchers also used Ni1-N–C to catalyze CO_2RR under low pressure. The results showed that even at 30% and 15% CO_2 concentrations, Ni1-N–C was highly selective and feasible in industrial production, which further demonstrated the superiority and ultra-high selectivity of Ni1-N–C over CO_2RR. In recent years, it has been discovered that bimetallic-N–C catalysts have attracted the attention and study of researchers with their bimetallic active sites and possible synergies. For example, Zhao and colleagues successfully synthesized isolated diatomic Ni–Fe anchored nitrogenated carbon (Ni/Fe–N–C) catalysts using ZIF-8 as a template [86]. The diatomic structure exposed a large number of active sites and improved the activity of the catalyst. Ni/Fe–N–C has suitable adsorption/desorption energy for ECR intermediates. Over a wide range of potential, CO_2 can be selectively reduced to CO, FE up to 98%, and has a robust stability (>30 h) at –0.7 V versus RHE. DFT calculation shows that when Co adsorbs Ni/Fe–N–C, the binding strength of

*COOH and *CO is weaker than that of bare Ni/Fe–N–C; therefore, after CO adsorption, the theoretical overpotential of Ni/Fe–N–C decreases and the potential barrier of catalytic formation of CO is greatly reduced.

By constructing suitable carbon precursor materials, atomic metals can be trapped and stabilized. Because the electronegativity difference between metal and carbon atoms is very large, sufficient charge transfer can be generated to make this structural unit (M–N–C/M–C) the active center of electrocatalysis, reducing the activation energy barrier and overpotential of the reaction. These strategies provide an important guidance for the preparation of high-performance ECR catalysts and are also one of the current research hotspots.

5.6.3 MOF-Derived Other Metal Materials for CO_2RR

MOF-derived other metal materials for CO_2RR include metal oxides, alloys, and metal nanoparticles. Among them, alloys and metal oxides are widely studied electrocatalytic CO_2 reduction catalysts. Metal alloys often show more excellent or completely different catalytic performances than single-metal catalytic materials, which not only improves the conversion efficiency of CO_2, but also reduces CO_2 to specific target products in a targeted manner, so as to achieve the purpose of regulating the product ratio. Metal oxides often form alloy oxides with metals to improve the CO_2RR performance of the catalyst. For example, Han's team first proposed a simple MOF-derived method in 2013 to synthesize porous In-Cu bimetallic oxide catalysts with various Cu/In ratios for CO_2 electroreduction (Fig. 5.16a–c) [87]. The tunable CO/H_2 ratio has been easily achieved by controlling the In-Cu ratios in the MOF precursors. The maximum Faradaic efficiency of CO could reach 92.1% with a current density of 11.2 mA cm^{-2} and has good stability (>24 h) (Fig. 5.16d and e). The excellent catalytic performance of In-Cu bimetallic oxides is mainly attributed to the high CO_2 adsorption efficiency, large mass diffusion space, and the incorporation of Cu into In_2O_3 resulting in higher electrochemical surface area, stronger CO_2 adsorption, and lower charge transfer resistance. Feng and co-workers used copper phthalocyanine as ligand and ZnO_4 as bond to prepare a two-dimensional c-MOF catalyst with bimetallic center (PcCu-O_8-Zn) by solvothermal method [88]. The PcCu-O8-Zn exhibits high CO selectivity of 88%, turnover frequency of 0.39 s^{-1}, and long-term durability (>10 h) under −0.7 V vs RHE. The results show that the ZnO_4 coordination in the PcCu-O_8-Zn catalyst has a high catalytic activity for the conversion of CO_2 to CO, while the CuN_4 complex in Pc macrocycle plays a synergistic role, promoting the protonation of adsorbed CO_2 during CO_2RR. Therefore, the bimetallic active sites in the catalyst have a good synergistic effect on CO_2RR. Reddy et al. used MOF as a template to derive Co/$Ce_{0.8}Zr_{0.2}O_2$, which also showed outstanding CO_2 methanation activity and stability [89]. Metal nanoparticles (NPs) have also been extensively studied in the field of catalysis due to their high conductivity, large specific surface area and high stability. Jeong et al. used Cu-based MOF (MOF-74) derivatization to synthesize highly isolated Cu NPs to achieve enhanced

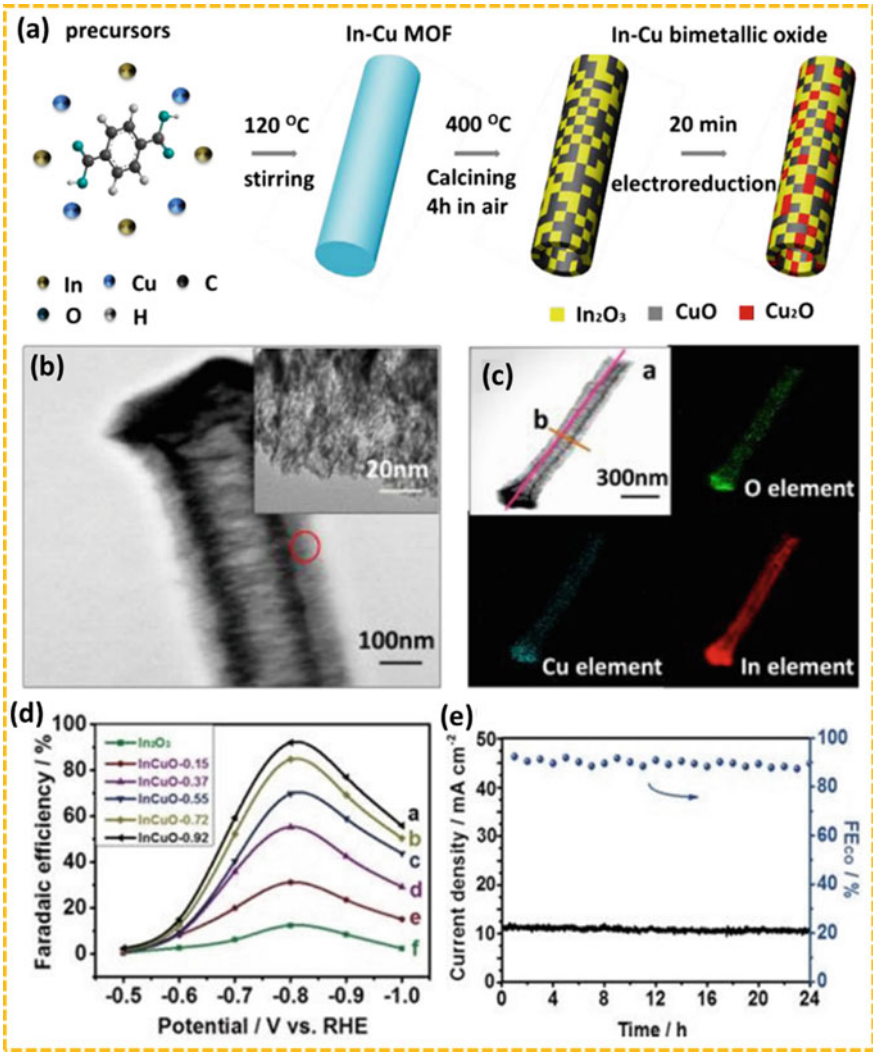

Fig. 5.16 **a** Schematic illustration for preparation process of InCuO. **b** TEM images of InCuO-0.92. **c** Elemental mapping image of InCuO-0.92. **d** Faradaic efficiency of CO for different catalysts at the applied potentials. **e** The long-term stability of InCuO-0.92 at −0.8 V vs. RHE during 24 h electrolysis

CH_4 production in the CO_2RR [90]. The experimental results found that MOF-derived Cu NPs have low aggregation, excellent electrocatalytic performance, and high activity and selectivity for C_1 product. The high selectivity of Cu NP catalysts to CH_4 is attributed to the isolated NP clusters inhibiting the coupling of C–C bonds.

In most of the cases, compared with MOF-derived other metal compounds, the pre-designed reaction sites and porous structure of the single-atom catalyst can facilitate

the adsorption or desorption step of CO_2 reduction. However, due to the high surface structure of the supported single-atom metal catalyst, the activity will be significantly reduced during the electrolysis process. Therefore, enhancing the metal–support interaction through rational design is of great significance for improving the long-term durability of MOF-derived single-atom catalysts in practical applications.

5.7 Conclusion

In summary, the recent progress of MOF-derived materials, such as MOF-derived metal-dispersed monatomic carbon-based materials, MOF-derived metal nanoparticle carbon-based materials, and MOF-derived metal-heteroatom-doped carbon-based materials, in various energy conversion reactions, such as hydrocracking, HER, OER, ORR, and CO_2RR, is reviewed. Relative to the prototype MOFs, MOF-derived materials heavily inherited the characteristics of porous MOF materials, at the same time with the unique advantages of the structure and composition of MOF material. These advantages can achieve derived materials in precise control of active ingredients, and can be very good to overcome the poor stability and electrical conductivity of MOFs. In addition, it also can provide a new type of reaction sites to expand the applicable scope of the reaction, and can provide great convenience for performance optimization. Therefore, this class of materials has been widely used in electrocatalytic applications. In addition, various synthetic strategies (water/solvent thermal synthesis) were demonstrated to prepare MOF-derived materials with good conductivity and controllable morphology. So far, various strategies have been developed to prepare MOF-derived materials to improve charge transfer and morphology control, component manipulation, and structural engineering, and some potential directions have been listed. First of all, the doping of heteroatoms can regulate the internal characteristics of functionalized carbon materials, such as internal microstructure and composition, electronic characteristics, and surface and partial electrochemical characteristics, which can significantly improve the electrocatalytic activity of the materials. Secondly, the high intrinsic activity (turnover frequency) of the active center in the single-atom catalyst mainly comes from the nitrogen coordination single-atom embedded in the carbon matrix. In addition, metal/metal compound nanoparticles showed higher activity in the electrocatalytic process, and the preparation process was simpler than that of single-atom catalysts. Therefore, various high-performance MOF derivative materials prepared by improving synthesis conditions have great application prospects in energy conversion.

MOF-derived materials have become very promising electrochemical catalysts for energy conversion, owing to their adjustable pore channels, high specific surface area, controllability of composition, and multiple morphological structures. Even though advances have been achieved in the exploration of MOF-derived materials as catalysts, there is still a long way to go before MOF-based catalysts are widely applied in industrial-level energy conversion applications.

It is still not enough for the reports about the electrochemical reaction mechanism of MOF-derived materials. Further study on this field will be beneficial for researchers to design structures and improve the performance of these materials rationally. Besides, the study of MOF-based single-/dual-atom and cluster catalyst is still in its primary stage. Therefore, more studies are needed to develop in this direction because of its potential electrochemical properties and attractive prospect toward huge energy conversion applications. Regarding the applications of MOF-derived catalysts, at present, most of the researchers mainly focus on ORR and CO_2RR, while less studies are about overall water splitting, HER, and OER. In addition, MOF-derived catalysts used in acid condition are especially scarce for water splitting and its half reactions.

For MOF-derived materials, regulating and controlling the coordination environments, more efficient characterization, and novel strategies for the designation of the structure are highly important to their further applications in catalysis.

References

1. Wen X, Guan J (2019) Recent progress on MOF-derived electrocatalysts for hydrogen evolution reaction. Appl Mater Today 16:146–168. https://doi.org/10.1016/j.apmt.2019.05.013
2. Lin L, Liu T, Xiao J, Li H, Wei P, Gao D, Nan B, Si R, Wang G, Bao X (2020) Enhancing CO_2 electroreduction to methane with cobalt phthalocyanine and zinc-nitrogen-carbon tandem catalyst. Angew Chem Int Ed 59:22408–22413. https://doi.org/10.1002/anie.202009191
3. Lee JW, Torres Pineda I, Lee JH, Kang YT (2016) Combined CO_2 absorption/regeneration performance enhancement by using nanoabsorbents. Appl Energ 178:164–176. https://doi.org/10.1016/j.apenergy.2016.06.048
4. Jiao L, Seow JYR, Skinner WS, Wang ZU, Jiang HL (2019) Metal-organic frameworks: Structures and functional applications. Mater Today 27:43–68. https://doi.org/10.1016/j.mattod.2018.10.038
5. Zhu B, Zou R, Xu Q (2018) Metal-organic framework based catalysts for hydrogen evolution. Adv Eng Mater 8:1801193. https://doi.org/10.1002/aenm.201801193
6. Li X, You S, Du J, Dai Y, Chen H, Cai Z, Ren N, Zou J (2019) ZIF-67-derived Co_3O_4@carbon protected by oxygen-buffering CeO_2 as an efficient catalyst for boosting oxygen reduction/evolution reactions. J Mater Chem A 7:25853–25864. https://doi.org/10.1039/C9TA08926H
7. Song Z, Zhang L, Doyle-Davis K, Fu X, Luo JL, Sun X (2020) Recent advances in MOF-derived single atom catalysts for electrochemical applications. Adv Eng Mater 10:2001561. https://doi.org/10.1002/aenm.202001561
8. Srinivas K, Lu Y, Chen Y, Zhang W, Yang D (2020) $FeNi_3$-Fe_3O_4 heterogeneous nanoparticles anchored on 2D MOF nanosheets/1D CNT matrix as highly efficient bifunctional electrocatalysts for water splitting. ACS Sustain Chem Eng 8:3820–3831. https://doi.org/10.1021/acssuschemeng.9b07182
9. Sankar SS, Ede SR, Anantharaj S, Karthick K, Sangeetha K, Kundu S (2019) Electrospun cobalt-ZIF micro-fibers for efficient water oxidation under unique pH conditions. Cat Sci Tec 9:1847–1856. https://doi.org/10.1039/C8CY02620C
10. Xing Z, Wang D, Meng T, Yang X (2020) Superb hydrogen evolution by a Pt nanoparticle-decorated Ni_3S_2 microrod array. ACS Appl Mater Inter 12:39163–39169. https://doi.org/10.1021/acsami.0c10476

11. Cui X, Ren P, Ma C, Zhao J, Chen R, Chen S, Rajan NP, Li H, Yu L, Tian Z, Deng D (2020) Robust interface Ru centers for high-performance acidic oxygen evolution. Adv Mater 32:1908126. https://doi.org/10.1002/adma.201908126
12. Yang M, Zhou YN, Cao YN, Tong Z, Dong B, Chai YM (2020) Advances and challenges of Fe-MOFs based materials as electrocatalysts for water splitting. Appl Mater Today 20:100692. https://doi.org/10.1016/j.apmt.2020.100692
13. Zhang J, Liu C, Zhang B (2019) Insights into single-atom metal-support interactions in electrocatalytic water Splitting. Small Methods 3:1800481. https://doi.org/10.1002/smtd.201800481
14. Ding M, Cai X, Jiang HL (2019) Improving MOF stability: approaches and applications. Chem Sci 10:10209–10230. https://doi.org/10.1039/C9SC03916C
15. Yang F, Zhao P, Hua X, Luo W, Cheng G, Xing W, Chen S (2016) A cobalt-based hybrid electrocatalyst derived from a carbon nanotube inserted metal-organic framework for efficient water-splitting. J Mater Chem A 4:16057–16063. https://doi.org/10.1039/C6TA05829A
16. Zhang E, Xie Y, Ci S, Cai P, Yi L, Wen Z (2016) Multifunctional high-activity and robust electrocatalyst derived from metal–organic frameworks. J Mater Chem A 4:17288–17298. https://doi.org/10.1039/C6TA06185K
17. Li X, Niu Z, Jiang J, Jia J, Ai L (2016) Cobalt nanoparticles embedded in porous N-rich carbon as an efficient bifunctional electrocatalyst for water splitting. J Mater Chem A 4:3204–3209. https://doi.org/10.1039/C6TA00223D
18. Cao C, Ma DD, Xu Q, Wu XT, Zhu QL (2018) Semisacrificial template growth of self-supporting MOF nanocomposite electrode for efficient electrocatalytic water oxidation. Adv Funct Mater 29:1807418. https://doi.org/10.1002/adfm.201807418
19. Wei X, Zhang Y, He H, Gao D, Hu J, Peng H, Peng L, Xiao S, Xiao P (2019) Carbon-incorporated NiO/Co_3O_4 concave surface microcubes derived from a MOF precursor for overall water splitting. Chem Commun 55:6515–6518. https://doi.org/10.1039/C9CC02037C
20. Zhang P, Zhan T, Rong H, Feng Y, Wen Y, Zhao J, Wang L, Liu X, Hou W (2020) NiFe-coordinated zeolitic imidazolate framework derived trifunctional electrocatalyst for overall water-splitting and zinc-air batteries. J Colloid Interface Sci 579:1–11. https://doi.org/10.1016/j.jcis.2020.06.052
21. Liang X, Zheng B, Chen L, Zhang J, Zhuang Z, Chen B (2017) MOF-derived formation of Ni_2P-CoP bimetallic phosphides with strong interfacial effect toward electrocatalytic water splitting. ACS Appl Mater Interfaces 9:23222–23229. https://doi.org/10.1021/acsami.7b06152
22. Shi X, Wu A, Yan H, Zhang L, Tian C, Wang L, Fu H (2018) A "MOFs plus MOFs" strategy toward Co-Mo_2N tubes for efficient electrocatalytic overall water splitting. J Mater Chem A 6:20100–20109. https://doi.org/10.1039/C8TA07906D
23. Shi L, Benetti D, Li F, Wei Q, Rosei F (2020) Phase-junction design of MOF-derived TiO_2 photoanodes sensitized with quantum dots for efficient hydrogen generation. Appl Catal B-Environ 263:118317. https://doi.org/10.1016/j.apcatb.2019.118317
24. Tourneur J, Fabre B, Loget G, Vacher A, Meriadec C, Ababou-Girard S, Gouttefangeas F, Joanny L, Cadot E, Haouas M, Leclerc-Laronze N, Falaise C, Guillon E (2019) Molecular and material engineering of photocathodes derivatized with polyoxometalate-supported Mo3S4 HER catalysts. J Am Chem Soc 141:11954–11962. https://doi.org/10.1021/jacs.9b03950
25. Liao T, Kou L, Du A, Gu Y, Sun Z (2018) Simplest MOF units for effective photodriven hydrogen evolution reaction. J Am Chem Soc 140:9159–9166. https://doi.org/10.1021/jacs.8b04599
26. Chen W, Pei J, He CT, Wan J, Ren H, Wang Y, Dong J, Wu K, Cheong WC, Mao J, Zheng X, Yan W, Zhuang Z, Chen C, Peng Q, Wang D, Li Y (2018) Single tungsten atoms supported on MOF-derived N-doped carbon for robust electrochemical hydrogen evolution. Adv Mater 30:1800396. https://doi.org/10.1002/adma.201800396
27. Zhao W, Wan G, Peng C, Sheng H, Wen J, Chen H (2018) Key single-atom electrocatalysis in metal-organic framework (MOF)-derived bifunctional catalysts. Chem Sus Chem 11:3473–3479. https://doi.org/10.1002/cssc.201801473

28. Chen Z, Wu R, Liu Y, Ha Y, Guo Y, Sun D, Liu M, Fang F (2018) Ultrafine Co nanoparticles encapsulated in carbon-nanotubes-grafted graphene sheets as advanced electrocatalysts for the hydrogen evolution reaction. Adv Mater 30:1802011. https://doi.org/10.1002/adma.201802011
29. Wu HB, Xia BY, Yu L, Yu XY, Lou XW (2015) Porous molybdenum carbide nano-octahedrons synthesized via confined carburization in metal-organic frameworks for efficient hydrogen production. Nat Commun 6:6512. https://doi.org/10.1038/ncomms7512
30. Yang Y, Lun ZY, Xia GL, Zheng F, He M, Chen Q (2015) Non-precious alloy encapsulated in nitrogen-doped graphene layers derived from MOFs as an active and durable hydrogen evolution reaction catalyst. Energ Environ Sci 8:3563–3571. https://doi.org/10.1039/C5EE02460A
31. Zhang X, Luo J, Wan K, Plessers D, Sels B, Song J, Chen L, Zhang T, Tang P, Morante JR, Arbiol J, Fransaer J (2019) From rational design of a new bimetallic MOF family with tunable linkers to OER catalysts. J Mater Chem A 7:1616–1628. https://doi.org/10.1039/C8TA08508K
32. Fang Z, Peng L, Qian Y, Zhang X, Xie Y, Cha JJ, Yu G (2018) Dual tuning of Ni-Co-A (A= P, Se, O) nanosheets by anion substitution and holey engineering for efficient hydrogen evolution. J Am Chem Soc 140:5241–5247. https://doi.org/10.1021/jacs.8b01548
33. Liu T, Li P, Yao N, Cheng G, Chen S, Luo W, Yin Y (2019) CoP-doped MOF-based electrocatalyst for pH-universal hydrogen evolution reaction. Angew Chem Int Ed 58:4679–4684. https://doi.org/10.1002/anie.201901409
34. Luo X, Zhou Q, Du S, Li J, Zhang L, Lin K, Li H, Chen B, Wu T, Chen D, Chang M, Liu Y (2018) One-dimensional porous hybrid structure of Mo2C-CoP encapsulated in N-doped carbon derived from MOF: an efficient electrocatalyst for hydrogen evolution reaction over the entire pH range. ACS Appl Mater Inter 10:42335–42347. https://doi.org/10.1021/acsami.8b15456
35. Hu S, Wang S, Feng C, Wu H, Zhang J, Mei H (2020) Novel MOF-derived nickel nitride as high-performance bifunctional electrocatalysts for hydrogen evolution and urea oxidation. ACS Sustain Chem Eng 8:7414–7422. https://doi.org/10.1021/acssuschemeng.0c01450
36. Zhou W, Lu J, Zhou K, Yang L, Ke Y, Tang Z, Chen S (2016) $CoSe_2$ nanoparticles embedded defective carbon nanotubes derived from MOFs as efficient electrocatalyst for hydrogen evolution reaction. Nano Energy 28:143–150. https://doi.org/10.1016/j.nanoen.2016.08.040
37. Hong W, Kitta M, Xu Q (2018) Bimetallic MOF-derived FeCo-P/C nanocomposites as efficient catalysts for oxygen evolution reaction. Small Methods 2:1800214. https://doi.org/10.1002/smtd.201800214
38. Zaman WQ, Sun W, Tariq M, Zhou Z, Farooq U, Abbas Z, Cao L, Yang J (2019) Iridium substitution in nickel cobaltite renders high mass specific OER activity and durability in acidic media. Appl Catal B: Environ 244:295–302. https://doi.org/10.1016/j.apcatb.2018.10.041
39. Kim JS, Kim B, Kim H, Kang K (2018) Recent progress on multimetal oxide catalysts for the oxygen evolution reaction. Adv Eng Mater 8:1702774. https://doi.org/10.1002/aenm.201702774
40. Dou S, Dong CL, Hu Z, Huang YC, Chen J, Tao L, Yan D, Chen D, Shen S, Chou S, Wang S (2017) Atomic-scale CoO_x species in metal-organic frameworks for oxygen evolution reaction. Adv Funct Mater 27:1702546. https://doi.org/10.1002/adfm.201702546
41. Zang W, Sumboja A, Ma Y, Zhang H, Wu Y, Wu S, Wu H, Liu Z, Guan C, Wang J, Pennycook SJ (2018) Single Co atoms anchored in porous N-doped carbon for efficient zinc-air battery cathodes. Appl Catal 8:8961–8969. https://doi.org/10.1021/acscatal.8b02556
42. Chen S, Cui M, Yin Z, Xiong J, Mi L, Li Y (2020) Single-atom and dual-atom electrocatalysts derived from metal organic frameworks: current progress and perspectives. ChemSusChem. https://doi.org/10.1002/cssc.202002098
43. Xu Y, Li B, Zheng S, Wu P, Zhan J, Xue H, Xu Q, Pang H (2018) Ultrathin two-dimensional cobalt-organic framework nanosheets for high-performance electrocatalytic oxygen evolution. J Mater Chem A 6:22070–22076. https://doi.org/10.1039/C8TA03128B
44. Ling X, Du F, Zhang Y, Shen Y, Li T, Alsaedi A, Hayat T, Zhou Y, Zou Z (2019) Preparation of an Fe_2Ni MOF on nickel foam as an efficient and stable electrocatalyst for the oxygen evolution reaction. RSC Adv 9:33558–33562. https://doi.org/10.1039/C9RA07499F

45. Liu Y, Wang C, Ju S, Li M, Yuan A, Zhu G (2020) FeCo-based hybrid MOF derived active species for effective oxygen evolution. Prog Nat Sci 30:185–191. https://doi.org/10.1016/j.pnsc.2020.02.006
46. Wang X, Chai L, Ding J, Zhong L, Du Y, Li TT, Hu Y, Qian J, Huang S (2019) Chemical and morphological transformation of MOF-derived bimetallic phosphide for efficient oxygen evolution. Nano Energy 62:745–753. https://doi.org/10.1016/j.nanoen.2019.06.002
47. Li X, Fang Y, Lin X, Tian M, An X, Fu Y, Li R, Jin J, Ma J (2015) MOF derived Co_3O_4 nanoparticles embedded in N-doped mesoporous carbon layer/MWCNT hybrids: extraordinary bi-functional electrocatalysts for OER and ORR. J Mater Chem A 3:17392–17402. https://doi.org/10.1039/C5TA03900B
48. Agarwal S, Yu X, Manthiram A (2020) A pair of metal organic framework (MOF)-derived oxygen reduction reaction (ORR) and oxygen evolution reaction (OER) catalysts for zinc-air batteries. Mater Today Energy 16:100405. https://doi.org/10.1016/j.mtener.2020.100405
49. Xu H, Yang Y, Yang X, Cao J, Liu W, Tang Y (2019) Stringing MOF-derived nanocages: a strategy for the enhanced oxygen evolution reaction. J Mater Chem A 7:8284–8291. https://doi.org/10.1039/C9TA00624A
50. Wang HF, Chen L, Pang H, Kaskel S, Xu Q (2020) MOF-derived electrocatalysts for oxygen reduction, oxygen evolution and hydrogen evolution reactions. Chem Soc Rev 49:1414–1448. https://doi.org/10.1039/C9CS00906J
51. Ren Q, Wang H, Lu XF, Tong Y-X, Li G-R (2018) Recent progress on MOF-derived heteroatom-doped carbon-based electrocatalysts for oxygen reduction reaction. Adv Sci (Weinh) 5:1700515. https://doi.org/10.1002/advs.201700515
52. Zhu Y, Zhang Z, Li W, Lei Z, Cheng N, Tan Y, Mu S, Sun X (2019) Highly exposed active sites of defect-enriched derived MOFs for enhanced oxygen reduction reaction. ACS Sustainable Chem Eng 7:17855–17862. https://doi.org/10.1021/acssuschemeng.9b04380
53. Song Z, Liu W, Cheng N, Banis MN, Li X, Sun Q, Xiao B, Liu Y, Lushington A, Li R, Liu L, Sun X (2017) Origin of the high oxygen reduction reaction of nitrogen and sulfur co-doped MOF-derived nanocarbon electrocatalysts. Mater Horiz 4:900–907. https://doi.org/10.1039/C7MH00244K
54. Deng Y, Chi B, Tian X, Cui Z, Liu E, Jia Q, Fan W, Wang G, Dang D, Li M, Zang K, Luo J, Hu Y, Liao S, Sun X, Mukerjee S (2019) g-C_3N_4 promoted MOF derived hollow carbon nanopolyhedra doped with high density/fraction of single Fe atoms as an ultra-high performance non-precious catalyst towards acidic ORR and PEM fuel cells. J Mater Chem A 7:5020–5030. https://doi.org/10.1039/C8TA11785C
55. Lin Y, Liu P, Velasco E, Yao G, Tian Z, Zhang L, Chen L (2019) Fabricating single-atom catalysts from chelating metal in open frameworks. Adv Mater 31:1808193. https://doi.org/10.1002/ADMA.201808193
56. Qiao Y, Yuan P, Hu Y, Zhang J, Mu S, Zhou J, Hao Li, Xia H, He J, Xu Q (2018) Sulfuration of an Fe-N-C catalyst containing FexC/Fe species to enhance the catalysis of oxygen reduction in acidic media and for use in flexible Zn-air batteries. Adv Mater 30:1804504. https://doi.org/10.1002/adma.201804504
57. Jin H, Zhou H, He D, Wang Z, Wu Q, Liang Q, Liu S, Mu S (2019) MOF-derived 3D Fe-N-S co-doped carbon matrix/nanotube nanocomposites with advanced oxygen reduction activity and stability in both acidic and alkaline media. Appl Catal B: Environ 250:143–149. https://doi.org/10.1016/j.apcatb.2019.03.013
58. Yin P, Yao T, Wu Y, Zheng L, Lin Y, Liu W, Ju H, Zhu J, Hong X, Deng Z, Zhou G, Wei S, Li Y (2016) Single Cobalt Atoms with Precise N-Coordination as Superior Oxygen Reduction Reaction Catalysts. Angew Chem Int Ed 55:10800–10805. https://doi.org/10.1002/anie.201604802
59. Ye W, Chen S, Lin Y, Yang L, Chen S, Zheng X, Qi Z, Wang C, Long R, Chen M, Zhu J, Gao P, Song L, Jiang J, Xiong Y (2019) Precisely tuning the number of Fe atoms in clusters on N-doped carbon toward acidic oxygen reduction reaction. Chem 5:2865–2878. https://doi.org/10.1016/j.chempr.2019.07.020

60. Liu J, Fan C, Liu G, Jiang L (2021) MOF-derived dual metal (Fe, Ni)-nitrogen-doped carbon for synergistically enhanced oxygen reduction reaction. Appl Surf Sci 538:148017. https://doi.org/10.1016/j.apsusc.2020.148017
61. Zhu Z, Yang Y, Guan Y, Xue J, Cui L (2016) Construction of a cobalt-embedded nitrogen-doped carbon material with the desired porosity derived from the confined growth of MOFs within graphene aerogels as a superior catalyst towards HER and ORR. J Mater Chem A 4:15536–15545. https://doi.org/10.1039/C6TA05196K
62. Wang Y, Pan Y, Zhu L, Yu H, Duan B, Wang R, Zhang Z, Qiu S (2019) Solvent-free assembly of Co/Fe-containing MOFs derived N-doped mesoporous carbon nanosheets for ORR and HER. Carbon 146:671–679. https://doi.org/10.1016/j.carbon.2019.02.002
63. Zhao X, He X, Chen B, Yin F, Li G (2019) MOFs derived metallic cobalt-zinc oxide@nitrogen-doped carbon/carbon nanotubes as a highly-efficient electrocatalyst for oxygen reduction reaction. Appl Surf Sci 487:1049–1057. https://doi.org/10.1016/j.apsusc.2019.05.182
64. Hori Y (2008) Electrochemical CO_2 reduction on metal electrodes. Mod Asp Electrochem 42:89–189. https://doi.org/10.1007/978-0-387-49489-0_3
65. Jiao Y, Zheng Y, Jaroniec M et al (2014) Origin of the electrocatalytic oxygen reduction activity of graphene-based catalysts: a roadmap to achieve the best performance. J Am Chem Soc 136:4394–4403. https://doi.org/10.1021/ja500432h
66. Zhang L, Niu J, Li M, Xia Z et al (2014) Catalytic mechanisms of sulfur-doped graphene as efficient oxygen reduction reaction catalysts for fuel cells. J Phys Chem C 118:3545–3553. https://doi.org/10.1021/jp410501u
67. Pei Z, Li H, Huang Y et al (2017) Texturing in situ: N, S-enriched hierarchically porous carbon as a highly active reversible oxygen electrocatalyst. Energy Environ Sci 10:742–749. https://doi.org/10.1039/c6ee03265f
68. Pei Z, Meng Q, Wei L, Fan J et al (2020) Toward efficient and high rate sodium-ion storage: A new insight from dopant-defect interplay in textured carbon anode materials. Energy Storage Mater 28:55–63. https://doi.org/10.1016/j.ensm.2020.02.033
69. Zhao J, Lai H, Lyu Z et al (2015) Hydrophilic hierarchical nitrogen-doped carbon nanocages for ultrahigh supercapacitive performance. Adv Mater 27:3541–3545. https://doi.org/10.1002/adma.201500945
70. Jia Y, Zhang L, Zhuang L et al (2019) Identification of active sites for acidic oxygen reduction on carbon catalysts with and without nitrogen doping. Nat Catal 2:688–695. https://doi.org/10.1038/s41929-019-0297-4
71. Jia Y, Chen J, Yao X (2018) Defect electrocatalytic mechanism: Concept, topological structure and perspective. Mater Chem Front 2:1250–1268. https://doi.org/10.1039/c8qm00070k
72. Jia Y, Zhang L, Du A et al (2016) Defect graphene as a trifunctional catalyst for electrochemical reactions. Adv Mater 28:9532–9538. https://doi.org/10.1002/adma.201602912
73. Earis P, Nugent N, Martinez-fresno M et al (2019) Defect engineering in earth-abundant electrocatalysts for CO_2 and N_2 reduction. Energy Environ Sci 12:1730–1750. https://doi.org/10.1039/C8EE03781G.Volume
74. Wu Q, Gao J, Feng J et al (2020) A CO_2 adsorption dominated carbon defect-based electrocatalyst for efficient carbon dioxide reduction. J Mater Chem A 8:1205–1211. https://doi.org/10.1039/c9ta11473d
75. Dong Y, Zhang Q, Tian Z et al (2020) Ammonia thermal treatment toward topological defects in porous carbon for enhanced carbon dioxide electroreduction. Adv Mater 2001300:1–10. https://doi.org/10.1002/adma.202001300
76. Wang A, Li J, Zhang T (2018) Heterogeneous single-atom catalysis. Nat Rev Chem 2:65–81. https://doi.org/10.1038/s41570-018-0010-1
77. Yang XF, Wang A, Qiao B et al (2013) Single-atom catalysts: A new frontier in heterogeneous catalysis. Acc Chem Res 46:1740–1748. https://doi.org/10.1021/ar300361m
78. Liu L, Corma A (2018) Metal catalysts for heterogeneous catalysis: from single atoms to nanoclusters and nanoparticles. Chem Rev 118:4981–5079. https://doi.org/10.1021/acs.chemrev.7b00776

79. Qin R, Liu P, Fu G et al (2018) Strategies for stabilizing atomically dispersed metal catalysts. Small Methods 2:1–21. https://doi.org/10.1002/smtd.201700286
80. Chen Y, Ji S, Zhao S et al (2018) Enhanced oxygen reduction with single-atomic-site iron catalysts for a zinc-air battery and hydrogen-air fuel cell. Nat Commun 9:5422. https://doi.org/10.1038/s41467-018-07850-2
81. Wei S, Wang Y, Chen W et al (2020) Atomically dispersed Fe atoms anchored on COF-derived N-doped carbon nanospheres as efficient multi-functional catalysts. Chem Sci 11:786–790. https://doi.org/10.1039/c9sc05005a
82. Yoo M, Yu Y-S, Ha H et al (2020) A tailored oxide interface creates dense Pt single-atom catalysts with high catalytic activity. Energy Environ Sci 13:1231–1239. https://doi.org/10.1039/c9ee03492g
83. Zhao C, Dai X, Yao T et al (2017) Ionic exchange of metal-organic frameworks to access single nickel sites for efficient electroreduction of CO_2. J Am Chem Soc 139:8078–8081. https://doi.org/10.1021/jacs.7b02736
84. Wang X, Chen Z, Zhao X et al (2018) Regulation of coordination number over single Co sites: triggering the efficient electroreduction of CO_2. Angew Chemie 130:1962–1966. https://doi.org/10.1002/ange.201712451
85. Jiao L, Yang W, Wan G et al (2020) Single-atom electrocatalysts from multivariate metal-organic frameworks for highly selective reduction of CO_2 at low pressures. Angew Chemie Int Ed 59:20589–20595. https://doi.org/10.1002/anie.202008787
86. Ren W, Tan X, Yang W et al (2019) Isolated diatomic Ni-Fe metal-nitrogen sites for synergistic electroreduction of CO_2. Angew Chemie Int Ed 58:6972–6976. https://doi.org/10.1002/anie.201901575
87. Guo W, Sun X, Chen C, Yang D et al (2019) Metal-organic framework-derived indium-copper bimetallic oxide catalysts for selective aqueous electroreduction of CO_2. Green Chem 21:503–508. https://doi.org/10.1039/c8gc03261k
88. Zhong H, Ghorbani-Asl M, Ly KH et al (2020) Synergistic electroreduction of carbon dioxide to carbon monoxide on bimetallic layered conjugated metal-organic frameworks. Nat Commun 11:1–10. https://doi.org/10.1038/s41467-020-15141-y
89. Jampaiah D, Damma D, Chalkidis A et al (2020) MOF-derived ceria-zirconia supported Co_3O_4 catalysts with enhanced activity in CO_2 methanation. Catal Today 356:519–526. https://doi.org/10.1016/j.cattod.2020.05.047
90. Kim MK, Kim HJ, Lim H et al (2019) Metal-organic framework-mediated strategy for enhanced methane production on copper nanoparticles in electrochemical CO_2 reduction. Electrochim Acta 306:28–34. https://doi.org/10.1016/j.electacta.2019.03.101

Chapter 6
Summary and Perspectives

Huan Pang

Research on the exploration of MOFs as platforms for electrochemical energy applications is certainly one of the most active topics among chemistry and materials community. Thanks to the efforts of researchers, significant progresses have been made in recent years in the development of MOFs, and MOF derivates for batteries, supercapacitors and water splitting. With these advanced functional materials, we can see both opportunities and challenges towards practical applications:

(1) The thermal, mechanical, and chemical stability of MOFs should be further improved. Up to now, most of MOFs undergo decomposition and skeleton collapse in water, acid, or base, extremely obstructing their extensive application in electrochemical energy fields. This problem can be solved by sensible choice of organic ligands and metal secondary building units. Moreover, special methods such as pressing and phase change treatment strategies can be applied to manufacture freestanding MOFs membranes, thereby overcoming inherent fragility and finite processability of MOFs without endowing their original properties.

(2) The conductivity of most MOFs are poor. However, how to further improve conductivity is of greatest importance. On the one hand, the conductivity of most MOFs should be further improved by deepening understanding the conductivity mechanism of MOFs so that to design and develop newly conductive MOFs. On the other hand, the conductivity of MOFs should be further enhanced by combining with highly conductive materials (CNT, GO, rGO, AC, and conducting polymer etc.).

(3) At present, there is a lack of systematic and comprehensive understanding of the mechanism of MOFs. The understanding of the mechanism is of great significance for the realization of electrode materials with high performance,

H. Pang (✉)
School of Chemistry and Chemical Engineering, Institute for Innovative Materials and Energy, Yangzhou University, Yangzhou 225009, Jiangsu, PR China
e-mail: panghuan@yzu.edu.cn

H. Pang (ed.), *Nano/Micro Metal-Organic Frameworks*,
https://doi.org/10.1007/978-981-16-4071-1_6

low cost and easy preparation. In order to systematically reveal the potential electrochemical mechanism, advanced characterization tools and theoretical calculations are essential. So far, only a few reports have provided a detailed explanation of this machine. Therefore, the electrochemical mechanism should be further explored.

(4) In comparison with MOFs, MOF-derived materials, including porous carbon, metal oxide, metal (oxide)/carbon composites and single-metal-atoms/carbon, obtained by the high-temperature pyrolysis, possess a large number of exposed (S, N, metal) active centers with excellent structural stability and electrical conductivity. They have been widely used as high-performance catalysts or catalyst supports in various electrocatalytic processes even at harsh conditions. However, the increased cost of the involved MOF precursors and the complex synthetic techniques usually reduce the economic viability of such MOF-derived nanomaterials. It should be noted that the high-temperature pyrolysis leads to considerable difficulties in precise control of the microstructures of MOF-derived nanomaterials. Though recent significant progresses have been made in precise control of the microstructures of MOF-derived materials, such as single-atom, di-atom, and metal-cluster catalysts, continuous efforts are still necessary for making this technique viable in practical applications.

(5) Choosing judiciously organic linker is significant for the construction of MOFs. For LIBs, organic linkers with abundant redox active sites in MOFs are preferred, making per formula of MOFs store more Li ions. For Li–S batteries, MOFs with functional organic linkers that can effectively confine polysulfides are advantageous, blocking the shuttle effect of soluble polysulfides. For SCs, opportune organic linkers contribute to construct electrically conductive MOFs, enhancing the electrochemical performance. In the field of energy conversion, a series of MOFs-derived materials are used in electrocatalytic reactions. These materials retain the original advantages of MOF materials to a great extent, such as ultra-high porosity and specific surface area, and at the same time well overcome the common problems of poor conductivity and stability of MOFs, and provide new reaction sites. It expands the applicable response range and also provides convenience for performance optimization.

There is no doubt that MOFs are useful platforms for electrochemical energy applications. The future work in this field should be focused on reducing the shortcomings of the current developed MOFs, MOF derivates, and on designing/developing new materials on the basis of MOFs without the current disadvantages. In addition, with the aid of advanced instrumentation techniques, deeper insights into the formation processes of MOFs and MOF derivates and their working mechanisms during electrochemical energy applications should be further explored. We hope that this book can help readers design and develop new electrochemical energy materials based on MOFs, and apply them to the world economy in the near future.